2023

Unraveling the metabolic pathway of dissimilatory sulfate reduction

Delfim Manuel Araújo Ferreira

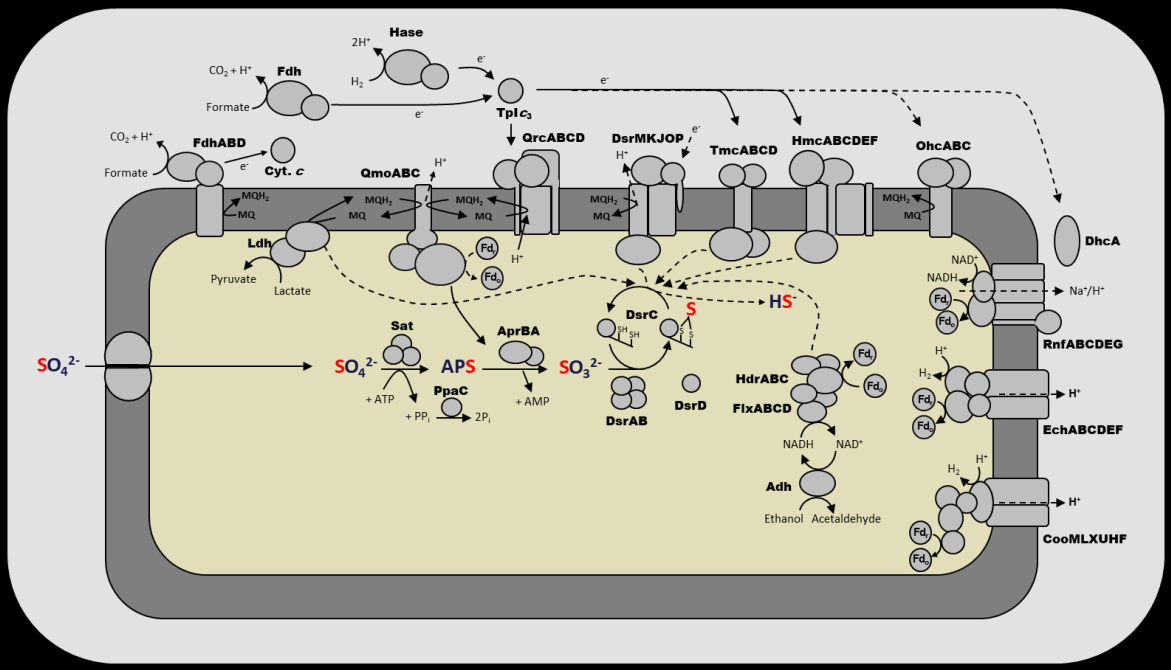

Dissertation presented to obtain the **Ph.D degree in**

Molecular Biosciences

Oeiras, December, 2023

INSTITUTO DE TECNOLOGIA QUÍMICA E BIOLÓGICA ANTÓNIO XAVIER | UNIVERSIDADE NOVA DE LISBOA

Unraveling the metabolic pathway of dissimilatory sulfate reduction

Delfim Manuel Araújo Ferreira

Dissertation presented to obtain the Ph.D degree in Molecular Biosciences

INSTITUTO DE TECNOLOGIA QUÍMICA E BIOLÓGICA ANTÓNIO XAVIER |
UNIVERSIDADE NOVA DE LISBOA

Oeiras, December, 2023

Contents

Acknowledgements

My PhD was a long and rocky journey, and its completion would not be possible without the support from those around me.

To my supervisor, Professor Inês Cardoso Pereira, for the unwavering commitment, insightful guidance, and mentorship throughout this journey. The constant encouragement and constructive feedback were influential in shaping my research and enhancing my skills as a researcher. I am truly indebted for your trust and belief in my abilities.

To my co-supervisor and “super old” friend, Dr Sofia Venceslau, whose valuable inputs, expertise, and encouragement have enriched this thesis. Thank you for the patience to interpret and discuss results, especially late in the afternoon when was time to go home. These discussions have broadened my perspective and significantly contributed to the quality of my research, and were equally important to build resilience. Till today, I remember the “good” motivational video.

I extend my warmest thanks to all my friends and ITQB colleagues, whose camaraderie, knowledge-sharing, and constructive discussions have fostered an intellectually stimulating environment. Their support has made the challenges of research more manageable.

To my family, I am deeply indebted to my family for their unwavering love, encouragement, and sacrifices they made to ensure my success. Their constant belief in my abilities has been a driving force behind my pursuit of knowledge, and I am eternally grateful for their unwavering support.

To Sara, which encouraged me in this last longing mile and with whom I celebrated the little wins that occur along the way. You have been my rock, my confidant, and my greatest source of happiness. This achievement would not have been possible without you by my side, and I am excited to embark on the next chapter of our journey together.

Thesis Outline

The work described in this thesis concerns the study of the metabolic pathways that enable several microorganisms to perform dissimilatory sulfate reduction, i.e., reducing sulfur-based molecules with the goal of energy production.

The thesis starts with an introduction to the sulfur cycle and description of the main metabolisms that use sulfur molecules to conserve energy. In the next chapter, the work focuses on the metabolism of sulfate-reducing organisms, more particularly on the role of DsrD, a protein which has been associated with an essential enzyme, but with no assigned function so far. In Chapter Three, by using strains with a defect in an essential protein, I see how both fermentation and respiration are affected by having an impaired pathway, also hypothesising alternative pathways and alternative protein complexes that may be relevant for sulfate reduction, namely the Flx-Hdr protein complex. The Flx-Hdr protein complex is analysed deeper in the next section, Chapter Four, through the performing biochemical and spectroscopic characterizations. This thesis is wrapped up in Chapter Five, which consists of final conclusions and future work perspectives.

List of Publications

Thesis publications

- **D. Ferreira***, A.C.C. Barbosa*, G.P. Oliveira, T. Catarino, S.S. Venceslau and I.A.C. Pereira (2022) “The DsrD functional marker protein is an allosteric activator of the DsrAB dissimilatory sulfite reductase” *PNAS* 119 (4): e2118880119

*These authors have contributed equally to this work

- **D. Ferreira**, S.S. Venceslau, R. Bernardino, A. Preto, L. Zhang, J.R. Waldbauer, W.D. Leavitt, I.A.C. Pereira (2023) “DsrC is involved in fermentative growth and interacts directly with the FlxABCD-HdrABC complex in *Desulfovibrio vulgaris* Hildenborough” *Environ Microbiol* 25(5): 962-976

- V. Pelmenschikov, **D. Ferreira**, S.S. Venceslau, P. Hildebrandt, I.A.C. Pereira and S. Todorovic (2023) “Substrate-Dependent Conformational Switch of the Noncubane [4Fe-4S] Cluster in Heterodisulfide Reductase HdrB" *J Am Chem Soc* 145(1): 7-11

Other publications

- A.G. Duarte, A.C.C. Barbosa, **D. Ferreira**, G. Manteigas, R.M. Domingos, I.A.C. Pereira (2021) “Redox loops in anaerobic respiration - The role of the widespread NrfD protein family and associated dimeric redox module” *Biochim Biophys Acta Bioenerg* 1862(7): 148416

Dissertation Summary

Sulfate-reducers are anaerobic organisms from the Bacteria and Archaea domains of life, which are able to use a wide variety of electron donors and couple them with the reduction of sulfur molecules to hydrogen sulfide. This process, known as dissimilatory sulfate reduction, drives the biogeochemical sulfur cycle and has a strong influence on other element cycles and on the redox balance of the oceans and atmosphere.

In this biochemical pathway, sulfite is reduced by the dissimilatory sulfite reductase DsrAB together with its cosubstrate DsrC to form a trisulfide in DsrC. The DsrC-trisulfide is suggested to be later reduced to hydrogen sulfide and DsrC by the DsrMKJOP transmembrane complex through menaquinol oxidation, coupled with proton translocation.

This thesis starts with a study of DsrD, a small protein whose gene *dsrD* is usually found downstream of *dsrAB* and has been used as a functional marker to distinguish organisms with reductive/disproportionating sulfur metabolism from sulfur-oxidizing metabolisms. The function of DsrD has remained unclear since it was identified in 1995, and in this work, we presented evidence that DsrD is a physiological partner of DsrAB and acts as an activator of its sulfite reduction activity. DsrD is expressed in respiratory and not in fermentative conditions and a Δ*dsrD* deletion strain could be obtained, indicating that its function is not essential. Analysis of *dsrD* genomic distribution reveals that three different sub-types of DsrD exist, which correlate with DsrAB phylogeny. Organisms with the earliest forms of *dsrAB* lack the *dsrD* gene, revealing that *dsrD* activating role arose later in evolution relative to *dsrAB*.

The focus of this thesis then goes to DsrC. As referred above, DsrC works as a co-substrate of DsrAB, having two conserved cysteines in its C-terminal arm that are converted to a trisulfide upon reduction of sulfite. This protein is essential in dissimilatory sulfur metabolism, with previous studies having already suggested additional interacting partners and additional roles in the energy metabolism. Here we confirm this hypothesis, by performing physiological, proteomic and biochemical studies with *Desulfovibrio vulgaris* Hildenborough wild-type and respective mutant strains affected in DsrC functionality. The results show that DsrC also plays a role during fermentative growth, since its impairment leads to reduced

growth under fermentative conditions. In both respiratory and fermentative growth conditions, the impairment of DsrC leads to an increased abundance of the FlxABCD-HdrABC complex and Adh alcohol dehydrogenase, which is reflected in higher production of ethanol. Subsequent pull-down experiments confirm a direct interaction between DsrC and the FlxABCD-HdrABC complex, through the HdrB subunit.

The next chapter is then dedicated to the characterization of the three subunits from the HdrABC complex from sulfate-reducers, namely the successful expression, purification and spectroscopic characterization of HdrA and HdrB, and the obstacles and strategies to overcome issues with HdrC expression and purification. HdrA is composed of six [4Fe-4S] clusters and one FAD cofactor, and HdrB is composed of two [4Fe-4S] clusters with paramagnetic spectroscopic characteristics corresponding to non-cubane [4Fe-4S] clusters. As for HdrC, several expression and purification approaches were tried, using several vectors, expression hosts, purification strategies and affinity tags. The best approach was via HdrC copurification with HdrB using *D*. *vulgaris* as expression host, but this yielded low amounts of HdrC and disproportional to the HdrB amount. To show electron transfer between HdrCB and DsrC, some biochemical experiments were done with no/low HdrC but were not successful.

Sumário da dissertação

Os organismos redutores de sulfato são micro-organismos anaeróbicos pertencentes aos domínios taxonómicos Bacteria e Archaea, e são capazes de usar uma ampla variedade de dadores eletrónicos e acoplá-los com a redução de compostos de enxofre a sulfureto de hidrogénio. Esse processo, conhecido como redução dissimilativa de sulfato, é essencial para o ciclo biogeoquímico do enxofre e tem forte influência nos ciclos de outros elementos e no equilíbrio redox dos oceanos e da atmosfera.

Nesta via bioquímica, o sulfito é reduzido pela enzima redutase de sulfito DsrAB juntamente com seu co-substrato DsrC para formar um trissulfureto na DsrC. Acredita-se que este DsrC-trissulfureto é posteriormente reduzido a sulfureto de hidrogénio e DsrC pelo complexo transmembranar DsrMKJOP através da oxidação do menaquinol, juntamente com a translocação de protões.

Este trabalho começa com um estudo da DsrD, uma pequena proteína cujo gene *dsrD* é geralmente encontrado a jusante de *dsrAB* e tem sido usado como um marcador funcional para distinguir organismos com metabolismo de redução/disproporcionação de enxofre de organismos com metabolismos de oxidação de enxofre. Desde que a DsrD foi identificada em 1995, a sua função permaneceu incerta. Neste trabalho apresentamos evidências de que DsrD é um parceiro fisiológico de DsrAB, atuando como um ativador da atividade de redução de sulfito. DsrD é expressa em condições respiratórias e não em condições fermentativas, sendo possível criar uma estirpe com o gene *dsrD* deletado, o que indica que sua função não é essencial. A análise da distribuição genómica de *dsrD* revela que existem três subtipos diferentes de DsrD, e que se correlacionam com a filogenia de DsrAB. Organismos com as primeiras formas de *dsrAB* não possuem o gene *dsrD*, revelando que seu papel ativador surgiu mais tarde na evolução em relação ao *dsrAB*.

A segunda parte deste trabalho foca-se na DsrC. Como referido anteriormente, DsrC funciona como um co-substrato de DsrAB, tendo duas cisteínas conservadas no seu extremo C-terminal e que são convertidas num trissulfureto após a redução do sulfito. Esta proteína é essencial no metabolismo dissimilativo do enxofre, tendo estudos anteriores já sugerido outros parceiros biológicos e funções adicionais da DsrC no metabolismo energético. Aqui confirmamos

esta hipótese, tendo realizado estudos fisiológicos, proteómicos e bioquímicos com *Desulfovibrio vulgaris* Hildenborough wild-type e respetivas estirpes mutantes com DsrC defeituosa. Os resultados mostram que DsrC também desempenha um papel durante o crescimento fermentativo, uma vez que o seu defeito leva a um menor crescimento em condições fermentativas. Tanto em condições de crescimento respiratório como fermentativo, este comprometimento da DsrC leva a um aumento da abundância do complexo proteico FlxABCD-HdrABC e da enzima álcool desidrogenase Adh, o que se reflete numa maior produção de etanol. Experiências de pull-down confirmam uma interação direta entre DsrC e o complexo FlxABCD-HdrABC, através da subunidade HdrB.

O capítulo seguinte é dedicado à expressão e purificação das subunidades do complexo HdrABC de organismos redutores de sulfato, nomeadamente o sucesso na expressão, purificação e caracterização espetroscópica de HdrA e HdrB, e os obstáculos e estratégias usadas com a expressão de HdrC e respetiva purificação. HdrA é composta por seis centros [4Fe-4S] e um cofator FAD, e HdrB é composta por dois centros [4Fe-4S] com características espetroscópicas paramagnéticas correspondentes a centros não cubanos [4Fe-4S]. Quanto à HdrC, foram tentadas várias abordagens de expressão e purificação, tendo usado vários vetores, hospedeiros de expressão, estratégias de purificação e tags de afinidade. A melhor abordagem foi através da copurificação de HdrC com HdrB usando *D*. *vulgaris* como hospedeiro de expressão, embora tenha resultado em quantidades baixas de HdrC e desproporcionais à quantidade de HdrB. Para mostrar a transferência de eletrões entre HdrCB e DsrC, algumas experiências bioquímicas foram feitos com nenhuma ou pouca HdrC, mas sem sucesso.

List of abbreviations

Amp^R	ampicillin resistance
APS	adenosine-5'-phophosulfate
BCA	bicinchoninic acid
Cm^R	chloramphenicol resistance
COG	cluster of orthologous groups
diDO-IPTL	dimethylation-deuteration and oxygen-exchange – – isobaric peptide terminal labelling
DMSO	dimethyl sulfoxide
DSR	dissimilatory sulfate reduction
DTT	dithiothreitol
EDTA	ethylenediaminetetraacetic acid
EPR	electron paramagnetic resonance
EMSA	electrophoretic mobility shift assay
FAD	flavin adenine dinucleotide
FBEB	flavin-based electron bifurcation
Fe-S	iron-sulfur cluster
FMN	flavin mononucleotide
g	EPR *g*-factor
GST	Glutathione S-transferase
HEPES	4-(2-hydroxyethyl)-1-piperazineethanesulfonic acid
HPLC	High Performance Liquid Chromatography
IPTG	isopropyl-β-D-thiogalactopyranoside
Kan^R	kanamycin resistance
LB	lysogeny broth, Luria broth, or Luria-Bertani medium
MALDI-TOF	Matrix-assisted laser desorption/ionization time-of-flight

MalPEG	Maleimide PEG
MK	menaquinone
MOPS	3-(N-morpholino)propanesulfonic acid
MS	mass spectrometry
NAD	nicotinamide adenine dinucleotide
OD	optical density
PIPES	piperazine-N,N′-bis(2-ethanesulfonic acid)
pmf	proton motive force
PP_i	pyrophosphate
PVDF	polyvinylidene fluoride
Rbs	ribosome-binding site
RT	room-temperature
SDS-PAGE	sodium dodecyl-sulfate polyacrylamide gel electrophoresis
SLP	substrate-level phosphorylation
SOB	Super Optimal Broth (Hanahan′s Broth)
SOP	sulfur-oxidizing prokaryotes
$Spec^R$	spectinomycin resistance
SRP	sulfate-reducing prokaryotes
TBS	tris-buffered saline
Tc^R	tetracycline resistance
TCEP	tris(2-carboxyethyl)phosphine
TEMED	tetramethylethylenediamine
WT	wild-type

Chapter I

Introduction

Contents

1.1 – The Earth earliest atmosphere

The Earth's earliest atmosphere was anoxic, being mainly composed of carbon dioxide (CO_2), nitrogen (N_2) and water vapor [1]. It is believed that the extensive activity of volcanoes and hydrothermal vents has released hydrogen sulfide (H_2S) and sulfur oxide (SO_2) gases into the atmosphere, and the penetration of UV-solar radiation deep in the atmosphere led to photochemical reactions such as SO_2 photolysis, resulting in the formation of sulfur compounds with higher oxidation states, such as elemental sulfur (S^0), sulfite (SO_3^{2-}) and sulfate (SO_4^{2-}) [2]. These conditions were ideal for the appearance of organisms capable of utilizing sulfur compounds for the generation of energy, such as sulfite-, thiosulfate- and sulfate-reducers, anoxygenic photosynthetic sulfur-oxidizers, and sulfur-disproportionators.

The reaction of sulfide with Fe^{2+}, resulting from volcano activity, generates the mineral pyrite (FeS_2). The gradual burial of sulfide minerals such as pyrite together with the appearance of oxygenic photosynthetic organisms, such as cyanobacteria, have contributed to a rise in the atmospheric oxygen levels, progressively changing it from a weakly reducing atmosphere to an oxidizing atmosphere. Over this time period, referred to as the Great Oxidation Event, the increasingly oxidized atmosphere caused the weathering of continental pyrite and subsequent gradual increase of sulfate concentration in the seawater, stabilizing in the concentrations observed today, 28 mM, and leading to the start of the modern sulfur cycle [3]. In fact, there is a correlation between oceanic sulfate levels and the oxygen content of the earth's atmosphere. In the current geologic eon, Phanerozoic, the largest sulfur reservoirs on Earth are in the form of pyrite and sulfate in the oceans [4].

1.2 – Sulfur cycle and sulfur-metabolizing organisms

The sulfur cycle is a biogeochemical process in which sulfur compounds are cycled, going from oxidation states ranging from +6 (sulfate) to -2 (sulfide). These transformations occur through both biotic (reducers, oxidizers, etc.) and abiotic (mineralization) processes. **Table 1** shows the most relevant inorganic compounds and respective oxidation state.

Table 1 – Inorganic sulfur compounds of biological relevance, and respective oxidation state. Table adapted from [5]

Compound	Chemical Formula	Sulfur Oxidation State
Sulfide	H_2S, HS^-, S^{2-}	-2
Polysulfides	$^-S\text{-}S_n\text{-}S^-$	-1 (terminal S)/0 (inner S)
Thiosulfate	$S_2O_3^{2-}$	-1 (sulfane S)/+5 (sulfone S)
Polythionates	$^-{}_3OS\text{-}S_n\text{-}SO_3^-$	0 (inner S)/+5 (sulfone S)
Elemental sulfur	S_n rings or chains	0
Sulfite	HSO_3^-, SO_3^{2-}	+4
Sulfate	SO_4^{2-}	+6

Microorganisms contribute to this cycle, being able to transform sulfur molecules in either an oxidative or reductive direction, both completely (from -2 to +6 or vice-versa) or partially, depending on their metabolism. In **Figure 1** are represented several metabolic pathways to metabolize sulfur molecules.

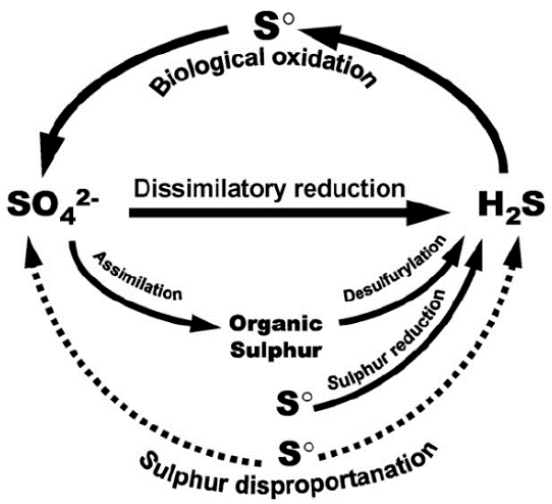

Figure 1 – Microbial sulfur cycle, with the main sulfur molecules and reactions represented. Figure from [6].

On the reductive side of the sulfur cycle, oxidized forms of sulfur (sulfate, thiosulfate, sulfite and S^0) work as electron acceptors for the oxidation of hydrogen (H_2) or a variety of organic acids (e.g., lactate, formate), which results in formation of H_2S and generation of energy. For the case of the most abundant molecule, sulfate, this process is known as dissimilatory sulfate reduction, which connects the sulfur and carbon cycles in anoxic environments, being quantitatively the most important process in the oxidation of organic matter in anoxic marine environments due to the very high concentration of sulfate in marine waters (28 mM). The environmental magnitude of this process is such that it has a direct impact on the redox balance of the oceans and atmosphere, and is estimated to account for up to 50% of the carbon mineralization in marine sediments [7], [8].

A small fraction of the resulting hydrogen sulfide is buried as pyrite [9], while the majority is oxidized, either chemically or biologically by diverse groups of microorganisms with oxygen, nitrate, and/or metal oxides as electron acceptors. On this oxidative part, microorganisms play an essential role in the oxidation of reduced forms of sulfur, such as H_2S, thiosulfate and S^0, to SO_4^{2-}. Depending on the metabolism of the microorganism, the electrons from this oxidation can be used for the reduction of terminal electron acceptors (chemolitotrophs) or for photosynthetic CO_2 fixation (photolitotrophs).

Sulfur disproportionators are another microbial group important for the sulfur cycle. These can use sulfur compounds with intermediate oxidation state to generate SO_4^{2-} and H_2S, coupled with substrate level phosphorylation of ATP.

The following sub-sections focus on these microbial groups: organisms that use sulfur molecules for dissimilatory reduction, oxidation and disproportionation.

1.2.1 – Sulfate-reducing organisms

Sulfate-reducing prokaryotes (SRP) are anaerobes able to use sulfate as a terminal electron acceptor and oxidizing hydrogen (H_2), alcohols, hydrocarbons, a variety of organic acids (e.g., lactate, formate), or sugars. These compounds can be partially oxidized to acetate, and others completely to carbon dioxide (CO_2).

The SRP group is phylogenetically disperse and can be found both in the Bacteria and Archaea domains of life. By using functional marker genes such as rRNA16S and *dsrAB*, the distribution of SRP has been steadily increasing, having been previously considered to be restricted to the bacterial lineages of Deltaproteobacteria, Firmicutes, Thermodesulfobacteria, Actinobacteria, Nitrospirae and Caldiserica, and the archaeal lineages Euryarchaeota (*Archaeoglobus* family), Crenarcheota (*Thermocladium* and *Caldivirga* family) and Aigarchaeota [10], [11]. In 2018, by taking advantage on the increasing genomic availability from uncultivated and unexplored microorganisms [12] and using metagenome-assembled genomes, several studies [13]–[15] have expanded the number of SRP to include the phylogenetic groups Acidobacteria, Armatimonadetes, *Bacteroidetes/Chlorobi*, *Candidatus* Desantisbacteria, *Candidatus* Falkowbacteria, *Candidatus* Hydrothermarchaeota, *Candidatus* Lambdaproteobacteria, *Candidatus* Omnitrophica, *Candidatus* Riflebacteria, *Candidatus* Schekmanbacteria, *Candidatus* Zixibacteria, Ignavibacteria, Planctomycetes and Verrucomicrobia. Although these new organisms have the genomic machinery needed to perform a dissimilatory sulfur metabolism, in some lineages it is not clear in which direction (reduction, oxidation or disproportionation) this metabolism works.

The canonical pathway for dissimilatory sulfate reduction involves the eight electron reduction of sulfate to sulfide, and starts with the import of sulfate into the cytoplasm, through sulfate permeases [16], [17]. Sulfate is chemically very stable, and the low redox potential of its reduction to sulfite ($E^{0'}$ = -516 mV) makes sulfate an inadequate electron acceptor [18]. Therefore, sulfate is phosphorylated by the sulfate adenylyltransferase Sat to Adenosine 5'-phosphosulfate (APS), at the expense of an ATP molecule, thus originating inorganic pyrophosphate (PP_i). Formation of PPi is not thermodynamically favorable, and so the reaction needs to be pulled to completion by an inorganic pyrophosphatase, according to equation (1) [19]. The higher midpoint redox potential for APS reduction to sulfite ($E^{0'}$ APS/SO_3^{2-} = -60 mV) allows this reaction (equation 2) to occur, catalyzed by the APS reductase enzyme AprAB, with 2 electrons received from the menaquinone pool. The menaquinol ($E^{0'}$ MKH_2/MK = -75 mV) by itself cannot donate electrons to APS, due to the small difference in redox potentials and the membrane potential (~150 mV) to be overcome. For the reaction to be favorable there is a redox loop mechanism between QmoABC and the QrcABCD membrane complex [20], in which electrons from the periplasmic TpIc_3 cytochrome, together with protons from the cytoplasm, are used by QrcABCD to reduce the menaquinone pool. QmoABC then oxidizes menaquinol to donate electrons to AprAB, together with proton transfer to the periplasm. After AprAB catalysis, sulfite binds to the siroheme of DsrAB, and DsrAB and its cosubstrate DsrC catalyse the four-electron reduction of SO_3^{2-} to a S^0 valence state, in the form of a trisulfide bound to DsrC by two strictly conserved cysteine residues. From these four electrons, two come from the reduced DsrC cysteine residues, and two come from a still unknown DsrAB physiological electron donor [21], [22]. The DsrC-trisulfide is suggested to be later reduced to sulfide and DsrC by the DsrMKJOP transmembrane complex through menaquinol oxidation, coupled with proton translocation. The stoichiometry of sulfite reduction reaction to sulfide is presented in equation (3). The origin of the two electrons for DsrAB reduction is not known, and it has been suggested that DsrMKJOP may also require an additional periplasmic electron donor donor through the DsrJ subunit or a cytoplasmic donor by electron confurcation in SRP lacking the DsrJOP module [18], [23]–[25]. A representation of the stepwise reduction of sulfate to sulfide is presented in **Figure 2**.

(1) $SO_4^{2-} + 2H^+ + ATP \rightarrow APS + PP_i$ ($\Delta G^{0'} = +46$ kJ mol^{-1} SO_4^{2-})

$PP_i + H_2O \rightarrow 2P_i$ ($\Delta G^{0'} = -22$ kJ mol^{-1} SO_4^{2-})

↓

$SO_4^{2-} + 2H^+ + ATP \rightarrow APS + 2Pi$ ($\Delta G^{0'} = +24$ kJ mol^{-1} SO_4^{2-})

(2) $APS + H_2$ (2 e^-) $\rightarrow SO_3^- + AMP$ ($\Delta G^{0'} = -69$ kJ mol^{-1} APS)

(3) $SO_3^- + 3H_2$ (6 e^-) $\rightarrow S^{2-} + 3H_2O$ ($\Delta G^{0'} = -172$ kJ mol^{-1} SO_3^-, for SO_3^-/S^{2-} reduction with H_2)

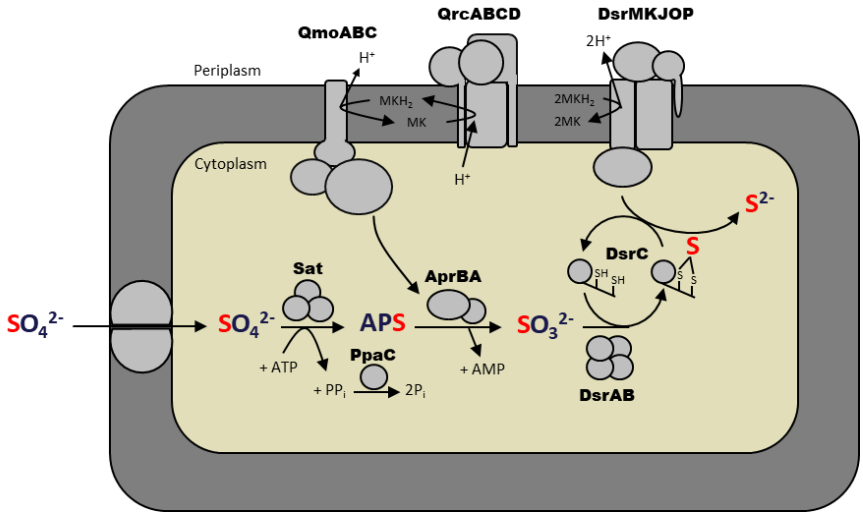

Figure 2 – Simplified version of the dissimilatory sulfate reduction pathway. Sulfate (SO_4^{2-}) is transported inside the cell, phosphorylated by Sulfate adenylyltransferase (Sat) to adenosine 5'-phosphosulfate (APS) and reduced by the APS reductase (AprAB) to sulfite (SO_3^{2-}), with electrons coming from the menaquinone pool (MKH_2/MK). The Dissimilatory sulfite reductase DsrAB reduces SO_3^{2-} to a S^0 in the form of a trisulfide between two cysteine residues of DsrC. The DsrC trisulfide will be later reduced to sulfide (S^{2-}) by the DsrMKJOP complex.

Despite the acceptance of this model as a general way to describe dissimilatory sulfate reduction, there are some differences to this typical metabolism, such as the absence of the QmoC subunit of the QmoABC complex in Gram-positive bacteria. In several Gram-positive organisms *qmoC* is replaced by the *hdrBC* genes from the soluble heterodisulfide reductases, suggesting that electrons for APS reduction may derive from soluble pathways, and not quinones [26], [27]. Zane *et al*. have deleted *qmoABC* from the genome of *Desulfovibrio vulgaris*, and showed this strain was still able to grow with sulfite or thiosulfate as electron acceptor, but not sulfate [28]. In fact, due to sulfite being an intermediary of dissimilatory sulfate reduction, many organisms able to respire sulfate are also able to use sulfite and thiosulfate as electron acceptors, with the latter being reduced to sulfite via thiosulfate reductase. The ability to respire sulfite is actually more widespread than sulfate and goes beyond the purpose of energy conservation [29].

The Gram-positive SRP and the archaeon *Caldivirga maquiliguensis,* only encode the DsrMK, but not the DsrJOP module. This is likely correlated with the fact that Gram positive bacteria are devoid of a periplasmic space. In these organisms, electrons for DsrC trisulfide reduction are suggested to come only from the menaquinone pool, and proton translocation might be coupled with pyrophosphate hydrolysis through membrane-associated proton-translocating pyrophosphatases and NADH oxidation through the presence of Complex I [26], [27], [30].

There are still several questions left to answer about the pathway of dissimilatory sulfate reduction, namely the nature of the two-electron donor of DsrAB, the confirmation of DsrC-trisulfide reduction by the DsrMKJOP, the respective mechanism and if there are other partners involved [22], [25], the function of the almost SRP-exclusive DsrD protein [13], [31], [32], and the presence of DsrL, a protein initially thought to be exclusive of sulfur-oxidizers and recently found in the genome of organisms encoding a reductive DsrAB [13], [33]. One of these questions, the function of DsrD, will be addressed in Chapter II of this thesis.

1.2.2 – Sulfur-oxidizing organisms

Sulfur oxidizers are organisms that can use reduced sulfur compounds, such as hydrogen sulfide, polysulfide, elemental sulfur, sulfite, thiosulfate or polythionates, to completely oxidize them to sulfate or partially oxidize them to sulfur globules that can be stored for future oxidation. There is no universal mechanism for the oxidation of reduced sulfur compounds, with several modules existing that occur alone or in different combinations [5], and sulfide oxidation may not always proceed completely to sulfate [34], [35]. Several proteins and protein complexes essential for dissimilatory sulfate reduction are also present in sulfur oxidizers, working reversibly [36].

The dissimilatory oxidation of sulfur compounds can be found in the Bacteria and Archaea domains of life, and organisms able to perform it can be phylogenetically and metabolically diverse. Many sulfur-oxidizers are litoautotrophs, i.e., use inorganic compounds (sulfur) as electron donors and use CO_2 as carbon source, and can be divided into chemolitotrophs able to grow under oxic conditions and phototrophs able to grow under anoxic conditions.

The chemolitotrophic sulfur-oxidizers couple the electrons from sulfur oxidation with the terminal acceptors O_2, NO_3^- or MnO_2, to fix CO_2 [37], [38]. The archaeal dissimilatory sulfur oxidation is restricted to this aerobic chemolitotrophic metabolism, and is represented by the extreme thermophilic obligate acidophilic organisms belonging to the order *Sulfolobales* of *Crenarchaeota* [39].

The photolitotrophic sulfur-oxidizers require light and use reduced sulfur compounds as electron donors for photosynthetic CO_2 fixation. These can be divided into Purple Sulfur Bacteria (PSB) and Green Sulfur Bacteria (GSB), depending on the pigment responsible for light harvesting, with bacteriochlorophylls (BChl) *a* or *b* being the major photosynthetic pigments in PSB, and BChl *c*, *d* or *e* in GSB. [40], [41].

Sulfur globules are insoluble and can be stored outside the cell or inside, in the periplasmic space [42]. When necessary, this stored sulfur is solubilized in the form of a sulfane sulfur in a low molecular weight organic persulfide (R-S-SH) to be later transported to the cytoplasmic space and oxidized by persulfide shuttling system constituted by rhodanese-, TusA- and DsrE-like proteins. Depending

on the sulfur-oxidizer organism, there are different pathways to go from this point to sulfite. To the best of my knowledge, the most studied and widespread pathway is through rDsr, but other routes can also occur, such as the recently unveiled heterodisulfide reductase-like system [43] or via non-energy conserving reactions with molecular oxygen [44].

The well-studied sulfur-oxidizer PSB *Allochromatium vinosum* performs the rDsr pathway, in which the sulfane sulfur is transfered to DsrEFH, a protein complex with a heterohexameric ($\alpha_2\beta_2\gamma_2$) structure [45], [46]. In *A. vinosum* DsrEFH, two conserved cysteine residues were found to be essential for sulfur oxidation, namely the DsrE-Cys78 and DsrH-Cys20 [45], [47]. The DsrE-Cys78 residue was found to bind sulfur and to be essential for further sulfur transfer to DsrC. No sulfur atoms bound to the cysteines in DsrH and DsrF were detected, but the DsrH-Cys20 residue is also essential for the enzyme catalytic activity, likely involved in the DsrEFH interaction with the sulfur donor. The persulfurated DsrEFH transfers the sulfur to DsrC, which is exclusively persulfurated at the C-terminal CysA, forming a persulfide [45]. Curiously, DsrEFH and DsrC are homologues of the *E. coli* TusBCD and TusE, respectively, and these proteins are part of the sulfur relay system required for 2-thiouridine biosynthesis [48].

The DsrC persulfide is believed to be later oxidized to DsrC trisulfide by the DsrMKJOP transmembrane complex, possibly using the electrons to feed respiratory or photosynthetic electron transport chains [49]. The DsrC trisulfide is oxidized by the reverse-acting dissimilatory sulfite reductase DsrAB together with the iron-sulfur flavoprotein DsrL, forming sulfite, regenerating DsrC for another catalytic cycle, and reducing $NAD(P)^+$ to NAD(P)H, which can be used for fixation of carbon dioxide and light-driven energy conservation [33]. A representation of S^0 oxidation to SO_3^{2-} in *A. vinosum* is presented in **Figure 3**. The resulting sulfite can be directly oxidized to sulfate by the membrane-bound iron-sulfur molybdoenzyme SoeABC, or can be oxidized in a reverse way to what occurs in dissimilatory sulfate reduction, to APS by AprAB and then to sulfate by Sat. In both ways, the electrons from sulfite oxidation are fed to the photosynthetic electron transport chain, via SoeC or AprM/QmoABC, respectively [50]–[52].

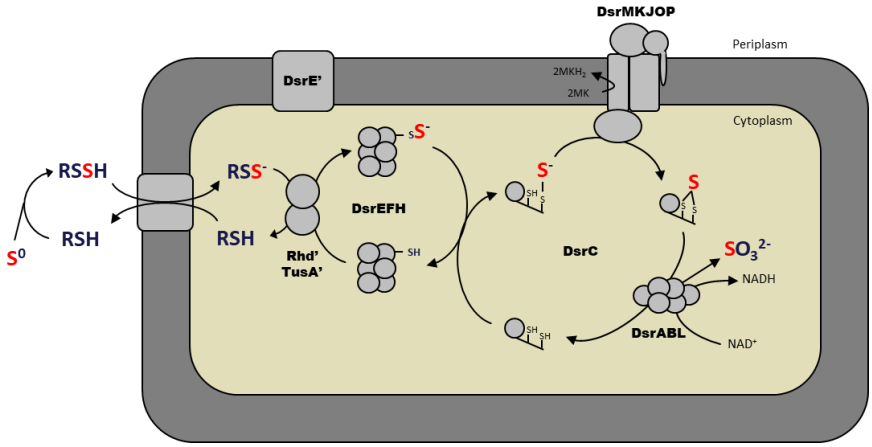

Figure 3 – Proposed model for the *Allochromatium vinosum* metabolism for sulfur oxidation to sulfite. Periplasmic sulfur globules are solubilized in the form of an organic persulfide, to be later transported to the cytoplasm, where a Rhd-TusA-DsrE-like complex will oxidize and transfer the sulfane sulfur to DsrEFH. This will be later transferred to DsrC, forming a persulfide, which is believed to be oxidized by the DsrMKJOP complex to for the DsrC trisulfide. This will be later oxidized by the DsrABL complex, forming sulfite and regenerating DsrC.

1.2.3 – Sulfur-disproportionators

Sulfur disproportionation was described in 1987 and is a chemolitotrophic process in which sulfur compounds with intermediate oxidation states (S^0, $S_2O_3^{2-}$, SO_3^{2-}) work both as electron donor and acceptor, generating H_2S and SO_4^{2-}. This process is comparable to the process of fermentation, in which electrons are redistributed among the carbon atoms and ATP is synthesized without the involvement of a membrane electron transport chain and proton gradients [53]–[55].

This process was first discovered in *Desulfovibrio sulfodismutans*, an organism from the *Desulfovibrio* family typically composed of sulfate-reducers. However, *D*. *sulfodismutans* could not grow in the presence of acetate and sulfate, being instead able to produce sulfide and sulfate from either sulfite or thiosulfate, according to the equations (4) and (5). The *D*. *sulfodismutans* growth required small

amounts of acetate as carbon source, but the growth yield was proportional to the amount of thiosulfate or sulfite added, and independent from the amount of acetate. Nonetheless, this strain was able to perform dissimilatory sulfate reduction when in the present of carbon substrates alternative to acetate.

(4) $4\ SO_3^{2-} + H^+ \rightarrow 3\ SO_4^{2-} + HS^-$ ($\Delta G^0 = -58.9$ kJ mol^{-1} SO_3^{2-})

(5) $S_2O_3^{2-} + H_2O \rightarrow SO_4^{2-} + HS^- + H^+$ ($\Delta G^0 = -21.9$ kJ mol^{-1} $S_2O_3^{2-}$)

The disproportionation of elemental sulfur to sulfate and sulfide was only later described in *Desulfocapsa thiozymogenes*, and is an endergonic process under standard conditions, as can be seen in equation (6). To be thermodynamically favorable and support growth, the produced H_2S must be chemically removed from the culture media, by sulfide-scavenging compounds such as ferric (equation 7) or manganic (equation 8) oxides [56]–[58]. The stoichiometry for elemental sulfur disproportionation in the presence of iron or manganese is displayed in equation (9) and (10), respectively.

(6) $4\ S^0 + 4\ H_2O \rightarrow SO_4^{2-} + 3\ HS^- + 5\ H^+$ ($\Delta G^0 = +10.2$ kJ mol^{-1} S^0)

(7) $3\ H_2S + 2FeOOH \rightarrow S^0 + 2FeS + 4H_2O$

(8) $H_2S + MnO_2 \rightarrow S^0 + Mn^{2+} + 2OH^-$

(9) $3\ S^0 + 2\ FeOOH \rightarrow SO_4^{2-} + 2FeS + 2H^+$

(10) $S^0 + 3MnO_2 + 2H_2O \rightarrow SO_4^{2-} + 3Mn^{2+} + 4OH^-$

Sulfur-disproportionation has so far been reported only in the Bacteria domain and is quite common among sulfate-reducers. In fact, with a few exceptions, most sulfur-disproportionating organisms possess the genes required for dissimilatory sufate reduction, and

most, but not all, can grow from reducing sulfate. Only a small list of sulfate-reducers can couple sulfur disproportionation with growth [53]–[55], [59]. On the other hand, there are some sulfur-disproportionating organisms lacking the ability for dissimilatory sulfate reduction while encoding the full set of genes required for this process, such as *Desulfocapsa sulfexigens* [60] and *Thermosulfurimonas dismutans* [61].

Slobodkin and Slobodkina [59] compiled a list of the 36 cultured microbial strains known to disproportionate sulfur compounds. These are so far represented by organisms of the phyla Proteobacteria, Thermodesulfobacteria and Firmicutes, being the majority Proteobacteria belonging to the Deltaproteobacteria class, recently reclassified as Desulfobacterota [62].

The metabolic pathway for sulfur disproportionation is different for different organisms. Krämer and Cypionka [54] showed that some *Desulfovibrio* species can reduce both sulfite and thiosulfate in the presence of the uncoupler carbonylcyanide m-chlorophenylhydrazone (CCCP), but not reduce sulfate or disproportionate sulfite or sulfate, suggesting the existence of an energy-driven step (phosphorylation) involved in disproportionation. Moreover, these strains grew by disproportionating sulfite or thiosulfate in the presence of the F_0F_1 ATP synthase inhibitor N,N'-dicyclohexylcarbodiimide (DCCD), but could not grow by reducing sulfate. This provides evidence that ATP synthesis during disproportionation is dependent on substrate-level phosphorylation, likely through ATP sulfurylase, and not by oxidative phosphorylation through ATP synthase. Thus, these organisms use the enzymatic machinery that catalyzes sulfate reduction reversely, to disproportionate thiosulfate and sulfite, with ATP being formed by substrate-level phosphorylation through ATP sulfurylase. In addition, these results strongly indicated that a reversed electron transport step was involved in the reduction of thiosulfate to sulfide, with the sulfite oxidation to APS being the source of these electrons. Another sulfur disproportionator is *Desulfocapsa sulfexigens*, whose metabolism is still not completely known: reduction of S^0 occurs through an unknown enzymatic machinery, and oxidization of S^0 to sulfite possibly occurs via the heterodisulfide reductase HdrABC [60]. Sulfite is then oxidized to sulfate using the sulfite-oxidoreductase (SOR) enzyme [55]. A representation of the sulfur disproportionation metabolism is presented in **Figure 4**.

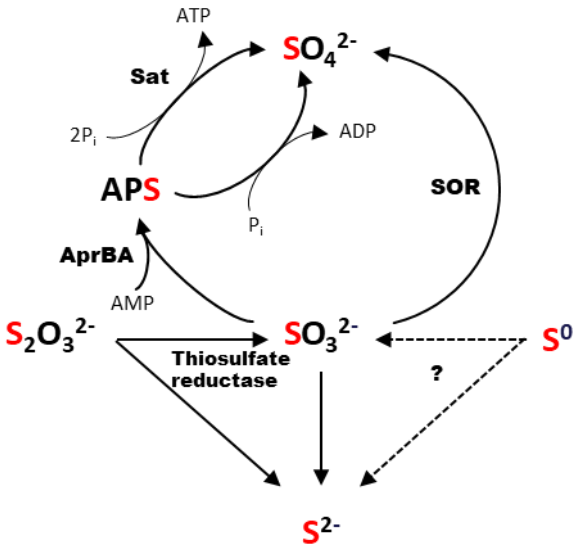

Figure 4 – Proposed pathways for sulfur disproportionation. Figure adapted from [55].

The chemical and biological oxidation of sulfide may not always proceed completely to sulfate. Consequently, the oxidized inorganic sulfur intermediates formed, such as elemental sulfur (S^0), thiosulfate and sulfite, can be utilized further by other sulfur metabolizing organisms.

1.2.4 – Cable bacteria

Cable bacteria are a group of microorganisms discovered in the last decade and have so far been detected only in marine and freshwater sediments. These organisms are characterized by being multicellular, filamentous bacteria capable of transporting electrons from cell to cell along the longitudinal axis of their centimeter-long filaments. The considerable size of each cable-bacterium filament, which can extend up to 3-7 cm in length and include over 10^4 cells, allows this organism to be exposed to an anoxic environment on one extremity, and an oxic environment on the other extremity [63]. On the anoxic side, the cable bacteria is composed of cells with a sulfide-oxidizing metabolism capable of oxidizing sulfide to sulfate, and the resulting electrons are transported along the filament to the

other extremity, composed of cells capable of using those electrons to reduce oxygen to water [64], [65], as depicted in **Figure 5**.

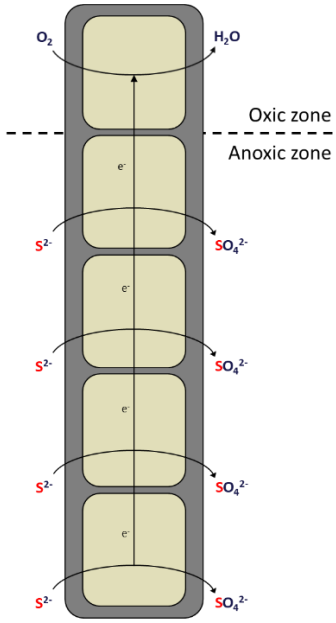

Figure 5 – Model for electrogenic sulfur oxidation in aquatic sediments by cable bacteria. Hydrogen sulfide is oxidized by anodic cells in the anoxic zone of the sediment, and the respective electrons are transported through the cable bacteria to the oxic zone, to be used to reduce oxygen by the cathodic cells. Figure adapted from [66].

This model has been confirmed by the direct electric current connection between the oxygen reduction at the surface and the sulfide oxidation in the subsurface of the sediments, at distances longer than 1 cm. Plus, this spatial separation of sulfide oxidation and oxygen reduction processes leads to steep pH gradients across the sediment, which in turn causes distinct dissolutions and precipitation of minerals [67], [68]. Cable bacteria also possess a gliding motility that helps them to orient themselves in the redox gradients that exist in aquatic sediments [69].

This electron transport between adjacent cells is not mediated by diffusive electron shuttles or contact between conductive elements, but rather through an electric cable-like structure (**Figure 6**): through electron microscopy and atomic force microscopy of a cross-section of the filament, it is possible to see the periplasmic space composed of 400-700 nm wide ridges, resembling a cartwheel structure. This invaginated shape of the outer cell membrane is due to the presence of a ~50 nm diameter fiber in each ridge compartment, these fibers being continuous along the bacterial filament and passing through the cell-cell junctions. The adjacent cells are 200 nm apart and bridged by the fibers, which also helps maintaining the integrity of individual cable bacteria as one united filament [64], [70], [71]. The composition of these continuous periplasmic fibers remains unresolved.

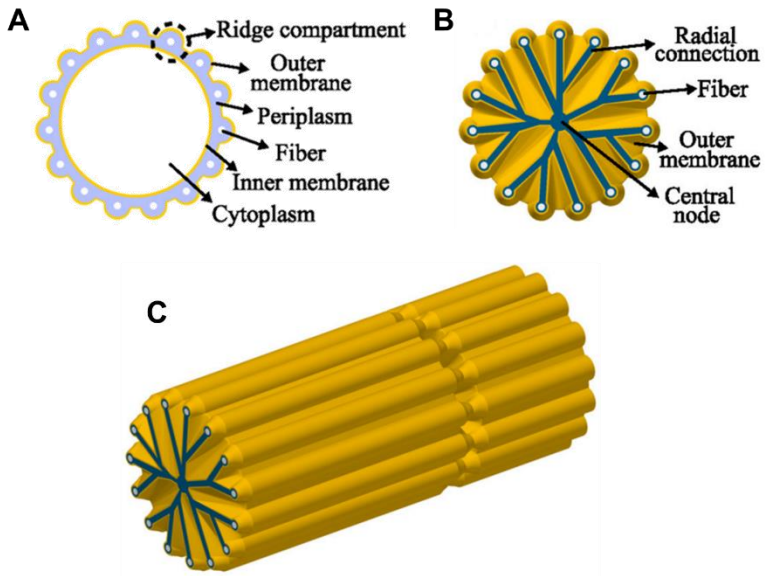

Figure 6 – Model representation of a cable bacteria cell. Model transverse cross-section of a cable bacterium cell, showing the outer membrane (ridges) and the fibers in the periplasm (**A**). Model transverse cross-section at a junction, the outer membrane folds in toward the central node, surrounding unknown radial connections (**B**). 3D-view of one and a half cell. Starting at a junction and ending at the middle of a cell, the fibers continue along the length of the filament (**C**). Figure taken from [71].

The 6 candidate species described so far are restricted to the genus *Candidatus* Electrothrix and *Candidatus* Electronema, which form a monophyletic group close to the *Desulfobulbus* genus [72], within the deltaproteobacterial *Desulfobulbaceae* family. The cable bacteria anodic cells exhibit a sulfide-oxidizing metabolism, that is followed by disproportionation of the sulfur compounds formed, similarly to members of the *Desulfobubaceae* family [66].

1.3 – Other energy metabolisms in sulfur-respiring organisms

Besides respiring sulfur compounds to generate ATP by oxidative phosphorylation, as mentioned in the previous sections, sulfur-metabolizing organisms have additional metabolic mechanisms to obtain energy, namely substrate-level phosphorylation and flavin-based electron bifurcation. Each of these metabolisms are briefly detailed in the following sub-sections.

1.3.1 – Substrate-level phosphorylation

In substrate-level phosphorylation (SLP), ATP is generated by the transfer of a phosphate group from the substrate or intermediate directly to ADP. This process can be divided in a donating and accepting part: the donating part comprises the flow of electrons from the donor substrate to the first electron carrier (NADH, for instance), being this associated with ATP formation. In the accepting part, the electrons flow from the first electron carriers to the final acceptor, with the carrier being regenerated.

Despite the large availability of carbon substrates, there are only a few reactions in anaerobes that conserve energy through SLP in comparison with the amount of electron donors/acceptors that can be used to generate energy by respiration [18].

Fermentative organisms were classically thought to conserve energy exclusively by SLP in a process where organic compounds function both as electron donors and acceptors, and the excess reductants are removed as reduced compounds. However, the identification of complex chemiosmotic mechanisms in fermentative organisms, such as electrogenic transport in lactic acid bacteria [73], electron transfer through energy conserving hydrogenases in fermentative hyperthermophiles [74] or sodium translocating NADH dehydrogenases in glutamate fermenting bacteria [75], indicate that fermentative organisms are more versatile in the way they conserve energy and are not limited to SLP.

1.3.2 – Flavin-Based Electron Bifurcation

In biological systems, energy conservation is mainly known to occur either through substrate-level phosphorylation or through electron

transport phosphorylation. However, in the last decade a new bioenergetic mechanism for energy coupling has been found to operate in several anaerobic organisms.

This mechanism is called flavin-based electron bifurcation (FBEB) and involves protein complexes containing flavins as a prosthetic group. Flavins can be found in the form of flavin adenine dinucleotide (FAD) or flavin mononucleotide (FMN) and are able to accept either one electron in a two-step process or two electrons at once, existing in an oxidized form (FAD^+ or FMN^+), as a semiquinone flavin radical (FADH• or FMNH•), or in a fully reduced form ($FADH_2$ or $FMNH_2$). In some flavoproteins, the exergonic one-electron oxidations of a fully reduced flavin can trigger the formation of a flavin semiquinone radical with a redox potential sufficiently negative to allow the reduction of ferredoxins (Fd). This mechanism was confirmed by Herrmann [76] and Li [77], and can be outlined as the following: a low-potential electron donor (H_2 or NAD(P)H, for instance) will fully reduce the flavin. The flavin will use one electron to reduce the first substrate with a higher redox potential, a reaction thermodynamically favourable. This leads to the formation of a low redox potential flavin semiquinone radical that can be responsible for an endergonic reaction, namely reduction of ferredoxin. With this, the reducing power of the second electron is increased at the cost of the first electron.

More than 90% of ferredoxins inside the cells are present in the reduced form, and the low redox potential of the Fd_{ox}/Fd_{red} couple of around -500 mV, makes reduced ferredoxin a good electron donor and a central player in the cell metabolism, working as energy and redox currency, and contributing to energy conservation by the reduction of protons to H_2 or by generating an electrochemical gradient. In many organisms, when ferredoxin is not present, flavodoxins can be used as substitute [78].

The FBEB topic will be addressed in Chapter III and Chapter IV.

1.4 – Bibliography

[1] K. Zahnle, L. Schaefer, and B. Fegley, “Earth’s earliest atmospheres”, *Cold Spring Harb. Perspect. Biol.*, vol. 2, no. 10, 2010.

[2] J. Farquhar, J. Savarino, S. Airieau, and M. H. Thiemens, “Sulfur isotope effects during SO_2 photolysis: Implications for the early atmosphere”, *J. Geophys. Res.*, vol. 106, no. 2000, pp. 32829–32839, 2001.

[3] D. E. Canfield, K. S. Habicht, and B. Thamdrup, “The Archean sulfur cycle and the early history of atmospheric oxygen”, *Science.*, vol. 288, no. 5466, pp. 658–661, 2000.

[4] J. Farquhar, W. U. Nanping, D. E. Canfield, and H. Oduro, “Connections between sulfur cycle evolution, sulfur isotopes, sediments and base metal sulfide deposits”, *Econ. Geol.*, vol. 105, no. 3, pp. 509–533, 2010.

[5] C. Dahl, “A biochemical view on the biological sulfur cycle”, in *Environmental Technologies to Treat Sulphur Pollution: Principles and Engineering*, 2020, pp. 55–96.

[6] K. Tang, V. Baskaran, and M. Nemati, “Bacteria of the sulphur cycle: An overview of microbiology, biokinetics and their role in petroleum and mining industries”, *Biochem. Eng. J.*, vol. 44, no. 1, pp. 73–94, 2009.

[7] M. W. Bowles, J. M. Mogollón, S. Kasten, M. Zabel, and K.-U. Hinrichs, “Global rates of marine sulfate reduction and implications for sub-sea-floor metabolic activities”, *Science*, vol. 344, no. 6186, pp. 889–891, 2014.

[8] B. B. Jørgensen, A. J. Findlay, and A. Pellerin, “The biogeochemical sulfur cycle of marine sediments”, *Front. Microbiol.*, vol. 10, no. 849, 2019.

[9] R. A. Berner, “Burial of organic carbon and pyrite sulfur in the modern ocean”, *American Journal of Science*, vol. 282, no. 4. pp. 451–473, 1982.

[10] G. Muyzer and A. J. M. Stams, “The ecology and biotechnology of sulphate-reducing bacteria”, *Nat. Rev. - Microbiol.*, vol. 6, pp. 441–454, 2008.

[11] A. L. Müller, K. U. Kjeldsen, T. Rattei, M. Pester, and A. Loy, “Phylogenetic and environmental diversity of DsrAB-type

dissimilatory (bi)sulfite reductases", *ISME J.*, vol. 9, no. 5, pp. 1152–1165, 2015.

[12] L. A. Hug *et al.*, "A new view of the tree of life", *Nat. Microbiol.*, vol. 1, no. 5, pp. 1–6, 2016.

[13] K. Anantharaman *et al.*, "Expanded diversity of microbial groups that shape the dissimilatory sulfur cycle", *ISME J.*, vol. 12, no. 7, pp. 1715–1728, 2018.

[14] B. Hausmann *et al.*, "Peatland Acidobacteria with a dissimilatory sulfur metabolism", *ISME J.*, vol. 12, no. 7, pp. 1729–1742, 2018.

[15] V. Thiel *et al.*, "'Candidatus Thermonerobacter thiotrophicus', A Non-phototrophic Member of the Bacteroidetes/Chlorobi With Dissimilatory Sulfur Metabolism in Hot Spring Mat Communities", *Front. Microbiol.*, vol. 9, no. 3159, 2019.

[16] A. Marietou, H. Røy, B. B. Jørgensen, and K. U. Kjeldsen, "Sulfate transporters in dissimilatory sulfate reducing microorganisms: A comparative genomics analysis", *Front. Microbiol.*, vol. 9, no. MAR, pp. 1–21, 2018.

[17] D. A. Smith, D. A. Fike, D. T. Johnston, and A. S. Bradley, "Isotopic Fractionation Associated With Sulfate Import and Activation by *Desulfovibrio vulgaris* str. Hildenborough", *Front. Microbiol.*, vol. 11, no. September, pp. 1–14, 2020.

[18] R. Thauer, K. Jungermann, and K. Decker, "Energy Conservation in Chemotrophic Anaerobic Bacteria", *Bacteriol. Rev.*, vol. 41, no. 1, pp. 100–180, 1977.

[19] G. D. Fauque and L. L. Barton, *Hemoproteins in Dissimilatory Sulfate- and Sulfur-Reducing Prokaryotes*, 1st ed., vol. 60. Elsevier Ltd., 2012.

[20] A. G. Duarte *et al.*, "An electrogenic redox loop in sulfate reduction reveals a likely widespread mechanism of energy conservation", *Nat. Commun.*, vol. 9, no. 1, pp. 1–11, 2018.

[21] T. F. Oliveira, C. Vonrhein, P. M. Matias, S. S. Venceslau, I. A. C. Pereira, and M. Archer, "The crystal structure of *Desulfovibrio vulgaris* dissimilatory sulfite reductase bound to DsrC provides novel insights into the mechanism of sulfate respiration", *J. Biol. Chem.*, vol. 283, no. 49, pp. 34141–34149, 2008.

[22] A. A. Santos *et al.*, “A protein trisulfide couples dissimilatory sulfate reduction to energy conservation”, *Science.*, vol. 350, no. 6267, pp. 1541–1545, 2015.

[23] R. H. Pires, S. S. Venceslau, F. Morais, M. Teixeira, A. V. Xavier, and I. A. C. Pereira, “Characterization of the *Desulfovibrio desulfuricans* ATCC 27774 DsrMKJOP complex - A membrane-bound redox complex involved in the sulfate respiratory pathway”, *Biochemistry*, vol. 45, no. 1, pp. 249–262, 2006.

[24] F. Grein *et al.*, “DsrJ, an essential part of the DsrMKJOP transmembrane complex in the purple sulfur bacterium *Allochromatium vinosum*, is an unusual triheme cytochrome c”, *Biochemistry*, vol. 49, no. 38, pp. 8290–8299, 2010.

[25] S. S. Venceslau, Y. Stockdreher, C. Dahl, and I. A. C. Pereira, “The ‘bacterial heterodisulfide’ DsrC is a key protein in dissimilatory sulfur metabolism”, *Biochim. Biophys. Acta - Bioenerg.*, vol. 1837, no. 7, pp. 1148–1164, 2014.

[26] P. Junier *et al.*, “The genome of the Gram-positive metal- and sulfate-reducing bacterium *Desulfotomaculum reducens* strain MI-1”, *Environ. Microbiol.*, vol. 12, no. 10, pp. 2738–2754, 2010.

[27] I. A. C. Pereira, A. R. Ramos, F. Grein, M. C. Marques, S. M. da Silva, and S. S. Venceslau, “A comparative genomic analysis of energy metabolism in sulfate reducing bacteria and archaea”, *Front. Microbiol.*, vol. 2, no. 69, pp. 1–22, 2011.

[28] G. M. Zane, H. C. Bill Yen, and J. D. Wall, “Effect of the deletion of *qmoABC* and the promoter-distal gene encoding a hypothetical protein on sulfate reduction in *Desulfovibrio vulgaris* Hildenborough”, *Appl. Environ. Microbiol.*, vol. 76, no. 16, pp. 5500–5509, 2010.

[29] J. Simon and P. M. H. Kroneck, “Microbial Sulfite Respiration”, in *Advances in Microbial Physiology*, vol. 62, 2013, pp. 45–117.

[30] A. Serrano, J. R. Pérez-Castiñeira, M. Baltscheffsky, and H. Baltscheffsky, “H^+-PPases: Yesterday, today and tomorrow”, *IUBMB Life*, vol. 59, no. 2, pp. 76–83, 2007.

[31] N. Mizuno, G. Voordouw, K. Miki, A. Sarai, and Y. Higuchi, “Crystal structure of dissimilatory sulfite reductase D (DsrD) protein - Possible interaction with B- and Z-DNA by its winged-

helix motif", *Structure*, vol. 11, no. 9, pp. 1133–1140, 2003.

[32] R. Rabus, S. S. Venceslau, L. Wöhlbrand, G. Voordouw, J. D. Wall, and I. A. C. Pereira, "A Post-Genomic View of the Ecophysiology, Catabolism and Biotechnological Relevance of Sulphate-Reducing Prokaryotes", *Adv. Microb. Physiol.*, vol. 66, pp. 55–321, 2015.

[33] M. Löffler *et al.*, "DsrL mediates electron transfer between NADH and rDsrAB in *Allochromatium vinosum*", *Environ. Microbiol.*, vol. 22, no. 2, pp. 783–795, 2020.

[34] B. B. Jørgensen, "A thiosulfate shunt in the sulfur cycle of marine sediments", *Science.*, vol. 249, no. 4965, pp. 152–154, 1990.

[35] B. B. Jørgensen, "The sulfur cycle of freshwater sediments: Role of thiosulfate", *Limnol. Oceanogr.*, vol. 35, no. 6, pp. 1329–1342, 1990.

[36] Andrea S. Pott and Christiane Dahl, "Sirohaem sulf ite reductase and other proteins encoded by genes at the dsr locus of *Chromatium vinosum* are involved in the oxidation of intracellular sulfur", *Microbiology*, vol. 144, pp. 1881–1894, 1998.

[37] C. Dahl, C. Friedrich, and A. Kletzin, "Sulfur Oxidation in Prokaryotes", *Encycl. Life Sci.*, 2008.

[38] J. V. Henkel, O. Dellwig, F. Pollehne, D. P. R. Herlemann, T. Leipe, and H. N. Schulz-Vogt, "A bacterial isolate from the Black Sea oxidizes sulfide with manganese(IV) oxide", *Proc. Natl. Acad. Sci. U. S. A.*, vol. 116, no. 25, pp. 12153–12155, 2019.

[39] W. Ghosh and B. Dam, "Biochemistry and molecular biology of lithotrophic sulfur oxidation by taxonomically and ecologically diverse bacteria and archaea", *FEMS Microbiol. Rev.*, vol. 33, no. 6, pp. 999–1043, 2009.

[40] N. U. Frigaard and C. Dahl, *Sulfur Metabolism in Phototrophic Sulfur Bacteria*, vol. 54, no. 08. 2008.

[41] C. Dahl, *Sulfur Metabolism in Phototrophic Bacteria*. 2017.

[42] C. L. Marnocha, A. T. Levy, D. H. Powell, T. E. Hanson, and C. S. Chan, "Mechanisms of extracellular S^0 globule production and degradation in *Chlorobaculum tepidum* via

dynamic cell-globule interactions", *Microbiol.*, vol. 162, no. 7, pp. 1125–1134, 2016.

[43] T. Koch and C. Dahl, "A novel bacterial sulfur oxidation pathway provides a new link between the cycles of organic and inorganic sulfur compounds", *ISME J.*, vol. 12, no. 10, pp. 2479–2491, 2018.

[44] R. Wang *et al.*, "Sulfur oxidation in the acidophilic autotrophic *Acidithiobacillus* spp.", *Front. Microbiol.*, vol. 10, no. JAN, pp. 1–20, 2019.

[45] Y. Stockdreher, S. S. Venceslau, M. Josten, H. G. Sahl, I. A. C. Pereira, and C. Dahl, "Cytoplasmic sulfurtransferases in the purple sulfur bacterium *Allochromatium vinosum*: Evidence for sulfur transfer from DsrEFH to DsrC", *PLoS One*, vol. 7, no. 7, 2012.

[46] F. Grein, A. R. Ramos, S. S. Venceslau, and I. A. C. Pereira, "Unifying concepts in anaerobic respiration: Insights from dissimilatory sulfur metabolism", *Biochim. Biophys. Acta*, vol. 1827, no. 2, pp. 145–160, 2013.

[47] C. Dahl *et al.*, "Structural and Molecular Genetic Insight into a Widespread Sulfur Oxidation Pathway", *J. Mol. Biol.*, vol. 384, no. 5, pp. 1287–1300, 2008.

[48] Y. Ikeuchi, N. Shigi, J. I. Kato, A. Nishimura, and T. Suzuki, "Mechanistic insights into sulfur relay by multiple sulfur mediators involved in thiouridine biosynthesis at tRNA wobble positions", *Mol. Cell*, vol. 21, no. 1, pp. 97–108, 2006.

[49] C. Dahl *et al.*, "Novel Genes of the *dsr* Gene Cluster and Evidence for Close Interaction of Dsr Proteins during Sulfur Oxidation in the Phototrophic Sulfur Bacterium *Allochromatium vinosum*", *J. Bacteriol.*, vol. 187, no. 4, pp. 1392–1404, 2005.

[50] J. Rodriguez, J. Hiras, and T. E. Hanson, "Sulfite oxidation in *Chlorobaculum tepidum*", *Front. Microbiol.*, vol. 2, no. MAY, pp. 1–7, 2011.

[51] A. R. Ramos, K. L. Keller, J. D. Wall, and I. A. Cardoso Pereira, "The membrane *qmoABC* complex interacts directly with the dissimilatory adenosine 5'-phosphosulfate reductase in sulfate reducing bacteria", *Front. Microbiol.*, vol. 3, pp. 1–10, 2012.

[52] C. Dahl, B. Franz, D. Hensen, A. Kesselheim, and R. Zigann, “Sulfite oxidation in the purple sulfur bacterium *Allochromatium vinosum*: Identification of SoeABC as a major player and relevance of SoxYZ in the process”, *Microbiol.*, vol. 159, pp. 2626–2638, 2013.

[53] F. Bak and H. Cypionka, “A novel type of energy metabolism involving fermentation of inorganic sulphur compounds”, *Nature*, vol. 326, no. 6116. pp. 891–892, 1987.

[54] M. Krämer and H. Cypionka, “Sulfate formation via ATP sulfurylase in thiosulfate- and sulfite-disproportionating bacteria”, *Arch. Microbiol.*, vol. 151, pp. 232–237, 1989.

[55] K. Finster, “Microbiological disproportionation of inorganic sulfur compounds”, *J. Sulfur Chem.*, vol. 29, no. 3–4, pp. 281–292, 2008.

[56] B. Thamdrup, K. Finster, J. W. Hansen, and F. Bak, “Bacterial disproportionation of elemental sulfur coupled to chemical reduction of iron or manganese”, *Appl. Environ. Microbiol.*, vol. 59, no. 1, pp. 101–108, 1993.

[57] D. R. Lovley and E. J. P. Phillips, “Novel processes for anaerobic sulfate production from elemental sulfur by sulfate-reducing bacteria”, *Appl. Environ. Microbiol.*, vol. 60, no. 7, pp. 2394–2399, 1994.

[58] K. Finster, W. Liesack, and B. Thamdrup, “Elemental sulfur and thiosulfate disproportionation by *Desulfocapsa sulfoexigens* sp. nov., a new anaerobic bacterium isolated from marine surface sediment.”, *Appl. Environ. Microbiol.*, vol. 64, no. 1, pp. 119–125, 1998.

[59] A. I. Slobodkin and G. B. Slobodkina, “Diversity of Sulfur-Disproportionating Microorganisms”, *Microbiol.*, vol. 88, no. 5, pp. 509–522, 2019.

[60] K. W. Finster *et al.*, “Complete genome sequence of *Desulfocapsa sulfexigens*, a marine deltaproteobacterium specialized in disproportionating inorganic sulfur compounds”, *Stand. Genomic Sci.*, vol. 8, no. 1, pp. 58–68, 2013.

[61] A. Mardanov, A. Beletsky, V. Kadnikov, A. Slobodkin, and N. Ravin, “Genome analysis of *Thermosulfurimonas dismutans*, the first thermophilic sulfur-disproportionating bacterium of the phylum Thermodesulfobacteria”, *Front. Microbiol.*, vol. 7,

p. 950, 2016.

[62] D. W. Waite *et al.*, “Proposal to reclassify the proteobacterial classes deltaproteobacteria and oligoflexia, and the phylum thermodesulfobacteria into four phyla reflecting major functional capabilities”, *Int. J. Syst. Evol. Microbiol.*, vol. 70, no. 11, pp. 5972–6016, 2020.

[63] R. Schauer *et al.*, “Succession of cable bacteria and electric currents in marine sediment”, *ISME J.*, vol. 8, no. 6, pp. 1314–1322, 2014.

[64] C. Pfeffer *et al.*, “Filamentous bacteria transport electrons over centimetre distances”, *Nature*, vol. 491, no. 7423, pp. 218–221, 2012.

[65] F. J. R. Meysman, “Cable Bacteria Take a New Breath Using Long-Distance Electricity”, *Trends Microbiol.*, vol. 26, no. 5, pp. 411–422, 2018.

[66] K. U. Kjeldsen *et al.*, “On the evolution and physiology of cable bacteria”, *PNAS*, vol. 116, no. 38, pp. 19116–19125, 2019.

[67] L. P. Nielsen, N. Risgaard-Petersen, H. Fossing, P. B. Christensen, and M. Sayama, “Electric currents couple spatially separated biogeochemical processes in marine sediment”, *Nature*, vol. 463, no. 7284, pp. 1071–1074, 2010.

[68] N. Risgaard-Petersen, A. Revil, P. Meister, and L. P. Nielsen, “Sulfur, iron-, and calcium cycling associated with natural electric currents running through marine sediment”, *Geochim. Cosmochim. Acta*, vol. 92, pp. 1–13, 2012.

[69] J. T. Bjerg, L. R. Damgaard, S. A. Holm, A. Schramm, and L. P. Nielsen, “Motility of electric cable bacteria”, *Appl. Environ. Microbiol.*, vol. 82, no. 13, pp. 3816–3821, 2016.

[70] Z. Jiang *et al.*, “In vitro single-cell dissection revealing the interior structure of cable bacteria”, *Proc. Natl. Acad. Sci. U. S. A.*, vol. 115, no. 34, pp. 8517–8522, 2018.

[71] R. Cornelissen *et al.*, “The Cell Envelope Structure of Cable Bacteria”, *Front. Microbiol.*, vol. 9, no. December, 2018.

[72] D. Trojan *et al.*, “A taxonomic framework for cable bacteria and proposal of the candidate genera Electrothrix and Electronema”, *Syst. Appl. Microbiol.*, vol. 39, no. 5, pp. 297–306, 2016.

[73] J. S. Lolkema, B. Poolman, and W. N. Konings, “Role of scalar protons in metabolic energy generation in lactic acid bacteria”, *J. Bioenerg. Biomembr.*, vol. 27, no. 4, pp. 467–473, 1995.

[74] R. Sapra, K. Bagramyan, and M. W. W. Adams, “A simple energy-conserving system: Proton reduction coupled to proton translocation”, *PNAS*, vol. 100, no. 13, pp. 7545–7550, 2003.

[75] C. D. Boiangiu *et al.*, “Sodium ion pumps and hydrogen production in glutamate fermenting anaerobic bacteria”, *J. Mol. Microbiol. Biotechnol.*, vol. 10, no. 2–4, pp. 105–119, 2005.

[76] G. Herrmann, E. Jayamani, G. Mai, and W. Buckel, “Energy conservation via electron-transferring flavoprotein in anaerobic bacteria”, *J. Bacteriol.*, vol. 190, no. 3, pp. 784–791, 2008.

[77] F. Li, J. Hinderberger, H. Seedorf, J. Zhang, W. Buckel, and R. K. Thauer, “Coupled ferredoxin and crotonyl coenzyme A (CoA) reduction with NADH catalyzed by the butyryl-CoA dehydrogenase/Etf complex from *Clostridium kluyveri*”, *J. Bacteriol.*, vol. 190, no. 3, pp. 843–850, 2008.

[78] W. Buckel and R. K. Thauer, “Energy conservation via electron bifurcating ferredoxin reduction and proton/Na^+ translocating ferredoxin oxidation”, *Biochim. Biophys. Acta - Bioenerg.*, vol. 1827, no. 2, pp. 94–113, 2013.

Chapter 2

The DsrD functional marker protein is an allosteric activator of the DsrAB dissimilatory sulfite reductase

Contents

Contributions

All experiments and analyses were performed by Delfim Ferreira, except the creation of the *Dv*H Δ*dsrD* mutant strain done by Gonçalo Oliveira, the mass spectrometry analysis performed by the ITQB/iBET UniMS Mass Spectrometry Unit, and the DsrD identity matrix and maximum likelihood phylogeny of DsrA and DsrD proteins done by Sinje Neukirchen and Filipa Sousa.

The experiment design was performed by Delfim Ferreira, Sofia Venceslau and Inês Cardoso Pereira.

This chapter was published as part of:

D. Ferreira, A.C.C. Barbosa, G.P. Oliveira, T. Catarino, S.S. Venceslau and I.A.C. Pereira (2022) “The DsrD functional marker protein is an allosteric activator of the DsrAB dissimilatory sulfite reductase” *PNAS* 119 (4): e2118880119

2.1 – Summary

The dissimilatory sulfur metabolism was recently shown to be much more widespread among bacteria and archaea than previously believed. One of the key pathways involved is the *dsr* pathway that is responsible for sulfite reduction in sulfate-reducing organisms, sulfur-, thiosulfate- and sulfite-reducers, sulfur-disproportionators and organosulphonate degraders, or for production of sulfite in many photo- and chemotrophic sulfur-oxidizing prokaryotes. The key enzyme is the dissimilatory sulfite reductase DsrAB, but a range of other Dsr proteins are involved, with different gene sets being present in organisms with a reductive or oxidative metabolism. The *dsrD* gene codes for a small protein of unknown function and has been widely used as a functional marker for reductive or disproportionating sulfur metabolism, although in some cases this has been disputed. This chapter presents *in vivo* and *in vitro* studies showing that DsrD is a physiological partner of DsrAB and acts as an activator of its sulfite reduction activity. DsrD is expressed in respiratory and not in fermentative conditions, and a Δ*dsrD* deletion strain could be obtained, which indicates its function to not be essential. Analysis of *dsrD* genomic distribution reveals that three different sub-types of DsrD exist, which correlate with DsrAB phylogeny. Organisms with the earliest forms of *dsrAB* lack the *dsrD* gene, revealing that its activating role arose later in evolution relative to *dsrAB*.

2.2 – Introduction

The reduction of sulfite is a key step in dissimilatory sulfate reduction (DSR), a microbial process performed by anaerobic bacteria or archaea, which derive energy from reducing sulfate to hydrogen sulfide [1], [2]. DSR drives the biogeochemical sulfur cycle and has a strong influence on other element cycles and on the redox balance of the oceans and atmosphere. It has a particular impact on marine sediments where it accounts for up to 50% of carbon mineralization [3], [4] and prevents methane emissions by its involvement in anaerobic methane oxidation [5], [6]. Remarkably, the existence of a cryptic sulfur cycle, involving several sulfur compounds, means that DSR and other sulfur metabolisms are also important in low-sulfate environments where fermentation and methanogenesis were thought to dominate [2], [4], [7], and through their action prevent methane production by diverting carbon flow and energy resources away from methanogens. In addition, sulfate-reducing prokaryotes (SRP) are members of the human gut flora, where their production of sulfide has been associated with inflammatory bowel diseases and cancer [8]–[10].

In DSR, sulfite reduction is performed by the DsrAB dissimilatory sulfite reductase, an $\alpha_2ß_2$ tetrameric enzyme that uses a [4Fe-4S]-coupled siroheme as a catalytic cofactor [1], [11], [12]. Beyond its role in sulfate reduction, DsrAB is also a key enzyme in other types of microbial sulfur metabolism, being present in a wide range of other organisms including sulfur-, thiosulfate- and sulfite-reducers, sulfur-disproportionators, organosulphonate degraders and in many photo- and chemotrophic sulfur-oxidizing prokaryotes (SOP), where it operates in the reverse direction and is designated as reverse-acting DsrAB (rDsrAB) [2], [7], [13]. DsrAB is an ancient enzyme whose two paralogous genes, *dsrA* and *dsrB*, evolved from duplication of a simpler sulfite reductase gene [14], [15], and phylogenetically it is organized in three main families comprising the archaeal and bacterial reductive enzymes, and the oxidative rDsrABs [16]–[18]. The phylogenetic studies support a reductive origin for this enzyme and indicate that dissimilatory sulfite reduction likely preceded DSR [19], [20]. The *dsrAB* genes are widely used as ecological and phylogenetic markers of dissimilatory sulfur metabolism and recent studies have uncovered that this metabolic trait is much more widespread in both bacteria and archaea than was previously believed [18], [20], [29], [21]–[28].

Contrary to assimilatory and other dissimilatory sulfite reductases [13], DsrAB does not reduce sulfite directly to sulfide. Instead, DsrAB requires the action of its partner protein DsrC [12] to catalyse a four electron reduction of sulfite to a S^0 valence state, in the form of a trisulfide bound to DsrC [30]. The DsrC-trisulfide is believed to be later reduced to HS^- and DsrC by the DsrMKJOP transmembrane complex [12], [30], [31]. All organisms that have *dsrAB* genes also have *dsrC* and minimally the *dsrMK* genes [12], [32], whereas other *dsr* genes seem to be characteristic of oxidative or reductive sulfite metabolism and have tentatively been used to discriminate between SRP, SOP and organisms with other types of dissimilatory sulfur metabolism. For example, genes that have been considered characteristic of SOP are the *dsrEFH* genes that code for a sulfur donor protein to DsrC [7], [12], [33] and *dsrL* that is essential for sulfur oxidation and codes for a $NAD(P)^+$-reductase that is a physiological partner for rDsrAB [34], [35], whereas the *dsrD* gene is considered to be characteristic of reductive sulfur metabolism [18], [21], [22], [29], [36]. However, as highlighted in several studies, metabolic assignments based solely on genetic composition are far from clear in some cases [18], [26], [29], [35], [37].

The *dsrD* gene, first identified in 1995 by Karkhoff-Schweizer and colleagues [38], is absent from SOP and is present in most organisms encoding a reductive enzyme (i.e., most SRP and sulfur disproportionators, and sulfite-, thiosulfate- and organosulfonate-reducing organisms), being even fused with *dsrB* in *Bilophila wadsworthia* [1], [12], [39], [40]. Notably, it is absent in archaea containing early diverging reductive DsrAB homologues [18], [20]. The *dsrD* gene is usually found immediately downstream of *dsrAB*, and DsrD is among the highest expressed proteins [37], [41], [42], which together with its widespread distribution and genetic location all suggest an important role in the dissimilatory reduction of sulfite. However, its function is still virtually unknown. In *Desulfovibrio vulgaris* Hildenborough (*Dv*H), a model SRP, *dsrD* was found to be downregulated under stationary phase conditions [43], and was the most downregulated gene when cells were exposed to high sulfide concentrations (10 mM vs. 1 mM) [44]. In this organism, DsrD is composed of 78 amino acids, and its crystallographic structure displays a winged helix-turn-helix (wHTH) motif characteristic of DNA-binding proteins (**Figure 2.1**), which led to the suggestion that this protein could be a transcription regulator of the genes involved in DSR [45]. DsrD also presents a high content of conserved lysine

residues that could point to a role in anion binding, such as SO_4^{2-} /SO_3^{2-}/HS^-, but this was not confirmed [38], [46]. In addition, *Desulfobacterota* DsrD proteins contain a well-conserved motif (YWSSGSTT) with no function assigned, and the absence of cysteine residues or cofactors suggests that this protein is unlikely to be involved in electron transfer or in sulfur chemistry like DsrC [30], [38], [45].

Figure 2.1 – *D. vulgaris* DsrD crystallographic structure. The "YWSSGSTT" conserved motif is highlighted.

Divergent data has been reported regarding a possible interaction between DsrD and DsrAB. Hittel & Voordouw [46] did not detect DsrD in partially purified DsrAB preparations, while Shatsky and colleagues [47] reported DsrAB being co-purified with tagged DsrD. This chapter reports *in vivo* and *in vitro* studies, together with genome distribution analysis, which provide the first detailed functional and physiological characterization of DsrD. The *in vivo* studies were performed with the bacterium *Dv*H from *Desulfobacterota* [48], which is genetically tractable, and the *in vitro* biochemical assays with proteins from the thermophilic euryarchaeon *Archaeoglobus fulgidus*, from which DsrAB can be purified in active form, in contrast to *Dv*H [30].

2.3 – Material & Methods

2.3.1 – Construction of *D. vulgaris* Hildenborough strains

A *Dv*H strain lacking the *dsrD* gene (Δ*dsrD*) was constructed by double homologous recombination: the vector for insertion of a ΩKm cassette in *dsrD* (locus tag: DVU0404) was constructed via SLIC (sequence ligation independent cloning) according to Li & Elledge (2007) [49], using *Dv*H chromosomal DNA as template and primers #1, #2, #3 and #4 to flank the upstream and downstream regions of *dsrD*, using the pSC27 vector and primers #5 and #6 for the kanamycin cassette, and using the pMO719 vector and primers #7 and #8 for the pUC-ori and spectinomycin resistance gene. The assembled plasmid (pMOIP17) was transformed into *E*. *coli* α-select Silver Efficiency (Bioline®) and plated on LB agar plates containing kanamycin and spectinomycin. After sequence confirmation, the plasmid was electroporated into *Dv*H cells, and double recombinants were selected in MOY solid medium with 30 mM of sodium pyruvate by secondary antibiotic screening, as described in Keller *et al*. (2011) [50]. G418 resistant but spectinomycin sensitive colonies were selected and grown in medium containing G418, an analogue of kanamycin but more effective in *Dv*H [51]. The absence of the *dsrD* gene in the *D*. *vulgaris* Δ*dsrD* mutant strain was verified by PCR using primers #9 and #10, and chromosomal DNA extracted from the screened cells.

A *Dv*H Δ*dsrD* + pMO-*dsrD* complemented strain was created by inserting the pMO-*dsrD* vector into *Dv*H Δ*dsrD* mutant cells also by electroporation. To create pMO-*dsrD*, *dsrD* was amplified from *Dv*H genomic DNA using primers #9 and #10, and cloned in pET22b(+) using *Nde*I and *Xho*I restriction sites, originating the pET-*dsrD*-*Dv*H vector. The *Xho*I restriction site was mutated to *Eco47*III using primer #11, and then *dsrD* was amplified using primers #12 and #13, and cloned in pMOIP12P using *Nde*I and *Eco47*III, inserting a Strep-tag at the C-terminus of *dsrD*, creating the pMO-*dsrD* vector.

All constructs were validated by sequencing. The several strains, plasmids and primers used in this study are summarized in **Table 2.1**, **Table 2.2** and **Table 2.3**, respectively.

Table 2.1 – List of strains used in this study

Strain	Genotype	Source or reference
E. coli strains		
E. coli NZY5α	*E. coli fhuA2*Δ(*argF-lacZ*)U169 *pho*A *glnV*44 Φ80 Δ(*lacZ*)M15 *gyrA*96 *recA*1 *relA*1 *endA*1 *thi*-1 *hsdR*17	Nzytech
E. coli BL21-Gold(DE3)	*E. coli* B F^- *ompT hsdS*(r_B^- m_B^-) *dcm*$^+$ Tet^R *gal λ*(DE3) *endA* Hte	Agilent Technologies
D. vulgaris strains		
*Dv*H WT	*D. vulgaris* Hildenborough ATCC 29579	ATCC
*Dv*H Δ*dsrD*	*Dv*H WT Δ*dsrD*::ΩKm	This work
*Dv*H Δ*dsrD* + pMO-*dsrD*	*Dv*H WT Δ*dsrD*::ΩKm + pMO-*dsrD*	This work
A. fulgidus strains		
A. fulgidus WT	*A. fulgidus* DSM 4304 / VC-16	DSMZ

Table 2.2 – List of plasmids used in this study

Plasmid	Relevant characteristics	Source or reference
pMO719	pCR8/GW/TOPO containing SRB replicon (pBG1); $Spec^R$	Keller *et al.*, 2009
pSC27	*Desulfovibrio* shuttle vector; source of *aph(3')-II*; Km^R	Rousset *et al.*, 1998
pMO9075	pCR8/GW/TOPO with pBG1, Km^R gene *aph(3')-II* promoter, multicloning site; $Spec^R$	Keller *et al.*, 2011
pMOIP17	*dsrD* deletion plasmid; $Spec^R$; Km^R	This work
pMOIP12P	pMO9075 expressing *flxA* with Strep-tag at C-terminal (using restriction sites NdeI and EcoRI); $Spec^R$	Ramos *et al.*, 2015
pET28a(+)	Bacterial protein expression vector with His6x-tag at N-terminal, Km^R	Novagen
pET-His-*dsrC*-AF	pET28a(+) containing *dsrC* from *A. fulgidus* (using restriction sites NdeI and HindIII), His6x-tag at N-terminal; Km^R	Santos *et al.*, 2015
pET-His-*dsrC*C77A/C85A-AF	pET28a(+) containing *dsrC* from *A. fulgidus* (using restriction sites NdeI and EcoRI) and with two point mutations C77A and C85A, His6x-tag at N-terminal; Km^R	Santos *et al.*, 2015
pET22b(+)	Bacterial protein expression vector with His6x-tag at C-terminal; Amp^R	Novagen
pET-*dsrD-Dv*H	pET22b(+) containing *dsrD* from *D. vulgaris* (using restriction sites NdeI and XhoI), His6x-tag at C-terminal; Amp^R	This work
pMO-*dsrD*	pMOIP12P with *flxA* replaced by *dsrD* from *D. vulgaris*; Strep-tag at C-terminal; $Spec^R$	This work
pET-*dsrD-Af*	pET-22b(+) containing *dsrD* from *A. fulgidus* (using restriction sites NdeI and XhoI), His6x-tag at C-terminal; Amp^R	This work
pRARE2	Ability to express tRNAs for the rare codons in *E. coli*: AGG, AGA, AUA, CUA, CCC, GGA, CGG; Cm^R	Novagen

Table 2.3 – List of primers used for plasmid and strains construction, and for DNA amplification

#	Primer	Primer sequence (5′ → 3′)	Observations
1	dsrD_upstream_forward	GCCTTTTGCTGGCCTTTTGCTCACATATGTCGATCACCCACATCCG	Construction of pMOIP17 by SLIC
2	dsrD_upstream_reverse	AAGACTGTAGCCGTACCTCGAATCTATTGCTCTTGCTACCAGACTTGG	Construction of pMOIP17 by SLIC
3	dsrD_downstream_forward	AATCCGCTCACTAAGTTCATAGACCGAGCCAGGAAGCGTATGAACC	Construction of pMOIP17 by SLIC
4	dsrD_downstream_reverse	CGAGGCATTTCTGTCCTGGCTGGCTGACGAAGGGCTTCAAGGT	Construction of pMOIP17 by SLIC
5	Kan_forward_SLIC	TAGATTCGAGGTACGGCTACAGTCTTACGGTCACAAACAGGTACGCCCCCAGAGTCCCGCTCAG	Construction of pMOIP17 by SLIC (Kan from pSC27 forward)
6	Kan_reverse_SLIC	CGGTCTATGAACTTAGTGAGCGGATTTCTCGTGTAGCCGATGCAGTGAGGTAGCTTGCAGTGGGCT	Construction of pMOIP17 by SLIC (Kan from pSC27 reverse)
7	Spec_forward_SLIC	CCAGCCAGGACAGAAATGCCTCG	Construction of pMOIP17 by SLIC (Spec from pMO719 forward)
8	pUCori_reverse_SLIC	ATGTGAGCAAAAGGCCAGCAAAAGGC	Construction of pMOIP17 by SLIC (pUCori from pMO719 reverse)
9	dsrD_DvH_forward	GGGGTACTCATATGGAAGAAGCC	Amplification of *dsrD* from *Dv*H genomic DNA to pET22b(+); NdeI restriction site
10	dsrD_DvH_reverse	TGAAGGCTCGAGTTCGTGCTC	Amplification of *dsrD* from *Dv*H genomic DNA to pET22b(+); XhoI restriction site
11	dsrD_XhoI_to_Eco47III	GTGGTGGTGAGCGCTTTCGTGCTC	Mutation of XhoI restriction site to Eco47III restriction site
12	dsrD_pMO_forward	CGACTCACTATAGGGGAATTGTGAGCG	Amplification of *dsrD* from pET22-*dsrD* to pMO-*dsrD*
13	dsrD_pMO_reverse	GTGGTGGTGAGCGCTTTCGTGCTC	Amplification of dsrD from pET22-*dsrD* to pMO-*dsrD*; Eco47III restriction site
14	dsrD_Af_forward	GACCTCATATGGCGGATTATAC	Amplification of *dsrD* from *Af* genomic DNA to pET22b(+); NdeI restriction site
15	dsrD_Af_reverse	AAGAAGAACTCGAGTTCAGCTC	Amplification of *dsrD* from *Af* genomic DNA to pET22b(+); XhoI restriction site
16	dsrAB_promoter_Af_forward	CGGGATTAGCTCCACCACATCG	Amplification of *dsrAB* promoter region from *Af*
17	dsrAB_promoter_Af_reverse	CTTTTCTAATTCATCAAGCAAAGG	Amplification of *dsrAB* promoter region from *Af*
18	KanR_forward	ATTGAACAAGATGGATTGCACGCAGG	Amplification of Kan^R gene from pSC27
19	KanR_reverse	GAAGAACTCGTCAAGAAGGCGATAGAAGG	Amplification of Kan^R gene from pSC27
20	dsrC_Af_forward	GGTGACCATATGCCAGAGTTAGAGG	Amplification of *dsrC* from *Af* genomic DNA to pET28a(+); NdeI restriction site
21	dsrC_Af_reverse	GCAGGAGGGACGGAATTCTAAAGG	Amplification of *dsrC* from *Af* genomic DNA to pET28a(+); EcoRI restriction site
22	dsrC_C77AC85A_forward	GTAAAGCACGCGAAGAAAGAGGTCAGGCCAGACGCGAACCTGCAG	Replacement of two structural Cys for Ala (Santos *et al*., 2015)
23	dsrC_C77AC85A_reverse	CTGCAGGTTCGCGTCTGGCCTGACCTCTTTCTTCGCGTGCTTTAC	Replacement of two structural Cys for Ala (Santos *et al*., 2015)

2.3.2 – Growth studies

*Dv*H wild-type (WT) and the two modified strains were grown anaerobically at 37 °C in MO medium [51]. Under respiratory conditions, 15 or 30 mM sodium lactate was added as electron donor, and sodium sulfate (30 mM), sodium sulfite (10 or 20 mM) or sodium thiosulfate (10 or 20 mM) were added as terminal electron acceptors. For fermentative conditions, 60 mM sodium pyruvate was used and lactate and sulfate were omitted from the culture media. No yeast extract was used in the growth experiments, but all media were inoculated with 2% (v/v) fresh precultured cells grown in MOY medium (0.5 g/L yeast extract) containing 60 mM sodium pyruvate and 3 mM sodium sulfate. The optical density (OD) at 600 nm of the cultures was monitored at various time points. Antibiotics G418 at 400 µg/mL and spectinomycin at 100 µg/mL were added to the media according to the strain. However, in the final growth curves only spectinomycin was used. Statistically significant relationships were determined using one-way analysis of variance (ANOVA), with a probability value (p) of < 0.05 considered as statistically significant.

2.3.3 – Electrophoretic mobility shift assay

A 981 bp fragment from the *dsrAB* promoter region was obtained by PCR using the *A*. *fulgidus* VC-16 genome as template, and primers #16 and #17. As negative control, the 803 bp gene for kanamycin resistance was amplified from the pSC27 plasmid, using primers #18 and #19. Based on Grimm *et al*. (2010) [52], 200 fmol of both DNA fragments were incubated with *A*. *fulgidus* DsrD (10-100 pmol) in incubation buffer (5 mM HEPES pH 7.8, 20 mM KCl, 0.02% (v/v) Tween 20 and 1 mM TCEP) during 15 min at 70 °C. The samples were loaded in a 1.5% agarose gel stained with GreenSafe Premium (NZYtech), in 0.5% TBE buffer. The electrophoresis was run at 90 V and the gel analyzed under UV light.

2.3.4 – Western blot analysis

*Dv*H WT and modified strains were grown in MO medium with the designated electron donor/acceptor, collected at the end of exponential phase, and centrifuged at 3000 x *g* for 10 min. The cell pellets were mechanically disrupted with glass beads using a Minilys

homogenizer (Bertin Technologies) and centrifuged at 17000 x *g* for 20 min at 4 °C. The protein concentration in the crude cell extracts was determined by the Bradford method (BioRad) with bovine serum albumin as standard (NZYTech). Crude cell extracts (40 µg) were analyzed in Tricine-SDS-PAGE gels (10% acrylamide (w/v)) and proteins transferred to 0.45 µm PVDF membranes (Roche) (transfer buffer: 48 mM Tris-HCl pH 9.2 and 39 mM glycine) using a Mini Trans-Blot® electrophoretic transfer cell (BioRad) at 100 V during 7 min (DsrD), 8 min (DsrC) or 30 min (DsrB), at 4 °C. Membranes for DsrD analysis were treated with blocking buffer (20 mM Tris-HCl pH 7.6, 150 mM NaCl and 5% (w/v) non-fat milk) during 1 h at room temperature (RT), incubated with TBST (20 mM Tris-HCl pH 7.6, 150 mM NaCl and 0.05% (v/v) Tween 20) plus anti-DsrD antibody at a 1:5000 dilution for 1 h at RT, and then incubated with TBST plus anti-rabbit IgG-alkaline phosphatase antibody (Sigma-Aldrich) at a 1:15000 dilution for 45 min at RT. Membranes for DsrB and DsrC analysis were incubated with TBST, 1.2% (w/v) non-fat milk and primary antibody (anti-DsrB at a 1:8300 dilution and anti-DsrC at a 1:3300 dilution) for 1 h at RT, and then incubated with anti-rabbit IgG-alkaline phosphatase antibody at a 1:15000 dilution in TBST for 45 min at RT. Between every incubation step the membranes were washed three times with TBS (20 mM Tris-HCl pH 7.6, 150 mM NaCl). All protein detections were performed by incubating the membranes in alkaline phosphatase buffer (100 mM Tris-HCl pH 9.5, 100 mM NaCl and 250 µM $MgCl_2$) and nitro-blue tetrazolium chloride/5-bromo-4-chloro-3-indolylphosphate toluidine (Sigma-Aldrich). The anti-DsrB antibody was produced in rabbits with synthesized peptides based on *Dv*H DsrB amino acid sequence, and anti-DsrC and anti-DsrD antibodies were produced from purified proteins at Davids Biotechnologie GmbH.

2.3.5 – Pull-down assay

*Dv*H WT and Δ*dsrD* + pMO-*dsrD* cells were grown in MO medium supplemented with 30 mM sodium lactate and 20 mM sodium sulfite. Cells were collected at the end of exponential phase, centrifuged, and disrupted as described previously for Western blot analysis. Crude extracts were loaded in gravity flow columns containing Strep-Tactin® resin (IBA Lifesciences) equilibrated with buffer W (50 mM Tris-HCl pH 7.5, 100 mM NaCl and 10% (v/v) glycerol). After five

column volumes of washing with buffer W, the Strep-tagged DsrD was eluted with buffer W plus 2.5 mM D-desthiobiotin. The pull-down assay of the two strains was normalized by loading in the Strep-Tactin column the same amount of total protein of each crude extract and performing elution with identical volumes throughout the process. The desthiobiotin eluted fractions (14 µg for Δ*dsrD* + pMO-*dsrD* and the equivalent volume for *Dv*H WT) were analyzed in a 10% Tricine-SDS-PAGE gel, and proteins identified by mass spectrometry.

2.3.6 – Production of recombinant *A. fulgidus* DsrD

The *dsrD* gene (locus tag: AF0425) was amplified by PCR from the *A. fulgidus* VC-16 genome, using primers #14 and #15. The digested PCR product was cloned into a pET-22b(+) expression vector (Novagen), which allows the insertion of a 6x-His tag sequence at the C-terminus of DsrD. The cloned vector was verified by sequencing. The recombinant plasmid was transformed into *E. coli* BL21-Gold(DE3) competent cells (Stratagene) containing the pRARE2 expression vector, for the expression of the rare codons present in *A. fulgidus*. Transformed cells were grown at 37 °C in LB medium supplemented with ampicillin (100 µg/mL) and chloramphenicol (30 µg/mL) until an OD_{600} of 0.5. At this point, isopropyl-β-D-thiogalactopyranoside (IPTG) was added to a final concentration of 500 µM, and growth was continued for another 5 h. Then, *E. coli* cells were collected by centrifugation at 7930 *g* for 12 min at 4 °C and stored at -20 °C.

The cell pellet was ressuspended in buffer K (25 mM potassium phosphate buffer pH 7.4, 300 mM NaCl and 20 mM imidazole) in the presence of DNase (Sigma-Aldrich) and a protease inhibitor cocktail (Roche) and disrupted in a French Press at 6.2 MPa. Cell lysates were centrifuged at 17000 x *g* for 20 min at 4 °C. After filtration with a 0.2 µm polyethersulfone (PES) membrane filter, the supernatant was loaded a HiTrap™ IMAC HP column (GE Healthcare) equilibrated with buffer K. An additional step of washing with 30 mM imidazole was performed in order to remove DNA contamination. DsrD was eluted with 25 mM potassium phosphate buffer pH 7.4, 300 mM NaCl and 150 mM imidazole, and then concentrated and dialyzed to 25 mM potassium phosphate buffer pH 7.4 by ultrafiltration (3 kDa cutoff, Amicon Millipore). Protein concentration

was determined using the BCA method (Merck Millipore) and purity was analyzed in a 10% Tricine-SDS-PAGE gel. The purified DsrD was also kept under anaerobic conditions.

2.3.7 – Mass Spectrometry

For protein identification, protein bands were excised from a 10% Tricine-SDS-PAGE gel and subjected to in-gel tryptic digestion followed by peptide identification in a MALDI-TOF/TOF analyzer (Applied Biosystems 4800plus). The data were analyzed in a combined mode using Mascot search engine and NCBI database.

For intact mass determination, DsrD was analyzed before and after addition to the sulfite reductase assay. The protein buffer was exchanged to 20 mM ammonium acetate pH 7.2 before analysis, using a Micro Bio-Spin™ 6 size exclusion spin column (Bio-Rad). The protein solution was mixed with 10 mg/mL Sinapinic acid (Sigma) in 50% (v/v) acetonitrile and 5% (v/v) formic acid (LC/MS grade, Fisher) in a 1:1 ratio and then this solution was applied directly onto the MALDI plate and allowed to air dry. The data was acquired in Linear Mid Mass Positive mode using a 5800 MALDI-TOF/TOF (AB Sciex) mass spectrometer and TOF/TOF Series Explorer Software v.4.1.0 (AB Sciex). External calibration was performed using Protein MALDI-MS Calibration Kit (MSCAL3, ProteoMass). MS data was obtained by the ITQB/iBET UniMS Mass Spectrometry Unit, Oeiras, Portugal.

2.3.8 – Bioinformatic analysis

Genomes of organisms performing sulfite reduction to sulfide with DsrAB (pathway 871) were retrieved from the JGI IMG/MER database, and joined with specific genomes whose relevance has been recently brought up, such as organisms belonging to phylogenetic groups of *Acidobacteria* [21], *Candidatus* Zixibacteria [18], *Candidatus* Falkowbacteria [18], *Bacteroidetes*/*Chlorobi* [26] and cable bacteria [53], [54] to generate a list with 480 genomes containing DsrD. DsrD sequences were retrieved from the JGI IMG/MER database using Blast based on the prototypical sequences for each DsrD type. Multiple alignments were performed using the ClustalW algorithm. All 504 DsrD sequences retrieved

were inspected for fusions with DsrB and manually trimmed. The pairwise global identities between all trimmed DsrD sequences were calculated using needleall (Emboss package, version 6.6.0) [55] with default gap penalties.

In addition, all DsrA protein sequences were extracted from the 480 genomes using either the DsrA protein list at IMG (Object ID 6635) or the *D. vulgaris* DsrA sequence (ID 637121620) as query for BLASTp at IMG. Selected early branching DsrA protein sequences from Rokubacteria and archaea (Thermoproteaceae, *Ca*. Hydrothermarchaeota), as well as oxidative-type DsrA from bacteria (*Allochromatium vinosum*, *Chlobaculum tepidum*, *Chlorobaculum parvum*, *Thioalkalivibrio nitratireducens*) were additionally added. The 510 DsrA protein sequences were aligned with Clustal Omega (version 1.2.3)[56] using both 100 guide tree and 100 HMM iterations and a DsrA maximum likelihood phylogeny reconstructed with IQ-TREE (version 1.6.12)[57] using best model selection and 1000 ultrafast bootstraps.

2.4 – Results

2.4.1 – DsrD interacts unspecifically with DNA

Since the 2003 determination of the DsrD crystal structure revealing a winged-helix motif similar to motifs present in Z-DNA and B-DNA binding proteins, DsrD was associated to a possible DNA-binding function, eventually regulating the *dsr* genes [45]. However, no experimental data has been reported so far supporting this possible function. It was tested whether DsrD is able to bind to DNA, and namely to the *dsrAB* promoter region. For this, a competitive electrophoretic mobility shift assay (EMSA) was performed by incubating *A. fulgidus* DsrD with a 981 bp DNA fragment from the *A. fulgidus dsrAB* promoter region and with the kanamycin-resistance gene (803 bp) as a control (non-specific DNA fragment). In both situations it is observed a DNA shift in the presence of DsrD, and dependent on the DsrD concentration (**Figure 2.2**), indicating that DsrD can bind to DNA but in an unspecific way. This does not support a regulatory function for DsrD, which is also disfavoured by its very high cellular levels [37], [41] that indicate a direct role in dissimilatory metabolism.

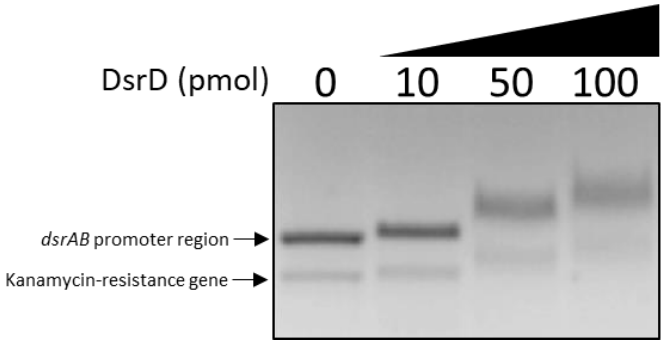

Figure 2.2 – DNA electrophoretic mobility shift assay of DsrD binding to the *A*. *fulgidus dsrAB* promoter region (981 bp), and the kanamycin-resistance gene (803 bp). The competitive assay used 200 fmol of each of the DNA fragments, which were incubated with 0 to 100 pmol of recombinant *A*. *fulgidus* DsrD.

2.4.2 – DsrD is produced in respiratory conditions

The presence of DsrD was analyzed in several growth conditions. For this, *Dv*H WT cells were grown in MO media in fermentative conditions (Pyr), and in respiratory conditions with lactate/sulfate (LS4), ethanol/sulfate (ES4), lactate/thiosulfate (LT), lactate/sulfite (LS3) and H_2/acetate/sulfate (HS4), and cells were collected at late exponential phase. The crude extracts were analyzed by Western blot against DsrD, and against DsrB as internal control (**Figure 2.3**). The Western blot results indicate that DsrD is more abundant under LS4, LT and LS3 conditions, less abundant in ES4 and HS4, and apparently absent in fermentative conditions. In contrast, the production of DsrB is constant in all growth conditions tested, in line with the constitutive expression of *dsrAB*. Interestingly, it was also under LS4, LT and LS3 growth conditions that *Dv*H WT reached higher cell densities. These findings suggest a role for DsrD under respiratory conditions and supporting a direct function in sulfite reduction.

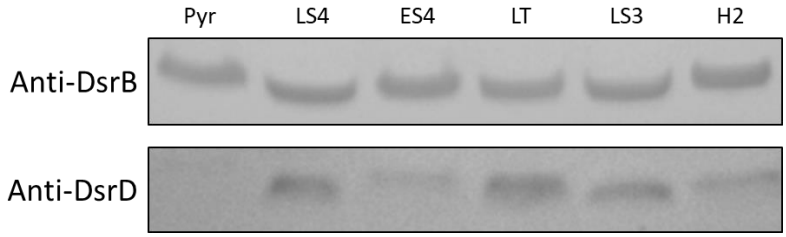

Figure 2.3 – Western blot of DsrD and DsrB expression in different growth media. Pyr – 60 mM pyruvate; LS4 – 30 mM lactate/30 mM sulfate; ES4 – 20 mM ethanol/20 mM sulfate; LT – 30 mM lactate/20 mM thiosulfate; LS3 – 30 mM lactate/20 mM sulfite; H2 – 2 bar H_2/ 10 mM acetate/30 mM sulfate.

2.4.3 – Deletion of *dsrD* affects respiratory growth

The *dsrD* gene was deleted in *Dv*H WT to create the *Dv*H Δ*dsrD* strain through replacement by a kanamycin cassette. A complemented strain *Dv*H Δ*dsrD* + pMO-*dsrD* was also generated by inserting a plasmid encoding *dsrD* (pMO-*dsrD*) in *Dv*H Δ*dsrD*. Strains *Dv*H WT, *Dv*H Δ*dsrD* and *Dv*H Δ*dsrD* + pMO-*dsrD* were grown in fermentative conditions with pyruvate and in respiratory conditions with lactate and sulfate or sulfite (**Figure 2.4, Table 2.4**).

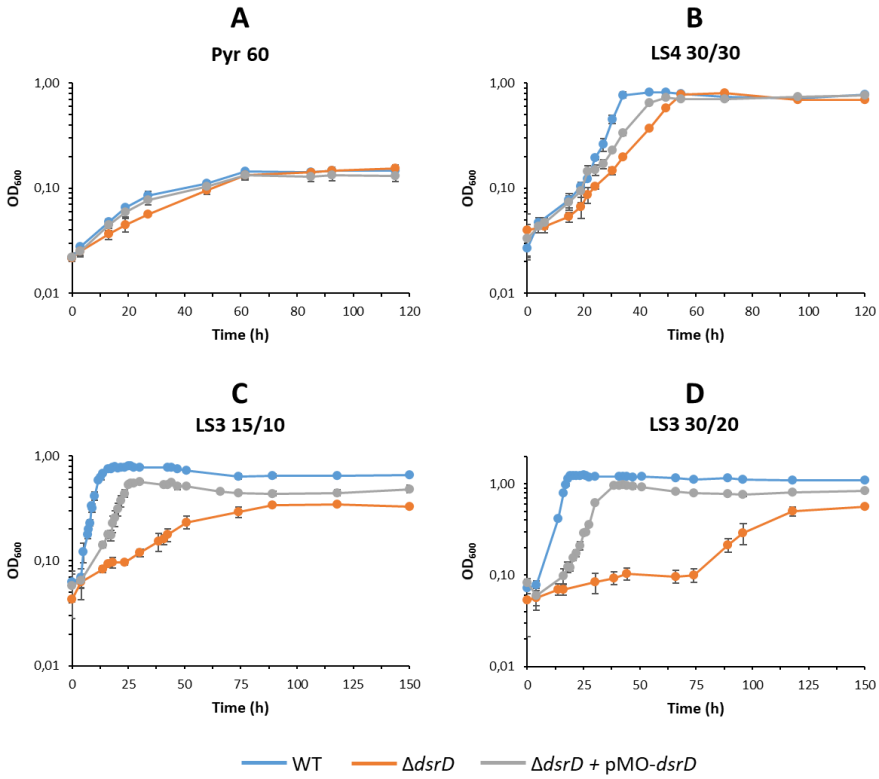

Figure 2.4 – Growth curves of *Dv*H WT (blue), *Dv*H Δ*dsrD* mutant (orange) and *Dv*H Δ*dsrD* + pMO-*dsrD* complemented strain (gray) in: **(A)** 60 mM pyruvate (Pyr 60); **(B)** 30 mM lactate/30 mM sulfate (LS4 30/30); **(C)** 15 mM lactate/10 mM sulfite (LS3 15/10); **(D)** 30 mM lactate/20 mM sulfite (LS3 30/20). Data points are mean ± SD, *n* = 3 independent experiments.

Table 2.4 – Doubling time (T_d) and maximum OD at 600 nm (Max. OD_{600}) for *Dv*H WT, Δ*dsrD* mutant and Δ*dsrD* + pMO-*dsrD* complemented strain in 60 mM pyruvate (Pyr 60), 30 mM lactate/30 mM sulfate (LS4 30/30), 15 mM lactate/10 mM sulfite (LS3 15/10) and 30 mM lactate/20 mM sulfite (LS3 30/20). Data are mean ± SD (n = 3 independent experiments).

	Pyr 60		LS4 30/30		LS3 15/10		LS3 30/20	
Strain	T_d (h)	Max. OD_{600}	T_d (h)	Max. OD_{600}	T_d (h)	Max. OD_{600}	T_d (h)	Max. OD_{600}
WT	31.1 ± 0.8	0.147 ± 0.005	5.0 ± 0.3	0.82 ± 0.02	2.8 ± 0.2	0.81 ± 0.02	2.9 ± 0.1	1.26 ± 0.02
Δ*dsrD*	27.6 ± 3.1	0.155 ± 0.017	10.0 ± 0.5	0.80 ± 0.02	30.3 ± 1.4	0.36 ± 0.01	24.6 ± 5.5	0.56 ± 0.02
Δ*dsrD* + pMO-*dsrD*	30.9 ± 3.5	0.133 ± 0.015	8.6 ± 0.4	0.76 ± 0.01	5.4 ± 0.7	0.58 ± 0.01	4.2 ± 0.3	0.99 ± 0.02

Under fermentative conditions, with pyruvate as sole carbon and electron source, all three strains presented a similar growth behaviour, with identical doubling times and maximum cell densities. However, the same was not observed under lactate/sulfate respiratory conditions (30 mM lactate/30 mM sulfate, LS4 30/30), where *Dv*H Δ*dsrD* presented a two-fold slower growth than *Dv*H WT ($p < 0.01$). This growth difference between WT and Δ*dsrD* strains is even more evident with sulfite as electron acceptor (15 mM lactate/10 mM sulfite, LS3 15/10), resulting in a higher difference in doubling time (10x slower) and a significant decrease in the maximum cell density attained ($p < 0.01$). In medium containing a higher sulfite concentration (30 mM lactate/20 mM sulfite, LS3 30/20), the Δ*dsrD* strain takes a long time to initiate exponential growth (≈ 75 h), while in LS3 15/10 there was virtually no lag phase. The effect on maximum cell density in the Δ*dsrD* strain *vs*. the *Dv*H WT was similar in LS3 15/10 and LS3 30/20, i.e., a decrease of ≈ 55% for the Δ*dsrD* strain. The *Dv*H WT phenotype in respiratory conditions was only partially recovered in the *Dv*H Δ*dsrD* + pMO-*dsrD* strain in LS4 and LS3 conditions, suggesting a reduced expression level of DsrD in the complemented strain relative to the WT. These results show that *Dv*H cannot grow as efficiently by sulfate or sulfite reduction in the absence of DsrD, whereas this is not involved in fermentative growth conditions.

2.4.4 – Identification of DsrD physiological partners

To identify potential physiological partners of DsrD a pull-down assay was performed, taking advantage of the strep-tagged DsrD expressed by the complemented strain. For that, cells of *Dv*H WT and *Dv*H Δ*dsrD* + pMO-*dsrD* were grown in MO LS3 30/20 conditions where a phenotype for Δ*dsrD* was more evident. The crude extracts were subjected to Strep-tag affinity chromatography to isolate DsrD and co-elute potential physiological partners. *Dv*H WT was used as a control, to discard proteins with an intrinsic ability to adhere to the resin. The eluted fractions from both strains were analyzed in a Tricine-SDS-PAGE gel (**Figure 2.5**), and six bands were evident in the eluted fraction of *Dv*H Δ*dsrD* + pMO-*dsrD*, expressing Strep-tagged DsrD. Only two of the six bands were also faintly visible in the *Dv*H WT control assay. The identity of the bands was determined by mass spectrometry (**Table 2.5**). Two bands of

≈ 140 kDa and ≈ 22 kDa were identified as pyruvate carboxylase (Pyc), an enzyme that contains biotin as prosthetic group, which explains its intrinsic binding to the Strep-tactin resin. However, only the ≈ 22 kDa band is present in the *Dv*H WT eluate, which is likely the result of protein degradation from the 140 kDa protein. GroL (a 60 kDa chaperonin) was also identified in both the *Dv*H Δ*dsrD* + pMO-*dsrD* and WT eluted fractions, suggesting also an intrinsic affinity of this highly expressed protein to bind the resin and/or its involvement in folding of recombinant DsrD. Two unique bands of ≈ 49 kDa and ≈ 43 kDa were present in *Dv*H Δ*dsrD* + pMO-*dsrD* eluted fraction and absent in the control eluate. These were identified as DsrA and DsrB, respectively, revealing that DsrD pulls down DsrAB, which indicates there is a direct interaction between these proteins. Curiously, a band corresponding to DsrC (≈ 12 kDa) was not detected in the *Dv*H Δ*dsrD* + pMO-*dsrD* eluate, and its absence was confirmed by Western-blot analysis (**Figure 2.6**).

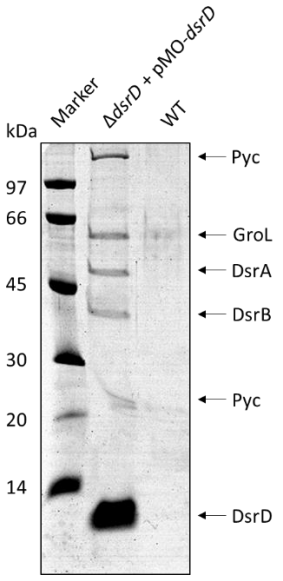

Figure 2.5 – Proteins co-eluting with DsrD-Strep in pull-down assay with the *Dv*H complemented strain (ΔdsrD + pMO-dsrD) and WT (negative control).

Table 2.5 – Identification by mass spectrometry of proteins co-eluted with DsrD-Strep from *Dv*H Δ*dsrD* + pMO-*dsrD* grown in MO LS3 30/20

Protein	Protein	Gene locus tag	Coverage (%)[a]	Peptides [b]	Mass (kDa)[c]
Pyc	Pyruvate carboxylase	DVU1834	35	33	136.3
GroL	60 kDa chaperonin	DVU1976	57	14	58.4
DsrA	Dissimilatory sulfite reductase alpha subunit	DVU0402	47	14	49.1
DsrB	Dissimilatory sulfite reductase beta subunit	DVU0403	44	11	42.5
DsrD	Dissimilatory sulfite reductase D	DVU0404	60	2	8.8

[a]Coverage is the protein sequence coverage by the matching peptides
[b]Peptides indicate the number of different peptides matching the protein sequence
[c]Mass corresponds to the theoretical molecular mass of the identified protein, based on its amino acid sequence

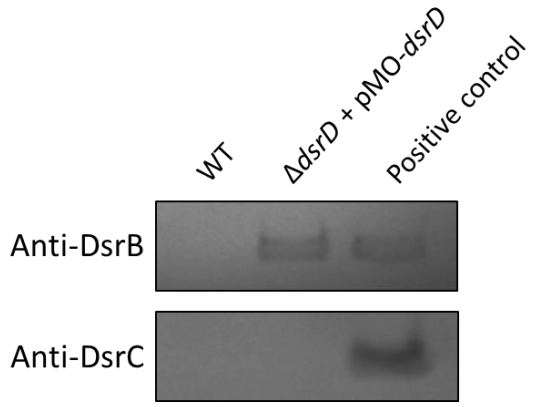

Figure 2.6 – Western blot of eluted fractions from *D*. *vulgaris* WT and *D*. *vulgaris* Δ*dsrD* + pMO-*dsrD* pull-down assay, using anti-DsrB and anti-DsrC antibodies. 1 µg of pure recombinant DsrC or DsrAB from *Dv*H were used as positive control. Samples are the same as loaded in the SDS-PAGE gel of Figure 4.

2.4.5 – Genomic distribution of *dsrD*

A survey of *dsrD* was performed in *dsrAB*-containing organisms (and also *Falkowbacteria*). Notably, using BLASTp and *Dv*H DsrD as query sequence a high number of organisms reported to contain this protein was missed. Closer inspection showed that *dsrD* was indeed present in the majority of organisms with a reductive-type DsrAB, but that three groups of DsrD proteins could be distinguished with low sequence identity between them. The three groups shared the characteristics of having a similar size, similar predicted 3D

structures including a helix-turn-helix motif, a low number of cysteines and presence generally immediately downstream of *dsrAB* genes. Some of these *dsrD* genes have already been identified in previous studies [18], [21], [26], [29], [36]. Three prototypical DsrD sequences were chosen, each belonging to one of three groups. These groups were named as “Type I DsrD” (homologous to *Desulfovibrio vulgaris* Hildenborough DsrD), “Type II DsrD” (homologous to *Thermodesulfobium narugense* DsrD) and “Type III DsrD” (homologous to *Desulfobacca acetoxidans* DsrD). From the 480 genomes containing DsrD analyzed in this study, 306 (64%) encode DsrD Type I, 72 (15%) DsrD Type II, and 102 (21%) DsrD Type III. Due to its small number of amino acids and the very low identity between the three types (in many cases below 20%) as can be seen in **Table 2.6**, it is not possible to generate a robust phylogenetic tree including all DsrD sequences. Instead, these 504 DsrD sequences from 480 genomes were compared based on their global identities. The identity matrix of the sequences showed clearly that the DsrD sequences fall into three different clusters with quite low identity between them (**Figure 2.7**). There is also a subtype within Type I, corresponding to DsrD from *Archaeoglobaceae* species. The *Archaeoglobaceae* DsrD sequences show higher identity to Type I sequences than to other types, and are more distinct from Type III.

Table 2.6 – Identity and similarity between the three types of DsrD, using the *Dv*H DsrD as representer of Type I, *Thermodesulfobium narugense* DsrD for Type II, and *Desulfobacca acetoxidans* DsrD for Type III

	Type I vs Type II	**Type I vs Type III**	**Type II vs Type III**
% Identity	13%	11%	20%
% Similarity	32%	34%	37%

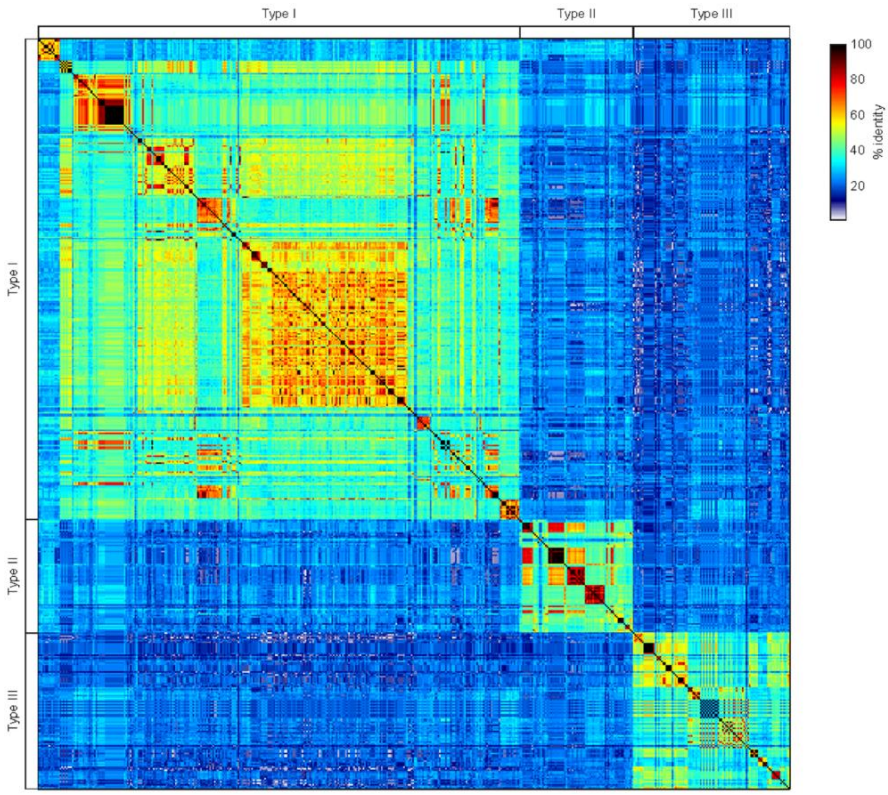

Figure 2.7 – Global identity matrix of DsrD sequences, ranging from low identity (white) to high identity (black) according to the scale shown. Comparison includes 504 DsrD proteins from 480 genomes used in this study.

Organisms with DsrD Type I include members of phylum *Desulfobacterota* (including orders *Desulfovibrionales*, *Desulfobulbales*, *Desulfobacterales*, *Desulfatiglanales*, *Syntrophobacterales*, *Desulfarculales*, *Desulfobaccales*, and the thermophilic class *Thermodesulfobacteria*), some species from the *Clostridia* class (families *Peptococcaceae* and *Thermoanaerobacteraceae*), a few organisms of the phyla *Nitrospirae, Chloroflexi* and *Candidatus* Falkowbacteria, and archaea from the *Archaeoglobaceae* order. An alignment of a few representative DsrD Type I sequences (**Figure 2.8A**) confirms that the previously described YWSSGSTT motif [45] is conserved within this group.

Organisms encoding DsrD Type II include some archaea from the *Aigarchaeota* phylum, bacterial species from *Actinobacteria* (*Coriobacteriia* class), some *Clostridia* organisms of the *Peptococcaceae* family (e.g., *Desulfitobacterium*, *Desulfosporosinus*, and some species of *Desulfotomaculum*), of the *Syntrophomonadaceae* and *Thermoanaerobacteraceae* (*Carboxydothermus* and *Calderihabitans*) families, and from the phyla *Chloroflexi* (*Dehalococcoides*) and *Caldiserica*. Despite not containing the "YWSSGSTT" conserved motif present in DsrD Type I, an 11–residue conserved motif is present closer to the C-terminus (**Figure 2.8B**). This type of DsrD is on average smaller than the other two types.

Organisms encoding DsrD Type III include species from the phyla *Acidobacteria* [18], [21], *Actinobacteria*, *Armatimonadetes*, *Ignavibacteriae*, *Nitrospirae* (e.g., *Nitrospirae* spp., *Candidatus* Magnetobacterium, and some *Thermodesulfovibrio* species), *Candidatus* Desantisbacteria, *Candidatus* Schekmanbacteria (both only 1 species), *Candidatus* Zixibacteria, as well as organisms from *Bacteroidetes*/*Chlorobi* Group, *Candidatus* Lambdaproteobacteria class, orders *Candidatus* Acidulodesulfobacterales, *Myxococcales* and *Desulfurellales* and some from the *Syntrophaceae* family (*Desulfobacca* species). No archaeal species were found encoding DsrD Type III. A conserved 10-residue motif is present in the region corresponding to the YWSSGSTT motif of DsrD Type I, but this region is not homologous to the corresponding region in DsrD Type I or DsrD Type II (**Figure 2.8C**). The majority of organisms containing DsrD Type III are organisms recently identified as belonging to newly-discovered phyla [18], [21], [26], [29]. Some of these organisms also encode DsrL and/or DsrEFH proteins, which are thought to be exclusive of SOP. However, a recent study revealed that several organisms with a reductive DsrAB contain a sub-group of DsrL proteins named DsrL-2 [35]. This search further showed that in all organisms containing DsrD, a reductive DsrAB and DsrL-2 and/or DsrEFH, the DsrD is of Type III. Some of these organisms with a reductive DsrAB and DsrL-2 and/or DsrEFH and DsrD Type III may be capable of sulfur disproportionation. The presence of the *dsrD*, *dsrL*, *dsrEFH* and YTD genes, recently suggested to be indicative of sulfur disproportionation [58], was analyzed in 30 genomes of confirmed sulfur disproportionators as well as three genomes of cable bacteria (*Candidatus* Electronema sp. GS, *Candidatus* Electrothrix aarhusiensis MCF and Deltaproteobacteria

bacterium 1MN72D_58_314), which also perform sulfur disproportionation [53], [54] (**Table 2.7**). All these genomes contain *dsrD*, which is Type I in most cases, except for two *Desulfurella* spp. (DsrD Type III), *Desulfotomaculum nigrificans* DSM 574 (DsrD Type II) and *Dethiobacter alkaliphilus* AHT1 that has no DsrD. No correlation was observed for the other genes, with *dsrL-2* only being observed for two *Desulfurella* spp., of which only *Desulfurella amilsii* contains a *dsrE*-like gene [59]. Of the 33 genomes analyzed 16 contain the YTD gene cluster.

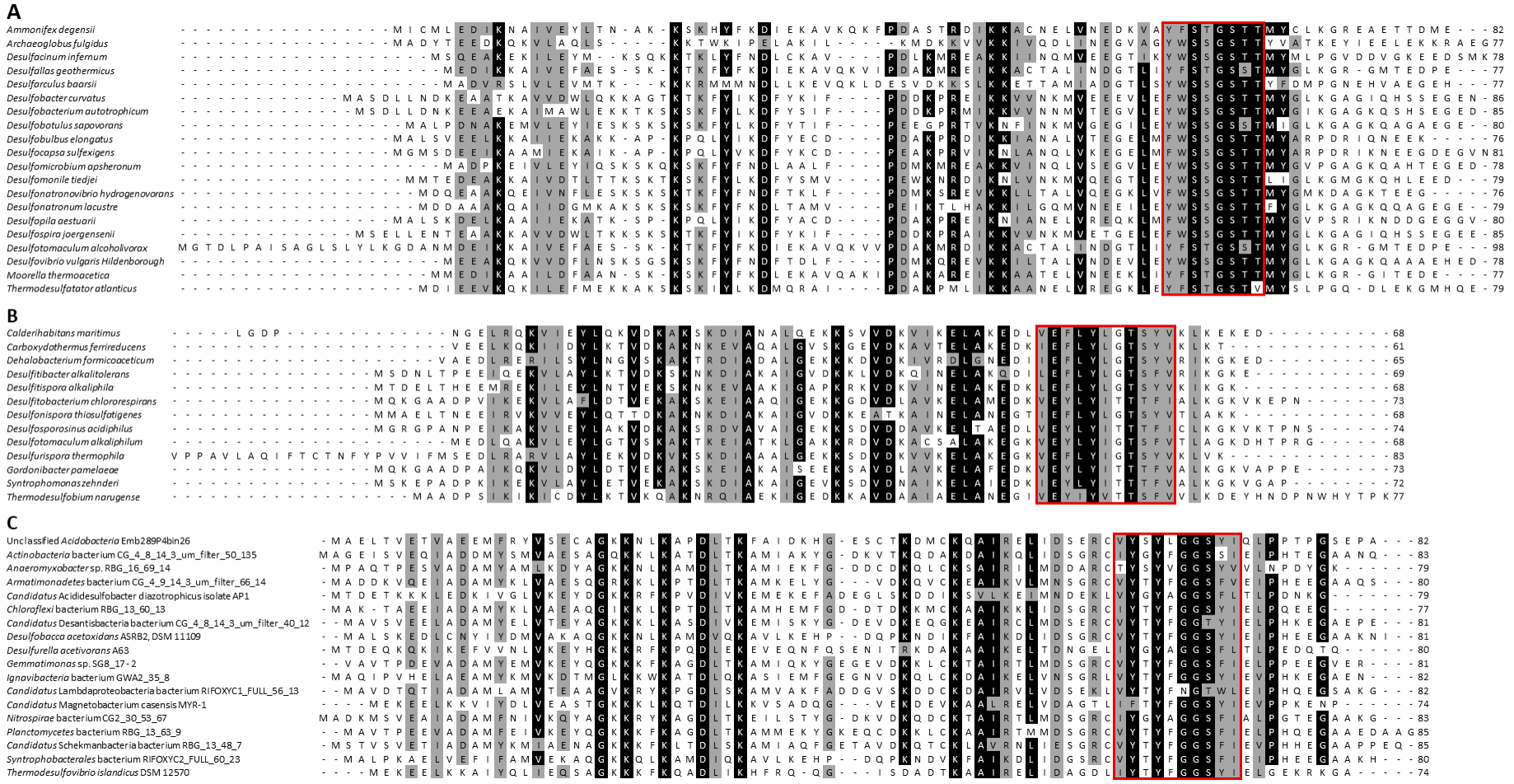

Figure 2.8 – Multiple sequence alignment of DsrD from representative archaeal and bacterial species. **(A)** Alignment of DsrD Type I. The conserved motif YWSSGSTT is outlined in red. **(B)** Alignment of DsrD Type II. A conserved motif is outlined in red. **(C)** Alignment of DsrD Type III. Conserved motifs are outlined in red.

Table 2.7 – Presence and type of DsrD and DsrL, as well as presence of DsrEFH and YDT clusters among sulfur-disproportionation organisms and cable bacteria able to perform sulfur-disproportionation

Sulfur-disproportionation organisms	DsrD type	DsrL type	DsrEFH cluster	YDT cluster
Caldimicrobium thiodismutans TF1	I	×	×	✓
delta proteobacterium sp. MLMS-1	I (x2)	×	×	✓
Desulfatiglans anilini DSM 4660	I	×	×	✓
Desulfobacter curvatus DSM 3379	I	×	×	×
Desulfobulbus propionicus 1pr3, DSM 2032	I	×	×	✓
Desulfocapsa sulfexigens DSM 10523	I	×	×	✓
Desulfocapsa thiozymogenes DSM 7269	I	×	×	✓
Desulfococcus multivorans DSM 2059	I	×	×	×
Desulfofustis glycolicus DSM 9705	I (x2)	×	×	✓
Desulfomonile tiedjei DCB-1, DSM 6799	I	×	×	×
Desulfonatronospira thiodismutans ASO3-1	I	×	×	✓
Desulfonatronovibrio hydrogenovorans DSM 9292	I	×	×	✓
Desulfonatronovibrio magnus AHT22	I	×	×	✓
Desulfonatronum thioautotrophicum ASO4-1	I	×	×	✓
Desulfonatronum thiodismutans MLF-1	I	×	×	×
Desulfonatronum thiosulfatophilum ASO4-2	I	×	×	×
Desulforhopalus singaporensis DSM 12130	I	×	×	✓
Desulfotomaculum nigrificans DSM 574	II	×	×	×
Desulfovibrio aminophilus DSM 12254	I	×	×	×
Desulfovibrio brasiliensis JCM 12178	I	×	×	×
Desulfovibrio cuneatus DSM 11391	I	×	×	×
Desulfovibrio longus DSM 6739	I	×	×	×
Desulfovibrio mexicanus DSM 13116	I	×	×	×
Desulfovibrio oxyclinae DSM 11498	I	×	×	×
Desulfurella acetivorans A63, DSM 5264	III	2	DsrE, DsrE'	×
Desulfurella amilsii TR1 Re-analysis	III	2	DsrE, DsrE'	×
Desulfurivibrio alkaliphilus AHT2	I	×	×	✓
Dethiobacter alkaliphilus AHT1	×	×	×	×
Dissulfuribacter thermophilus S69	I	×	×	✓
Thermosulfurimonas dismutans S95	I	×	×	✓
Cable bacteria				
Candidatus Electronema sp. GS	I	×	×	✓
Candidatus Electrothrix aarhusiensis MCF	I	×	×	×
Deltaproteobacteria bacterium 1MN72D_58_314	I	N.a.	N.a.	N.a.

The *dsrD* gene distribution reveals that some phylogenetic groups contain species with different types of DsrD, reflecting gene acquisition by lateral gene transfer, as described for DsrAB [17], [18]. Notable examples are members of the *Syntrophaceae* family where some organisms contain DsrD Type I (e.g., *Syntrophus*, *Desulfomonile*) and others of Type III (*Desulfobacca*), members of the *Nitropsira* class where most organisms contain DsrD Type II but a few have Type I, members of the phylum *Chloroflexi* where most organisms have DsrD Type II, but there are examples with the other two types, and finally in the *Thermoanaerobacterales* order and the *Peptococcaceae* family of Clostridia where some organisms contain DsrD type I and others DsrD type II. In fact, distribution of the three DsrD types matches well with the phylogenetic groups of DsrAB

(**Figure 2.9**), as might be expected, supporting joint evolutionary pathways for *dsrAB* and *dsrD*.

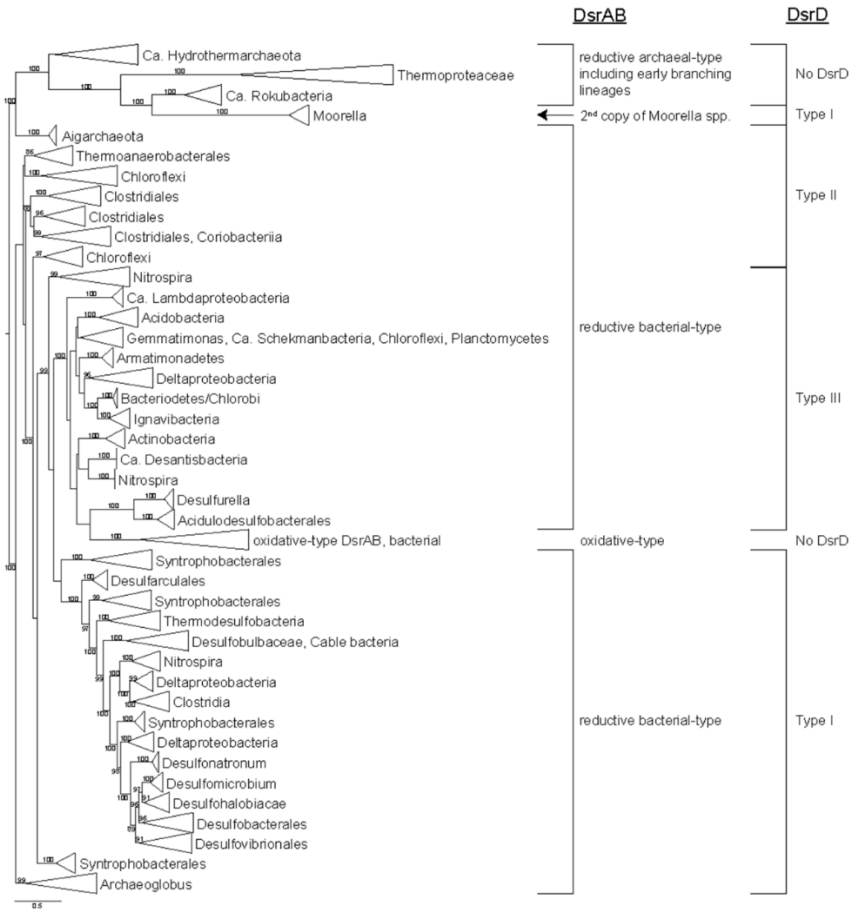

Figure 2.9 – Maximum likelihood phylogeny of 510 DsrA sequences (best model: LG+I+G4), and respective types of DsrA and DsrD proteins. Only bootstrap values ≥ 85 are shown.

As previously reported, no *dsrD* was found in the genome of SOP with oxidative-type rDsrAB [18], [35]. In addition, a few organisms with a reductive DsrAB do not have DsrD, such as *Thermosinus carboxydivorans, Thermanaeromonas toyohensis* and others [18], [21]. Notably, *dsrD* genes were not found in organisms containing the putative earliest evolved forms of *dsrAB*, such as *Crenarchaeota*,

Verrucomicrobia, *Candidatus* Rokubacteria and *Candidatus* Hydrothermarchaeota.

Independently of the DsrD type, in 95% of the genomes analyzed the *dsrD* gene was found immediately downstream of *dsrAB*, in a *dsrABD* arrangement. However, in some organisms, namely in *Acidobacteria*, *dsrD* was not found next to *dsrAB* but was still present within the *dsr* operon or in proximity to other *dsr* genes. Several organisms have two copies of *dsrD* in a *dsrABD* arrangement. In all genomes where several copies of *dsrD* are found, all belong to the same type. In a few cases (all Type I), *dsrD* is found immediately upstream of *dsrAB*, instead of downstream. A striking event of gene fusion between *dsrB* and *dsrD* was detected only in *Bilophila* spp. [40], and in *Mailhella massiliensis* Marseille-P3199, an organism from the same family. In *Gordonibacter* spp. and Coriobacteriaceae bacterium 68-1-3, organisms encoding DsrD Type II, the operon has a *dsrAB*$(X)_n$*D* arrangement (where X is not a *dsr* gene and n = 3 or 4).

2.5 – Discussion

The dissimilatory reduction of sulfite and sulfate, and also sulfur disproportionation, are likely very ancient metabolisms [14], [60], [61]. Their evolutionary history is difficult to clarify, but it is likely that sulfite reduction preceded sulfate reduction [19], [20]. Recently, the analysis of metagenome-assembled genomes revealed that the range of organisms capable of dissimilatory sulfur metabolism, namely sulfate/sulfite reduction and/or disproportionation is much larger than previously believed [18], [20], [29], [21]–[28]. This identification often takes into account the presence of genes for the key *dsr* pathway, which can include up to 15 genes, and is involved in either sulfite reduction or sulfite production in a large range of sulfur energy metabolisms. The presence of *rdsrAB*, *dsrEFH* and *dsrL* are typically taken as an indication for oxidative sulfur metabolism, whereas the presence of reductive-type *dsrAB* and *dsrD* are taken as indicative of reductive sulfur metabolism or disproportionation. However, several cases have been found where identification of the type of metabolism is not straightforward, as for example some organisms have *dsrEFH* and/or *dsrL* along with reductive *dsrAB* [18], [21], [26], [29]. For a clear assignment of genes to metabolisms it is obviously critical to have a good understanding of the function performed by the proteins encoded in those genes. An important advancement was the recent elucidation of the function of DsrL as an electron acceptor for rDsrAB coupled to the reduction of NAD^+ [62], and the subsequent identification of different classes of DsrL proteins, with DsrL-2 being present in organisms with a reductive sulfur metabolism, where it acts as an electron donor for DsrAB while oxidizing NADPH [35]. These studies were critical to clarify that DsrL is also present in organisms with a reductive/disproportionating type metabolism.

The function of the small protein DsrD has long remained enigmatic. Based on the crystal structure of the *Dv*H protein and its winged helix-turn-helix (wHTH) motif, it has generally been assumed that DsrD has a DNA-binding function, acting as a regulator of the *dsr* genes. Although DsrD can bind to DNA, as might be expected from its high lysine content, this binding is unspecific and so a possible role as a transcriptional regulator seems unlikely. Here it was provided evidence to assign the function of DsrD as an activator of DsrAB. This protein is very highly abundant, in the same order as DsrAB or even more [37], [41], [42], which is characteristic of energy

metabolism but not gene regulation proteins. This study shows that DsrD is highly abundant in respiratory conditions but practically absent during fermentative growth, and that this protein is not strictly essential as a Δ*dsrD* deletion strain could be obtained for *Dv*H, in contrast to DsrC [30]. The Δ*dsrD* strain is not affected in fermentative growth with pyruvate but is affected in respiratory growth with sulfate and more prominently with sulfite, indicating that *Dv*H grows more efficiently with these sulfur compounds in the presence of DsrD, particularly in the case of sulfite.

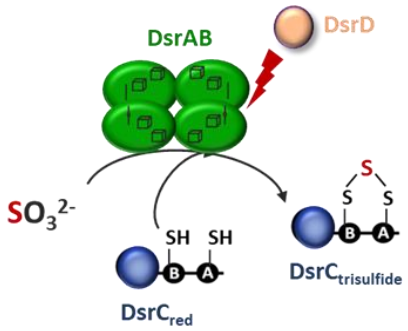

Figure 2.10 – Representation of the DsrD function as an allosteric activator of DsrAB in DsrC catalysis.

The *Dv*H Δ*dsrD* + pMO-*dsrD* complemented strain, containing a tagged version of DsrD, allowed us to do a pull-down experiment and identify DsrAB as its direct physiological partner. Previous studies have looked at a possible interaction between DsrD and DsrAB. Hittel & Voordouw did not detect DsrD in partially purified DsrAB preparations [46], whereas Shatsky and colleagues reported DsrAB being co-purified with tagged DsrD, and DsrD being co-purified with tagged DsrA or DsrB with lower yields [47], suggesting a transient binding of DsrD to DsrAB and not the formation of a stable complex. Both studies corroborate the our findings, since DsrD was not detected when purifying DsrAB/C from *Dv*H [11]. Nevertheless, the affinity of DsrD for DsrAB is very high, with a K_d of 350 ± 60 nM as revealed by microscale thermophoresis (MST) and supported by surface plasmon resonance (SPR), and revealing a direct physiological interaction between the two proteins. Interestingly, DsrC was not detected together with DsrAB in the pull-down assay,

confirming that the previously observed covalent cross-link between *Dv*H DsrC and the DsrAB siroheme [11] is not physiological and occurs during the long DsrAB purification process.

By using isolated proteins from *A. fulgidus* and *in vitro* activity assays, we show that DsrD acts as an activator of the sulfite reductase activity of DsrAB. In the presence of the co-substrate DsrC, the DsrAB activity increases by 25%, while the affinity for sulfite is not affected. These results go in line with the observations that DsrD is not essential for growth in *Dv*H, but that a Δ*dsrD* strain cannot grow as efficiently as the wild-type during sulfate/sulfite respiration. Since DsrD is not modified during DsrAB catalysis it is likely that the activating role of DsrD is associated with a conformational alteration in DsrAB that leads to increased activity, meaning that DsrD acts as an allosteric activator of DsrAB. In the gut pathogen *B. wadsworthia*, the dissimilatory sulfite reductase was isolated as DsrABD, and the *dsrD* gene is fused to *dsrB* [40]. The C-terminal of DsrB is distant from the active site [11], which suggests that DsrD binds far away from the substrate pocket. Future modelling studies will be performed to try to elucidate the DsrD binding site and possible conformational alterations induced by DsrD on DsrAB.

Analysis of *dsrD* distribution in 480 genomes containing the *dsr* pathway, revealed the presence of three phylogenetically distinct types of DsrD, with very low sequence identity between them, and confirmed the absence of this gene from SOP. The three types are likely to have similar 3D structures including a wHTH motif that is likely involved in the interaction with DsrAB. The distribution of DsrD types agrees with DsrAB phylogeny supporting co-evolution of these genes and a specific protein-protein interaction. The most abundant is DsrD Type I, present in *Desulfobacterota* and others, with DsrD from the *Archaeoglobaceae* forming a sub-group within this type. Organisms recently described to encode DsrAB and DsrD together with DsrL and/or DsrEFH [18], [21], [26], [29], encode exclusively DsrD of Type III. For some of these organisms it is not clear if sulfur metabolism occurs in a reductive or oxidative direction, and it has been suggested that the presence of reductive DsrAB and DsrD may not be indicative of reductive metabolism and that DsrAB may be operating in an oxidative mode. Some of the cases where DsrAB is present together with DsrD and DsrL are organisms capable of disproportionation, where reductive and oxidative sulfur metabolism occur concurrently. One example is *Desulfurivibrio alkaliphilus*,

which couples sulfide oxidation to nitrate reduction with production of elemental sulfur, which is then disproportionated [37], as shown before for other *Desulfobulbaceae* [63]–[65], including recently for cable bacteria [54]. The fate of elemental sulfur during this process has not been clarified and may involve its oxidation to sulfite, which has been shown to be an intermediate during disproportionation of sulfur or thiosulfate [64], [65]. Disproportionation of sulfite then involves its oxidation to sulfate by ATP sulfurylase and APS reductase, both of which are readily reversible enzymes, as well as its reduction to sulfide, performed by DsrABCD. Cable bacteria are another interesting example of organisms performing sulfide oxidation coupled with oxygen or nitrate reduction and containing reductive DsrABCD [53]. They also belong to the *Desulfobulbaceae* and are closely related to the genus *Desulfobulbus* that contain several disproportionators, suggesting also the involvement of elemental sulfur disproportionation in their energy metabolism [53], which was recently confirmed [54]. Thus, it is reasonable to assume that disproportionation of sulfur, thiosulfate and sulfite involves DsrAB operating in a reductive direction. Reversibility of the reductive DsrAB, although theoretically possible, has never been shown and may imply protein adaptation, as suggested by the existence of separate phylogenetic groups of rDsrAB and DsrC for the reverse reaction, operating with different proteins (e.g., DsrEFH). The presence of DsrEFH indicates the need for dedicated proteins to transfer sulfur onto DsrC, which are not present in simple sulfate reducers and many disproportionators. Nevertheless, disproportionation of elemental sulfur can apparently occur also without the involvement of DsrAB, as suggested by proteomic studies of *D. amilsii*, an organism that can grow by elemental sulfur or thiosulfate reduction and also by elemental sulfur disproportionation [59]. In *D. amilsii*, high abundance of DsrAB, DsrC and DsrMKJOP was only observed during thiosulfate reduction, and not during sulfur disproportionation. This organism also does not have ATP sulfurylase and APS reductase, and sulfite was not detected during disproportionation, suggesting a different mechanism for this process [59]. Thus, sulfur compound disproportionation and/or reduction of intracellularly formed sulfite (from thiosulfate or organosulfonates) can explain the presence of reductive DsrAB/DsrC/DsrD in organisms that do not perform DSR. In these cases, disproportionation is likely to involve the intermediate production of elemental sulfur and/or sulfite and thus would not be a

simple reversal of the canonical sulfate reduction pathway. Thus, the presence of DsrAB, DsrD and DsrL-2 are in line with a reductive or disproportionating metabolism. However, as previously noted, the presence of *dsrD* alone cannot be taken as an indication of reductive sulfur metabolism as this gene is also present in some organisms that lack other *dsr* genes, such as symbiotic bacteria of the candidate phyla radiation (CPR), where this small protein may be involved in modulating host metabolism, as reported for viruses [18], [66].

In conclusion, these results clarify the functional role of DsrD as an allosteric activator of DsrAB catalysis in sulfite reduction, providing important insights into our molecular understanding of dissimilatory sulfur metabolism. The absence of DsrD in organisms encoding the putative earliest forms of DsrAB indicates that DsrD appeared later in the evolutionary history of the *dsr* genes. This is in line with its non-essential function, observed in this study. In terms of its use as a functional marker gene we believe that *dsrD*, when found together with *dsrAB*, *dsrC* and *dsrMK* genes are most likely evidence of reductive sulfur metabolism, which may be part of a larger disproportionating scheme.

2.6 – Acknowledgements

I would like to thank Ana Catarina Barbosa, who was involved in this study and whose PhD work complements the findings described in this chapter, having co-authored the paper that resulted from this work. I would also like to thank Filipa Sousa and Sinje Neukirchen from University of Vienna, which contributed to the phylogenetic analysis. This work was funded by the Fundação para a Ciência e Tecnologia (Portugal) through Fellowships PD/BD/128204/2016 (D.F.), PD/BD/135488/2018 (A.C.C.B.) and SFRH/BPD/79823/2011 (S.S.V.); Grants PTDC/BIA-MIC/6512/2014 and PTDC/BIA-BQM/29118/2017; and Research unit Molecular and Structural Microbiology (MOSTMICRO-ITQB) (Grants UIDB/04612/2020 and UIDP/04612/2020). The European Union's Horizon 2020 Research and Innovation Program (Grant Agreement No. 810856) is also acknowledged.

2.6 – Bibliography

[1] R. Rabus, S. S. Venceslau, L. Wöhlbrand, G. Voordouw, J. D. Wall, and I. A. C. Pereira, “A Post-Genomic View of the Ecophysiology, Catabolism and Biotechnological Relevance of Sulphate-Reducing Prokaryotes”, *Adv. Microb. Physiol.*, vol. 66, pp. 55–321, 2015.

[2] K. Wasmund, M. Mußmann, and A. Loy, “The life sulfuric: microbial ecology of sulfur cycling in marine sediments,” *Environ. Microbiol. Rep.*, vol. 9, no. 4, pp. 323–344, 2017.

[3] M. W. Bowles, J. M. Mogollón, S. Kasten, M. Zabel, and K.-U. Hinrichs, “Global rates of marine sulfate reduction and implications for sub-sea-floor metabolic activities”, *Science*, vol. 344, no. 6186, pp. 889–891, 2014.

[4] B. B. Jørgensen, A. J. Findlay, and A. Pellerin, “The biogeochemical sulfur cycle of marine sediments”, *Front. Microbiol.*, vol. 10, no. 849, 2019.

[5] S. E. McGlynn, G. L. Chadwick, C. P. Kempes, and V. J. Orphan, “Single cell activity reveals direct electron transfer in methanotrophic consortia”, *Nature*, vol. 526, no. 7574, pp. 531–535, 2015.

[6] G. Wegener, V. Krukenberg, D. Riedel, H. E. Tegetmeyer, and A. Boetius, “Intercellular wiring enables electron transfer between methanotrophic archaea and bacteria”, *Nature*, vol. 526, no. 7574, pp. 587–590, 2015.

[7] C. Dahl, “A biochemical view on the biological sulfur cycle”, in *Environmental Technologies to Treat Sulphur Pollution: Principles and Engineering*, 2020, pp. 55–96.

[8] F. Carbonero, A. C. Benefiel, A. H. Alizadeh-Ghamsari, and H. R. Gaskins, “Microbial pathways in colonic sulfur metabolism and links with health and disease”, *Front. Physiol.*, vol. 3, no. 448, 2012.

[9] S. Devkota and E. B. Chang, “Interactions between diet, bile acid metabolism, gut microbiota, and inflammatory bowel diseases”, *Dig. Dis.*, vol. 33, no. 3, pp. 351–356, 2015.

[10] J. M. Ridlon, P. G. Wolf, and H. R. Gaskins, “Taurocholic acid metabolism by gut microbes and colon cancer”, *Gut Microbes*, vol. 7, no. 3, pp. 201–215, 2016.

[11] T. F. Oliveira, C. Vonrhein, P. M. Matias, S. S. Venceslau, I. A. C. Pereira, and M. Archer, “The crystal structure of *Desulfovibrio vulgaris* dissimilatory sulfite reductase bound to DsrC provides novel insights into the mechanism of sulfate respiration”, *J. Biol. Chem.*, vol. 283, no. 49, pp. 34141–34149, 2008.

[12] S. S. Venceslau, Y. Stockdreher, C. Dahl, and I. A. C. Pereira, “The ‘bacterial heterodisulfide’ DsrC is a key protein in dissimilatory sulfur metabolism”, *Biochim. Biophys. Acta - Bioenerg.*, vol. 1837, no. 7, pp. 1148–1164, 2014.

[13] J. Simon and P. M. H. Kroneck, “Microbial Sulfite Respiration”, in *Advances in Microbial Physiology*, vol. 62, 2013, pp. 45–117.

[14] M. Wagner, A. J. Roger, J. L. Flax, G. A. Brusseau, and D. A. Stahl, “Phylogeny of dissimilatory sulfite reductases supports an early origin of sulfate respiration”, *J. Bacteriol.*, vol. 180, no. 11, pp. 2975–2982, 1998.

[15] A. Dhillon, S. Goswami, M. Riley, A. Teske, and M. Sogin, “Domain Evolution and Functional Diversification of Sulfite Reductases”, *Astrobiology*, vol. 5, no. 1, pp. 18–29, 2005.

[16] A. Loy *et al.*, “Reverse dissimilatory sulfite reductase as phylogenetic marker for a subgroup of sulfur-oxidizing prokaryotes”, *Environ. Microbiol.*, vol. 11, no. 2, pp. 289–299, 2009.

[17] A. L. Müller, K. U. Kjeldsen, T. Rattei, M. Pester, and A. Loy, “Phylogenetic and environmental diversity of DsrAB-type dissimilatory (bi)sulfite reductases”, *ISME J.*, vol. 9, no. 5, pp. 1152–1165, 2015.

[18] K. Anantharaman *et al.*, “Expanded diversity of microbial groups that shape the dissimilatory sulfur cycle”, *ISME J.*, vol. 12, no. 7, pp. 1715–1728, 2018.

[19] N. A. Chernyh *et al.*, “Dissimilatory sulfate reduction in the archaeon ‘*Candidatus* Vulcanisaeta moutnovskia’ sheds light on the evolution of sulfur metabolism”, *Nat. Microbiol.*, vol. 5, no. 11, pp. 1428–1438, 2020.

[20] D. R. Colman, M. R. Lindsay, M. J. Amenabar, M. C. Fernandes-Martins, E. R. Roden, and E. S. Boyd, “Phylogenomic analysis of novel Diaforarchaea is consistent with sulfite but not sulfate reduction in volcanic environments

on early Earth", *ISME J.*, vol. 14, no. 5, pp. 1316–1331, 2020.

[21] B. Hausmann *et al.*, "Peatland Acidobacteria with a dissimilatory sulfur metabolism", *ISME J.*, vol. 12, no. 7, pp. 1729–1742, 2018.

[22] P. Dalcin Martins *et al.*, "Viral and metabolic controls on high rates of microbial sulfur and carbon cycling in wetland ecosystems", *Microbiome*, vol. 6, no. 1, pp. 1–17, 2018.

[23] B. J. Baker, C. S. Lazar, A. P. Teske, and G. J. Dick, "Genomic resolution of linkages in carbon, nitrogen, and sulfur cycling among widespread estuary sediment bacteria", *Microbiome*, vol. 3, no. 14, 2015.

[24] L. J. McKay *et al.*, "Co-occurring genomic capacity for anaerobic methane and dissimilatory sulfur metabolisms discovered in the Korarchaeota", *Nat. Microbiol.*, vol. 4, no. 4, pp. 614–622, 2019.

[25] S. Zecchin *et al.*, "Rice paddy Nitrospirae carry and express genes related to sulfate respiration: Proposal of the new genus 'Candidatus Sulfobium,'" *Appl. Environ. Microbiol.*, vol. 84, no. 5, 2018.

[26] V. Thiel *et al.*, "'*Candidatus* Thermonerobacter thiotrophicus', A Non-phototrophic Member of the Bacteroidetes/Chlorobi With Dissimilatory Sulfur Metabolism in Hot Spring Mat Communities", *Front. Microbiol.*, vol. 9, no. 3159, 2019.

[27] S. A. Carr *et al.*, "Carboxydotrophy potential of uncultivated Hydrothermarchaeota from the subseafloor crustal biosphere", *ISME J.*, vol. 13, no. 6, pp. 1457–1468, 2019.

[28] Z. S. Hua *et al.*, "Genomic inference of the metabolism and evolution of the archaeal phylum Aigarchaeota", *Nat. Commun.*, vol. 9, no. 2832, 2018.

[29] S. Tan *et al.*, "Insights into ecological role of a new deltaproteobacterial order *Candidatus* Acidulodesulfobacterales by metagenomics and metatranscriptomics", *ISME J.*, vol. 13, no. 8, pp. 2044–2057, 2019.

[30] A. A. Santos *et al.*, "A protein trisulfide couples dissimilatory sulfate reduction to energy conservation", *Science.*, vol. 350, no. 6267, pp. 1541–1545, 2015.

[31] R. H. Pires, S. S. Venceslau, F. Morais, M. Teixeira, A. V. Xavier, and I. A. C. Pereira, “Characterization of the *Desulfovibrio desulfuricans* ATCC 27774 DsrMKJOP complex - A membrane-bound redox complex involved in the sulfate respiratory pathway”, *Biochemistry*, vol. 45, no. 1, pp. 249–262, 2006.

[32] F. Grein, A. R. Ramos, S. S. Venceslau, and I. A. C. Pereira, “Unifying concepts in anaerobic respiration: Insights from dissimilatory sulfur metabolism”, *Biochim. Biophys. Acta*, vol. 1827, no. 2, pp. 145–160, 2013.

[33] Y. Stockdreher, S. S. Venceslau, M. Josten, H. G. Sahl, I. A. C. Pereira, and C. Dahl, “Cytoplasmic sulfurtransferases in the purple sulfur bacterium *Allochromatium vinosum*: Evidence for sulfur transfer from DsrEFH to DsrC”, *PLoS One*, vol. 7, no. 7, 2012.

[34] Y. J. Lübbe, H. S. Youn, R. Timkovich, and C. Dahl, “Siro(haem)amide in *Allochromatium vinosum* and relevance of DsrL and DsrN, a homolog of cobyrinic acid a,c-diamide synthase, for sulphur oxidation”, *FEMS Microbiol. Lett.*, vol. 261, no. 2, pp. 194–202, 2006.

[35] M. Löffler, K. B. Wallerang, S. S. Venceslau, I. A. C. Pereira, and C. Dahl, “The Iron-Sulfur Flavoprotein DsrL as NAD(P)H:Acceptor Oxidoreductase in Oxidative and Reductive Dissimilatory Sulfur Metabolism”, *Front. Microbiol.*, vol. 11, no. 578209, 2020.

[36] M. Flieder *et al.*, “Novel taxa of Acidobacteriota implicated in seafloor sulfur cycling”, *ISME J.*, 2021.

[37] C. Thorup, A. Schramm, L. Schreiber, A. J. Findlay, and K. W. Finster, “Disguised as a Sulfate Reducer: Growth of the Deltaproteobacterium *Desulfurivibrio alkaliphilus* by Sulfide Oxidation with Nitrate”, *MBio*, vol. 8, no. 4, 2017.

[38] R. R. Karkhoff-Schweizer, D. P. W. Huber, and G. Voordouw, “Conservation of the genes for dissimilatory sulfite reductase from *Desulfovibrio vulgaris* and *Archaeoglobus fulgidus* allows their detection by PCR”, *Appl. Environ. Microbiol.*, vol. 61, no. 1, pp. 290–296, 1995.

[39] Ø. Larsen, T. Lien, and N. K. Birkeland, “A novel organization of the dissimilatory sulfite reductase operon of *Thermodesulforhabdus norvegica* verified by RT-PCR”,

FEMS Microbiol. Lett., vol. 203, no. 1, pp. 81–85, 2001.

[40] H. Laue, M. Friedrich, J. Ruff, and A. M. Cook, “Dissimilatory sulfite reductase (Desulfoviridin) of the taurine-degrading, non-sulfate-reducing bacterium *Bilophila wadsworthia* RZATAU contains a fused DsrB-DsrD subunit”, *J. Bacteriol.*, vol. 183, no. 5, pp. 1727–1733, 2001.

[41] K. L. Keller and J. D. Wall, “Genetics and molecular biology of the electron flow for sulfate respiration in *Desulfovibrio*”, *Front. Microbiol.*, vol. 2, no. 135, 2011.

[42] A. E. Otwell, S. J. Callister, E. M. Zink, R. D. Smith, and R. E. Richardson, “Comparative Proteomic Analysis of *Desulfotomaculum reducens* MI-1: Insights into the Metabolic Versatility of a Gram-Positive Sulfate- and Metal-Reducing Bacterium”, *Front. Microbiol.*, vol. 7, no. 191, 2016.

[43] W. Zhang, D. E. Culley, J. C. M. Scholten, M. Hogan, L. Vitiritti, and F. J. Brockman, “Global transcriptomic analysis of *Desulfovibrio vulgaris* on different electron donors”, *Antonie van Leeuwenhoek, Int. J. Gen. Mol. Microbiol.*, vol. 89, no. 2, pp. 221–237, 2006.

[44] S. M. Caffrey and G. Voordouw, “Effect of sulfide on growth physiology and gene expression of *Desulfovibrio vulgaris* Hildenborough”, *Antonie Van Leeuwenhoek*, vol. 97, no. 1, pp. 11–20, 2010.

[45] N. Mizuno, G. Voordouw, K. Miki, A. Sarai, and Y. Higuchi, “Crystal structure of dissimilatory sulfite reductase D (DsrD) protein - Possible interaction with B- and Z-DNA by its winged-helix motif”, *Structure*, vol. 11, no. 9, pp. 1133–1140, 2003.

[46] D. S. Hittel and G. Voordouw, “Overexpression, purification and immunodetection of DsrD from *Desulfovibrio vulgaris* Hildenborough”, *Antonie Van Leeuwenhoek*, vol. 77, no. 3, pp. 271–280, 2000.

[47] M. Shatsky *et al.*, “Bacterial interactomes: interacting protein partners share similar function and are validated in independent assays more frequently than previously reported.”, *Mol. Cell. Proteomics*, vol. 15, no. 5, pp. 1539–1555, 2016.

[48] D. W. Waite *et al.*, “Proposal to reclassify the proteobacterial classes deltaproteobacteria and oligoflexia, and the phylum thermodesulfobacteria into four phyla reflecting major

functional capabilities", *Int. J. Syst. Evol. Microbiol.*, vol. 70, no. 11, pp. 5972–6016, 2020.

[49] M. Z. Li and S. J. Elledge, "Harnessing homologous recombination in vitro to generate recombinant DNA via SLIC", vol. 4, no. 3, pp. 251–256, 2007.

[50] K. L. Keller, J. D. Wall, and S. Chhabra, *Methods for engineering sulfate reducing bacteria of the genus Desulfovibrio*, 1st ed., vol. 497. Elsevier Inc., 2011.

[51] G. M. Zane, H. C. Bill Yen, and J. D. Wall, "Effect of the deletion of *qmoABC* and the promoter-distal gene encoding a hypothetical protein on sulfate reduction in *Desulfovibrio vulgaris* Hildenborough", *Appl. Environ. Microbiol.*, vol. 76, no. 16, pp. 5500–5509, 2010.

[52] F. Grimm, N. Dobler, and C. Dahl, "Regulation of *dsr* genes encoding proteins responsible for the oxidation of stored sulfur in *Allochromatium vinosum*", *Microbiology*, vol. 156, no. 3, pp. 764–773, 2010.

[53] K. U. Kjeldsen *et al.*, "On the evolution and physiology of cable bacteria", *Proc. Natl. Acad. Sci. U. S. A.*, vol. 116, no. 38, pp. 19116–19125, 2019.

[54] H. Müller, S. Marozava, A. J. Probst, and R. U. Meckenstock, "Groundwater cable bacteria conserve energy by sulfur disproportionation", *ISME J.*, vol. 14, no. 2, pp. 623–634, 2020.

[55] P. Rice, L. Longden, and A. Bleasby, "EMBOSS: The European Molecular Biology Open Software Suite", *Trends Genet.*, vol. 16, no. 6, pp. 276–277, 2000.

[56] F. Sievers and D. G. Higgins, "Clustal Omega for making accurate alignments of many protein sequences", *Protein Sci.*, vol. 27, no. 1, pp. 135–145, 2018.

[57] L. T. Nguyen, H. A. Schmidt, A. Von Haeseler, and B. Q. Minh, "IQ-TREE: A fast and effective stochastic algorithm for estimating maximum-likelihood phylogenies", *Mol. Biol. Evol.*, vol. 32, no. 1, pp. 268–274, 2015.

[58] K. Umezawa, H. Kojima, Y. Kato, and M. Fukui, "Disproportionation of inorganic sulfur compounds by a novel autotrophic bacterium belonging to Nitrospirota", *Syst. Appl. Microbiol.*, vol. 43, no. 5, 2020.

[59] A. P. Florentino, I. A. C. Pereira, S. Boeren, M. van den Born, A. J. M. Stams, and I. Sánchez-Andrea, “Insight into the sulfur metabolism of *Desulfurella amilsii* by differential proteomics”, *Environ. Microbiol.*, vol. 21, no. 1, pp. 209–225, 2019.

[60] Y. Shen, R. Buick, and D. E. Canfield, “Isotopic evidence for microbial sulphate reduction in the early Archaean era.”, *Nature*, vol. 410, no. 6824, pp. 77–81, 2001.

[61] P. Philippot, M. Van Zuilen, K. Lepot, C. Thomazo, J. Farquhar, and M. J. Van Kranendonk, “Early Archaean microorganisms preferred elemental sulfur, not sulfate.”, *Science*, vol. 317, no. 5844, pp. 1534–1537, 2007.

[62] M. Löffler *et al.*, “DsrL mediates electron transfer between NADH and rDsrAB in *Allochromatium vinosum*”, *Environ. Microbiol.*, vol. 22, no. 2, pp. 783–795, 2020.

[63] K. Fuseler, D. Krekeler, U. Sydow, and H. Cypionka, “A common pathway of sulfide oxidation by sulfate-reducing bacteria”, *FEMS Microbiol. Lett.*, vol. 144, no. 2–3, pp. 129–134, 1996.

[64] H. Cypionka, A. M. Smock, and M. E. Böttcher, “A combined pathway of sulfur compound disproportionation in *Desulfovibrio desulfuricans*”, *FEMS Microbiol. Lett.*, vol. 166, pp. 181–186, 1998.

[65] K. Finster, “Microbiological disproportionation of inorganic sulfur compounds”, *J. Sulfur Chem.*, vol. 29, no. 3–4, pp. 281–292, 2008.

[66] K. Anantharaman, M. B. Duhaime, J. A. Breier, K. Wendt, B. M. Toner, and G. J. Dick, “Sulfur Oxidation Genes in Diverse Deep-Sea Viruses”, *Science.*, vol. 344, no. 6185, pp. 757–760, 2014.

Chapter 3

DsrC is involved in fermentative growth and interacts directly with the FlxABCD-HdrABC complex in *Desulfovibrio vulgaris* Hildenborough

Contents

Contributions

All experiments and analyses were performed by Delfim Ferreira, except the whole cell proteomic analysis and respective statistic analysis done by Lichun Zhang, Jacob Waldbauer and William Leavitt, and the mass spectrometry analysis performed by the ITQB/iBET UniMS Mass Spectrometry Unit.

The experiment design was performed by Delfim Ferreira, Sofia Venceslau and Inês Cardoso Pereira.

This section was published as

D. Ferreira, S.S. Venceslau, R. Bernardino, A. Preto, L. Zhang, J.R. Waldbauer, W.D. Leavitt, I.A.C. Pereira (2023) “DsrC is involved in fermentative growth and interacts directly with the FlxABCD-HdrABC complex in Desulfovibrio vulgaris Hildenborough” Environ Microbiol 25(5)

3.1 – Summary

DsrC is a key protein in dissimilatory sulfur metabolism, where it works as co-substrate of the dissimilatory sulfite reductase DsrAB. DsrC has two conserved cysteines in a C-terminal arm that are converted to a trisulfide upon reduction of sulfite. In sulfate-reducing bacteria, DsrC is essential and previous works suggested additional functions beyond sulfite reduction. In this chapter it is studied whether DsrC also plays a role during fermentative growth of *Desulfovibrio vulgaris* Hildenborough, by studying two strains, one where the functionality of DsrC is impaired by a lower level of expression (IPFG07) and another additionally absent of one conserved Cys (IPFG09). Growth studies coupled with metabolite and proteomic analyses reveal that fermentation leads to lower levels of DsrC, but impairment of its function results in reduced growth by fermentation and a shift towards more fermentative metabolism during sulfate respiration. In both respiratory and fermentative conditions there is increased abundance of the FlxABCD-HdrABC complex and Adh alcohol dehydrogenase in IPFG09 versus the wild type, which is reflected in higher production of ethanol. Pull-down experiments confirmed a direct interaction between DsrC and the FlxABCD-HdrABC complex, through the HdrB subunit. Dissimilatory sulfur metabolism, where sulfur compounds are used for energy generation, is a key process in the ecology of anoxic environments and is more widespread among bacteria than previously believed. Two central proteins for this type of metabolism are DsrAB dissimilatory sulfite reductase and its co-substrate DsrC. Using physiological, proteomic and biochemical studies of *Desulfovibrio vulgaris* Hildenborough and mutants affected in DsrC functionality, this study shows that DsrC is also relevant for fermentative growth of this model organism and that it interacts directly with the soluble FlxABCD-HdrABC complex that links the NAD(H) pool with dissimilatory sulfite reduction.

3.2 – Introduction

Sulfate-reducing prokaryotes (SRP) are a group of microorganisms characterized by being able to obtain energy through the reduction of sulfate, using electrons resultant from the oxidation of hydrogen or organic acids [1]. Some of these organisms also grow by fermentation through oxidation of substrates such as pyruvate and lactate, with substrate-level phosphorylation [2]–[4].

The DsrAB and DsrC proteins play an essential role in the respiratory metabolism of SRP [5]–[7]. DsrAB contains a coupled siroheme-[4Fe-4S] cofactor which covalently binds sulfite, being this reduced and incorporated in a S^0 valence state between two conserved cysteine residues of DsrC, forming a trisulfide bridge [5], [7]. The trisulfide in DsrC is proposed to be reduced by the DsrMKJOP transmembrane complex, resulting in the reduction of DsrC and release of sulfide, coupled with proton translocation [7]–[11].

The formation of the trisulfide bridge in DsrC involves two conserved Cys residues: the penultimate residue, CysA, and another located 11 residues before, CysB [7]. The CysA residue was found next to the DsrAB substrate-binding site in the DsrABC crystal structure [5] and is the first to react with sulfite, forming a persulfide. Its mutation to an alanine residue generates a DsrC with an altered catalytic profile, and did not yield viable cells [7]. CysB is responsible for the later reduction of the CysA-persulfide, yielding the S^0 trisulfide product, and its mutation to Ala results in the formation of a persulfide sulfenate in CysA, which cannot react further and is released as a product. The CysB residue is not strictly essential for cell viability, but its mutation results in cells displaying a growth deficit, by having a higher duplication time and achieving a lower biomass yield [7], [12].

DsrC is widespread among organisms containing DsrAB and able to metabolize sulfur compounds for their energy metabolism [10], but the role of this protein seems not to be restricted to intermediating DsrAB and DsrMKJOP catalysis. Previous studies have shown the *dsrC* gene expression to be higher than of *dsrAB* [13], which results in a higher abundance of DsrC compared with DsrAB, being most of it not associated with DsrAB [14]. In fact, *dsrC* was shown to be more expressed in stationary rather than exponential phase under lactate-sulfate growth conditions [3], [15], [16], stressing an additional function for DsrC besides the respiratory energy metabolism. The

importance of DsrC is such that creating a mutant strain carrying the *dsrC* deletion was not viable in the sulfate-reducer *Desulfovibrio vulgaris* Hildeborough, even under fermentative conditions [7], and the same was observed for the sulfur oxidizer *Allochromatium vinosum* [17]. Moreover, in *A*. *vinosum*, DsrC was shown to bind a region upstream of *dsrAB*, which supports a regulatory function for this protein [18]. In some organisms, the *dsrC* gene is present close to the operon of several transmembrane complexes other than *dsrMKJOP* [10], hinting towards DsrC having additional interacting partners and additional roles in the energy metabolism. In fact, it has been already suggested that DsrC could work as a redox hub in dissimilatory sulfur metabolism, linking oxidation of several substrates to the reduction of sulfate [10].

Some predicted interacting partners of DsrC are proteins containing the CCG motif (CX_nCCGX_mCXXC) [10], such as the subunits DsrK from DsrMKJOP [8], HdrB from HdrABC [19], [20], HmcF from HmcABCDEF [21] and TmcB from TmcABCD [22]. The CCG motif is well characterized in the methanogenic heterodisulfide reductase HdrABC, and harbors a non-cubane [4Fe–4S] center with distinct spectroscopic properties [19], [23], responsible for catalyzing the reduction of the heterodisulfide formed between coenzymes M and B in the last step of methanogenesis [24]–[26]. In SRP, the same CCG motif is present in DsrK and is suggested to be catalytically responsible for DsrC-trisulfide reduction [8], [10], [11]. Some SRP also encode the HdrABC protein complex, and in *D*. *vulgaris* this is associated with the flavin oxidoreductase FlxABCD, being essential when ethanol is the electron donor for sulfate reduction [27]. In the sulfate-reducer archaeon *Archaeoglobus fulgidus*, the HdrABC complex is associated with the [NiFe]-hydrogenase MvhAGD, suggesting a link between hydrogen oxidation and sulfate reduction [23], [27]. The HdrABC can couple disulfide reduction with ferredoxin reduction through flavin-based electron bifurcation (FBEB), and is suggested to serve as an alternative electron route for sulfate reduction through DsrC, with energy coupling occurring by electron bifurcation instead of chemiosmotically by DsrMKJOP [21].

In the present study, *D*. *vulgaris* Hildenborough (*Dv*H) was used as a model SRP to investigate other possible roles of DsrC, trying to identify further physiological partners. For this, both growth and metabolite analyses were performed for *Dv*H wild type (WT) and two strains partially impaired in DsrC function, having complemented this

with measurement of protein expression patterns during respiration and fermentation. The results show that DsrC also plays a role during fermentative growth and provide evidence for a direct interaction between DsrC and the FlxABCD-HdrABC complex through HdrB. During fermentation, sulfur compounds are not turned over in energy metabolism, and the extra sulfur in the DsrC trisulfide is likely to derive from the intracellular sulfur pool from sulfur assimilation.

3.3 – Material and Methods

3.3.1 – Strains, plasmids and growth conditions

Desulfovibrio vulgaris Hildenborough wild-type (*Dv*H WT) was used for the construction of the mutant strains *Dv*H IPFG07 and *Dv*H IPFG09, according to Santos *et al*., 2015 [7].

The genes *hdrC* (locus tag: AF1376) and *hdrB* (locus tag: AF1375) were individually amplified from *Archaeoglobus fulgidus* VC-16 (DSM 4304) genomic DNA. The first using primers #1 and #2, and cloned in pETDuet-1 using *Nco*I and *Afl*II restriction sites, and the second using primers #3 and #4 and cloned into a modified pET22b(+) vector encoding a Strep-tag sequence, using *Nde*I and *BamH*I restriction sites. The *hdrB*-Strep gene fragment from pET22b(+)-AF*hdrB*-Strep was later cloned into pETDuet-1 already encoded with *hdrC*, using primers #5 and #6 and *Nde*I and *EcoR*V restrictions sites, resulting in pETDuet-1-AF*hdrC*-Strep-AF*hdrB*-Strep. This vector contains both *hdrC* and *hdrB* genes, each with a Strep-tag and a dedicated promoter. Then, the "*hdrC*-Strep-*hdrB*-Strep" fragment was subcloned into pMO719, a vector designed for use in *D*. *vulgaris* [28]. This vector, pMO719-AF*hdrC*-Strep-AF*hdrB*-Strep, was constructed via SLIC (sequence ligation independent cloning) according to Li & Elledge (2007) [29] using vector pETDuet-1-AF*hdrC*-Strep-AF*hdrB*-Strep as template and primers #7 and #8 to flank the upstream and downstream regions of "*hdrC*-Strep-*hdrB*-Strep", and pMO719 vector and primers #9 and #10, #11 and #12, for the vector backbone. The assembled plasmid was transformed into *E*. *coli* α-select Silver Efficiency (Bioline®) and selected with spectinomycin. After sequence confirmation, the plasmid pMO719-AF*hdrC*-Strep-AF*hdrB*-Strep was electroporated into *Dv*H WT cells using the method described in Keller *et al*., 2011 [30], creating *D*. *vulgaris* strain IPDF01. A descriptive list of strains, plasmids and primers used throughout this study are summarized in **Table 3.1**, **Table 3.2** and **Table 3.3**, respectively.

Table 3.1 – List of strains used in this study

Strain	Genotype	Source or reference
D. vulgaris strains		
*Dv*H WT	*D. vulgaris* Hildenborough ATCC 29579	ATCC
*Dv*H IPFG07	*Dv*H Δ*dsrC* + pMODsrC	Santos *et al.*, 2015
*Dv*H IPFG09	*Dv*H Δ*dsrC* + pMODsrC (C26A, C93A)	Santos *et al.*, 2015
*Dv*H IPDF01	*Dv*H WT + pMO719-AF*hdrC*-Strep-AF*hdrB*-Strep	This work
A. fulgidus strains		
A. fulgidus WT	*A. fulgidus* DSM 4304 / VC-16	DSMZ
E. coli strains		
E. coli α-select Silver Efficiency	F- *deo*R *end*A1 *rec*A1 *rel*A1 *gyr*A96 *hsd*R17(r_k^-, m_k^+) *sup*E44 *thi*-1 *pho*A Δ(*lac*ZYA *arg*F)U169 Φ80*lac*ZΔM15λ-	Bioline

Table 3.2 – List of plasmids used in this study

Plasmid	Relevant characteristics	Source or reference
pET22b(+)	Bacterial protein expression vector with His6x-tag at C-terminal; Amp^R	Novagen
pETDuet-1	Bacterial protein expression vector containing two multiple cloning sites (MCS), each of which preceded by a T7 promoter/lac operator and a ribosome binding site; Amp^R	Novagen
pET22b(+)-AF*hdrB*-Strep	pET-22b(+) encoding *hdrB* from *A. fulgidus* (using restriction sites *Nde*I and *BamH*I), Strep-tag at C-terminal; Amp^R	This work
pETDuet-1-AF*hdrC*-Strep-AF*hdrB*-Strep	pETDuet-1 encoding *hdrC* and *hdrB* from *A. fulgidus* (using restriction sites *Nco*I/*Afl*II, and *Nde*I/*EcoR*V, respectively), each gene with a Strep-tag at C-terminal; Amp^R	This work
pMO719	pCR8/GW/TOPO containing SRB replicon (pBG1); $Spec^R$	Keller *et al.*, 2009
pMO719-AF*hdrC*-Strep-AF*hdrB*-Strep	pMO719 encoding *hdrC* and *hdrB* from *A. fulgidus*, each with a Strep-tag at C-terminal; $Spec^R$	This work
pMO9075	pCR8/GW/TOPO with pBG1, Km^R gene *aph(3')-II* promoter, multicloning site; $Spec^R$	Keller *et al.*, 2011
pMODsrC	pMO9075 encoding *dsrC* with N-terminal His6x-tag; $Spec^R$	Santos *et al.*, 2015
pMODsrC (C26A, C93A)	pMO9075 encoding *dsrC* with N-terminal His6x-tag and C26A and C93A substitutions; $Spec^R$	Santos *et al.*, 2015

Table 3.3 – List of primers used for plasmid construction

#	Primer	Primer sequence (5' → 3')	Observations
1	hdrC_AF_forward	CATCCATGGCGAGAGTTGTGAGGCTGCC	Amplification of *hdrC* from *Af* genomic DNA to pETDuet-1 *Nco*I restriction site
2	hdrC_AF_reverse	TCTCTTAAGTTATTATTTTTCGAACTGCGGGTGGCTCCACCGAATTAAGCCCAGCT	Amplification of *hdrC* from *Af* genomic DNA to pETDuet-1 *Afl*II restriction site; primer includes sequence for Strep-tag
3	hdrB_AF_forward	GGCTTAATTCGGTCATATGTTTATGAAGTACG	Amplification of *hdrB* from *Af* genomic DNA to pET22b(+) *Nde*I restriction site
4	hdrB_AF_reverse	CAAAACCGATAAGGATCCTTCTCTCCC	Amplification of *hdrB* from *Af* genomic DNA to pET22b(+) *BamH*I restriction site
5	hdrB_pET22b_AF_forward	GGCTTAATTCGGTCATATGTTTATGAAGTACG	Amplification of *hdrB* from pET22b(+)-HdrB-AF to pETDuet-1 *Nde*I restriction site
6	hdrB_pET22b_AF_reverse	CGGCCGATATCTTATTATTTTTCGAACTGCG	Amplification of *hdrB* from pET22b(+)-HdrB-AF to pETDuet-1 *EcoR*V restriction site
7	hdrC-s-hdrB-s_forward	CCCAGGAGGTACCATATGGCGAGAGTTGTGAGGCT	Construction of pMO719-HdrC-Strep-HdrB-Strep by SLIC (amplification of the HdrC-Strep-HdrB-Strep fragment)
8	hdrC-s-hdrB-s_reverse	ATCGGGTCTTTTCGTTTATTATTTTTCGAACTGCGGGTGG	Construction of pMO719-HdrC-Strep-HdrB-Strep by SLIC (amplification of the HdrC-Strep-HdrB-Strep fragment)
9	pMO719_1_forward	TTCGAAAAATAATAAACGAAAAGACCCGATCATGAAGGGG	Construction of pMO719-HdrC-Strep-HdrB-Strep by SLIC (amplification of the pMO719 backbone)
10	pMO719_2_reverse	CGACTGAGCCTTTCGTTTTATTTGATGCCTGGCAGTTCCC	Construction of pMO719-HdrC-Strep-HdrB-Strep by SLIC (amplification of the pMO719 backbone)
11	pMO719_3_forward	GGGAACTGCCAGGCATCAAATAAAACGAAAGGCTCAGTCG	Construction of pMO719-HdrC-Strep-HdrB-Strep by SLIC (amplification of the pMO719 backbone)
12	pMO719_4_reverse	CACAACTCTCGCCATATGGTACCTCCTGGGACTGCATTGC	Construction of pMO719-HdrC-Strep-HdrB-Strep by SLIC (amplification of the pMO719 backbone)

D. *vulgaris* respiratory and fermentative growths were performed anaerobically at 37 °C in 100 ml flasks containing 50 mL MO medium, using 2% (v/v) fresh precultured cells grown in pyruvate/sulfate (60 mM/3 mM) as inoculum. For respiratory conditions, 30 mM sodium lactate was used as electron donor and 30 mM sodium sulfate as electron acceptor. For fermentative conditions, 60 mM sodium pyruvate was used as carbon and electron source. The culture medium of mutant strains was supplemented with 400 µg/mL G418 and 100 µg/mL spectinomycin [31]. To avoid masking the growth profiles and outcomes, yeast extract was intentionally not used. The optical density (OD) of the cultures was monitored at the wavelength of 600 nm with a DR3900 VIS Spectrophotometer (Hach). Statistically significant relationships were determined using one-way analysis of variance (ANOVA), with a probability value (p) of < 0.05 being the statistical significance considered.

3.3.2 – Metabolites' measurement

Concentration of pyruvate, acetate and lactate was measured by high-performance liquid chromatography (HPLC), using an Alliance 2695 Waters system equipped with an IR detector (2124 Differential Refractometer, LKB Bromma). By using an injection volume of 20 µL, the compounds were separated on an Aminex HPX-87H column (Bio-Rad) under isocratic conditions, with 0.005 N H_2SO_4 as mobile phase and a flow rate of 0.4 $mL.min^{-1}$ at 36 °C. Ethanol concentration was assessed with an enzymatic kit (AK00061, NZYTech). Production of hydrogen was measured from sampling the flask headspace into a gas chromatographer, using a TraceGCUltra (Thermo Scientific) equipped with a thermal conductivity detector (TCD), using a MolSieve 5A 80/100 column (Alltech) and nitrogen as carrier gas.

3.3.3 – Whole cell proteomic analysis

Bacterial growths were performed as previously described. At late exponential phase, the content of each anaerobic flask, approximately 50 mL, was collected anoxically and aseptically, and then centrifuged at 5000 x *g* for 15 min at 4 °C. The supernatant was discarded and the cell pellet was flash-frozen in liquid nitrogen, and

then stored at -80 °C. Cell pellets were extracted by vortexing and heating (95 °C, 20 min) in a reducing and denaturing buffer composed of 1% SDS, 10 mM DTT and 200 mM Tris (pH 8.0), and cysteine thiols alkylated with 40 mM iodoacetamide. Proteins were purified by a modified eFASP (enhanced filter-aided sample preparation) protocol [32], using Sartorius Vivacon 500 concentrators (30 kDa nominal cutoff). Proteins were digested overnight at 37 °C with MS-grade trypsin, and peptides were eluted from the concentrator dried by vacuum centrifugation. For quantitative analysis, digested peptides were isotopically labeled at both N- and C-termini using the diDO-IPTL (dimethylation-deuteration and oxygen-exchange – isobaric peptide terminal labelling) methodology [33]. Briefly, C-termini were labeled with either oxygen-16 or -18 by enzymatic exchange in isotopic water of > 98 atom % enrichment. N-termini were labeled with either un- or dideuterated formaldehyde via reductive alkylation using sodium cyanoborohydride. Peptide extracts from each sample were split and aliquots labeled separately with $CD_2O/^{16}O$ and $CH_2O/^{18}O$, the latter were pooled to serve as a common internal standard for quantification. Aliquots of the ^{16}O-labeled peptides and ^{18}O-labeled internal standard were mixed 1:1 (v/v) and analyzed by LC-MS for protein expression quantification. For LC-MS analysis, peptide samples were separated on a monolithic capillary C18 column (GL Sciences Monocap Ultra, 100 µm I.D. × 200 cm length) using a water-acetonitrile + 0.1% formic acid gradient (2%-50% AcN over 180 min) at 360 nl/min using a Dionex Ultimate 3000 LC system with nanoelectrospray ionization (Proxeon Nanospray Flex source). Mass spectra were collected on an Orbitrap Elite mass spectrometer (Thermo) operating in a data-dependent acquisition (DDA) mode, with one high-resolution (120,000 $m/\Delta m$) MS1 parent ion full scan triggering Rapid-mode 15 MS2 CID fragment ion scans of selected precursors. Proteomic mass spectral data were analyzed using MorpheusFromAnotherPlace (MFAP) [33], using the predicted proteome of *Dv*H as a search database. Precursor and product ion mass tolerances for MFAP searches were set to 20 ppm and 0.6 Da, respectively. Static cysteine carbamidomethylation and variable methionine oxidation, N-terminal (d4)-dimethylation, and C-terminal $^{18}O_2$ were included as modifications. False discovery rate for peptide-spectrum matches was controlled by target-decoy searching to < 0.5%. Protein-level relative abundances and standard errors

were calculated in R using the Arm postprocessing scripts for diDO-IPTL data (github.com/waldbauerlab) [33].

Significantly differential protein expression between experimental conditions was determined by calculating a *Z*-score for protein abundance differences by taking the difference in the mean (log_2-transformed) protein abundance between conditions and dividing it by the sum of the total uncertainly estimate for that protein in the two conditions. This total uncertainty estimate for a given condition was taken as the root-square sum of the standard deviation of a protein's abundance across the biological replicates of that condition plus the average standard error of the protein's abundance across quantified spectra within each replicate. Proteins were considered valid for analysis when presenting a number of spectra equal or higher than 3 in the two conditions used for comparison. False discovery rate for differential protein abundance between conditions was controlled by the Benjamini-Hochberg method [34], with a *p*-value threshold of < 0.1. Information about Clusters of Orthologous Groups (COGs) of proteins was obtained from the MicrobesOnline database (http://www.microbesonline.org/).

3.3.4 – Pull-down assays

For the pull-down of His-tagged DsrC, *Dv*H WT and *Dv*H IPFG07 cells were grown in 1) MO medium supplemented with 40 mM ethanol, 20 mM sodium sulfate and 1 g/L yeast extract, and in 2) MO medium supplemented with 60 mM sodium pyruvate and 1 g/L yeast extract. For the Strep-tagged HdrB pull-down, *Dv*H WT and *Dv*H IPDF01 cells were grown in MO medium supplemented with 30 mM sodium lactate, 30 mM sodium sulfate and 0.5 g/L yeast extract. In both cases, expression of the plasmid-encoded protein was assured with addition of 100 µg/mL spectinomycin.

Cells were collected by centrifugation at the end of exponential phase. Pelleted cells were mechanically disrupted with glass beads using the Minilys homogenizer (Bertin Technologies), and soluble fraction separated by centrifugation (17000 x *g*, 20 min, 4 °C). The protein concentration was determined by the Bradford method (BioRad) with bovine serum albumin as standard (NZYTech). The same amount of total soluble proteins was loaded for *Dv*H WT (negative control) and IPFG07 pull-down assays.

For pull-down of His-tagged DsrC, pelleted cells of *Dv*H WT or IPFG07 strain were resuspended in 25 mM KH_2PO_4/K_2HPO_4 (pH 7.4), 100 mM NaCl and 10% glycerol before disruption. Soluble fractions were injected in a HiTrap™ IMAC HP column (GE Healthcare, 1 mL) charged with Ni^{2+} and assembled on a FPLC AKTA™ system. His-tagged DsrC was eluted with increasing imidazole concentrations, and eluted fractions (10 µg) were separated in an SDS-PAGE (12% acrylamide (w/v)) and transferred to 0.45 µm PVDF membranes (Roche) (transfer buffer: 48 mM Tris-HCl pH 9.2 and 39 mM glycine) using a Mini Trans-Blot® electrophoretic transfer cell (BioRad) at 100 V during 30 min at 4 °C. The membrane was incubated with a buffer containing 20 mM Tris-HCl (pH 7.6), 150 mM NaCl, 0.015% (v/v) Tween 20, 1.2% (w/v) non-fat milk and the anti-FlxA primary antibody (FlxA locus tag: DVU2399; polyclonal antibody produced by Davids Biotechnologie GmbH) at a 1:3000 dilution, for 1 h at RT, followed by incubation with the same buffer but containing the anti-rabbit IgG-alkaline phosphatase antibody at a 1:15000 dilution, for 45 min at RT. Between every incubation step, membranes were washed three times with TBS buffer. The protein detection was performed by incubating with alkaline phosphatase buffer (100 mM Tris-HCl pH 9.5, 100 mM NaCl and 250 µM $MgCl_2$) and NBT-BCIP (nitro-blue tetrazolium chloride/5-bromo-4-chloro-3-indolylphosphate toluidine) substrates (Sigma-Aldrich).

For the pull-down of Strep-tagged HdrB from *A. fulgidus*, the *Dv*H WT or IPDF01 strain cell resuspension and disruption was performed in 50 mM Tris-HCl (pH 7.5), 100 mM NaCl and 10% (v/v) glycerol. Soluble fractions were loaded in a gravity flow column containing Strep-Tactin® resin (IBA Lifesciences). After five washing steps, the Strep-tagged HdrB was eluted with 2.5 mM D-desthiobiotin. The elution fractions (20 µg) were analyzed in a 10% Tricine-SDS-PAGE gel, and protein bands identified by MALDI-TOF/TOF (ITQB/iBET UniMS Mass Spectrometry Unit, Oeiras, Portugal).

3.4 – Results

3.4.1 – Growth in respiratory and fermentative conditions

The consequences of interfering with DsrC were assessed in strains *Dv*H IPFG07, which has lower DsrC expression, and in *Dv*H IPFG09 that additionally has a CysB to Ala point mutation, preventing formation of the DsrC trisulfide. Growth experiments were performed under respiratory and fermentative conditions coupled with metabolite and quantitative whole cell proteomic analysis (**Table 3.4**, **Figure 3.1** and **Figure 3.2**).

Table 3.4 – Doubling time (T_d) and maximum OD at 600 nm (Max. OD_{600}) for *Dv*H WT, IPFG07 and IPFG09, in sulfate respiration conditions (30 mM lactate and 30 mM sulfate) and pyruvate fermentation conditions (60 mM pyruvate). Data are mean ± SD (n = 3 independent experiments)

	Sulfate Respiration		Pyruvate Fermentation	
Strain	**T_d (h)**	**Max. OD_{600}**	**T_d (h)**	**Max. OD_{600}**
***Dv*H WT**	2.8 ± 0.1	0.915 ± 0.004	30.6 ± 2.0	0.160 ± 0.001
***Dv*H IPFG07**	4.0 ± 0.1	0.896 ± 0.008	51.1 ± 4.5	0.125 ± 0.012
***Dv*H IPFG09**	8.2 ± 0.1	0.656 ± 0.003	89.8 ± 4.7	0.072 ± 0.008

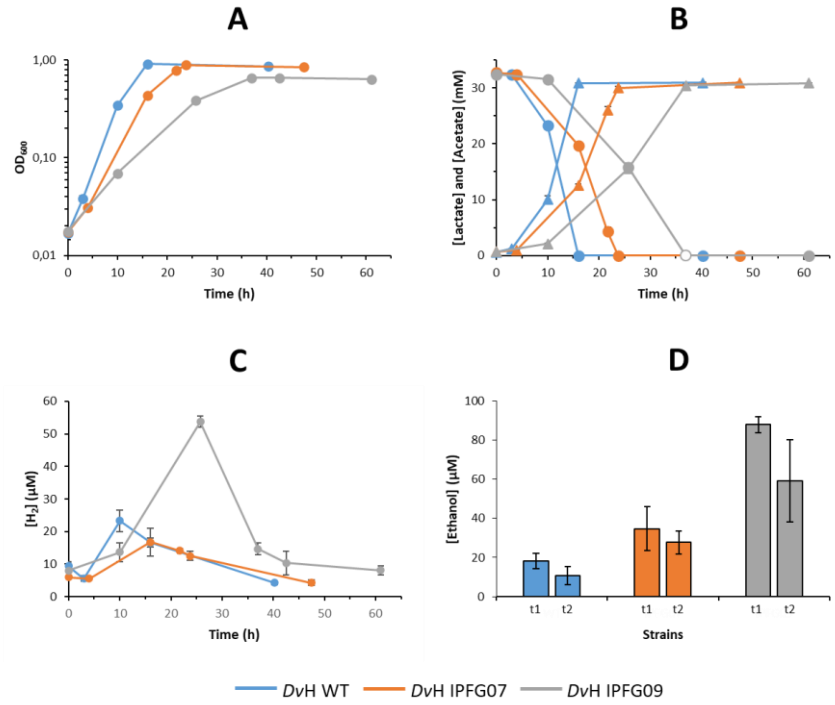

Figure 3.1 – Growth of *Dv*H wild-type (blue), *Dv*H IPFG07 (orange) and *Dv*H IPFG09 (gray) in MO medium with lactate and sulfate **(A)**, respective lactate consumption (circles) and acetate production (triangles) **(B)**, and hydrogen production **(C)**. Ethanol production **(D)** was measured only at the mid-exponential phase (t1) and at late-exponential phase (t2). All data are mean ± standard deviation (n = 3).

As observed in **Figure 3.1A**, when using lactate as electron donor and sulfate as electron acceptor for respiratory growth, *Dv*H WT grew faster (T_d = 2.8 h ± 0.1 h) and reached an higher cell density (OD_{max} = 0.915 ± 0.004), followed by *Dv*H IPFG07 (T_d = 4.0 h ± 0.1 h; OD_{max} 0.896 ± 0.008) and then by *Dv*H IPFG09, whose duplication time was significantly higher (T_d = 8.2 h ± 0.1 h) and achieved ≈ 30% lower cell density when compared with the WT (OD_{max} = 0.656 ± 0.003), which is in line with previous results [7], [12] (**Table 3.4**), particularly when yeast extract is not added into medium. This bacterial growth was complemented with the measurement of consumed carbon substrates and main metabolites produced,

namely the consumption of lactate and the production of acetate (**Figure 3.1B**), production of hydrogen (**Figure 3.1D**) and production of ethanol (**Figure 3.1E**). The growth pattern for each strain follows the rate for lactate consumption and acetate production, with *Dv*H WT consuming lactate and producing acetate at a higher rate, followed by *Dv*H IPFG07 and then by *Dv*H IPFG09, as expected from growth rates and already observed [12]. All three strains produced low amounts of hydrogen during the mid-exponential phase, which was consumed during second half part of exponential phase, with *Dv*H IPFG09 standing out by producing approximately twice more hydrogen than the other two strains: 53.8 ± 1.7 µM by *Dv*H IPFG09, in comparison with 23.3 ± 3.3 µM for *Dv*H WT and 16.7 ± 4.4 µM for *Dv*H IPFG07. The concentration of ethanol was also measured namely at four time-points: beginning of growth, mid-exponential, late-exponential and stationary phases. Similarly, to what was observed for hydrogen, all three strains produced low amounts of ethanol during growth being the higher concentration during mid-exponential phase, in which *Dv*H IPFG09 was the highest producer strain of ethanol by 5-fold versus *Dv*H WT (88.0 µM ± 4.2 µM for *Dv*H IPFG09 in comparison with 18.1 µM ± 4.0 µM for *Dv*H WT and 34.8 µM ± 11.3 µM for *Dv*H IPFG07). No ethanol was detected at the beginning of growth and at stationary phase of all strains.

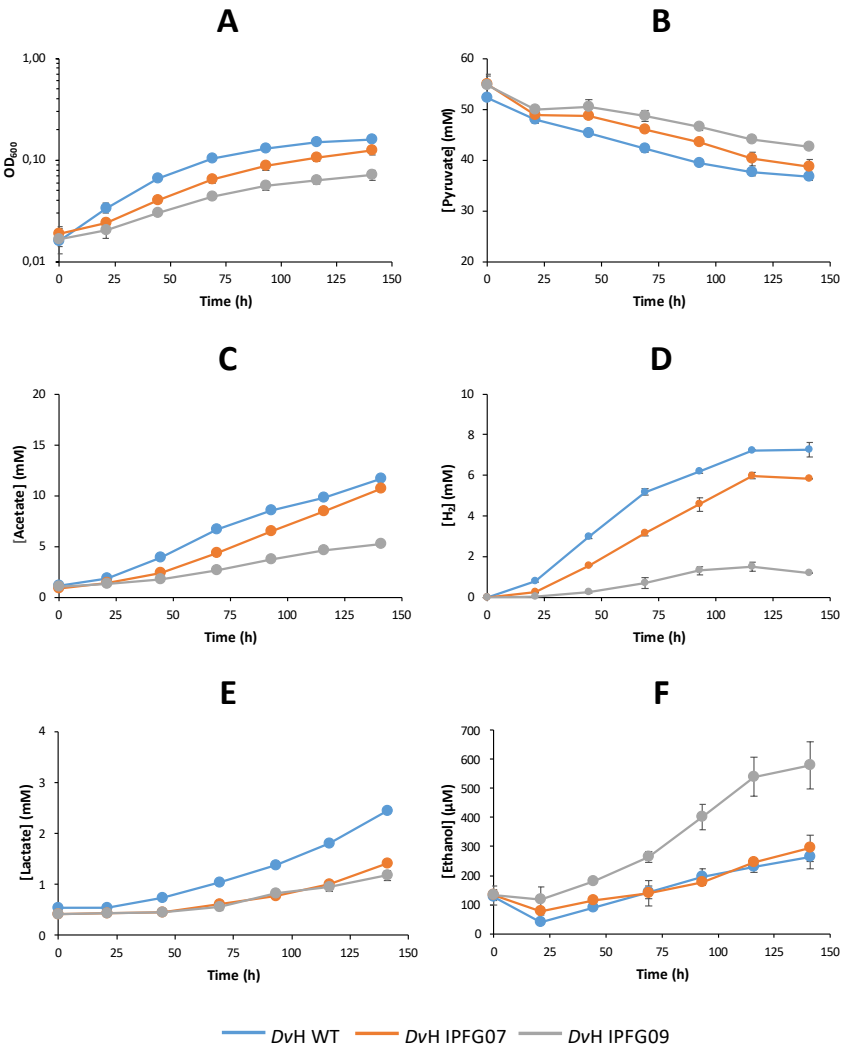

Figure 3.2 – Growth of *Dv*H wild-type (blue), *Dv*H IPFG07 (orange) and *Dv*H IPFG09 (gray) in MO medium with 30 mM pyruvate **(A)**, and respective pyruvate consumption **(B)**, and acetate **(C)**, hydrogen **(D)**, lactate **(E)** and ethanol **(F)** production. All data are mean ± standard deviation (n = 3).

In fermentative conditions, surprisingly the phenotypic growth behaviour was similar to the one observed in respiration for the three strains (**Figure 3.2A**), with *Dv*H WT presenting a fastest growth (T_d = 30.6 h ± 2.0 h) and reaching a highest bacterial density (OD_{max} =

0.160 ± 0.001) than *Dv*H IPFG07 (T_d = 51.1 h ± 4.5 h, OD_{max} = 0.125 ± 0.012) and *Dv*H IPFG09, being the latest the slower (T_d = 89.8 h ± 4.7 h) and not able to achieve a similar cell density (OD_{max} = 0.072 ± 0.008) (**Table 3.4**). This shows that *Dv*H IPFG09 strain grew 3 times slower and it was only able to obtain energy to reach half of the cellular density than *Dv*H WT.

The fermentative growth was complemented with measurement of the substrate pyruvate (**Figure 3.2B**), and the main products acetate (**Figure 3.2C**), hydrogen (**Figure 3.2D**), lactate (**Figure 3.2E**) and ethanol (**Figure 3.2F**). As observed for respiration, the rate for substrate consumption and product formation matches the bacterial growth rate, being *Dv*H WT able to consume pyruvate at a faster rate, which results in a higher rate for acetate, lactate and hydrogen production, and therefore a highest growth rate. Acetate was the main organic product resultant from pyruvate fermentation, with lactate also being detected at lower concentrations. These were produced in higher amounts by *Dv*H WT and 2-fold less in *Dv*H IPFG09. Hydrogen, a typical end product from bacterial fermentation [2], followed the same pattern of being produced at a higher concentration in *Dv*H WT. As opposed to what was observed in respiration, there was accumulation of the produced hydrogen and it was not consumed back, with *Dv*H IPFG09 showing an inability to produce as much as *Dv*H WT and *Dv*H IPFG07 even when taking into consideration the cell density of each strain, since *Dv*H IPFG09 produced 36% of the hydrogen when normalized by the final OD. All three strains also produced small amounts of ethanol, another end product of fermentation, which was not consumed at a later stage, as observed in respiration. *Dv*H IPFG09 strain produced nearly the double amount of ethanol from nearly half of maximum cell density, when compared with the other strains, meaning that normalized per OD, *Dv*H IPFG09 produced nearly five times more than the *Dv*H WT.

3.4.2 – Effect on whole cell proteome

To further evaluate the effects of modifying DsrC, the proteomes of *Dv*H WT and *Dv*H IPFG09 were measured under respiratory and fermentative conditions. For this purpose, cells were collected at the late exponential phase, and their whole cell proteome analyzed by Mass Spectrometry using the diDO-IPTL methodology [33]. Various MS runs were performed, in order to allow comparison of all the

possible combinations, namely *Dv*H WT in fermentation versus respiration, *Dv*H IPFG09 in fermentation versus respiration, *Dv*H IPFG09 versus *Dv*H WT in respiration, and *Dv*H IPFG09 versus *Dv*H WT in fermentation.The genome of *D*. *vulgaris* ATCC 29579 contains 3545 predicted protein-coding genes, and the several analysis performed could cover between 33% and 39% of its genome, which is in line with coverages previously observed using the same strain and method [35]. In all analysis, most proteins affected, positively or negatively, belong to cluster of orthologous groups (COG) related with energy generation and growth, such as “energy production and conversion” (COG classification: C), “amino acid transport and metabolism” (COG classification: E) and “translation, ribosomal structure and biogenesis” (COG classification: J). The MS proteomic analysis has a particular limitation, since there are two protein classes known to be difficult or barely detected due to technical reasons, namely small cytochrome *c* proteins and integral membrane proteins. The prior because it generates peptides linked to the heme giving rise to unidentifiable peaks, while the latter is characterized by its hydrophobic nature that results in being insoluble in aqueous solutions and therefore less likely to extract and derivatize without special protocols. *Dv*H has several proteins belonging to these groups, particularly membrane-bound redox complexes, which are of special interest here. However, both cases require a specialized extraction and/or analytical regime, and was out of the scope of this study.

3.4.3 – *Dv*H WT proteomic changes

For the analysis of the *Dv*H WT proteome under respiratory and fermentative conditions, a total of 550 proteins were considered valid. Of these, 84 proteins were found to be more abundant and 89 proteins less abundant in fermentation conditions compared with respiration (**Figure 3.3**).

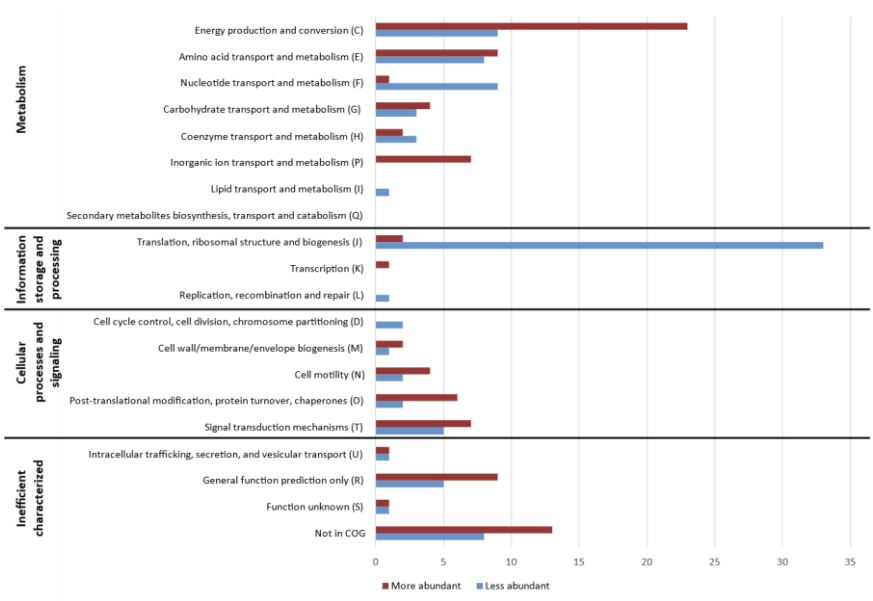

Figure 3.3 – Number of more abundant (red) and less abundant (blue) proteins in fermentation versus respiration, for *Dv*H WT. Proteins are categorized by general function and respective COG. Only proteins presenting $Log_2 > 0.5$ and $p < 0.1$ are considered.

As can be seen in **Figure 3.4**, the majority of proteins involved in the sulfate reduction pathway were more abundant during fermentative conditions, namely sulfate adenylyltransferase (Sat), pyrofosfatase (PpaC), adenosine-5'-phosphosulfate reductase (ApsAB) (DVU0846-7), QmoAB and QrcB. The abundance of DsrAB was not affected by the growth conditions here tested. This result is in line with previous reports [36], [37] and likely reflects the more reducing status of the cell in fermentative conditions, since the genes for these proteins belong to the Rex regulon that responds to NADH levels [38].

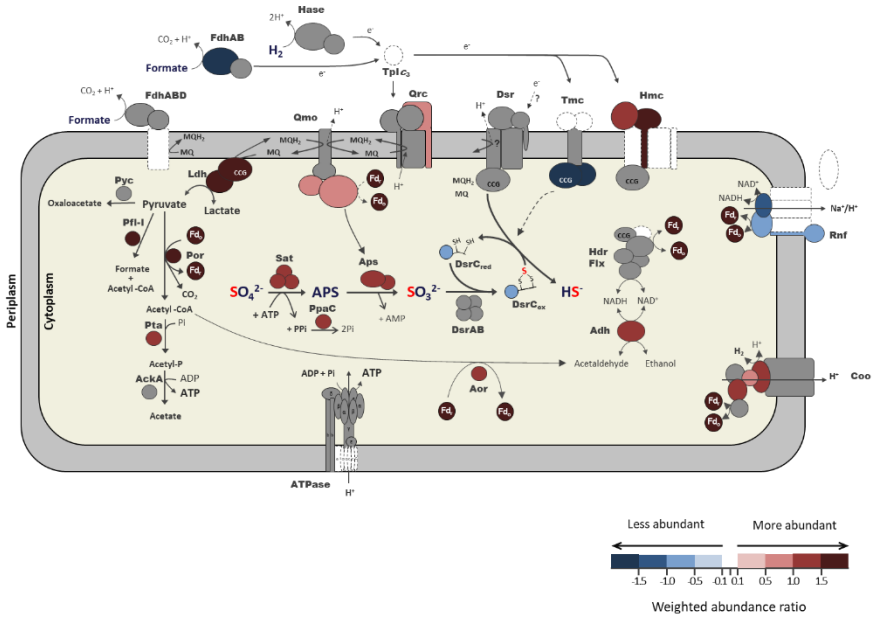

Figure 3.4 – Representation of more abundant (red) and less abundant (blue) energy metabolism proteins in fermentation versus respiration for *Dv*H wild-type. Color intensity reflects weighted abundance in a Log_2 scale ($p < 0.1$). Proteins barely affected (abundance between -0.1 and 0.1, $p < 0.1$) are shown in white, proteins detected in low amounts and/or not statistically affected in gray, and proteins not detected in dashed lines.

Additionally, proteins involved in the lactate oxidation pathway, such as lactate dehydrogenase (Ldh), pyruvate-formate lyase (Pfl-I) (DVU2824), pyruvate oxidoreductase (Por), phosphotransacetylase (Pta) (DVU3029), aldehyde oxidoreductase (Aor) (DVU1179) and aldehyde dehydrogenase (Adh), followed the same pattern of higher abundance in fermentation, as well as the transmembrane hydrogenase complex Coo (CooLXH subunits) and ferredoxin-I (DVU3276). Only a few energy-related proteins were significantly more abundant in *Dv*H WT during respiration, namely the Tmc (TmcBD subunits; DVU0264,6) and Rnf (RnfCGB; DVU2792,4,7) transmembrane complexes, the periplasmic FdhAB formate dehydrogenase (FdhA catalytic subunit, DVU0587) and, notably, DsrC.

3.4.4 – *Dv*H IPFG09 proteomic changes

Regarding *Dv*H IPFG09, 538 proteins were considered valid for analysis, of which 53 were more abundant and 51 less abundant in fermentation conditions, compared with respiration (**Figure 3.5**).

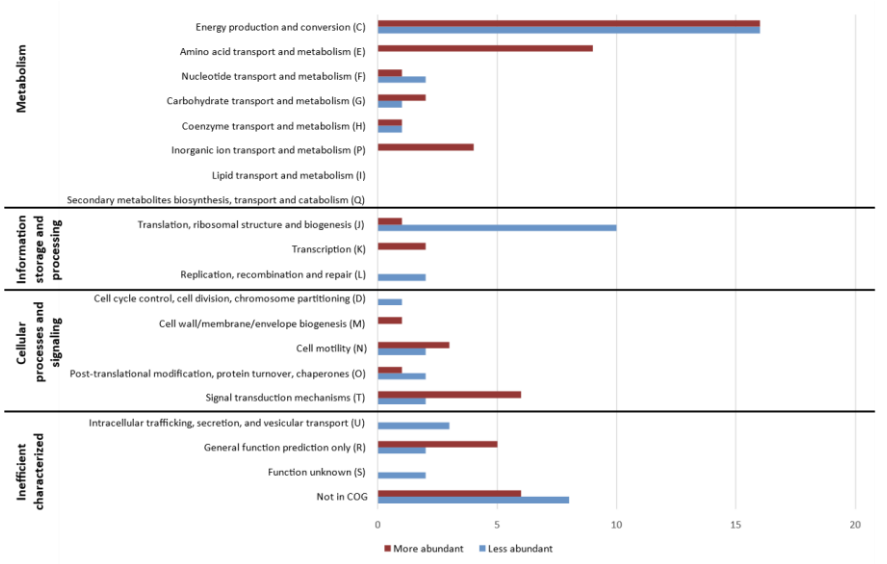

Figure 3.5 – Number of more abundant (red) and less abundant (blue) proteins in fermentation versus respiration, for *Dv*H IPFG09. Proteins are categorized by general function and respective COG. Only proteins presenting $Log_2 > 0.5$ and $p < 0.1$ are considered.

As observed in **Figure 3.6**, most of the changes observed for *Dv*H IPFG09 were consistent with the pattern found in *Dv*H WT (**Figure 3.4**). This includes proteins involved in sulfate respiration that were more abundant in fermentation, such as PpaC, ApsA (ApsB also detected in lower abundance, but below the threshold), QmoB (QmoA also detected in lower abundance, but below the threshold) and QrcB, as well as proteins involved in carbon oxidation, such as Ldh, Por and Pta. The transmembrane Coo hydrogenase (CooH subunit) was also more abundant.

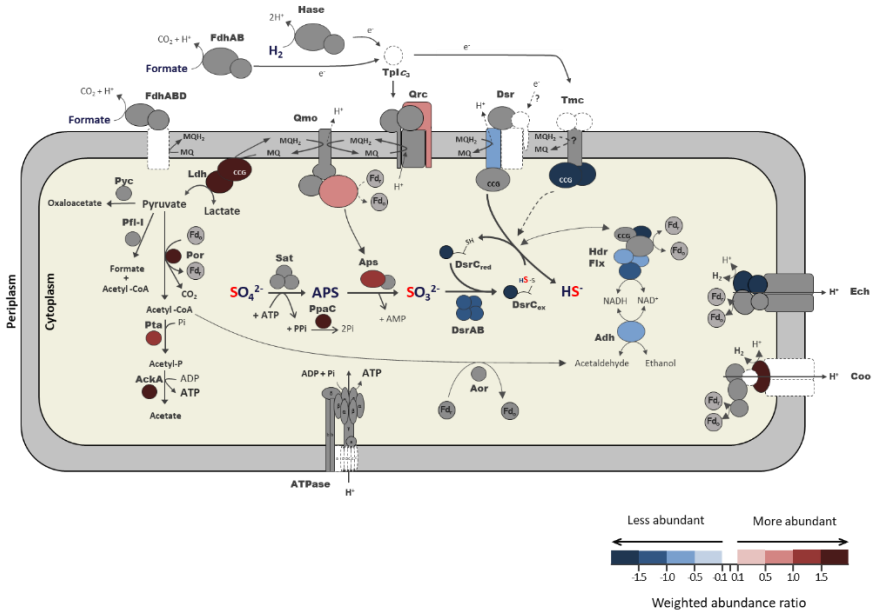

Figure 3.6 – Representation of more abundant (red) and less abundant (blue) energy metabolism proteins in fermentation versus respiration for *Dv*H IPFG09. Color intensity reflects weighted abundance in a Log_2 scale ($p < 0.1$). Proteins barely affected (abundance between -0.1 and 0.1, $p < 0.1$) are shown in white, proteins detected in low amounts and/or not statistically affected in gray, and proteins not detected in dashed lines.

As for proteins more abundant in respiration, also a similar pattern was observed for *Dv*H IPFG09 and WT, namely a higher abundance of DsrC, of the TmC (TmcBD subunits) and Rnf (Rnf CGB subunits, although below the significance treshold) transmembrane complexes. However, a few energy metabolism proteins were more abundant in respiration only for *Dv*H IPFG09, namely Adh, proteins of the Flx-Hdr complex (FlxABC, DVU2399-401 and HdrC, DVU2404) and the Ech energy conserving hydrogenase (EchED subunits; DVU0430-1), and DsrAB and DsrM (DVU1290).

3.4.5 – Effect of DsrC in respiratory conditions

When comparing *Dv*H IPFG09 with *Dv*H WT in sulfate respiration, a total of 208 proteins were considered valid for analysis. Of these, 56 proteins were more abundant and 85 proteins were less abundant in the *Dv*H IPFG09 than *Dv*H WT, while the remaining proteins were not affected (**Figure 3.7**).

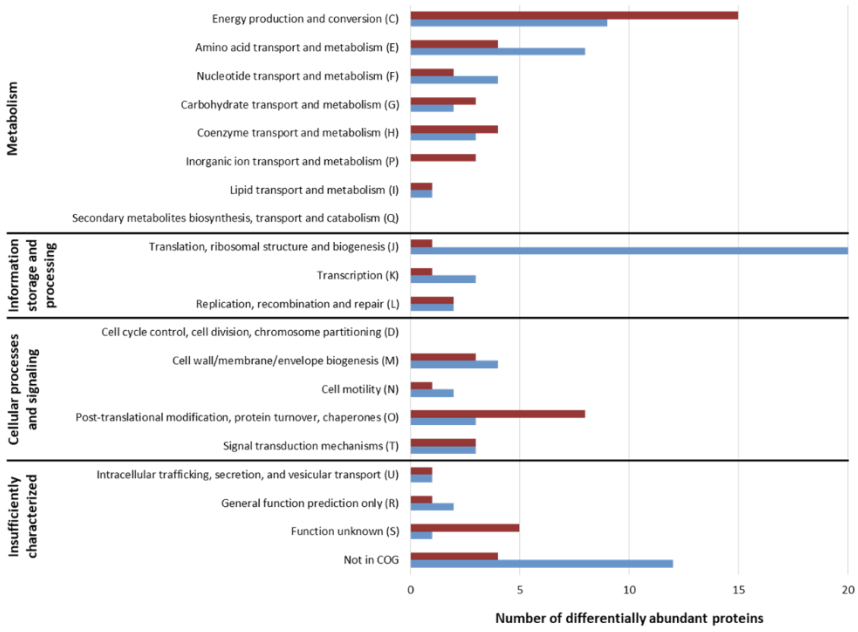

Figure 3.7 – Number of more abundant (red) and less abundant (blue) proteins in *Dv*H IPFG09 compared with *Dv*H WT, for respiration. Proteins are categorized by general function and respective COG. Only proteins presenting $Log_2 > 0.5$ and $p < 0.1$ are considered.

DsrC is the protein less abundant of all in *Dv*H IPFG09 but only when considering the threshold of 2 spectra instead of 3 cut off threshold upper mentioned, which was in line to the expected [7] and intrinsically validates the results here obtained. The majority of proteins involved in sulfate respiration, namely QmoB (DVU0849), PpaC (DVU1636), ApsA (DVU0847), DsrC (DVU2776) and an ATP synthase subunit (AtpA, DVU0777) were less abundant in *Dv*H

IPFG09 than in *Dv*H WT (**Figure 3.8**), which is consistent with this strain growing slower and not being able to reach the same cell density as *Dv*H WT.

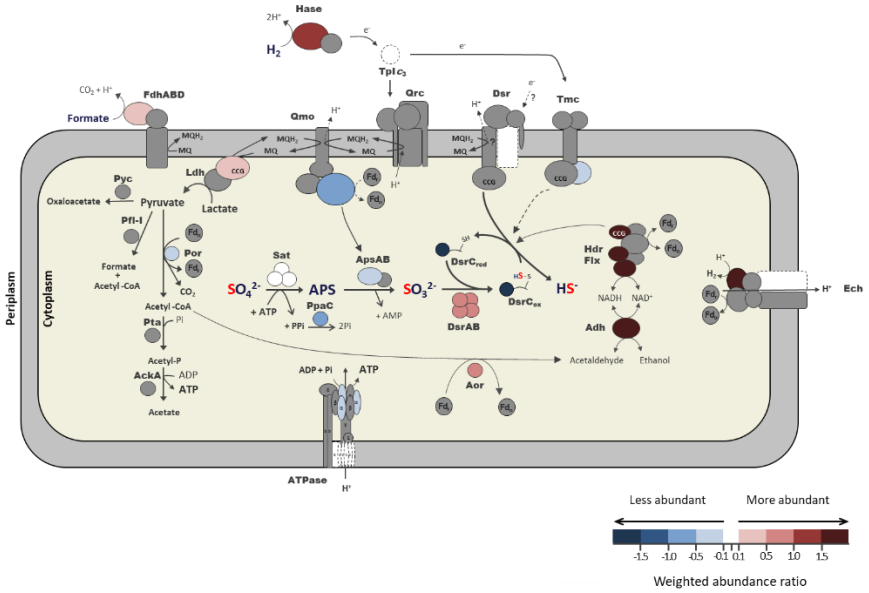

Figure 3.8 – Representation of more abundant (red) and less abundant (blue) energy metabolism proteins in *Dv*H IPFG09 compared with *Dv*H WT, for respiration. Color intensity reflects the weighted abundance measured in a Log_2 scale ($p < 0.1$). Proteins barely affected are shown in white (abundance between -0.1 and 0.1, $p < 0.1$), proteins detected in low amounts and/or not statistically affected in gray, and proteins not detected in dashed lines.

On the other hand, the DsrAB (DVU0402-3) central for sulfate respiration, was more abundant in *Dv*H IPFG09, possibly to compensate the lower level of DsrC. In addition, the Adh alcohol dehydrogenase (DVU2405) and 3 out of 6 subunits from the Flx-Hdr protein complex (FlxA, DVU2399; FlxC, DVU2401; HdrB, DVU2403) are more abundant in the *Dv*H IPFG09 strain, which is consistent with its higher ethanol production. These proteins are among the group of the most abundant protein detected in the mutant strain. The EchE subunit (DVU0430) from the transmembrane Ech hydrogenase and the HysA catalytic subunit (DVU1918) from the

periplasmic [NiFeSe] hydrogenase were also more abundant, justifying the higher hydrogen production by this strain in respiration.

3.4.6 – Effect of DsrC in fermentative conditions

When comparing *Dv*H WT and *Dv*H IPFG09 under fermentative growth conditions, 708 proteins were considered valid for analysis, of which 66 were more abundant and 57 were less abundant in the *Dv*H IPFG09 strain (**Figure 3.9**).

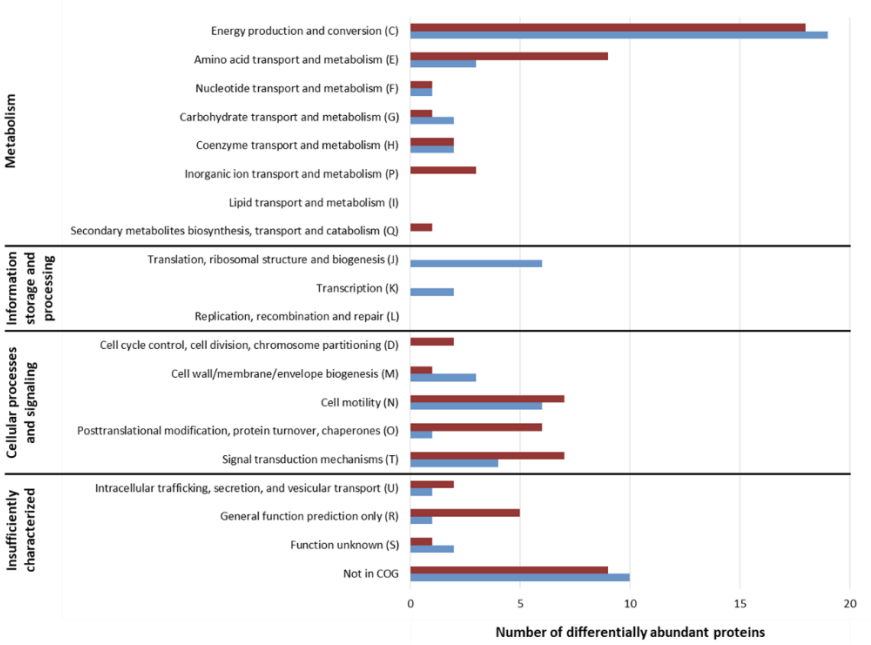

Figure 3.9 – Number of more abundant (red) and less abundant (blue) proteins in *Dv*H IPFG09 compared with *Dv*H WT, for fermentation. Proteins are categorized by general function and respective COG. Only proteins presenting $Log_2 > 0.5$ and $p < 0.1$ are considered.

As expected, proteins less abundant in *Dv*H IPFG09 in fermentation included DsrC and proteins from the sulfate reduction pathway (Sat, DVU1295; PpaC; DsrAB, DVU0402-3; QmoA, DVU0848; QrcB, DVU0694; DsrK, DVU1289) and proteins involved in carbon

oxidation, namely Ldh (DVU3027-8) and Por (DVU3025) (**Figure 3.10**), in line with the lower lactate production by this strain (**Figure 3.2D**). The Coo transmembrane hydrogenase was also among the less abundant protein complexes in *Dv*H IPFG09 (all the soluble cytoplasmic subunits, CooLXUHF, DVU2288-91,93), which correlates with the lower hydrogen production measured in *Dv*H IPFG09 under fermentative conditions.

Proteins more abundant in *Dv*H IPFG09 included the soluble subunits from both Tmc (TmcBD subunits; DVU0264,6) and Rnf (RnfCGB; DVU2792,4,7) membrane complexes, as well as the Adh alcohol dehydrogenase (DVU2405) and 3 out of 6 subunits from the Flx-Hdr protein complex (FlxB, DVU2400; HdrA, DVU2402; HdrB, DVU2403), which is consistent with its higher ethanol production by this mutant strain (**Figure 3.2F**). Another protein significantly more abundant in *Dv*H IPFG09 is ferredoxin-II (DVU0305).

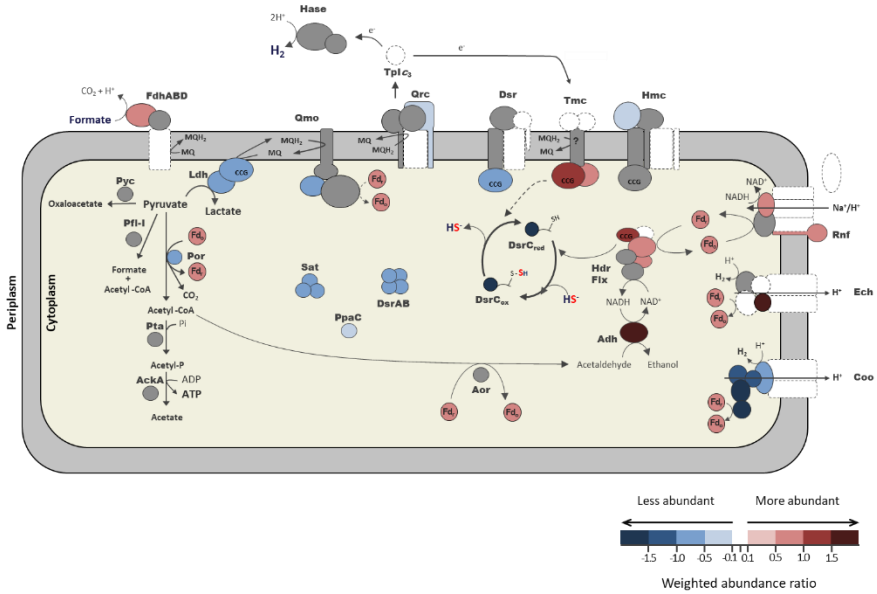

Figure 3.10 – Representation of more abundant (red) and less abundant (blue) energy metabolism proteins in *Dv*H IPFG09 compared with *Dv*H WT, for fermentation. Color intensity reflects the weighted abundance measured in a Log_2 scale ($p < 0.1$). Proteins barely affected are shown in white (abundance between -0.1 and 0.1, $p < 0.1$), proteins detected in low amounts and/or not statistically affected in gray, and proteins not detected in dashed lines.

3.4.7 – DsrC as a physiological partner of FlxABCD-HdrABC

The investigation on the relationship between DsrC and FlxABCD-HdrABC complex was pursued by studying the interaction between DsrC and this complex by pull-down assays, using two distinct approaches.

The first approach was using the *Dv*H IPFG07 strain since it expresses DsrC with a His-tag at its N-terminal. This strain was grown in ethanol/sulfate respiration and pyruvate fermentation, which are growth conditions previously shown to enhance the expression of the Flx-Hdr complex [27]. *Dv*H WT, which expresses the chromosomal DsrC with no tag, was used as control and therefore grown in the same conditions and subjected to the same disruption and pull-down protocol. The elution fractions from *Dv*H WT and IPFG07 soluble fractions were separated by SDS-PAGE.

The Western blot against FlxA showed a positive band at approximately 31 kDa that corresponds to the theoretical MW of 31 kDa expected for FlxA. This band was observed in both ethanol respiration and pyruvate fermentation conditions for *Dv*H IPFG07 and not detected in *Dv*H WT control (**Figure 3.11A**), which indicates FlxA eluting together with His-tagged DsrC and in a specific way. Despite FlxA having been detected in both growth conditions, the band is stronger in ethanol respiration conditions, which is in line with the previous result from Ramos *et al*., 2015 [27] presenting ethanol respiration to be the condition with the highest *flxA* expression.

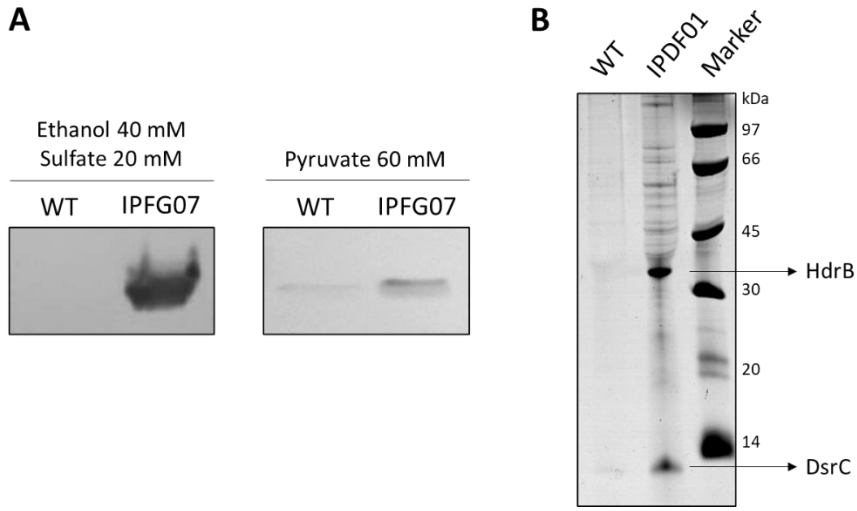

Figure 3.11 – Pull-down assays with DsrC and HdrCB. **(A)** Western blot detection of FlxA in eluted proteins from *Dv*H WT (negative control) and *Dv*H IPFG07, grown in MOY with ethanol/sulfate and MO pyruvate. **(B)** SDS-PAGE of eluted proteins from the soluble fraction of *Dv*H WT (negative control) and *Dv*H IPDF01 cells expressing Strep-tagged *Af* HdrCB. DsrC and HdrB bands were identified by mass spectrometry.

A similar approach was performed using *Dv*H IPDF01, a strain encoding HdrC and HdrB from *A*. *fulgidus*, where both proteins contain a Strep-tag at their C-terminal. *Dv*H WT and *Dv*H IPDF01 were grown in lactate/sulfate respiration, a condition where cell biomass is maximized, and so is the expression of these plasmid

constitutively-expressed proteins. *D*. *vulgaris* native *hdrA*/*flxA* were also shown to be highly expressed under these conditions [27]. As previously, *Dv*H WT served as control, and eluted proteins from both *Dv*H WT and *Dv*H IPDF01 soluble fractions were separated by Tricine-SDS-PAGE, as observed in **Figure 3.11B**. The two most salient protein bands were identified by mass spectrometry, and corresponded to the plasmid encoded HdrB-Strep (with 41% sequence coverage) and the native DsrC from *Dv*H (with 29% sequence coverage). This observation of DsrC coeluting with HdrB highlights the physiological interaction between DsrC and the FlxABCD-HdrABC complex. Despite the fact that the plasmid-expressed also HdrC encoding a Strep-tag, this protein was not observed in the SDS-PAGE of the pull-down assay at approximately 20 kDa, probably due to difficulties in HdrC expression and purification aforementioned.

3.4 – Discussion

DsrC is a key protein in dissimilatory sulfur metabolism, due to its function as a co-substrate of the widespread DsrAB sulfite reductase [7], [10]. However, DsrC is also part of a larger protein family including two other functionally and phylogenetically distinct proteins, namely TusE and RspA [10]. TusE contains only CysA and no CysB in the C-terminal arm and is involved in sulfurtransfer reactions for the biosynthesis of thio-uridine in bacterial tRNAs [39], having also been shown to modulate the intracellular redox state of *E*. *coli* [40]. The *tusE* genes are mostly found in organisms that do not have a dissimilatory sulfur metabolism. RspA proteins lack both Cys in the C-terminal arm and their function is still unclear but may be involved in gene regulation [10]. The *rspA* genes are mostly present in sulfur-oxidizing bacteria (some of which may also contain *tusE* genes). In contrast, SRP only encode *dsrC* [10], suggesting that DsrC may play multiple roles in SRP. Previous attempts to create a *dsrC* deletion strain were not successful even in fermentative conditions [7], [17], also suggesting a more general role of DsrC than only sulfite reduction.

This work focused on investigating other physiological functions for this protein, by studying in more detail two *Dv*H strains where DsrC functionality is partially impaired: *Dv*H IPFG07, which has lower DsrC expression, and *Dv*H IPFG09 that besides lower expression has also a CysB to Ala point mutation [7]. Strain *Dv*H IPFG09 is of particular interest since the absence of CysB means that it cannot form a trisulfide species and may only form a persulfenate in CysA that decomposes to a persulfide, which corresponds to a more reduced state of DsrC than the trisulfide. If DsrC is also involved in modulating the intracellular redox state and/or in regulating gene expression, these changes are likely to have an impact. Strain *Dv*H IPFG07 was previously shown to have a slower growth rate and achieve lower cell density than *Dv*H WT in sulfate respiration, a phenotype that was even more pronounced in *Dv*H IPFG09 [7], [12]. In this work, IPFG07 and IPFG09 strains were compared with *Dv*H WT in sulfate respiration in conditions that differed from previous studies by the absence of yeast extract in the media, by measuring metabolic products, and studying also pyruvate fermentation [7], [12], [35].

As previously observed, both IPFG07 and IPFG09 grew slower than *Dv*H WT by sulfate respiration, and strain IPFG09 only achieved 70% of the bacterial density of the other two strains, in line with impaired sulfate reduction. In IPFG09, sulfite reduction leads to the formation of a DsrC persulfide or a persulfide sulfenate instead of a trisulfide [7]. This means that the DsrC pool will be in a more reduced state and that fewer electrons will be involved in its reduction by DsrMKJOP, which may lead to a reduced proton motive force (pmf). The present results show that these factors are reflected in a shift towards fermentation in IPFG09 during lactate/sulfate growth, which is expressed in increased production of the fermentative products hydrogen and ethanol, and also the decreased abundance of several proteins from the sulfate reduction pathway, such as QmoB, PpaC, ApsA and AtpA. Most hydrogen produced in IPFG09 is later consumed for sulfate reduction in agreement with the hydrogen cycling model [41], [42]. This is supported by the increased abundance of the transmembrane [NiFe] Ech hydrogenase and the periplasmic [NiFe] Hys hydrogenase in *Dv*H IPFG09 when compared with *Dv*H WT. IPFG09 also produced more ethanol, and the Adh alcohol dehydrogenase (DVU2405) was also more abundant in *Dv*H IPFG09 versus the *Dv*H WT. This Adh is believed to be linked to reduction of the DsrC trisulfide via FlxABCD-HdrABC, a protein complex likely able to perform FBEB (**Figure 3.8** and **Figure 3.10**) [25], [27]. In line with this, FlxA, FlxCD and HdrB, are significantly more abundant in *Dv*H IPFG09 versus *Dv*H WT in lactate/sulfate growth. The higher transient flux of reducing power to hydrogen and ethanol during respiration, in IPFG09 relative to IPFG07 and WT, may also decouple the sulfate from sulphide S-isotope signals in IPFG09, but not WT or IPFG07, as previously observed [12].

When switching from respiratory to fermentative growth, *Dv*H WT and *Dv*H IPFG09 show a similar proteomic response, with higher abundance of many proteins involved in sulfate reduction (e.g., PpaC, ApsAB, QmoAB, QrcB), and proteins involved in lactate oxidation to acetate (Ldh, Pta and Por), due to the more reducing redox status of the cell during fermentation. The Coo hydrogenase is also increased in fermentation for both strains. The Tmc and Rnf complexes are both less abundant in the two strains when switching from respiration to fermentation, while the Hmc complex is more abundant (in the WT only). The Tmc complex is involved in transmembrane electron transfer from periplasmic hydrogen

oxidation to cytoplasmic reduction of the DsrC trisulfide [22], based on the CCG domain present in the TmcB subunit, similar to that observed in DsrK and HdrB [10], [21], [22], [43]. This complex is upregulated in *D*. *vulgaris* under hydrogen/sulfate conditions [37], and in *D*. *alaskensis* G20, a *tmc* deletion mutant was affected under these conditions. The Rnf complex [44], [45] is an electrogenic complex that links the cellular NADH and ferredoxin pools, and during fermentation it can allow for reduction of NAD^+ from reduced ferredoxin (produced by Por) coupled to energy conservation, as suggested for *D*. *alaskensis* [46]. The Hmc complex was previously reported to be involved in syntrophic growth [47], and it may be involved in reducing oxidized DsrC formed by the FlxABCD-HdrABC complex.

In both strains, DsrC is less abundant in fermentation than respiration. However, since this is such a highly abundant protein, its expression level should still be significant during fermentation. Both strain *Dv*H IPFG07 and even more so *Dv*H IPFG09 grow slower and to lower cell density than *Dv*H WT in fermentative conditions, supporting the involvement of DsrC in fermentation. Strain *Dv*H IPFG09 produces a lot more ethanol than the other two strains, revealing a shift in fermentation, whereas the other fermentation products acetate, hydrogen and lactate are reduced in both *Dv*H IPFG07 and *Dv*H IPFG09 versus *Dv*H WT, following the reduced growth pattern. The increased ethanol production can be explained by the higher abundance of the FlxABCD-HdrABC complex, Adh and Rnf in *Dv*H IPFG09 versus *Dv*H WT in fermentation. In contrast, *Dv*H WT shows no effect for the Flx–Hdr complex when switching from respiration to fermentation, whereas Adh is increased. The higher production of ethanol is not observed for *Dv*H IPFG07, suggesting that it is linked to the changed redox state of DsrC in *Dv*H IPFG09, and not to the reduced level of this protein, which is similar for both IPFG07 and IPFG09 strains. The results suggest that the likely more reduced state of DsrC in *Dv*H IPFG09 versus *Dv*H WT is associated with the increased expression of the Flx–Hdr complex as well as Adh, leading to increased production of ethanol. This is also supported by the increased production of NADH by the more abundant Rnf contributing to the pmf. Overall, the results support the previous suggestion of a direct interaction between DsrC and the Flx–Hdr complex [10], [27], [46], [48]. This interaction was finally proven by the pull-down experiments reported here, where the tagged *Dv*H DsrC protein could pull down the FlxABCD-HdrABC

complex (detected by Western blot against the FlxA protein, which will not interact directly with DsrC), and the *A*. *fulgidus* HdrB expressed in *Dv*H could pull down native *Dv*H DsrC in high amounts, which enabled direct detection by SDS-PAGE. HdrB is the subunit containing two CCG domains that is homologous to the methanogenic HdrB responsible for CoM-CoB reduction and is expected to interact directly and reduce the DsrC trisulfide.

In conclusion, these results indicate that DsrC is important for other cellular functions besides sulfite reduction and suggest that it may also be involved in redox regulation, since its redox status is linked to the expression of several proteins, most notably Adh and the FlxABCD-HdrABC complex, for which a direct interaction with DsrC was confirmed. Further work will be required to confirm this regulatory function.

3.5 – Acknowledgements

I would like to thank Lichun Zhang and Jacob Waldbauer from University of Chicago, and William Leavitt from Dartmouth College, which contributed to the proteomic analysis. This work was funded by the Fundação para a Ciência e Tecnologia (Portugal) through fellowship PD/BD/128204/2016, grants PTDC/BIA-MIC/6512/2014 e PTDC/BIA-BQM/29118/2017, R&D unit MOSTMICRO-ITQB (UIDB/04612/2020 and UIDP/04612/2020) and LS4FUTURE Associated Laboratory (LA/P/0087/2020).

3.6 – Bibliography

[1] W. Liamleam and A. P. Annachhatre, “Electron donors for biological sulfate reduction”, *Biotechnol. Adv.*, vol. 25, no. 5, pp. 452–463, 2007.

[2] I. P. Pankhania, A. M. Spormann, W. A. Hamilton, and R. K. Thauer, “Lactate conversion to acetate, CO_2 and H_2 in cell suspensions of *Desulfovibrio vulgaris* (Marburg): indications for the involvement of an energy driven reaction”, *Arch. Microbiol.*, vol. 150, no. 1, pp. 26–31, 1988.

[3] K. L. Keller and J. D. Wall, “Genetics and molecular biology of the electron flow for sulfate respiration in *Desulfovibrio*”, *Front. Microbiol.*, vol. 2, no. 135, 2011.

[4] K. L. Keller, B. J. Rapp-Giles, E. S. Semkiw, I. Porat, S. D. Brown, and J. D. Wall, “New model for electron flow for sulfate reduction in *Desulfovibrio alaskensis* G20”, *Appl. Environ. Microbiol.*, vol. 80, no. 3, pp. 855–868, 2014.

[5] T. F. Oliveira, C. Vonrhein, P. M. Matias, S. S. Venceslau, I. A. C. Pereira, and M. Archer, “The crystal structure of *Desulfovibrio vulgaris* dissimilatory sulfite reductase bound to DsrC provides novel insights into the mechanism of sulfate respiration”, *J. Biol. Chem.*, vol. 283, no. 49, pp. 34141–34149, 2008.

[6] A. L. Müller, K. U. Kjeldsen, T. Rattei, M. Pester, and A. Loy, “Phylogenetic and environmental diversity of DsrAB-type dissimilatory (bi)sulfite reductases”, *ISME J.*, vol. 9, no. 5, pp. 1152–1165, 2015.

[7] A. A. Santos *et al.*, “A protein trisulfide couples dissimilatory sulfate reduction to energy conservation”, *Science.*, vol. 350, no. 6267, pp. 1541–1545, 2015.

[8] R. H. Pires, S. S. Venceslau, F. Morais, M. Teixeira, A. V. Xavier, and I. A. C. Pereira, “Characterization of the *Desulfovibrio desulfuricans* ATCC 27774 DsrMKJOP complex - A membrane-bound redox complex involved in the sulfate respiratory pathway”, *Biochemistry*, vol. 45, no. 1, pp. 249–262, 2006.

[9] F. Grein, I. A. C. Pereira, and C. Dahl, “Biochemical characterization of individual components of the *Allochromatium vinosum* DsrMKJOP transmembrane complex aids understanding of

complex function *in vivo*", *J. Bacteriol.*, vol. 192, no. 24, pp. 6369–6377, 2010.

[10] S. S. Venceslau, Y. Stockdreher, C. Dahl, and I. A. C. Pereira, "The 'bacterial heterodisulfide' DsrC is a key protein in dissimilatory sulfur metabolism", *Biochim. Biophys. Acta - Bioenerg.*, vol. 1837, no. 7, pp. 1148–1164, 2014.

[11] F. Grein, A. R. Ramos, S. S. Venceslau, and I. A. C. Pereira, "Unifying concepts in anaerobic respiration: Insights from dissimilatory sulfur metabolism", *Biochim. Biophys. Acta*, vol. 1827, no. 2, pp. 145–160, 2013.

[12] W. D. Leavitt, S. S. Venceslau, I. A. C. Pereira, D. T. Johnston, and A. S. Bradley, "Fractionation of sulfur and hydrogen isotopes in *Desulfovibrio vulgaris* with perturbed DsrC expression", *FEMS Microbiol. Lett.*, vol. 363, no. 20, 2016.

[13] S. A. Haveman, V. Brunelle, J. K. Voordouw, G. Voordouw, J. F. Heidelberg, and R. Rabus, "Gene expression analysis of energy metabolism mutants of *Desulfovibrio vulgaris* Hildenborough indicates an important role for alcohol dehydrogenase", *J. Bacteriol.*, vol. 185, no. 15, pp. 4345–4353, 2003.

[14] S. S. Venceslau *et al.*, "Redox states of desulfovibrio vulgaris dsrC, a key protein in dissimilatory sulfite reduction", *Biochem. Biophys. Res. Commun.*, vol. 441, no. 4, pp. 732–736, 2013.

[15] R. A. R. Karkhoff-Schweizer, M. Bruschi, and G. Voordouw, "Expression of the γ-subunit gene of desulfoviridin-type dissimilatory sulfite reductase and of the α- and β-subunit genes is not coordinately regulated", *Eur. J. Biochem.*, vol. 211, no. 3, pp. 501–507, 1993.

[16] W. Zhang *et al.*, "A proteomic view of *Desulfovibrio vulgaris* metabolism as determined by liquid chromatography coupled with tandem mass spectrometry", *Proteomics*, vol. 6, no. 15, pp. 4286–4299, 2006.

[17] J. R. Cort, U. Selan, A. Schulte, F. Grimm, M. A. Kennedy, and C. Dahl, "*Allochromatium vinosum* DsrC: Solution-State NMR Structure, Redox Properties, and Interaction with DsrEFH, a Protein Essential for Purple Sulfur Bacterial Sulfur Oxidation", *J. Mol. Biol.*, vol. 382, no. 3, pp. 692–707, 2008.

[18] F. Grimm, N. Dobler, and C. Dahl, “Regulation of *dsr* genes encoding proteins responsible for the oxidation of stored sulfur in *Allochromatium vinosum*”, *Microbiology*, vol. 156, no. 3, pp. 764–773, 2010.

[19] S. Madadi-Kahkesh, E. C. Duin, S. Heim, S. P. J. Albracht, M. K. Johnson, and R. Hedderich, “A paramagnetic species with unique EPR characteristics in the active site of heterodisulfide reductase from methanogenic archaea”, *Eur. J. Biochem.*, vol. 268, no. 9, pp. 2566–2577, 2001.

[20] N. Hamann, G. J. Mander, J. E. Shokes, R. A. Scott, M. Bennati, and R. Hedderich, “A cysteine-rich CCG domain contains a novel [4Fe-4S] cluster binding motif as deduced from studies with subunit B of heterodisulfide reductase from Methanothermobacter marburgensis”, *Biochemistry*, vol. 46, no. 44, pp. 12875–12885, 2007.

[21] I. A. C. Pereira, A. R. Ramos, F. Grein, M. C. Marques, S. M. da Silva, and S. S. Venceslau, “A comparative genomic analysis of energy metabolism in sulfate reducing bacteria and archaea”, *Front. Microbiol.*, vol. 2, no. 69, pp. 1–22, 2011.

[22] P. M. Pereira, M. Teixeira, A. V. Xavier, R. O. Louro, and I. A. C. Pereira, “The Tmc complex from *Desulfovibrio vulgaris* Hildenborough is involved in transmembrane electron transfer from periplasmic hydrogen oxidation”, *Biochemistry*, vol. 45, no. 34, pp. 10359–10367, 2006.

[23] G. J. Mander, A. J. Pierik, H. Huber, and R. Hedderich, “Two distinct heterodisulfide reductase-like enzymes in the sulfate-reducing archaeon *Archaeoglobus profundus*”, *Eur. J. Biochem.*, vol. 271, no. 6, pp. 1106–1116, 2004.

[24] R. Hedderich, N. Hamann, and M. Bennati, “Heterodisulfide reductase from methanogenic archaea: A new catalytic role for iron-sulfur cluster”, *Biol. Chem.*, vol. 386, no. 10, pp. 961–970, 2005.

[25] A.-K. Kaster, J. Moll, K. Parey, and R. K. Thauer, “Coupling of ferredoxin and heterodisulfide reduction via electron bifurcation in hydrogenotrophic methanogenic archaea”, *Proc Natl Acad Sci U S A*, vol. 108, no. 7, pp. 2981–2986, 2011.

[26] T. Wagner, J. Koch, U. Ermler, and S. Shima, “Methanogenic

heterodisulfide reductase (HdrABC-MvhAGD) uses two noncubane [4Fe-4S] clusters for reduction", *Science.*, vol. 357, no. 6352, pp. 699–703, 2017.

[27] A. R. Ramos *et al.*, "The FlxABCD-HdrABC proteins correspond to a novel NADH dehydrogenase/heterodisulfide reductase widespread in anaerobic bacteria and involved in ethanol metabolism in *Desulfovibrio vulgaris* Hildenborough", *Environ. Microbiol.*, vol. 17, no. 7, pp. 2288–2305, 2015.

[28] K. L. Keller, K. S. Bender, and J. D. Wall, "Development of a markerless genetic exchange system for *Desulfovibrio vulgaris* Hildenborough and its use in generating a strain with increased transformation efficiency", *Appl. Environ. Microbiol.*, vol. 75, no. 24, pp. 7682–7691, 2009.

[29] M. Z. Li and S. J. Elledge, "Harnessing homologous recombination *in vitro* to generate recombinant DNA via SLIC", vol. 4, no. 3, pp. 251–256, 2007.

[30] K. L. Keller, J. D. Wall, and S. Chhabra, *Methods for engineering sulfate reducing bacteria of the genus Desulfovibrio*, 1st ed., vol. 497. Elsevier Inc., 2011.

[31] G. M. Zane, H. C. Bill Yen, and J. D. Wall, "Effect of the deletion of *qmoABC* and the promoter-distal gene encoding a hypothetical protein on sulfate reduction in *Desulfovibrio vulgaris* Hildenborough", *Appl. Environ. Microbiol.*, vol. 76, no. 16, pp. 5500–5509, 2010.

[32] J. Erde, R. R. O. Loo, and J. A. Loo, "Enhanced FASP (eFASP) to Increase Proteome Coverage and Sample Recovery for Quantitative Proteomic Experiments", *J. Proteome Res.*, vol. 13, no. 4, pp. 1885–1895, Apr. 2014.

[33] J. Waldbauer, L. Zhang, A. Rizzo, and D. Muratore, "DiDO-IPTL: A Peptide-Labeling Strategy for Precision Quantitative Proteomics", *Anal. Chem.*, vol. 89, no. 21, pp. 11498–11504, 2017.

[34] Yoav Benjamini and Yosef Hochberg, "Controlling the False Discovery Rate: A Practical and Powerful Approach to Multiple Testing", *J. R. Stat. Soc. Ser. B*, vol. 57, no. 1, pp. 289–300, 1995.

[35] W. D. Leavitt, S. S. Venceslau, J. Waldbauer, D. A. Smith, I. A. Cardoso Pereira, and A. S. Bradley, "Proteomic and Isotopic

Response of *Desulfovibrio vulgaris* to DsrC Perturbation", *Front. Microbiol.*, vol. 10, no. APR, pp. 1–13, 2019.

[36] B. Meyer *et al.*, "The energy-conserving electron transfer system used by *Desulfovibrio alaskensis* strain G20 during pyruvate fermentation involves reduction of endogenously formed fumarate and cytoplasmic and membrane-bound complexes, Hdr-Flox and Rnf", *Environ. Microbiol.*, vol. 16, no. 11, pp. 3463–3486, 2014.

[37] P. M. Pereira *et al.*, "Energy metabolism in *Desulfovibrio vulgaris* Hildenborough: Insights from transcriptome analysis", *Antonie van Leeuwenhoek, Int. J. Gen. Mol. Microbiol.*, vol. 93, no. 4, pp. 347–362, 2008.

[38] G. A. Christensen *et al.*, "Rex (encoded by DVU_0916) in *Desulfovibrio vulgaris* Hildenborough is a repressor of sulfate adenylyl transferase and is regulated by NADH", *J. Bacteriol.*, vol. 197, no. 1, pp. 29–39, 2015.

[39] Y. Ikeuchi, N. Shigi, J. I. Kato, A. Nishimura, and T. Suzuki, "Mechanistic insights into sulfur relay by multiple sulfur mediators involved in thiouridine biosynthesis at tRNA wobble positions", *Mol. Cell*, vol. 21, no. 1, pp. 97–108, 2006.

[40] T. Nakayashiki *et al.*, "The tRNA thiolation pathway modulates the intracellular redox state in *Escherichia coli*", *J. Bacteriol.*, vol. 195, no. 9, pp. 2039–2049, 2013.

[41] G. Kulkarni, T. D. Mand, and W. W. Metcalf, "Energy Conservation via Hydrogen Cycling in the Methanogenic Archaeon *Methanosarcina barkeri*", vol. 9, no. 4, pp. 1–10, 2018.

[42] J. M. Odom and H. D. Peck, "Hydrogen cycling as a general mechanism for energy coupling in the sulfate-reducing bacteria, *Desulfovibrio* sp.", *FEMS Microbiol. Lett.*, vol. 12, no. 1, pp. 47–50, 1981.

[43] M. N. Price *et al.*, "The genetic basis of energy conservation in the sulfate-reducing bacterium *Desulfovibrio alaskensis* G20.", *Front. Microbiol.*, vol. 5, p. 577, 2014.

[44] M. Kuhns, D. Trifunović, H. Huber, and V. Müller, "The Rnf complex is a Na^+ coupled respiratory enzyme in a fermenting bacterium, Thermotoga maritima", *Commun. Biol.*, vol. 3, no. 1, pp. 1–10, 2020.

[45] L. Westphal, A. Wiechmann, J. Baker, N. P. Minton, and V. Müller, “The Rnf complex is an energy-coupled transhydrogenase essential to reversibly link cellular NADH and ferredoxin pools in the acetogen *Acetobacterium woodii*”, *J. Bacteriol.*, vol. 200, no. 21, 2018.

[46] B. Meyer *et al.*, “The energy-conserving electron transfer system used by *Desulfovibrio alaskensis* strain G20 during pyruvate fermentation involves reduction of endogenously formed fumarate and cytoplasmic and membrane-bound complexes, Hdr-Flox and Rnf”, *Environ. Microbiol.*, vol. 16, no. 11, pp. 3463–3486, 2014.

[47] C. B. Walker *et al.*, “The electron transfer system of syntrophically grown *Desulfovibrio vulgaris*”, *J. Bacteriol.*, vol. 191, no. 18, pp. 5793–5801, 2009.

[48] L. Appel, M. Willistein, C. Dahl, U. Ermler, and M. Boll, “Functional diversity of prokaryotic HdrA(BC) modules: Role in flavin-based electron bifurcation processes and beyond”, *Biochim. Biophys. Acta - Bioenerg.*, vol. 1862, no. 4, p. 148379, 2021.

Chapter 4

Expression, Purification and Characterization of the Hdr complex

Contents

Contributions

All experiments and analyses were performed by Delfim Ferreira, except the mass spectrometry analysis done by the ITQB/iBET UniMS Mass Spectrometry Unit, and the expression of codon-optimized *A*. *fulgidus* HdrC by Raquel Bernardino

The experiment design was performed by Delfim Ferreira, Sofia Venceslau and Inês Cardoso Pereira.

Part of this section was published as:

V. Pelmenschikov, D. Ferreira, S.S. Venceslau, P. Hildebrandt, I.A.C. Pereira and S. Todorovic (2023) “Substrate-Dependent Conformational Switch of the Noncubane [4Fe-4S] Cluster in Heterodisulfide Reductase HdrB" J Am Chem Soc 145(1): 7–11

4.1 – Summary

Several hints point towards an interaction between the HdrABC protein complex and DsrC, in sulfate reducing organisms. To confirm this *in vitro*, it is required to purify both the Hdr protein complex and DsrC. This chapter is focused on the expression, purification and characterization of the three subunits from the HdrABC complex from sulfate-reducers. HdrA includes six [4Fe-4S] clusters and one FAD cofactor, and HdrB includes two non-cubane [4Fe-4S] clusters. Both these proteins were successfully expressed. HdrC includes two conventional [4Fe-4S] clusters, but its expression was very challenging. Several expression and purification approaches were tried, using several vectors, expression hosts, purification strategies and affinity tags. The best approach was via HdrC coexpression with HdrB using *D. vulgaris* as expression host, but this still yielded low amounts of HdrC, which were disproportional to HdrB. Electron transfer between HdrCB (with no/low HdrC) and DsrC was tested but was not successful.

4.2 – Introduction

Energy conservation involves a set of chemical processes necessary to produce the universal carrier for biological energy: adenosine 5'-triphosphate (ATP). Substrate-level phosphorylation (SLP) and oxidative phosphorylation (OP) are the two most known mechanisms for energy conservation in chemotrophic organisms, and can be broadly described as catabolic and exergonic processes comprising electron-accepting and -donating reactions, in which the first stage includes the flow of electrons from the donor substrate to an electron carrier, usually nicotinamide adenine dinucleotide (NAD), and the second stage involves the flow from the electron carrier to the final acceptor. Both partial reactions can be coupled with phosphorylation of ADP to ATP [1].

Recently, a new mechanism of energy coupling has been revealed: Electron Bifurcation. This is a mechanism in which there is a reduction of a redox cofactor (quinone or flavin), and its subsequent partial oxidation by a high-potential one electron acceptor, which leads to the formation of a reactive semiquinone intermediate, and then its oxidation by a low-potential one electron acceptor. This results in the electron pair splitting in one electron with a more positive reduction potential and another electron with a more negative reduction potential, when compared with the initial electron pair. A simplified version of this mechanism is shown in **Figure 4.1**.

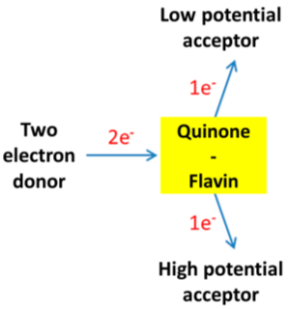

Figure 4.1 – Simplified version of the Electron Bifurcation mechanism. An electron-donor protein provides two electrons to a quinone- or flavin-containing protein, which in turn reduces a high potential acceptor protein, leaving the flavin in an unstable semiquinone state, which can reduce a low potential acceptor protein. Figure adapted from [2].

Quinone-based electron bifurcation (QBEB) is present in mitochondria, chloroplasts, phototrophic bacteria, and respiring bacteria and archaea, and was first described for the bc_1 complex by Peter Mitchell [3] as the mechanism responsible for the reduction of a low-potential acceptor, cytochrome *b*, and for generating an electrochemical proton gradient ($\Delta\mu H^+$).

Flavin-based electron bifurcation (FBEB) has been found only in strictly anaerobic bacteria and archaea. This mechanism requires a flavin cofactor (FAD or FMN) that can be reduced by a two-electron step and oxidized by two one-electron steps, and the two-electron donor, usually NADH, fully reduces the flavin cofactor to its hydroquinone state. The potentials of the two oxidation states of the flavin cofactor must be crossed-over from what would be expected for a typical hydroquinone one-electron oxidation. Normally, the first electron to leave the hydroquinone state (hydroquinone → semiquinone) state has a lower reduction potential, i.e., higher reductive power, than the second electron leaving the semiquinone state (semiquinone → quinone). In contrast, in electron bifurcation the inversion of this order ensures that the first electron (hydroquinone → semiquinone) will reduce a high-potential acceptor, giving the remaining semiquinone a very low reduction potential able to reduce a low-potential acceptor. Whether the potentials are normal or crossed over is dependent on the stability of the semiquinone intermediate. Thus, by having a higher redox potential for the semiquinone/hydroquinone couple than the quinone/semiquinone, the first electron transfer from the fully reduced hydroquinone state to the high-potential acceptor generates an extremely unstable semiquinone from which one second electron can be transferred to the low-potential acceptor. This would not be possible with one-electron donors, which are not able to reduce the quinone state of electron-bifurcating flavins to the hydroquinone state [2], [4], [5].

The low-potential acceptor for FBEB is usually ferredoxin (Fd) or flavodoxin, and this process is an effective way to overcome the thermodynamic challenge of reducing ferredoxin, since it has a very low redox potential ($E^{0'}$ = -450 mV) and is mainly present in its reduced state (> 90%) inside the cells. Under iron deprivation, many anaerobes synthesize flavodoxin instead of ferredoxin to overcome

the shortage of iron, and this can substitute ferredoxin in most functions [6], [7]. Ferredoxins are small cytoplasmic proteins containing either one [2Fe-2S] cluster or one or more [4Fe-4S] clusters, each of which can be reduced by one electron, and are very important proteins that act as general electron donors for redox reactions. Reduced ferredoxin can also be used to drive otherwise endergonic reactions, such as generation of $\Delta\mu H^+/Na^+$ via the ferredoxin:NAD reductase (Rnf) or ferredoxin:proton reductase (Ech), which can later be used for ATP formation [7].

Despite Electron Bifurcation being known since 1975, FBEB was only hypothesized by Herrmann *et al*. [8] and confirmed by Li *et al*. [9] in 2008. These authors described the butyryl-CoA dehydrogenase/electron-transferring flavoprotein (Bcd/EtfAB) complex from *Clostridium kluyvery* to be able to use two NADH ($E^{0'}$ = -320 mV) to reduce the FAD prosthetic group to its hydroquinone form ($FADH_2$), with one electron being used to reduce crotonyl-CoA to butyryl-CoA ($E^{0'}$ = -10 mV) and another to reduce ferredoxin ($E^{0'}$ = -410 mV) (**Figure 4.2)**.

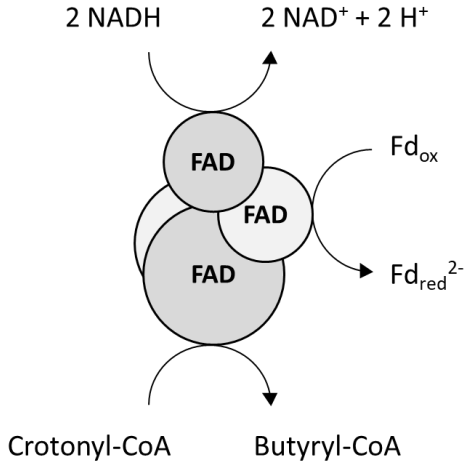

Figure 4.2 – Flavin-based electron bifurcation mechanism of the butyryl-CoA dehydrogenase/electron-transferring flavoprotein complex from *Clostridium kluyvery*. Image adapted from [9].

The reverse reaction of FBEB, flavin-based electron confurcation (FBEC), can also occur and be essential for some organisms to cope with thermodynamically unfavorable conditions, for instance in syntrophic bacteria as a way to consume their substrates and produce hydrogen [10]–[12]. A postulated example of FBEC in dissimilatory sulfate reduction, still not experimentally confirmed, is the mechanism operating in the quinone-interacting membrane-bound oxidoreductase QmoABC [13], which acts as electron donor for the APS reductase that reduces APS to sulfite. The membrane-bound QmoC subunit is proposed to oxidize menaquinol and transfer the electrons to the flavin-containing subunits QmoAB. The reduction of APS ($E^{0'}$ APS/sulfite = -60 mV) driven by the menaquinone pool ($E^{0'}$ menaquinone/menaquinol = -75 mV) is endergonic when considering that menaquinol oxidation must occur against the membrane potential (≈ -150 mV) due to protons being released to the periplasm. Therefore, coupling the reduction with the exergonic oxidation of ferredoxin makes this reaction viable [13]. The proposed mechanism for QmoABC confurcation is displayed in **Figure 4.3**. The DsrMK complex in sulfur-based organisms has also been suggested to perform FBEC using a cytoplasmic electron donor, as one of the hypothesis to reduce the DsrC trisulfide [14].

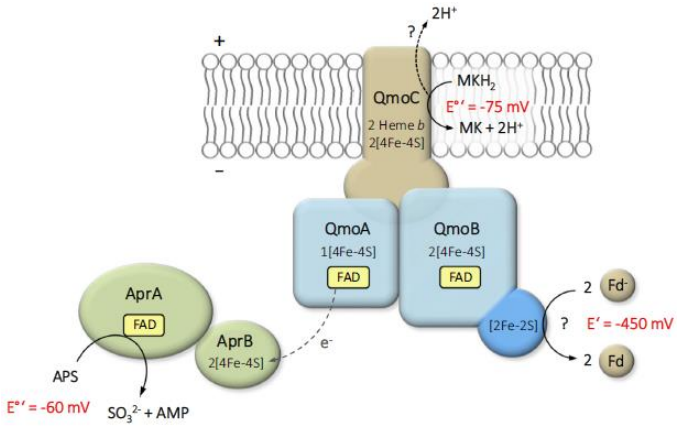

Figure 4.3 – Proposed mechanism for flavin-based electron confurcation in QmoABC. The electron transfer from the menaquinone pool to APS is endergonic. Coupling menaquinol oxidation with the exergonic ferredoxin oxidation, through electron confurcation, enables the less favorable APS reduction. Image from [5].

Since the discovery of FBEB, several protein complexes have been described to be able to perform this mechanism, requiring the presence of a flavin cofactor (either FAD or FMN) and generally having ferredoxin as the endergonic electron acceptor. A list of protein complexes able to perform FBEB is presented in **Table 4.1.**

Table 4.1 – Examples of electron bifurcating protein complexes. Data from [5].

Prototypical complex	Cellular function	Electron donor	Low-potential acceptor	High-potential acceptor
EtfAB-Bcd	Fermentation	NADH	Fd	Crotonyl-CoA
HydABC (NuoF-like)	Glucose fermentation	H_2	Fd	NAD^+
NfnAB	Fermentation	NADPH	Fd	NAD^+
HdrABC-MvhAGD	Methanogenesis from H_2/CO_2	H_2	Fd	CoM-S-S-CoB

It is of particular interest how FBEB is used for energy conservation in hydrogenotrophic methanogens, which are organisms that produce CH_4 from CO_2 and H_2. The first steps of methanogenesis involve the H_2-driven endergonic reduction of CO_2 with methanofuran ($\Delta G^{0'}$ = +20 kJ/mol), while the last step involves the exergonic reduction of the heterodisulfe CoM-S-S-CoB to coenzyme M (CoM-SH) and coenzyme B (CoB-S) ($\Delta G^{0'}$ = -55 kJ/mol). Kaster and coworkers [15] answered the question of how these two cytoplasmic reactions were energetically coupled, by observing that cell extracts from *Methanothermobacter marburgensis* catalyzed the reduction of the *Clostridium pasteurianum* ferredoxin with H_2 at significant rates only in the presence of CoM-S-S-CoB. This was followed by the confirmation of the H_2:CoM-S-S-CoB oxidoreductase activity by the cytoplasmic MvhADG/HdrABC complex, composed of the [NiFe]-hydrogenase MvhADG and the heterodisulfide reductase HdrABC, which showed a complete reduction of ferredoxin with H_2 (100% at 1 bar) only when coupled to the reduction of CoM-S-S-

CoB. In this process, H_2 donates two electrons to the bifurcating flavin present in the HdrA subunit, which will bifurcate one electron to reduce the heterodisulfide and the other to reduce ferredoxin, followed by another round of electron-donation and bifurcation, which will complete the reduction of CoM-S-S-CoB to HS-CoB and HS-CoM and two equivalents of reduced ferredoxin, as depicted in **Figure 4.4A**. At Fd_{red}^{2-}/Fd_{ox} ratios >100 the redox potential of *C. pasteurianum* Fd (E_0' = -400 mV) approaches -500 mV, and the redox potential of the 2 H^+/H_2 couple is -414 mV. Therefore, ferredoxin can be fully reduced with H_2 (100% at 1 bar) at pH 7 only if the reduction is energy driven. The ferredoxin reduced by H_2 in the last step of methanogenesis allows the first steps of methanogenesis to occur, by donating the electrons for the endergonic CO_2 reduction.

Whilst the MvhADG/HdrABC FBEB mechanism was proposed since 2011, the MvhADG/HdrABC protein tridimensional structure from the methanogen *Methanothermococcus thermolithotrophicus* was solved only in 2017 by Wagner and colleagues [16] (**Figure 4.4B**), where a hypothesis for the electron route through the protein complex was also presented (**Figure 4.4C**).

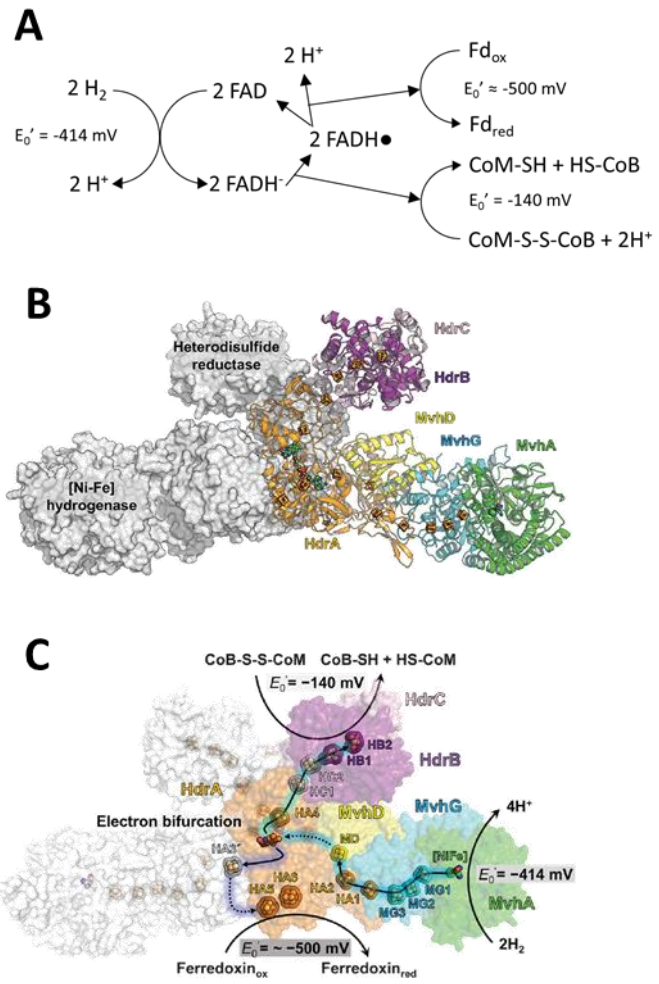

Figure 4.4 – MvhAGD-HdrABC from *M*. *thermolithotrophicus*. Scheme for the electron route from hydrogen to the flavin cofactor, followed by transfer to the high potential acceptor and then the low potential acceptor (**A**). Crystal structure of the heterodimer, with each subunit highlighted (**B**), and with the electron route depicted (**C**). Image taken from [16].

The HdrA subunit contains one FAD cofactor and six [4Fe-4S] clusters and is one of the most highly conserved proteins in methanogens. However, its presence is not restricted to methanogens, corroborating the formerly mentioned idea that electron bifurcation might be used in several metabolisms and

contexts [5]. The HdrA subunit contains an inserted ferredoxin domain, which is believed to go through conformational rearrangements to allow electron flow between FAD and the ferredoxin at its surface [16].

HdrB is the catalytic subunit directly involved in the CoM-S-S-CoB reduction. This subunit encodes two motifs characterized by the cysteine-rich sequence "CX_nCCGX_mCXXC" and named as CCG motifs, which were assigned to the binding of two Fe-S clusters with distinct spectroscopic characteristic [17], [18]. After solving the protein structure, each motif was found to harbor a non-cubane [4Fe-4S] cluster (by opposition to the well-known cubane [4Fe-4S]), which is composed of fused [3Fe-4S]-[2Fe-2S] units sharing 1 iron and 1 sulfur (**Figure 4.5**). It was postulated that the CoM-S-S-CoB disulfide bridge clamps between two exposed iron atoms of each non-cubane [4Fe-4S] clusters. Then, the disulfide is homolytically cleaved and the two coenzymes are released upon one-by-one electron transfer, with the electron of the first FBEB round reducing the [4Fe-4S]-S-CoB adduct, and HS-CoB being released. In the second round, electron transfer to the oxidized [4Fe-4S]-S-CoM adduct results in dissociation of HS-CoM.

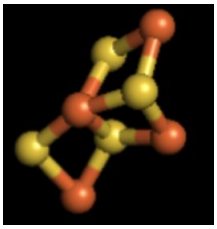

Figure 4.5 – Non-cubane [4Fe-4S] cluster. Image adapted from [16].

The HdrC subunit harbors two conventional [4Fe-4S] clusters and works as a linker module that electronically wires HdrA to HdrB [16].

Despite the Hdr complex having been extensively studied and already purified from some methanogenic organisms [16], [19], the study of the homologous complex in sulfate-reducers is still insufficient. As examples of Hdr homologues in sulfate-reducers, *Archaeoglobus fulgidus* contains the MvhAGD-HdrABC complex, while in *Desulfovibrio vulgaris*, the HdrABC is coupled with the flavin

oxidoreductase FlxABCD, forming the FlxABCD-HdrABC complex [20], [21]. However, the energy metabolism of sulfate-reducers is quite distinct from that of methanogens, and the coenzymes M and B do not exist. Ramos *et al*. [21] proposed that the *D*. *vulgaris* FlxABCD-HdrABC complex was able to accept electrons from NADH and transfer them to ferredoxin and DsrC, via a similar mechanism to the one described for MvhAGD-HdrABC. The FlxABCD-HdrABC complex is essential for *Dv*H when using ethanol as electron donor for sulfate respiration, and it is hypothesized to operate in the reverse direction during pyruvate fermentation, reducing NAD^+ for ethanol production [21]. In the case of *A*. *fulgidus*, the MvhAGD unit is present instead of FlxABCD [20], suggesting this organism may be able to couple hydrogen oxidation with ferredoxin and DsrC reduction.

Nonetheless, the interaction between these complexes and DsrC has not been shown yet, due to challenges regarding protein purification. Issues regarding purification of the Hdr complex, or some of its subunits, have already been mentioned for other organisms, such as HdrC from *Acidithiobacillus ferrooxidans* [22], [23] and HdrAB2C2 from *Methanosarcina acetivorans* [19]. In these studies, where the several Hdr subunits were expressed and purified separately, the presence of HdrC in inclusion bodies was recurrent. This obstacle was surpassed either by coexpressing HdrC together with HdrB [19], or by expressing HdrC in *E. coli* and purifying it from inclusion bodies [22], [23].

This chapter is focused on the expression and purification of the three subunits from the HdrABC complex from sulfate-reducers (*Desulfovibrio vulgaris* Hildenborough and *Archaeoglobus fulgidus*), namely the successful expression, purification and spectroscopic characterization of HdrA and HdrB, and the obstacles and strategies to overcome HdrC expression and purification.

4.3 – Material and Methods

4.3.1 – Strains, plasmids and primers

The *hdrB* gene from *D. vulgaris* Hildenborough (locus tag DVU2403) was amplified from its genomic DNA using the primers #1 and #2 and cloned into a modified pET22b(+) vector encoding a Strep-tag

sequence, using the *Nde*I and *BamH*I restriction sites, creating the vector pET22b(+)-HdrB-DvH.

The *hdrA-2* gene from *A. fulgidus* (locus tag AF1377) was amplified from its genomic DNA using the primers #3 and #4 and cloned into a modified pET22b(+) vector encoding a Strep-tag sequence, using the *Nde*I and *BamH*I restriction sites, creating the vector pET22b(+)-HdrA-Af .

The *hdrB* gene from *A. fulgidus* (locus tag AF1375) was amplified from its genomic DNA using the primers #5 and #6 and the restriction sites *Nde*I and *BamH*I, into a modified pET22b(+) vector encoding the strep-tag sequence, creating the vector pET22b(+)-HdrB-Af.

The plasmid pETDuet-1-HdrC-HdrB-Af was created by amplification of the *hdrB*-strep gene fragment from the pET22b(+)-HdrB-Af vector using the primers #7 and #8 and the restriction sites *Nde*I and *EcoR*V, and by amplification of the *A. fulgidus hdrC* gene (locus tag AF1376) using the primers #9 and #10 and the restriction sites *Nco*I and *Afl*II.

The plasmid pET22b(+)-HdrC-Af was created by amplification of the *hdrC*-strep gene fragment from the pETDuet-1-HdrC-HdrB-Af vector using the primers #11 and #12 and the restriction sites *Nde*I and *BamH*I, into the pET22b(+)-HdrB-Af, substituting *hdrB* from *hdrC* and maintaining the Strep-tag sequence, creating the pET22b(+)-HdrC-Af.

The plasmid pGEX4T2-GST-HdrC-Af was created by amplification of the *A. fulgidus hdrC* gene using the primers #13 and #14 and the restriction sites *BamH*I and *Xho*I, into the pGEX-4-T2 vector. The primer #14 contained a sequence for the Strep-tag, creating a plasmid that could express HdrC with a GST-tag at the N-terminus and a Strep-tag at the C-terminus.

The plasmids pET22b(+)-HdrB*-Af and pET22b(+)-HdrC*-Af, encode a codon-optimized version of *hdrB* and *hdrC*, respectively, for *A*. *fulgidus*. These genes were designed and synthetically produced by IDT Technologies (USA). The vector pET22b(+)-HdrA-Af served as cloning backbone to substitute HdrA for HdrB*/HdrC* and keep the Strep-tag sequence, by using the primers #15/#16 (HdrB) and #17/#18 (HdrC), and the restriction sites *Nde*I and *BamH*I.

All these plasmids were used together with pRARE and/or pRKISC. *Escherichia coli* BL21 and *Escherichia coli* BL21 Δ*iscR* competent cells were first transformed with the pRARE and/or the pRKISC plasmids by heat shock, and then treated by the TSS method to be again transformed by heat shock with the pET/pETDuet/pGEX plasmid. For the preparation of competent cells, the aforementioned *E. coli* strains were grown overnight in LB media at 37 °C, 180 rpm. On the next day, 250 µL of the culture were inoculated in 25 mL in SOB media (2% (w/v) tryptone, 0.5% (w/v) yeast extract, 10 mM NaCl, 2.5 mM KCl, 2 mM $MgCl_2$ and 2 mM $MgSO_4$) and incubated at 37 °C, 180 rpm until reaching an optical density of ≈ 0.6. The cell culture was then centrifuged (2100 *g*, 10 min at 4 °C), and the pellet resuspended in 8 mL of cold TB buffer (10 mM HEPES, 15 mM $CaCl_2$, 250 mM KCl and 55 mM $MnCl_2$, pH adjusted to 6.7), incubated 10 min on ice and centrifuged again (2100 *g*, 10 min at 4 °C). The cell pellet was resuspended in 2 mL cold TB Buffer with 7% (v/v) DMSO, stored in 50 µL aliquots and flash-frozen in liquid nitrogen. For transformation by heat shock, 50 µL of these competent cells were incubated with the plasmid (100 ng) on ice for 30 min, subjected to 42 °C for 45 seconds, 1 minute on ice, and then 950 µL of SOC media (SOB + 20 mM glucose) was added to the cells, followed by incubation for 1 h at 37 °C. The cells were then pelleted by centrifugation (5000 x *g*, 2 min), and the cell pellet plated into LB agar plates containing the desired antibiotic. For transformation by the TSS method, the *E. coli* cells containing the pRARE and/or pRKISC vector were grown overnight at 37 °C in LB media, with the appropriate antibiotic. On the following day, 500 µL of the overnight culture were inoculated into 50 mL LB media and grown until reaching an optical density of ≈ 0.4. The cells were then centrifuged (1000 x *g*, 10 min, 4 °C) and the cell pellet resuspended in 5 mL of cold TSS buffer (LB media containing 10% PEG 8000, 5% DMSO, 20 mM $MgCl_2$) [24], stored in 50 µL aliquots and flash-frozen in liquid nitrogen. These cells, already containing pRARE and/or pRKSIC vectors, were now receptive to be transformed with the pET/pETDuet/pGEX plasmid by the heath shock, as already referred, being able to carry more than one vector.

The *D. vulgaris* strain IPDF01 was created by electroporating the plasmid pMO719-HdrC-HdrB-Af in *D. vulgaris* Hildenborough wild-type (*Dv*H WT), using the method described in Keller *et al*. (2011) [25]. For the creation of the pMO719-HdrC-HdrB-Af plasmid, the fragment "*hdrC*-strep-*hdrB*-strep" from pETDuet-1-HdrC-HdrB-Af

was cloned into pMO719, a vector designed for use in *D*. *vulgaris* [26]. This was constructed via SLIC (Sequence Ligation Independent Cloning) according to Li & Elledge (2007) [27], by using the vector pETDuet-1-HdrC-HdrB-Af as a template and the primers #19 and #20 to flank the upstream and downstream regions of "*hdrC*-strep-*hdrB*-strep", and the pMO719 vector and primers #21 and #22, #23 and #24, for the vector backbone. The assembled plasmid was transformed into *E*. *coli* α-select Silver Efficiency (Bioline®), and the cells then plated on LB agar plates containing spectinomycin. The plasmid was then extracted and electroporated into *Dv*H cells, with the positive colonies selected in MOY solid medium.

All constructs were validated by sequencing. All strains, plasmids and primers used in this study are summarized in **Table 4.2**, **Table 4.3** and **Table 4.4**, respectively.

Table 4.2 – List of strains used in this study

Strain	Genotype	Source or reference
E. coli strains		
Escherichia coli BL21(DE3)	*E. coli* F$^-$ *ompT hsdS*$_B$(r_B^- m_B^-) *gal dcm* (DE3)	Novagen
Escherichia coli BL21(DE3) + pET28b(+)-DsrC-Af + pRARE	*E. coli* BL21(DE3) strain containing the vectors pET28b(+)-DsrC-Af and pRARE	[28]
Escherichia coli BL21(DE3) Δ*iscR*	F$^-$ *ompT hsdS*$_B$(r_B^- m_B^-) *gal dcm iscR*::kan (DE3)	[29]
E. coli Δ*iscR* + *p*ET22b(+)-HdrB-DvH	*E. coli* BL21 Δ*iscR* strain containing the vectors pET22b(+)-HdrB-DvH	This work
E. coli Δ*iscR* + *p*ET22b(+)-HdrA-Af	*E. coli* BL21 Δ*iscR* strain containing the vectors pET22b(+)-HdrA-Af	This work
E. coli Δ*iscR* + pET22b(+)-HdrB-Af	*E. coli* BL21 Δ*iscR* strain containing the vectors pET22b(+)-HdrB-Af	This work
E. coli Δ*iscR* + pET22b(+)-HdrC-Af + pRARE	*E. coli* BL21 Δ*iscR* strain containing the vectors pET22b(+)-HdrC-Af and pRARE	This work
E. coli Δ*iscR* + pETDuet-1-HdrC-HdrB-Af + pRARE	*E. coli* BL21 Δ*iscR* strain containing the vectors pETDuet-1-HdrC-HdrB-Af and pRARE	This work
E. coli BL21 + *p*ET22b(+)-HdrC-Af + pRKISC + pRARE	*E. coli* BL21 strain containing the vectors pET22b(+)-HdrC-Af, pRKISC and pRARE	This work
E. coli BL21 Δ*iscR* + pGEX4T2-GST-HdrC-Af + pRARE	*E. coli* BL21 Δ*iscR* strain containing the vectors pGEX4T2-GST-HdrC-Af and pRARE	This work
E. coli BL21 Δ*iscR* + pET22b(+)-HdrB*-Af	*E. coli* BL21 Δ*iscR* strain containing the vector pET22b(+)-HdrB*-Af	This work
E. coli BL21 Δ*iscR* + pET22b(+)-HdrB*-Af + pRARE	*E. coli* BL21 Δ*iscR* strain containing the vectors pET22b(+)-HdrB*-Af and pRARE	This work
E. coli BL21 Δ*iscR* + pET22b(+)-HdrC*-Af	*E. coli* BL21 Δ*iscR* strain containing the vector pET22b(+)-HdrC*-Af	This work
E. coli BL21 Δ*iscR* + pET22b(+)-HdrC*-Af + *pRARE*	*E. coli* BL21 Δ*iscR* strain containing the vectors pET22b(+)-HdrC*-Af and pRARE	This work
D. vulgaris strains		
*Dv*H WT	*D. vulgaris* Hildenborough ATCC 29579	ATCC
*Dv*H IPFG04	*Dv*H WT FlxA-Strep tag	[21]
*Dv*H IPDF01	*Dv*H WT + pMO719-HdrC-HdrB-Af	This work
A. fulgidus strains		
A. fulgidus WT	*A. fulgidus* DSM 4304 / VC-16	DSMZ

Table 4.3 – List of plasmids used in this study

Plasmid	Relevant characteristics	Source or reference
pET22b(+)	Bacterial protein expression vector with His6x-tag at C-terminal; Amp^R	Novagen
pET22b(+)-DsrJ-Strep	pET-22b(+) containing *dsrJ* from *Allochromatium vinosum*, with a Strep-tag at its C-terminal. This vector was already available at the laboratory, and was used to switch the *dsrJ* gene with the genes of interest for this study, while maintaining the C-terminal Strep-Tag	Laboratory collection
pET22b(+)-HdrB-DvH	pET-22b(+) containing *hdrB* from *D. vulgaris* (using restriction sites Nde*I* and BamH*I*), Strep-tag at C-terminal; Amp^R	This work
pET22b(+)-HdrA-Af	pET-22b(+) containing *hdrA* from *A. fulgidus* (using restriction sites NdeI and BamH*I*), Strep-tag at C-terminal; Amp^R. This plasmid was used for HdrA expression, and also used as backbone for the creation of pET22b(+)-HdrB*-Af and pET22b(+)-HdrC*-Af	This work
pET22b(+)-HdrB-Af	pET-22b(+) containing *hdrB* from *A. fulgidus* (using restriction sites Nde*I* and BamH*I*), Strep-tag at C-terminal; Amp^R. This plasmid was used for HdrB expression, and also used for *hdrB* amplification for construction of pETDuet-1-HdrC-HdrB-Af	This work
pET22b(+)-HdrC-Af	pET-22b(+) containing *hdrC* from *A. fulgidus* (using restriction sites Nde*I* and BamH*I*), Strep-tag at C-terminal; Amp^R	This work
pETDuet-1	Bacterial protein expression vector containing two multiple cloning sites (MCS), each of which preceded by a T7 promoter/lac operator and a ribosome binding site; Amp^R	Novagen
pETDuet-1-HdrC-HdrB-Af	pETDuet-1 containing *hdrC* and *hdrB* from *A. fulgidus* (using restriction sites NcoI/AflII, and NdeI/EcoR*V*, respectively), each gene with a Strep-tag at C-terminal; Amp^R	This work
pET22b(+)-HdrB*-Af	pET-22b(+) containing codon-optimized *hdrB* from *A. fulgidus* (using restriction sites Nde*I* and BamH*I*), Strep-tag at C-terminal; Amp^R	This work
pET22b(+)-HdrC*-Af	pET-22b(+) containing codon-optimized *hdrC* from *A. fulgidus* (using restriction sites Nde*I* and BamH*I*), Strep-tag at C-terminal; Amp^R	This work
pRARE2	Ability to express tRNAs for the rare codons in *E. coli*: AGG, AGA, AUA, CUA, CCC, GGA, CGG; Cm^R	Novagen
pRKISC	Vector encoding the *isc* gene cluster (*iscRSUA-hscBA-fdx-iscX*) from *E. coli*, and has been shown to enhance biogenesis of Fe-S clusters; Tc^R	[30]
pGEX-4T-2	Bacterial protein expression vector with GST-tag; Amp^R	Addgene
pGEX4T2-GST-HdrC-Af	pGEX-4T-2 containing *hdrC* from *A. fulgidus*, with Strep-tag at C-terminal (using restriction sites BamH*I* and Xho*I*); Amp^R	This work
pMO719	pCR8/GW/TOPO containing SRB replicon (pBG1); $Spec^R$	[26]
pMO719-HdrC-HdrB-Af	pMO719 expressing *hdrC* and *hdrB*, each with a Strep-tag at C-terminal; $Spec^R$	This work
pET28b(+)-DsrC-Af	pET-28b(+) expressing *dsrC* from *A. fulgidus*, containing the mutations C77→A and C85→A, and His6x-tag at N-terminal; Amp^R	[28]

Table 4.4 – List of primers used for plasmids construction

#	Primer	Primer sequence (5' → 3')	Observations
1	hdrB_DvH_forward_pET22	GGAGGAGAGGACCATATGAATCTCGCCTACTATCC	Amplification of *hdrB* from *D. vulgaris* genomic DNA to pET22b(+); Nde*I* restriction site
2	hdrB_DvH_reverse_pET22	GAAAACACCTAGGATCCTGCCCTGCCC	Amplification of *hdrB* from *D. vulgaris* genomic DNA to pET22b(+); BamH*I* restriction site
3	hdrA_Af_forward_ pET22	GGTCATATGAAAATTGGCGTTTACG	Amplification of *hdrA* from *A. fulgidus* genomic DNA to pET22b(+); Nde*I* restriction site
4	hdrA_ Af_reverse_pET22	CCTCACAAGGATCCTAATATCGC	Amplification of *hdrA* from *A. fulgidus* genomic DNA to pET22b(+); BamH*I* restriction site
5	hdrB_ Af_forward_pET22	GGCTTAATTCGGTCATATGTTTATGAAGTACG	Amplification of *hdrB* from *A. fulgidus* genomic DNA to pET22b(+); Nde*I* restriction site
6	hdrB_ Af_reverse_pET22	CAAAACCGATAAGGATCCTTCTCTCCC	Amplification of *hdrB* from *A. fulgidus* genomic DNA to pET22b(+); BamH*I* restriction site
7	hdrB_forward_pDuet	GGCTTAATTCGGTCATATGTTTATGAAGTACG	Amplification of *hdrB* from pET22b(+)-HdrB-*Af* to pETDuet-1; Nde*I* restriction site
8	hdrB_reverse_pDuet	CGGCCGATATCTTATTATTTTTCGAACTGCG	Amplification of *hdrB* from pET22b(+)-HdrB-*Af* to pETDuet-1; EcoR*V* restriction site
9	hdrC_Af_forward_pDuet	CATCCATGGCGAGAGTTGTGAGGCTGCC	Amplification of *hdrC* from *A. fulgidus* genomic DNA to pETDuet-1; Nco*I* restriction site
10	hdrC_Af_reverse_pDuet	TCTCTTAAGTTATTATTTTTCGAACTGCGGGTGGCTCCACCGAATTAAGCCCAGCT	Amplification of *hdrC* from *A. fulgidus* genomic DNA to pETDuet-1; Afl*II* restriction site; primer includes sequence for Strep-tag
11	hdrC_forward_pET22	GGAGATATCATATGGCGAGAGTTG	Amplification of *hdrC* from pETDuet-1-HdrC-HdrB-*Af* to pET22b(+)-HdrB-*Af* (substitution of *hdrB* to *hdrC* in pET22b); Nde*I* restriction site
12	hdrC_reverse_pET22	GTTCGACTTGGATCCCCGAATTAAG	Amplification of *hdrC* from pETDuet-1-HdrC-HdrB-*Af* to pET22b(+)-HdrB-*Af* (substitution of *hdrB* to *hdrC* in pET22b); BamH*I* restriction site
13	hdrC_Af_forward_pGEX4T2	ATAGGATCCATGAGAGTTGTGAGGC	Amplification of *hdrC* from *A. fulgidus* genomic DNA to pGEX-4T-2; BamH*I* restriction site
14	hdrC_Af_reverse_pGEX4T2	ATATCTCGAGTTATTATTTTTCGAACTGCGGGTGGCTCCACCGAATTAAGCCCAGC	Amplification of *hdrC* from *A. fulgidus* genomic DNA to pGEX-4T-2; Xho*I* restriction site; primer includes sequence for Strep-tag
15	hdrB_Af_optimized_forward	ATACATATGTTCATGAAATATGCC	Amplification of *hdrB* from *A. fulgidus* codon-optimized genomic DNA to pET22b(+)-HdrA-*Af*; Nde*I* restriction site
16	hdrB_Af_optimized_reverse	TATGGATCCCTCGCGGCCCTCC	Amplification of *hdrB* from *A. fulgidus* codon-optimized genomic DNA to pET22b(+)-HdrA-*Af*; BamH*I* restriction site
17	hdrC_Af_optimized_forward	ATACATATGCGTGTTGTTCGTTTGC	Amplification of *hdrC* from *A. fulgidus* codon-optimized genomic DNA to pET22b(+)-HdrA-*Af*; Nde*I* restriction site
18	hdrC_Af_optimized_reverse	TATGGATCCACGGATTAAGCCCAGC	Amplification of hdrC from *A. fulgidus* codon-optimized genomic DNA to pET22b(+)-HdrA-*Af*; BamH*I* restriction site
19	hdrC-s-hdrB-s_forward	CCCAGGAGGTACCATATGGCGAGAGTTGTGA GGCT	Construction of pMO719-HdrC-HdrB-Af by SLIC (amplification of the *hdrC*-strep-*hdrB*-strep fragment)
20	hdrC-s-hdrB-s_reverse	ATCGGGTCTTTTCGTTTATTATTTTTCGAACTGCGGGTGG	Construction of pMO719-HdrC-HdrB-Af by SLIC (amplification of the *hdrC*-strep-*hdrB*-strep fragment)
21	pMO719_1_forward	TTCGAAAAATAATAAACGAAAAGACCCGATCATGAAGGGG	Construction of pMO719-HdrC-HdrB-Af by SLIC (amplification of the pMO719 backbone)
22	pMO719_2_reverse	CGACTGAGCCTTTCGTTTTATTTGATGCCTGGCAGTTCCC	Construction of pMO719-HdrC-HdrB-Af by SLIC (amplification of the pMO719 backbone)
23	pMO719_3_forward	GGGAACTGCCAGGCATCAAATAAAACGAAAGGCTCAGTCG	Construction of pMO719-HdrC-HdrB-Af by SLIC (amplification of the pMO719 backbone)
24	pMO719_4_reverse	CACAACTCTCGCCATATGGTACCTCCTGGGACTGCATTGC	Construction of pMO719-HdrC-HdrB-Af by SLIC (amplification of the pMO719 backbone)

4.3.2 – Growth conditions for *Escherichia coli*

For the strains *E. coli* BL21 Δ*iscR* strains encoding pET22b(+)-HdrB-DvH, pET22b(+)-HdrA-Af + pRARE, pET22b(+)-HdrB-Af + pRARE, pET22b(+)-HdrC-Af + pRARE or pETDuet-1-HdrC-HdrB-Af + pRARE, a colony was picked and grown overnight at 37 °C. On the next day, 20 mL of this inoculum was added to a total of 500 mL LB media containing 100 mM MOPS, 25 mM glucose, 2 mM ammonium iron(III) chloride, and the antibiotics 50 µg/mL kanamycin, 100 µg/ml ampicillin and 30 µg/mL chloramphenicol. Cells were grown aerobically at 37 °C and 180 rpm until reaching the optical density of 0.45, 1.5, 2.0 or 2.2. At this point, the cell growth was interrupted, and 25 mM fumarate and 2 mM L-cysteine were added [31], [32]. The 500 mL culture media were transferred from a 2 L Erlenmeyer to a 500 mL Erlenmeyer flask, which was then transported inside an anaerobic Coy chamber with an atmosphere composed of 98% N_2 and 2% H_2. Once inside, 200 µM IPTG was added to the media, and the Erlenmeyer neck sealed with a rubber stopper. The Erlenmeyer was then removed from the anaerobic chamber, and placed at 20 °C, 150 rpm for 24h.

For the strain *E. coli* Δ*iscR* + pGEX4T2-GST-HdrC-Af + pRARE, the same growth conditions were applied, with the cells being induced when reaching an optical density of 2.0.

As for *E. coli* BL21 + pET22b(+)-HdrC-Af + pRKISC + pRARE, this strain was grown in LB media, first aerobically and then anaerobically at 20 °C for 24h, after inducing the cells with 200 µM IPTG when the cells reached an optical density of 3.3.

With this method, the Erlenmeyer's aerobic headspace was removed when the flasks entered the anaerobic chamber, and the rubber stopper avoids oxygen entrance from that point onwards. The oxygen dissolved in the culture media will be consumed and the protein expression under this anaerobic environment is advantageous to prevent oxidation of the iron-sulfur clusters.

The cell growth was monitored by measuring the optical density at the wavelength of 600 nm, using a DR3900 VIS Spectrophotometer (Hach).

4.3.3 – Growth conditions for *Desulfovibrio vulgaris*

*Dv*H WT, *Dv*H IPFG04 and *Dv*H IPDF01 strains were anaerobically grown at 37 °C in MO medium supplemented with 0.5 g/L yeast extract, with *Dv*H WT and *Dv*H IPDF01 supplemented with 30 mM sodium lactate and 30 mM sodium sulfate, and *Dv*H IPFG04 supplemented with 40 mM ethanol and 20 mM sodium sulfate, as described in [33]. MO medium is composed of 8 mM $MgCl_2$, 20 mM NH_4Cl, 600 µM $CaCl_2$, 2 mM K_2HPO_4-NaH_2PO_4, 0.6% (v/v) of a trace element solution (composed of 2.5 mM $MnCl_2.4H_2O$, 1.5 mM $CoCl_2.4H_2O$, 1.5 mM $ZnCl_2$, 0.2 mM $Na_2MoO_4.4H_2O$, 0.3 mM H_3BO_3, 0.4 mM $NiSO_4.6H_2O$, 0.01 mM $CuCl_2.2H_2O$, 0.02 mM $Na_2SeO_3.5H_2O$ and 0.025 mM $Na_2WO_4.2H_2O$) [34], 60 µM/120 µM $FeCl_2$/EDTA, 30 mM Tris-HCl, 1x Thauers Vitamins (14 mM Choline Chloride, 500 µM pyridoxine hydrochloride, 400 µM nicotinic acid, 360 µM *p* aminobenzoic acid, 240 µM lipoic acid, 230 µM D-pantothenic acid, 150 µM thiamine hydrochloride, 130 µM riboflavin, 80 µM biotin, 45 µM folic acid, 7.4 µM Vitamin B_{12}) [34], and the pH adjusted to 7.2. For the growth of *Dv*H IPDF01, containing the vector pMO719-HdrC-HdrB-Af, 100 µg/mL spectinomycin was also added to the medium.

4.3.4 – Growth conditions for *Archaeoglobus fulgidus*

Growth under lactate/sulfate conditions was performed by inoculating 10% inoculum in a total volume of 50 mL of growth media containing 30 mM lactate, 30 mM Na_2SO_4, 0.8 mM K_2HPO_4, 5.1 µM $Fe(NH_4)_2(SO_4)_2.6H_2O$, 0.5 g/L Yeast Extract, 20 mM PIPES, 1.2 mM thioglycolate, 1x mineral solution composed of 0.33 g/L KCl, 2.75 g/L $MgCl_2.6H_2O$, 0.25 g/L NH_4Cl, 0.14 g/L $CaCl_2.2H_2O$ and 18 g/L NaCl, and 1x Wolfe mineral solution composed of 15 mg/L nitrilotriacetic acid, 30 mg/L $MgSO_4.7H_2O$, 4.5 mg/L $MnSO_4.2H_2O$, 10 mg/L NaCl, 1 mg/L $FeSO_4.7H_2O$, 1.8 mg/L $CoSO_4.6H_2O$, 0.1 mg/L $CuSO_4.5H_2O$, 0.2 mg/L $KAl(SO_4)_2.12H_2O$, 0.1 mg/L H_3BO_3, 0.1 mg/L $Na_2WO_4.2H_2O$, 0.1 mg/L $Na_2MoO_4.2H_2O$, 3 mg/L Na_2SeO_3 and 0.25 mg/L $NiCl_2.6H_2O$. The pH was adjusted to 6.8, and cells were grown at 83 °C.

Growth under acetate/H_2/sulfate conditions was performed by inoculating 10% inoculum in a total volume of 25 mL growth media containing 48.8 mM sodium acetate, 28.2 mM Na_2SO_4, 6.7 mM KCl, 14.8 mM $MgCl_2.6H_2O$, 4.7 mM NH_4Cl, 1 mM $CaCl_2.2H_2O$, 0.8 mM

K_2HPO_4, 342 mM NaCl, 12 mM $NaHCO_3$, 1 g/L Yeast Extract, 13.2 mM PIPES, 1.2 mM thioglycolate and 1x Wolfe mineral solution. The pH was adjusted to 6.8. Before starting the growth, the headspace was sparged with H_2/CO_2 (80:20 (v/v)) during 30 min, and then overpressured with 1.5 bar. Cells were grown at 83 °C.

4.3.5 – Protein purification from the soluble fraction

When using *E*. *coli* as expression host, the cells were centrifuged anaerobically (10000 x *g*, 15 min, 4 °C) after growth, and the cell pellet was stored at -20 °C. After this point, all procedures were performed anaerobically under the N_2/H_2 (98%/2%) atmosphere inside the Coy anaerobic chamber. Around 3 g of cell pellet was resuspended in buffer composed of 100 mM Tris (pH 8.0), 150 mM NaCl, 0.005 mg/mL DNAse (Sigma) and Protease inhibitor (cOmplete™ Protease Inhibitor Cocktail, Roche), and anaerobically disrupted by sonication (80% amplitude, 0.7 pulse, 20 min) using the ultrasonic homogenizer UP200St coupled with the S2 sonotrode (Hielscher Ultrasonics, Germany). The resulting extract was promptly subjected to a heat shock at 70 °C for 10 min, followed by centrifugation (17000 x *g*, 30 min, 4 °C). The resultant soluble fraction was then immediately subjected to affinity purification, by loading in the gravity flow column containing Strep®-Tactin resin (IBA Lifesciences, Germany) equilibrated with 100 mM Tris-HCl (pH 7.5) and 150 mM NaCl (Buffer W). After five washing steps with Buffer W, the Strep-tagged protein was eluted with Buffer W containing 2.5 mM desthiobiotin. The eluted fraction, i.e., the purified protein, was concentrated and subjected to buffer change to 20 mM Tris (pH 7.5) using the Amicon Ultra-0.5 mL Centrifugal Filters (Merck). The purified proteins were anaerobically stored in glass vials.

For protein purification from *Dv*H cells, these were collected after growth and the cell pellet was stored at -20 °C. In contrast to what was performed for *E*. *coli*, the *Dv*H cells had to be disrupted outside the anaerobic chamber, due to the presence of hydrogen sulfide in the *Dv*H cell pellet that can irreversibly damage the palladium catalyst used in the Coy chamber for oxygen removal. The *Dv*H cells were broken in a French® Pressure Cell Press (Thermo IEC) with 1000 psi of pressure, using a system designed to maintain the cell's anaerobic environment. The cell debris was separated from the cell

extract by centrifugation (5000 x *g*, 20 min, 4 °C), and the cell extract (supernatant) then ultracentrifuged (68000 x *g*, 2 h, 4 °C) to separate the soluble from the membrane fraction. The soluble fraction was then subjected to heat shock and centrifugation, as previously described, and transferred to the anaerobic chamber for purification. The purification was performed by affinity chromatography, as described for the *E*. *coli* cells.

Protein concentration was determined using the BCA protein quantification method (Merck Millipore). The eluted fractions (20 µg) were analyzed in SDS-PAGE gels [12% acrylamide (v/v)] and stained with Coomassie Brilliant Blue (Bio-Rad).

4.3.6 – Protein purification from the membrane fraction

The cell pellet from strains *E*. *coli* BL21 Δ*iscR* + pETDuet-1-HdrC-HdrB-Af + pRARE and *E*. *coli* BL21 Δ*iscR* + pET22b(+)-HdrC*-Af + pRARE was anaerobically disrupted on a French Pressure Cell Press, as previously described. The cell debris was separated from the cell extract by centrifugation (5000 x *g*, 20 min, 4 °C) and the cell extract was ultracentrifuged (68000 x *g*, 2 h, 4 °C). The resultant pellet, the membrane fraction, was resuspended in Buffer W containing 2% n-dodecyl β-D-maltoside (DDM) and incubated with shaking for 1 h at 4 °C, followed by centrifugation (68000 x *g*, 2 h, 4 °C). The supernatant was loaded in the gravity flow column containing Strep®-Tactin resin and equilibrated with Buffer W + 0.1% (v/v) DDM, and purification proceeded as described above.

Protein concentration was determined using the BCA protein quantification method. The elution fractions (20 µg) were analyzed in SDS-PAGE gels [12% acrylamide (v/v)] stained with Coomassie Brilliant Blue, and by Western Blot (WB).

4.3.7 – Protein purification from inclusion bodies

E. *coli* BL21 Δ*iscR* + pET22b(+)-HdrC-Af + pRARE cells were grown and induced at OD of 2.2, as previously referred in **section 4.3.2**. Several protocols were tested for the purification and renaturation of HdrC from inclusion bodies, as described in **Table 4.5**.

Table 4.5 – Protocols tested for denaturation and renaturation of HdrC from inclusion bodies

Step	Protocol #1	Protocol #2	Protocol #3	Protocol #4	Protocol #5	Protocol #6
Cell resuspension	Resuspend cells in: 50 mM Tris-HCl (pH 8) 500 mM NaCl 1 mM EDTA	Resuspend cells in: 50 mM Tris-HCl (pH 8) 200 mM NaCl				
Cell disruption	Sonicate cells (20 min, 0.7 pulse, 70% amplitude) Centrifuge (6500 *g*, 30 min, 4 °C) Store the pellet					
Inclusion bodies washing	Resuspend pellet in: 50 mM Tris-HCl (pH 8) 500 mM NaCl 2% Triton X-100 2 M Urea	Resuspend pellet in: 50 mM Tris-HCl (pH 8) 200 mM NaCl 2% Triton X-100	Resuspend pellet in: 50 mM Tris-HCl (pH 8) 200 mM NaCl 2% Triton X-100 2 M Urea			
	Incubate 15 min at room temperature Wash: centrifuge 3x (12000 x *g*, 15 min, 4 °C) and change buffer					
Inclusion bodies denaturation	Resuspend pellet in: 50 mM Tris-HCl (pH 8) 500 mM NaCl 8 M Urea	Resuspend pellet in: 50 mM Tris-HCl (pH 8) 200 mM NaCl 5 mM DTT 6 M Guanidine-HCl	Resuspend pellet in: 50 mM Tris-HCl (pH 8) 200 mM NaCl 5 mM DTT 8 M Urea			
	3 h at 4 °C, with shaking	3 h at 4 °C, with shaking	3 h at 4 °C, with shaking	3 h at 4 °C, with shaking	1 h at 60 °C	1 h at 60 °C
	Centrifuge (48000 x *g*, 30 min, 4 °C) Collect supernatant					
Protein renaturation	Gradual dialysis – Step 1					
	20 mM Tris-HCl (pH 8) 150 mM NaCl 3 M Urea 5% Glycerol 0.005% Tween 2 mM reduced glutathione 0.02 mM oxidized glutathione	20 mM Tris-HCl (pH 8) 200 mM NaCl 3 M Guanidine-HCl 10% Glycerol 0.4 M L-Arginine	20 mM Tris-HCl (pH 8) 200 mM NaCl 3 M Urea 10% Glycerol 0.4 M L-Arginine 1 mM β-Mercaptoethanol	20 mM Tris-HCl (pH 8) 200 mM NaCl 3 M Urea 10% Glycerol 0.4 M L-Arginine	20 mM Tris-HCl (pH 8) 200 mM NaCl 3 M Urea 10% Glycerol 0.4 M L-Arginine 1 mM β-Mercaptoethanol	20 mM Tris-HCl (pH 8) 200 mM NaCl 3 M Urea 10% Glycerol 0.4 M L-Arginine
Protein renaturation	Gradual dialysis – Step 2					
	20 mM Tris-HCl (pH 8) 150 mM NaCl 1 M Urea 5% Glycerol 0.005% Tween 2 mM reduced glutathione 0.02 mM oxidized glutathione	20 mM Tris-HCl (pH 8) 200 mM NaCl 10% Glycerol 0.4 M L-Arginine	20 mM Tris-HCl (pH 8) 200 mM NaCl 10% Glycerol 0.4 M L-Arginine 1 mM β-Mercaptoethanol	20 mM Tris-HCl (pH 8) 200 mM NaCl 10% Glycerol 0.4 M L-Arginine	20 mM Tris-HCl (pH 8) 200 mM NaCl 10% Glycerol 0.4 M L-Arginine 1 mM β-Mercaptoethanol	20 mM Tris-HCl (pH 8) 200 mM NaCl 10% Glycerol 0.4 M L-Arginine
	Gradual dialysis – Step 3					
	20 mM Tris-HCl (pH 8) 150 mM NaCl 5% Glycerol	20 mM Tris-HCl (pH 8)				

The *E*. *coli* cells were disrupted by sonication, and several protocols were tested to assess the one with the best purification performance. Protocol #1 was adapted from [22], [23], while protocols #2 to #6 were formed based on various literature [35]–[38]. The variables tested between the several protocols were the use of 8 M Urea or 6 M Guanidine-HCl as denaturing agent, the use of high temperature (60 °C) to help denaturation, and the use of β-Mercaptoethanol to help reduce intra- and intermolecular disulphide bridges. The renaturation step occurred gradually using the Amicon Ultra-0.5 mL Centrifugal Filters. Due to protein precipitation during renaturation clogging the membrane and the difficulty of handling it in the anaerobic chamber, this step was carried out aerobically as a compromise.

The protocol with the most promising result was protocol #3, which was repeated and adjusted for the renaturation steps, as summarized in **Table 4.6**. The renaturation occurred anaerobically, and the urea's gradual removal was assessed by centricon concentration and by dialysis, with additional transitional urea concentrations: starting from 8 M to 5 M, 3 M, 1 M and finally 0 M. The Fe-S cluster reconstitution was also tested, during the last renaturation steps and at the end of renaturation. Fe-S cluster reconstitution was performed enzymatically using IscS from *E*. *coli*, according to Singh *et al*. [39]. Protein renaturation was performed inside an anaerobic Coy chamber with an atmosphere composed of 98% N_2 and 2% H_2.

Table 4.6 – Variations of Protocol #3 tested for renaturation of HdrC

Renaturation	Renaturation & Fe-S reconstitution
Gradual dialysis – Step 1	
20 mM Tris-HCl (pH 8) 200 mM NaCl 5 M Urea 10% Glycerol 0.4 M L-Arginine 1 mM β-Mercaptoethanol	
Gradual dialysis – Step 2	
20 mM Tris-HCl (pH 8) 200 mM NaCl 3 M Urea 10% Glycerol 0.4 M L-Arginine 1 mM β-Mercaptoethanol	
Gradual dialysis – Step 3	
20 mM Tris-HCl (pH 8) 200 mM NaCl 1 M Urea 10% Glycerol 0.4 M L-Arginine 1 mM β-Mercaptoethanol	20 mM Tris-HCl (pH 8) 200 mM NaCl 1 M Urea 10% Glycerol 0.4 M L-Arginine 500 µM $FeCl_2$ 5 mM DTT 55 nM IscS 2 mM L-Cysteine
Gradual dialysis – Step 4	
20 mM Tris-HCl (pH 8) 200 mM NaCl 10% Glycerol 0.4 M L-Arginine 1 mM β-Mercaptoethanol	20 mM Tris-HCl (pH 8) 200 mM NaCl 10% Glycerol 0.4 M L-Arginine 500 µM $FeCl_2$ 5 mM DTT 55 nM IscS 2 mM L-Cysteine
Gradual dialysis – Step 5	
20 mM Tris-HCl (pH 8)	

The renaturated samples (20 µg) were quantified by the BCA method and analyzed in SDS-PAGE gels, as previously described.

4.3.8 – Fe-S cluster reconstitution

Fe-S cluster reconstitution was performed enzymatically using IscS from *E. coli*, according to Singh *et al*. [39], inside an anaerobic COY chamber with an atmosphere composed of 98% N_2 and 2% H_2. Iron quantification was performed with pure protein preparations using the 2,4,6-tripyridyl-1,3,5-triazine (TPTZ) colorimetric method [40]. Protein concentration was determined using the BCA Protein Assay Kit (Merck Millipore). FAD detection and quantification was performed by reverse-phase HPLC.

4.3.9 – Spectroscopic characterizations

UV-visible absorption spectroscopies were performed inside a Coy anaerobic chamber (98% N_2, 2% H_2 atmosphere), using quartz cuvettes (Hellma) and a Shimadzu UV-1800 spectrophotometer. For this, 10 µM of protein was used, and protein reduction was performed by adding small amounts of dithionite powder. The protein samples were scanned through the wavelengths of 250 to 650 nm.

For characterization by Electron Paramagnetic Resonance (EPR), the titration of *D*. *vulgaris* HdrB was also performed inside the anaerobic chamber. For this purpose, 80 µM of this protein was incubated in 50 mM MOPS buffer (pH 7.5) containing 5 mM EDTA and a mixture of redox mediators at the concentration of 150 µM. This mixture included: 1,2-naphthoquinone, phenazine methosulfate, phenazine ethosulfate, methylene blue, indigo tetrasulfonate, indigo disulfonate, 2-hydroxy-1,4-naphthoquinone, antraquinone-2-sulfonate, safranine, neutral red, benzyl viologen and methyl viologen. The protein was first reduced with increasing amounts of dithionite and then oxidized with increasing amounts of ferricyanide, with samples being taken at several redox potentials. The reduction potentials were measured with a combined Ag/AgCl electrode calibrated against a saturated quinhydrone solution at pH 7 and referenced to the standard hydrogen electrode.

EPR spectroscopy was recorded on a Brucker EMX spectrometer equipped with an Oxford Instruments ESR-900 continuous flow helium cryostat. Protein samples were prepared anaerobically to a final concentration of 80 µM. The reduced sample was prepared by incubation with dithionite in excess amount.

4.3.10 – Western Blot analysis

For the protein purification from the *E*. *coli* membrane fraction, 10 µg of each sample was run on an SDS-PAGE and then transferred to a 0.45 µm PVDF membranes (Roche) (transfer buffer: 48 mM Tris-HCl and 39 mM glycine, pH 9.2) using a Mini Trans-Blot® electrophoretic transfer cell (BioRad) at 100 V during 30 min, at 4 °C. The membrane was incubated with PBS Blocking Buffer [4 mM KH_2PO_4, 16 mM Na_2HPO_4, 115 mM NaCl, 3% BSA, 0.5% (v/v) Tween 20, pH 7.4] during 1 h at room temperature (RT), washed three times with PBST [4 mM KH_2PO_4, 16 mM Na_2HPO_4, 115 mM NaCl, 0.1% (v/v) Tween

20, pH 7.4]. Following this, the membrane was incubated with 10 mL PBST together with 10 µL biotin blocking buffer for 10 min at RT, being the Strep-Tactin alkaline phosphatase conjugate then added at a 1:4000 dilution, and the membrane incubated for 1 h at RT. After two washes with PBST buffer and two washes with PBS buffer (4 mM KH_2PO_4, 16 mM Na_2HPO_4, 115 mM NaCl, pH 7.4), the protein revelation was performed by incubating the membrane in a 10 mL composed of 100 mM Tris-HCl pH 8.8, 100 mM NaCl, 5 mM $MgCl_2$ and 10µL of the NBT/BCIP (nitro-blue tetrazolium chloride/5-bromo-4-chloro-3-indolylphosphate toluidine) solution.

For the protein purification from the *D*. *vulgaris* IPFG04 soluble fraction, 10 µg of each sample was run on an SDS-PAGE and transferred to a PVDF membrane as described above. The membrane was incubated with TBS Blocking Buffer [20 mM Tris-HCl, 150 mM NaCl, 1.2% milk powder, 0.015% (v/v) Tween 20, pH 7.6] containing the anti-FlxA antibody at a 1:3000 dilution, during 1 h at RT, and then incubated with TBS Blocking Buffer containing anti-rabbit IgG-alkaline phosphatase antibody at a 1:15000 dilution, for 45 min at RT. At the end of each incubation step, membranes were washed three times with TBS (20 mM Tris-HCl, 150 mM NaCl, pH 7.6). Protein revelation was performed as above mentioned.

The anti-FlxA antibody was produced in rabbits with synthesized peptides based on *D*. *vulgaris* Hildenborough FlxA amino acid sequence (DGPVFSYAELKELPNEL), at Davids Biotechnologie GmbH®.

4.3.11 – Measurement of hydrogenase activity

A. *fulgidus* cells grown in H_2/CO_2/thiosulfate were treated with BugBuster protein extraction reagent (Merck Millipore), and the hydrogenase activity was measured on 500 µg of soluble fraction and 50 µg of the membrane fraction. The soluble fraction from *A*. *fulgidus* grown on lactate/thiosulfate was subjected to ionic exchange chromatography, and 300 µg of total protein of each eluted fraction was gel loaded to analyze the hydrogenase activity. The NiFeSe hydrogenase from *D*. *vulgaris* (2 µg) was used as positive control. These samples were run on a native acrylamide gel composed of 25 mM Tris, 190 mM Glycine, 7.5% (w/v) acrylamide, 0.1% (w/v) Triton, 0.06% (w/v) APS, and 0.1% TEMED for the

resolving part, and composed of 25 mM Tris, 190 mM Glycine, 3.75% (w/v) acrylamide, 0.1% (w/v) Triton, 0.06% (w/v) APS, and 0.1% TEMED for the stacking part. The gel was run at 4 °C in a buffer composed of 25 mM Tris, 190 mM Glycine and 0.1% Triton (w/v). After finishing the run, the gel is inserted in a Schott glass bottle containing N_2-degassed 50 mM Tris-HCl (pH 8) and 500 µM methyl viologen, and sparged with H_2. After the appearance of blue bands, a fixating agent (Triphenyltetrazolium chloride) is added to final concentration of 30 mM.

4.3.12 – Enzymatic assays with DsrC

The *A*. *fulgidus* DsrC was expressed in *E*. *coli* BL21(DE3) containing the plasmids pET28b(+)-DsrC-Af and pRARE. This strain grew in LB medium at 37 °C until reaching an optical density (OD) of 0.4 at the wavelength of 600 nm, being then induced with 200 µM IPTG for 5 h. The cell pellet was collected by centrifugation and stored at -20 °C, being then resuspended in a buffer composed of 25 mM KH_2PO_4/K_2HPO_4 (pH 7.4), 300 mM NaCl, 30 mM imidazole, 0.005 mg/mL DNAse and Protease inhibitor, and lysed in the French Pressure Cell Press [28].

DsrC was purified by taking advantage of the His-tag present at its N-terminus, by immobilized metal affinity chromatography (IMAC) using a 1 ml HisTrap HP column. DsrC was eluted with 25 mM KH_2PO_4/K_2HPO_4 (pH 7.4), 300 mM NaCl and 150 mM imidazole, with the salt and imidazole later removed by sequential centrifugations using a centrifugal filter unit with a 10 kDa cutoff. 1 mL of purified DsrC at the concentration of 1.5 mM was reduced by incubating with 5 mM DTT for 30 min at 37 °C, with the DTT later removed by sequencing centrifugations using a centrifugal filter unit. The reduced DsrC was then used to produce enzymatically DsrC-trisulfide, by anaerobically incubating 150 µM of reduced DsrC with 1 mM methyl viologen, 500 µM SO_3^{2-} and 200 nM *A*. *fulgidus* DsrAB. The reaction occurred anaerobically at 60 °C in a quartz cuvette, and DsrC oxidation was followed by the methyl viologen oxidation at 732 nm, using a Shimadzu UV-1800 spectrophotometer [28].

For the interaction between *A*. *fulgidus* DsrC and *A*. *fulgidus* HdrB, the reaction was performed anaerobically at 60 °C in a buffer composed of 50 mM K_2HPO_4/KH_2PO_4 (pH 7.0), 1 mM methyl

viologen, 500 nM of HdrB and 30 µM of DsrC trisulfide. The reduction was followed by the methyl viologen oxidation at 732 nm. After the reaction, a sample of the mixture was incubated with Maleimide PEG (MalPEG) for 15 minutes at 37 °C, and then analyzed in a 10% Tricine-SDS-PAGE gel [41].

For the interaction between the *Dv*H IPDF01 cell extract (with expressed *A*. *fulgidus* HdrB and HdrC) and *A*. *fulgidus* DsrC, the reaction was performed anaerobically at either 70 °C or 80 °C, in a buffer composed of 50 mM K_2HPO_4/KH_2PO_4 (pH 7.0), 1 mM methyl viologen, 0.01 µg/µL or 0.05 µg/µL of DvH IPDF01 cell extract and 30 µM of DsrC trisulfide. The reduction was followed by the methyl viologen oxidation at 732 nm. After the reaction, a sample of the mixture was incubated with MalPEG for 15 minutes at 37 °C, and then analyzed in a 10% Tricine-SDS-PAGE gel.

4.4 – Results

4.4.1 – The HdrA subunit

4.4.1.1 – Expression, purification & spectroscopic characterization of *A. fulgidus* HdrA

The *A. fulgidus* HdrA subunit was heterologously expressed using the *Escherichia coli* Δ*iscR* strain as expression host. This strain carries a deletion mutation for the *iscR* gene, the repressor of the *isc* operon expression, enhancing the overexpression of [Fe-S]-cluster-containing proteins [29]. The effectiveness of this strain was already proven in the production of [FeFe] hydrogenases, as well as Hdr complexes from methanogenic organisms [19], [29], [31], [42]. Besides the pET22b(+) plasmid encoding *hdrA*, this strain was also transformed with pRARE, a plasmid suited for the expression of genes encoding for tRNA cognate to codons rare in the *E. coli* host, and which have a higher usage frequency in eukaryotic cells and archaeal cells, such as the case for *A. fulgidus* [43].

HdrA was purified by affinity chromatography, presenting a molecular weight matching its theoretical value of 73 kDa (**Figure 4.5A**). After protein purification, HdrA was submitted to incubation with the IscS protein to assist in the Fe-S assemblage, and also with FAD. This resulted in a FAD/Protein ratio increase from 0.69 ± 0.02 to 0.84 ± 0.04 upon reconstitution, and the Fe/Protein ratio from 16.7 ± 1.0 to 20.7 ± 1.6, experimental values close to the expected values of 1 FAD/Protein and 24 Fe/Protein, corresponding to six [4Fe-4S] clusters. The UV-Visible scanning of *A. fulgidus* HdrA presented absorption bands centered at 320 nm and 420 nm corresponding to the Fe-S clusters, with the 320 nm band enhanced after incubation with IscS (**Figure 4.5B**).

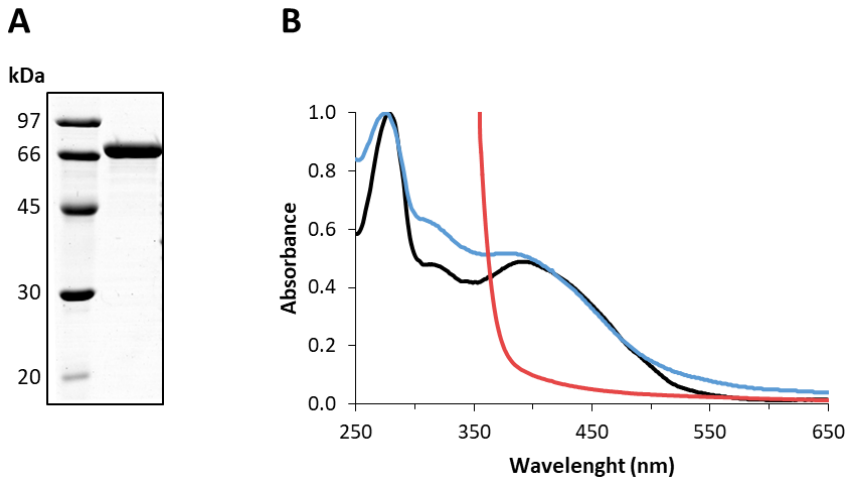

Figure 4.5 – Purification of *A*. *fulgidus* HdrA-Strep using *E*. *coli* Δ*iscR* as expression host. SDS-PAGE with the eluted band corresponding to HdrA **(A)** and UV-Visible spectra of *A*. *fulgidus* HdrA as purified (black), after Fe-S and FAD reconstitution (blue) and after reduction with dithionite in excess (red) **(B)**.

4.4.2 – The HdrB subunit

4.4.2.1 – Expression, purification & spectroscopic characterization of *D. vulgaris* HdrB

The *D*. *vulgaris* HdrB subunit could also be expressed using the *E*. *coli* Δ*iscR* strain as expression host. This protein subunit was purified by affinity chromatography, presenting a molecular weight matching its theoretical value of 39 kDa (**Figure 4.6A**). The UV-Vis scanning of *D*. *vulgaris* HdrB shows absorption bands centered at 320 nm and 420 nm, corresponding to the presence of Fe-S clusters (**Figure 4.6B**). Unlike *A. fulgidus* HdrA, there was no apparent difference in the UV-Visible spectra before and after Fe-S centers reconstitution, which is in accordance with the observation that the Fe amount did not change after IscS incubation, presenting a Fe/Protein ratio of 4.4 ± 0.2, against the expected value of 8 Fe/Protein.

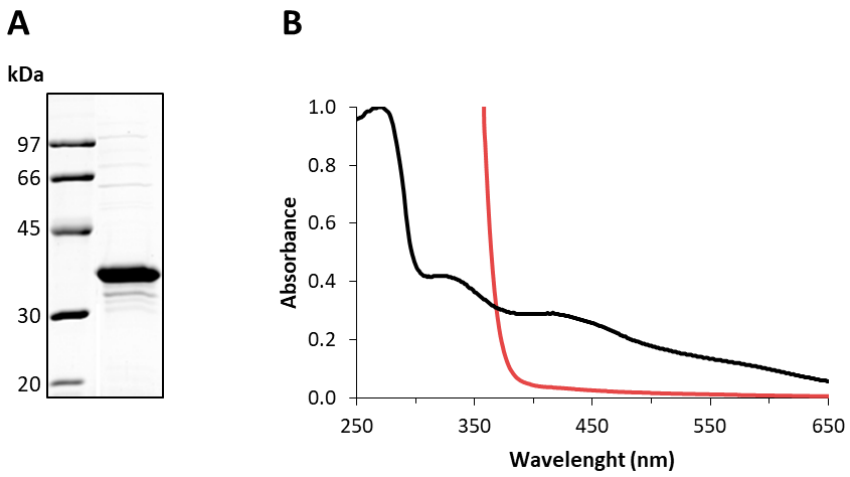

Figure 4.6 – Purification of *D*. *vulgaris* HdrB-Strep using *E*. *coli* Δ*iscR* as expression host. SDS-PAGE with the eluted band corresponding to HdrB **(A)** and UV-Visible spectra of *D*. *vulgaris* HdrB as purified (black) and after reduction with dithionite in excess (red) **(B)**.

Samples of *D*. *vulgaris* HdrB protein, namely as purified, dithionite reduced and oxidized by air exposure, were subjected to EPR spectroscopy. The protein presented a distinctive rhombic signal (g_{xyz} = 2.016, 1.989, and 1.948) (**Figure 4.7A**) characteristic of proteins containing a non-cubane [4Fe-4S] cluster, which has a spin of ½ in the oxidized state. Examples of proteins containing this unusual Fe-S cluster are HdrABC from *M*. *marburgensis* (g_{xyz} = 2.013, 1.991 and 1.938) [17], Mvh-Hdr from *A*. *profundus* [18], DsrMKJOP (previously designated as Hme) from *A. fulgidus* [44] and DsrMKJOP from *D*. *desulfuricans* (g_{xyz} = 2.027, 1.991 and 1.943) [45]. This result confirms the assembly of the non-cubane Fe-S cluster in the *D*. *vulgaris* HdrB protein. To the best of my knowledge, this is the first demonstration of heterologous expression of a protein encoding a non-cubane [4Fe-4S] cluster using *E*. *coli* as expression host.

This protein was also redox titrated in order to determine the redox potential of its center(s). An overlay of the several spectra obtained during the titration can be seen in **Figure 4.7B.** By focusing on *g* = 2.016 (*g* max), it is possible to see two signals with distinct redox potentials, suggesting the existence of two centers. However, their

midpoint potential could not be determined due to the fact that experimental data do not perfectly fit the Nernst equation for simple situations (such as non-cooperative). One explanation could be that, despite the detection of non-cubane 4Fe-4S clusters in EPR, other redox center populations can be present and be interfering with the signal. Moreover, a signal near $g = 2$ is observed (typically assigned to mediators radical), particularly visible in the titrations between +9 and -74 mV. This signal interferes with the signal for the non-cubane [4Fe-4S] center with the higher midpoint potential and does not affect the signal from the non-cubane [4Fe4S] center with lower the midpoint potential. Madadi-Kahkesh *et al*. [17] reported similar observations when performing EPR spectroscopy of the HdrABC complex from *M. marburgensis*, where a signal appeared next to the signal of redox centers with a midpoint potential of -30 mV, and did not appear on the center with the lower midpoint potential, -185 mV. The authors reported this as radical signals from the redox dyes used for the sample titration, having to simulate the EPR signal to obtain the signal intensity for the non-cubane [4Fe-4S] center.

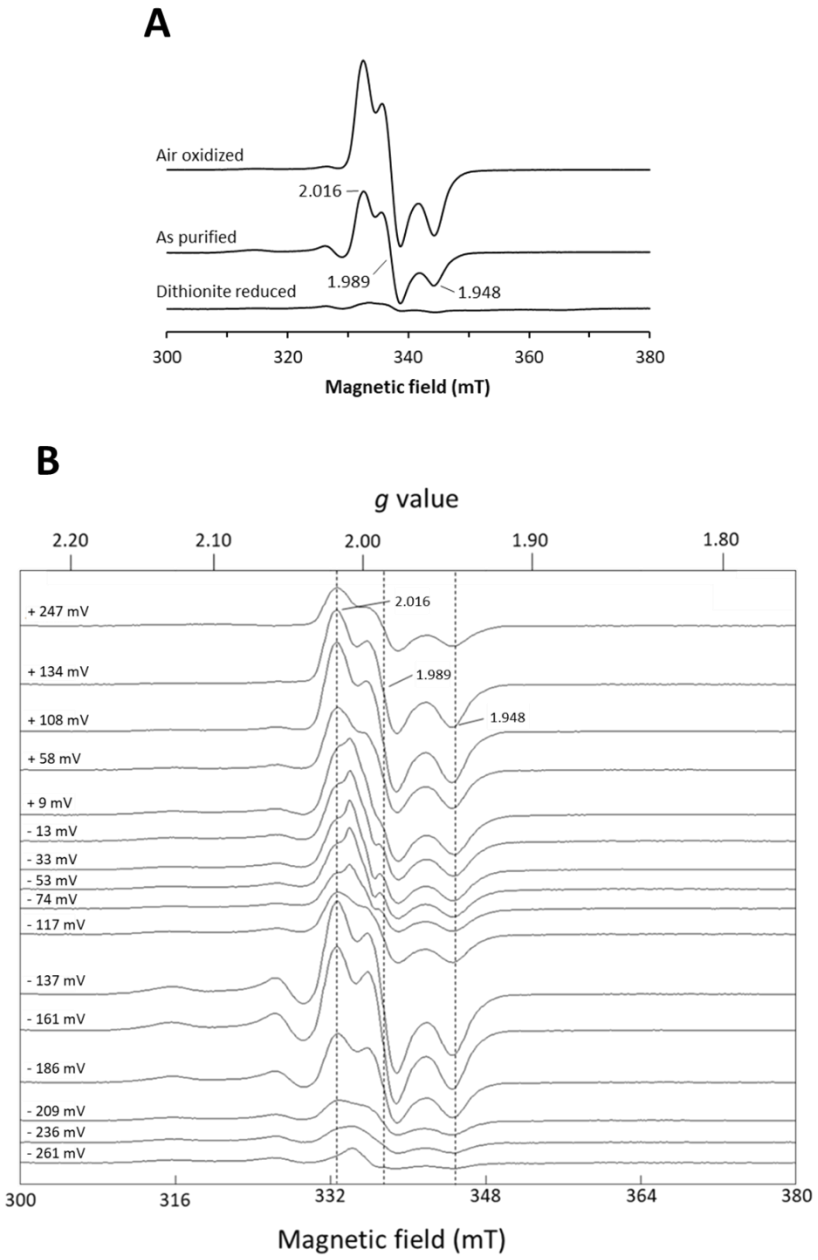

Figure 4.7 – EPR characterization of *D*. *vulgaris* HdrB. EPR signal for HdrB as purified, reduced with dithionite, and oxidized by air exposure **(A)**, and EPR spectra of HdrB under several redox potentials at 15 K **(B)**.

4.4.2.2 – Expression, purification & spectroscopic characterization of *A. fulgidus* HdrB

The *A*. *fulgidus* HdrB protein subunit was also successfully expressed using the same methodology as for *A*. *fulgidus* HdrA and *D*. *vulgaris* HdrB. This protein subunit was purified by affinity chromatography, presenting a molecular weight matching its theoretical value of 35 kDa (**Figure 4.8A**). The UV-Visible spectrum of *A*. *fulgidus* HdrB shows also absorption bands centered at 320 nm and 420 nm, corresponding to the presence of Fe-S clusters (**Figure 4.8B**). As with *D*. *vulgaris* HdrB, there was no apparent difference in the UV-Visible spectra before and after Fe-S centers reconstitution, which is also in accordance with the Fe quantification that did not change after IscS incubation. Quantification showed that Fe/Protein ratio is of 6.7 ± 0.6, closer to its expected value of 8 Fe/Protein and better than the one obtained for *D. vulgaris* HdrB. However, the total protein expressed and isolated was much less than the counterpart from *D.vulgaris*, which did not allow to run EPR characterization.

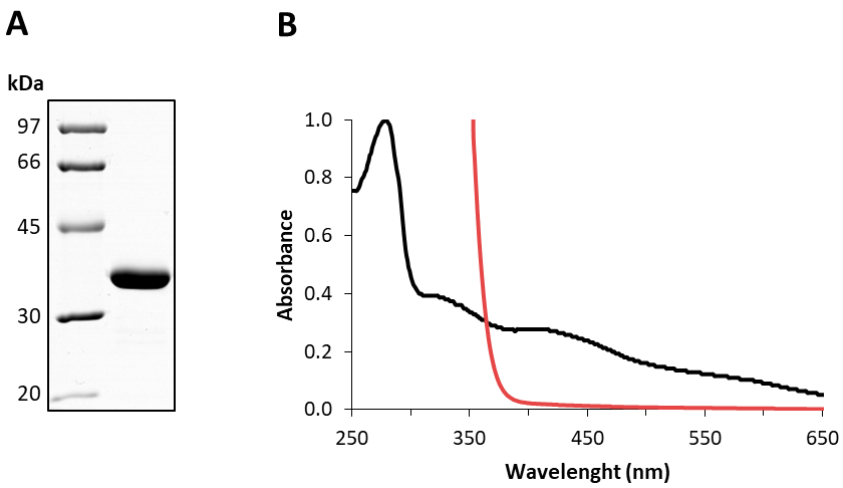

Figure 4.8 – Purification of *A*. *fulgidus* HdrB-Strep using *E*. *coli* Δ*iscR* as expression host. SDS-PAGE showing the eluted band corresponding to HdrB **(A)** and UV-Visible spectra of *A*. *fulgidus* HdrB as purified (black) and after reduction with dithionite in excess (red) **(B)**.

4.4.3 – The HdrC subunit

4.4.3.1 – Expression of *A*. *fulgidus* HdrC using the *E*. *coli* Δ*iscR* strain

The first approach used to express *A*. *fulgidus* HdrC was using the *E*. *coli* Δ*iscR* strain, i.e., the same approach previously used to successfully express HdrA and HdrB subunits from *A*. *fulgidus*, and HdrB subunit from *D*. *vulgaris*. The strain was transformed with a pET22b(+) plasmid encoding HdrC with a Strep-tag at its C-terminal (theoretical molecular weight of 19 kDa), together with the pRARE.

Besides pET22b(+)-HdrC-Af, an expression vector in which HdrC could be co-expressed with HdrB was also created. This approach was based on previous report from Yan *et al*. [19], referring problems upon purifying HdrC alone due to the formation of inclusion bodies, which was circumvented by coexpressing HdrC together with HdrB, using the pETDuet-1 expression system. For this purpose, both *hdrC*-strep and *hdrB*-strep genes were cloned into pETDuet-1, with each gene containing its own ribosomal binding site and strep-tag at C-terminal, creating the strain *E*. *coli* BL21 Δ*iscR* + pDuet-1- HdrC-HdrB-Af + pRARE.

Figure 4.9 presents a simplified plasmid map for both pET22b(+)-HdrC-Af and pDuet-1-HdrC-HdrB-Af (**Figure 4.9A**), together with SDS-PAGE results showing expression profile before and after induction (**Figure 4.9B** and **Figure 4.9C**), the expression of the eluted fractions after Strep-tag purification (**Figure 4.9D**), and a SDS-PAGE of the solubilized inclusion bodies (**Figure 4.9E**).

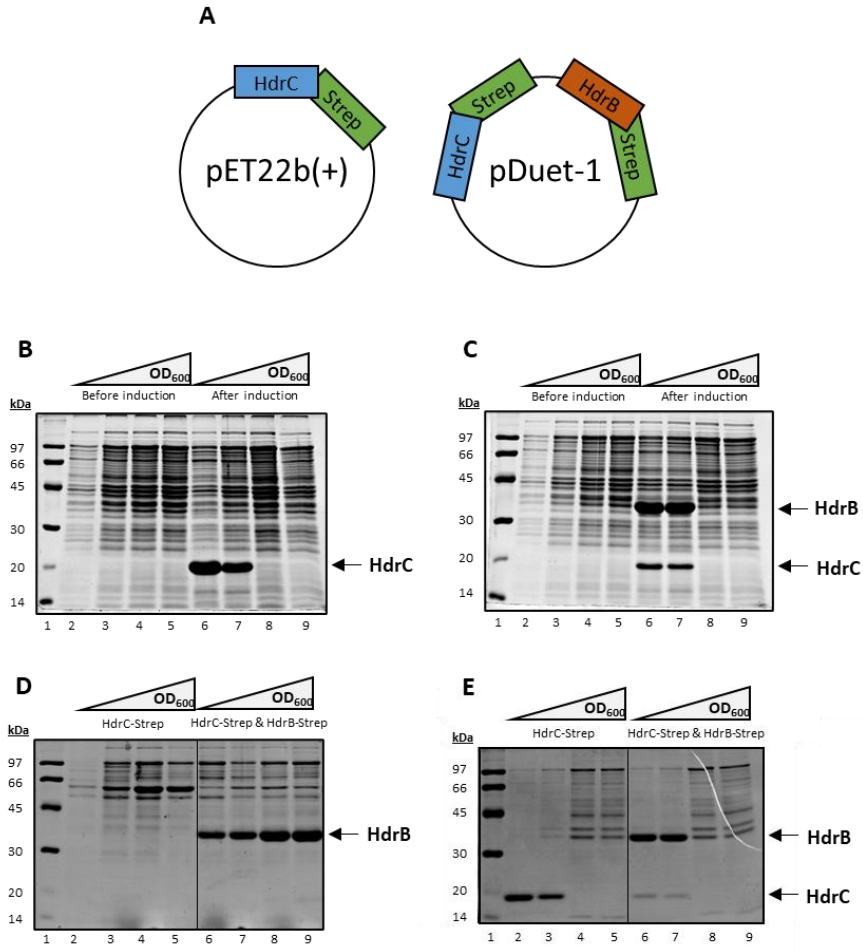

Figure 4.9 – Plasmid organization for pET22b(+)-HdrC-Af and pDuet-1-HdrC-HdrB-Af **(A)**; Cell pellet before induction and after induction, for several induction optical densities tested in *E*. *coli* + pET22b(+)-HdrC-Af + pRARE **(B)** and *E*. *coli* BL21 Δ*iscR* + pDuet-1-HdrC-HdrB-Af + pRARE **(C)**; Eluted fraction for the two vectors and several induction optical densities tested **(D)**; Solubilized resulting pellet from centrifugation after sonication, which includes unbroken cells, cell debris and insoluble material such as inclusion bodies **(E)**. Protein bands corresponding to HdrC and HdrB are indicated.

By looking at **Figure 4.9**, it is possible to see that a higher expression of HdrC (**Figure 4.9B**) and HdrC/HdrB (**Figure 4.9C**) occurs when

IPTG is added at lower optical densities such as 0.45 and 1.5 (lanes 6 and 7), and this is in accordance with the cells being on exponential phase at the moment of induction, which is when there is a lot of nutrients still available. This together with lower growth temperatures of 20 °C, forces the cells to shift their metabolism from growth to protein massive expression. For induction at higher bacterial densities, such as 2.0 and 2.2 when cells are in stationary phase, there is no distinguishable band for HdrC and/or HdrB when comparing the cell pellet before and after IPTG induction (**Figure 4.9B** and **Figure 4.9C**, lanes 8 and 9). After breaking the cells and applying the soluble fraction into a Strep-tactin column, no HdrC was found in any case (**Figure 4.9D**). However, in the case of the pDuet-HdrC-HdrB plasmid, HdrB was detected in higher amounts when higher optical densities were used for protein expression.

Common strategies to enhance the yield of protein expression usually includes lowering the concentration of inducer in the media and/or lowering the temperature, in order to slow down the protein expression rate and consecutively decrease the amount of misfolded proteins and proteins deposited in the form of inclusion bodies [46], [47]. In this case, the induction at a time-point where the cells are metabolically less active, such as stationary phase, is likely causing the cells to express less, but soluble, protein. This is also supported by the higher amounts of HdrC and HdrB detected in the cell pellet (**Figure 4.9E**, lanes 2, 3, 6 and 7), which is composed in part by the inclusion bodies. Despite the observed coexpression with HdrB (**Figure 4.9C**, lanes 6 and 7), HdrC could not be purified successfully (**Figure 4.9D**, lanes 6 and 7).

4.4.3.2 – Expression of *A. fulgidus* HdrC using the pRKISC vector

One alternative was the use of the pRKISC vector, instead of using the *E. coli* strain with a mutation in the repressor for the *isc* operon. The pRKISC vector encodes the entire *isc* gene cluster (*iscRSUA-hscBA-fdx-iscX*) and has been shown to enhance the biogenesis of Fe-S clusters [30]. This strategy focused on the overexpression of the *isc* operon instead of deletion of its repressor. *E. coli* BL21 was transformed with 3 plasmids: pET22b(+)-HdrC-Af, pRKISC and pRARE, and grown in LB media. **Figure 4.10** shows a simplification of the expression vectors present in this host strain (**Figure 4.10A**),

as well as the results for the protein purification using this expression system (**Figure 4.10B**).

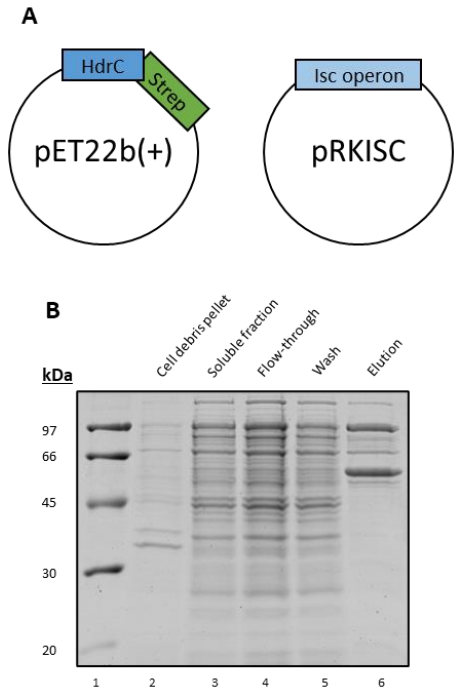

Figure 4.10 – Plasmid organization for pET22b(+)-HdrC-Af and pRKISC **(A)**; SDS-PAGE showing the band pattern for the resulting pellet from centrifugation after sonication, and respective soluble fraction, the flow-through, wash, and elution fractions from affinity purification **(B)**.

In **Figure 4.10B** it is possible to observe that the band pattern for soluble fraction, flow-through and wash are very similar between them, which is expected given the type of chromatography used. On the other hand, there was no evidence of HdrC in the elution fraction (expected band of ≈ 19 kDa). This elution fraction protein content was quite low, indicative of a defective expression system in HdrC and, therefore, it was necessary to perform acetone precipitation prior to gel loading. Still, only high-molecular weights bands were observed in this fraction, which do not match with HdrC molecular weight. As a consequence of this precipitation procedure, proteins

present in considerable low amounts were concentrated and became visible, despite being present in low amounts.

4.4.3.3 – Expression of *A. fulgidus* HdrC using a tag solubility enhancer

One issue related with soluble expression of HdrC could be related with the lower solubility of this protein. A way to circumvent this is the addition of a soluble fusion tag that will create and express a protein that is overall more soluble. There are several tags designed to increase solubility properties of recombinant proteins, with Glutathione S-transferase (GST), Thioredoxin (Trx), Small Ubiquitin-like Modifier (SUMO) and Maltose Binding Protein (MBP) being the most relevant ones. These tags are often designed with cleavage sites between the tag moiety and the protein of interest, which are recognized by specific proteases to allow removal of the tag moiety from the target recombinant protein [48], [49].

For this purpose, the strain *E. coli* BL21 Δ*iscR* + pGEX4T2-GST-HdrC-Af + pRARE was created. In this strain, a GST tag was added upstream of HdrC aiming to enhance its solubility. GST is a highly soluble enzyme of 26 kDa, which can help in the solubility of the overall GST-HdrC amino acid sequence. The GST-tag is of significantly high molecular weight in comparison with HdrC, which can affect the native HdrC functional activity after purification. For this purpose, in the linker region between GST and HdrC, it was introduced an amino acid sequence composed of Leu-Val-Pro-Arg-Gly-Ser, which will be recognized and cleaved between the arginine and glycine residues by the thrombin protease [50], [51]. The GST-tag has the advantage of combining increase of solubility with the possibility to perform affinity purification [50].

Figure 4.11 presents a simplified plasmid map for pGEX4T2-GST-HdrC-Af (**Figure 4.11A**), as well as the SDS-PAGE analysis of the cell expression profile before and after IPTG induction, the pellet resulting from cell lysis and soluble fraction, and fractions from the several affinity purification steps (**Figure 4.11B**).

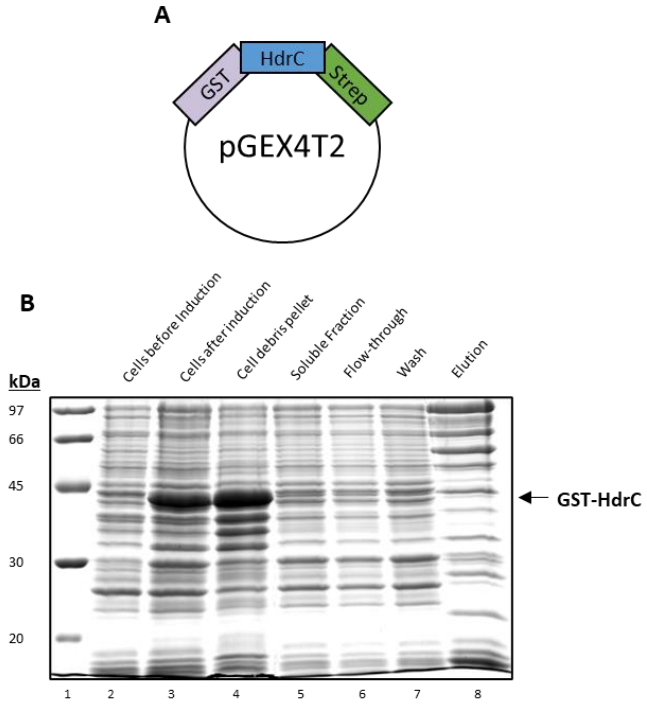

Figure 4.11 – Plasmid organization for pGEX4T2-GST-HdrC-Af **(A)** and a SDS-PAGE showing the band pattern for cell pellet before induction and after induction (lanes 2 and 3), the cell debris and soluble fraction after cell lysis (lanes 4 and 5), and the flow-through, wash and elution fractions from Strep-tag affinity purification (lanes 6, 7 and 8) **(B).**

The cloning of a fused GST-HdrC results in a protein of 45 kDa versus 19 kDa of HdrC. It is possible to observe the expression of GST-HdrC after induction (lane 3) corresponding to the approx. 45 kDa protein band on the SDS-PAGE gel. However, a high amount of this protein was still present in the cell debris fraction and, therefore in inclusion bodies. In the elution fraction (lane 8), despite the existence of a band that could correspond to GST-HdrC, this was present in lower amounts than the contaminant bands. Additionally, even if GST-HdrC was solubly expressed it should have been in low amounts, since it was necessary to concentrate the elution fraction in order to have 20 µg of total protein for the SDS-PAGE analysis,

and as it can be seen this elution fraction is very impure for an affinity purification from an induction-expressing system.

Despite the high solubility of GST, not all GST-tagged fusion proteins get necessarily solublized [52], and *A*. *fulgidus* HdrC seems to be one of these cases.

4.4.3.4 – Expression of codon-optimized *A*. *fulgidus* HdrC

The HdrC protein was so far recombinantly expressed and purified in *E*. *coli* from its original DNA sequence from *A*. *fulgidus*, which is an archaeal organism. The tRNA variety and availability during translation is tuned to the codon usage for a determined species, and this codon usage varies across species, being quite distinctive between archaeal and bacterial organisms, and also eukaryotic organisms. Therefore, the unavailability of certain tRNA during protein expression can affect the translation rate and misincorporation of amino acids, and consequent protein folding [43], [53], [54]. This issue was partially circumvented by co-expressing the protein of interest together with the pRARE plasmid, which expresses genes of tRNAs that are rare in *E*. coli, namely the ones that recognize and bind the mRNA codons AGG, AGA, AUA, CUA, CCC, GGA and CGG. However, since this did not provide soluble HdrC, the work proceeded to optimize the DNA sequence of *hdrC* prior to its expression. For this purpose, the *hdrC* gene was synthesized by Integrated DNA Technologies (Iowa, USA), using a codon-optimization tool in which the algorithm provides the best sequence option by screening and filtering sequences to lower complexity and minimize secondary structures, through rebalancing codon usage, decreasing sequence complexity and avoiding rare codons. This procedure also avoids the use of pRARE, which requires the usage of chloramphenicol and can have a fitness cost [43], [55]. The codon optimized HdrC is referred from here on as HdrC*.

The growth conditions were similar to those previously described, and cells were grown by testing IPTG induction at an OD_{600} of 0.4 and 2.2, and inducing with IPTG at a final concentration of 50 µM and 200 µM. **Figure 4.12** shows the SDS-PAGE analysis of the cell expression profile before and after induction, the insoluble fraction after cell lysis which includes cell debris and inclusion bodies, and

the eluted fractions after Strep-tag purification, both for *E*. *coli* BL21 Δ*iscR* + pET22b(+)-HdrC*-Af (**Figure 4.12A**) and *E*. *coli* BL21 Δ*iscR* + pET22b(+)-HdrC*-Af + pRARE (**Figure 4.12B**).

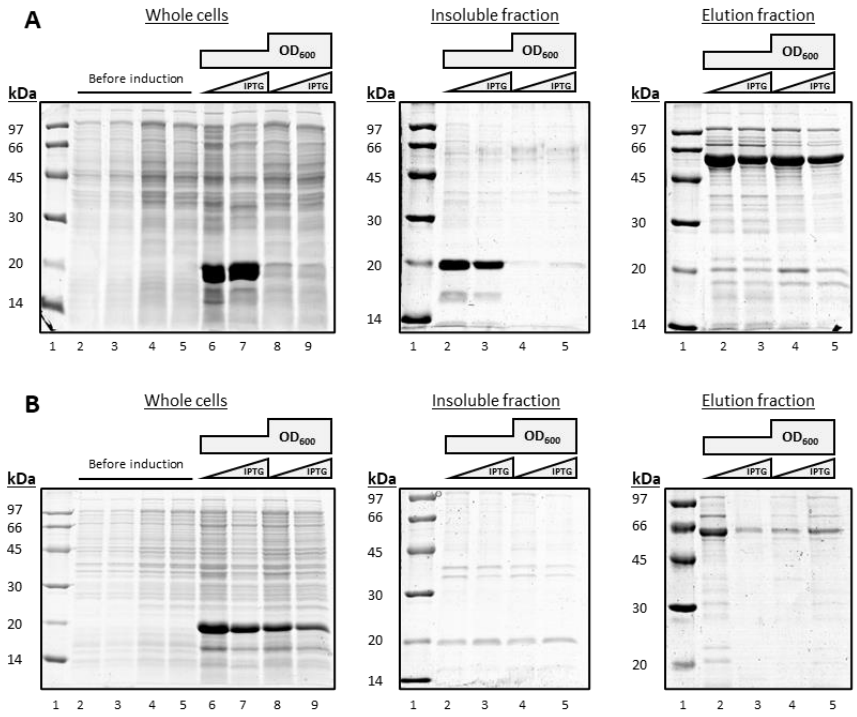

Figure 4.12 – Cell pellet for the several induction optical densities and IPTG concentrations tested, before induction and after induction; resulting pellet from centrifugation after sonication, the insoluble fraction, which includes unbroken cells, cell debris and insoluble material such as inclusion bodies; and the eluted fraction for the several induction optical densities and IPTG concentrations tested, for *E*. *coli* BL21 Δ*iscR* + pET22b(+)-HdrC*-Af (**A**) and *E*. *coli* BL21 Δ*iscR* + pET22b(+)-HdrC*-Af + pRARE (**B**).

By looking at the insoluble fraction, it is possible to see two strong band corresponding to HdrC* after induction at lower OD_{600}, and four bands for all the induction tests for HdrC* in the presence of pRARE. These results resemble the ones from **Figure 4.9**, in which there was a higher expression at lower OD_{600}, although this did not correspond

later to an increased amount of protein in the elution fraction. By looking at the insoluble fraction, which is composed of inclusion bodies, among other debris, it is possible to see also a clear band corresponding to HdrC*. After affinity purification of the soluble fraction, there is a faint band around 20 kDa that could be assigned to HdrC*. However, most of the bands present in the elution fraction are of much higher molecular weights, which correspond to contaminant proteins that result from acetone precipitation of the elution fraction in order to have a satisfactory amount of protein to run in an SDS-PAGE analysis. Overall, these results resemble previous data obtained (such as in **Figure 4.9**), where it is possible to see a clear expression of HdrC after IPTG induction, but this protein is being accumulated in the form of inclusion bodies and little or nothing is in the soluble form.

4.4.3.5 – Purification of *A. fulgidus* HdrC from the membrane fraction

The struggle to obtain a soluble HdrC subunit led us to hypothesize that HdrC could have a higher content of non-polar amino acids and/or a higher affinity to the cellular membrane, which could lead to it being present in the membrane fraction during purification. HdrC from *A. fulgidus* has a content of non-polar amino acids (glycine, alanine, proline, valine, leucine, isoleucine, methionine, tryptophan, phenylalanine) of 52%, which is similar to the 50% content from HdrA or HdrB from the same organism. Bioinformatic tools were also used to analyse the possibility of HdrC attaching or interacting with the cell membrane. Both softwares TMHMM Server v. 2.0 [56] and MemBrain 3.1 [57], used for prediction of transmembrane helices in proteins, predicted zero transmembrane helices. AmphipaSeeK v1.3.5 [58] did not detect an in-plane membrane anchoring segments.

Despite HdrC not having a theoretical affinity to the membrane, still an attempted purification of HdrC was performed from the membrane fraction, as opposed to the soluble fraction that was used so far. For that, two strains were used: *E. coli* BL21 Δ*iscR* + pET22b(+)-HdrC*-Af + pRARE, encoding the codon-optimized version of HdrC, and *E. coli* Δ*iscR* + pETDuet-1-HdrC-HdrB-Af + pRARE, encoding HdrB and HdrC, both containing a Strep-tag. The resulting pellet from the ultracentrifugation (i.e., membrane pellet) of

the cell extract was resuspended in buffer containing DDM, which is a mild detergent frequently used for solubilization of membrane proteins in *D. vulgaris*, *A. fulgidus* and others, while still preserving the proteins activity. The purification step was performed by affinity chromatography, taking advantage of the Strep-tag, as performed before.

Figure 4.13 presents the results for the SDS-PAGE gel (**Figure 4.13A**) and the Western-blot using anti-Strep tag antibodies (**Figure 4.13B**) from the soluble and membrane fractions before affinity purification, and the solubilized membrane eluted fraction, for both strains.

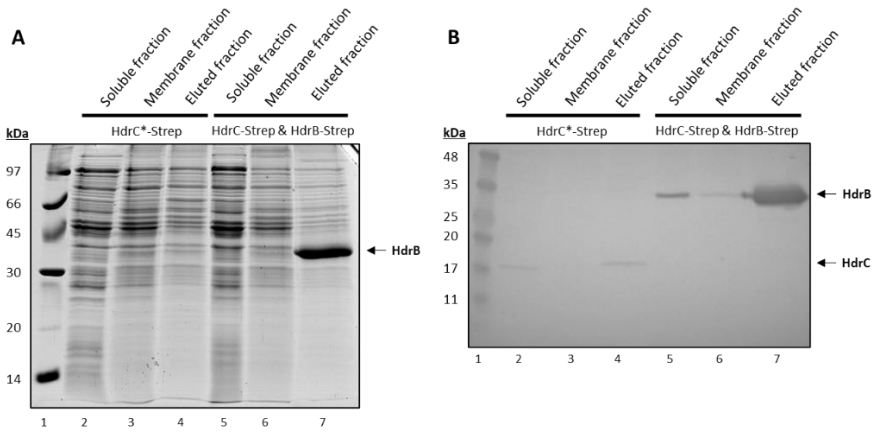

Figure 4.13 – SDS-PAGE (**A**) and Western-blot (**B**) showing the band pattern for the cell extract's soluble and membrane fraction, and solubilized membrane eluted fraction after affinity purification, for *E*. *coli* BL21 Δ*iscR* + pET22b(+)-HdrC*-Af + pRARE and *E*. *coli* Δ*iscR* + pETDuet-1-HdrC-HdrB-Af + pRARE.

By observing the SDS-PAGE analysis (**Figure 4.13A**), it is possible to see that no particular band corresponding to HdrC-Strep (MW = 19 kDa) is visible. While the band corresponding to HdrB-Strep from the *E*. *coli* strain encoding pETDuet-1-HdrC-HdrB-Af (lane 7) is noticeable, which is in line with the results previously obtained for the soluble fraction from the same strain. The apparent absence of HdrC was subsequently analyzed by Western blot using an anti-Strep antibody (**Figure 4.13B**), and it is possible to detect a faint

band assigned to the HdrC-Strep in the soluble and eluted fractions. This suggests that HdrC is present in higher abundance in the soluble fraction than in the membrane fraction (lanes 2 and 3). However, the amount of HdrC detected by WB in the eluted fraction from solubilized membranes is quite low, compared with the contaminant proteins observed in the SDS-PAGE gel. HdrB expressed from the pETDuet-1-HdrC-HdrB-Af strain is also more present in the soluble fraction, still there is a faint band of this protein associated to the membrane fraction. Overall, these results show HdrC to be more present in the soluble fraction rather than membrane fraction, as expected from bioinformatic tools, but still it could not be purified in reasonable quantities and without contaminant proteins.

4.4.3.6 – Purification of *A. fulgidus* HdrC from inclusion bodies

Inclusion bodies are amorphous aggregates formed mainly by hydrophobic interactions resulting from disordered and misfolded proteins [38], [59]. The cause for formation of inclusion bodies is generally expression-related, such as high temperature of induction or high inducer concentration, or protein-intrinsic such as high content of hydrophobic amino acids or it represents an unrecognizable protein to the host cell system [38], [60]. Techniques used to circumvent this issue generally include lowering the induction temperature or the inducer concentration, which still may not solve the problem.

On the other hand, the considerable amount of HdrC as inclusion bodies in the insoluble fraction, can be seen as an advantage in protein purification, by separating the crude extract from the inclusion bodies which are almost solely composed by HdrC, and renaturating HdrC from there. This technique was already used for HdrC from *Acidithiobacillus ferrooxidans* [22], [23], where the authors faced similar struggles to obtain soluble HdrC, and were successful in recovering it from inclusion bodies. This acidophilic organism contains two HdrC's, HdrC1 (locus tag AFE_2555) and HdrC2 (locus tag AFE_2551), both encoding two motifs for Fe-S cluster binding ($CX_2CX_2CX_3C$), like the HdrC from *A. fulgidus*. However, only one motif of each HdrC was demonstrated to harbor a Fe-S cluster. Despite sharing a similar operon, and likely the same function, HdrC from *A. fulgidus* shares a low % of similarity and % of

identity with the two HdrC's from *A*. *ferrooxidans*, being 28% similar and 12% identical with HdrC1, and 24% similar and 15% identical with HdrC2 (alignment performed using ClustalW, and identity/similarity calculated on Bioinformatics.org). In both alignments, the Fe-S binding motifs ($CX_2CX_2CX_3C$) were conserved.

A total of six protocols were tested to purify *A*. *fulgidus* HdrC from the inclusion bodies from the same *E. coli* expression conditions, as described in **Table 4.5**. Protocol #1 was reproduced from the previously referred experiments with HdrC from *A*. *ferrooxidans* [22], [23]. Protocols #2 to #6 share a similar operational structure with Protocol #1, being the main differences related with the buffer composition selected for denaturation and renaturation.

Inclusion bodies are commonly solubilized using a chaotropic agent, such as urea or guanidine hydrochloride [35], [38]. Protocol #2 mainly differed from the rest by the usage of 6 M guanidine-HCl as denaturing agent, while the rest used 8 M urea. Protocols #2 to #6 also included 5 mM DTT in the solubilization buffer, used to keep all cysteines in the reduced state [38]. Depending on the protocol, the solubilization of inclusion bodies was performed by incubating them for 3 h at either 4 °C or 60 °C. The temperature of 4 °C is a standard for protein renaturation, while the incubation at 60 °C was tested due to *A*. *fulgidus* HdrC being a thermophilic protein, and in this case the higher temperature could help protein renaturation without affecting the protein itself. In fact, guanidine-HCl and urea are both know to be more effective at elevated temperatures such as 60 °C [61]. After incubation, the inclusion bodies were centrifuged, and **Figure 4.14A** shows the resulting supernatants and pellets.

The renaturation was performed using centrifugal filters and continuously lowering the denaturant concentration. The use of 0.4 M arginine during renaturation aimed to suppress protein aggregation during the protein refolding process, although little is known about the arginine mechanism of action [36], [37]. Protocol #1 included a mixture of glutathione, in the reduced and oxidized form, which serves as facilitator of disulfide bond formation during the protein renaturation [35], [62]. Protocols #3 and #5 included β-mercaptoethanol, which is commonly used for proteins containing multiple cysteine residues, since it works as reducing agent to keep all cysteines in the reduced state, this way reducing the amount of incorrect intra- and intermolecular disulfide bonds during

renaturation [38]. **Figure 4.14** shows the color characterization and purity by SDS-PAGE analysis of the soluble fractions after several denaturation treatments (**Figure 4.14A** and **Figure 4.14B**), as well as the respective results after protein renaturation (**Figure 4.14C**).

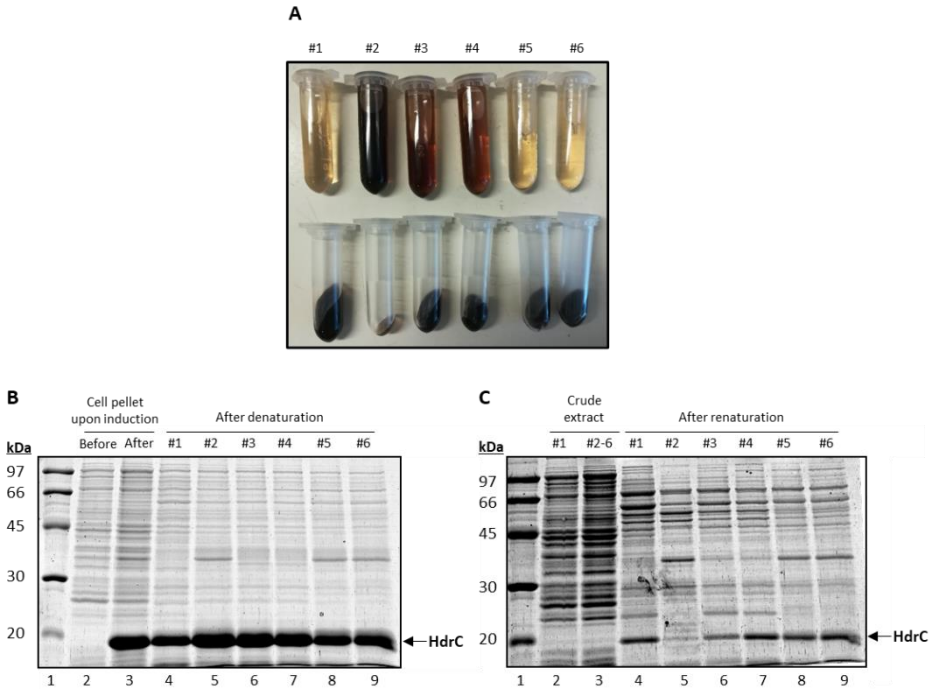

Figure 4.14 – Color characterization of soluble fractions (first row) and pellets (second row) after treatment with the denaturing agents (urea or guanidine-HCl) **(A)**; SDS-PAGE analysis of cell pellet before and after IPTG induction, and soluble fractions after treatment with the denaturing agents **(B)**; SDS-PAGE analysis of crude extracts after cell pellet sonication for protocol #1 and protocols #2 to #6, and soluble fractions that result from each protocol after renaturation **(C)**.

Figure 4.14B shows the protein pattern before induction (lane 2) and after 24 h induction (lane 3). The same cell pellet was used in the several denaturation protocols. Despite the protocol of cell lysis being different between protocol #1 and protocols #2-6, the crude extract pattern was similar (**Figure 4.14C**, lanes 2 and 3). Several renaturation protocols were performed, and the outcome is in **Figure**

4.14C (lanes 4 to 9). In **Figure 4.14B** it is possible to observe (lanes 4 to 9) that the pattern after renaturation is somewhat similar across all protocols, except for protocol #2 where no obvious HdrC was obtained. Protocol #1 seemed to contain higher amounts of contaminant proteins. The amount of purified HdrC by lysing the cells with Guanidine-HCl (protocol #2) was very low. The protein pattern for protocols #3 to #6 was similar in the overall context, with protocols #3-4 and #5-6 being more similar between them, since they show a similar pattern for contaminant proteins.

In all protocols, there was a high amount of protein precipitation during the renaturation step. The gradual reduction of Urea/Guanidine-HCl from 8 M/6 M to 1 M could occur with no precipitation, with precipitation being quite significant at concentrations lower than 1 M Urea/Guanidine-HCl, whether the renaturation was performed by a centricon device concentration or by dialysis methodology using a diffusion membrane. This instability of HdrC during the renaturation process could be due to the lack of iron-sulfur clusters, which can have a role in the stabilization of the protein structure besides electron transport, by binding to available cysteine residues [63]–[66]. After purification, washing and lysis of the inclusion bodies, the protein presented a brown color, which is indicative of the presence of iron-sulfur clusters.

To overcome the precipitation issue due to the possible lack of Fe-S clusters, the HdrC renaturation was repeated, this time including Fe-S cluster enzymatic reconstitution, by means of the IscS enzyme. For this purpose, protocol #3 was chosen due to its highest yield of total protein (as seen in **Figure 4.14A**), and the renaturation and Fe-S reconstitution was tested in two different ways: by incubating with the IscS protein at the end of renaturation, and by including IscS and the necessary iron and sulfur sources during the renaturation process at urea concentrations lower than 1 M. Changes in the protocol included addition of $FeCl_2$ and L-Cysteine as an iron and sulfur source, respectively, for the formation of Fe-S clusters, adding DTT for a reducing environment, and IscS, the enzyme. The protocols and respective results are shown in **Figure 4.15**.

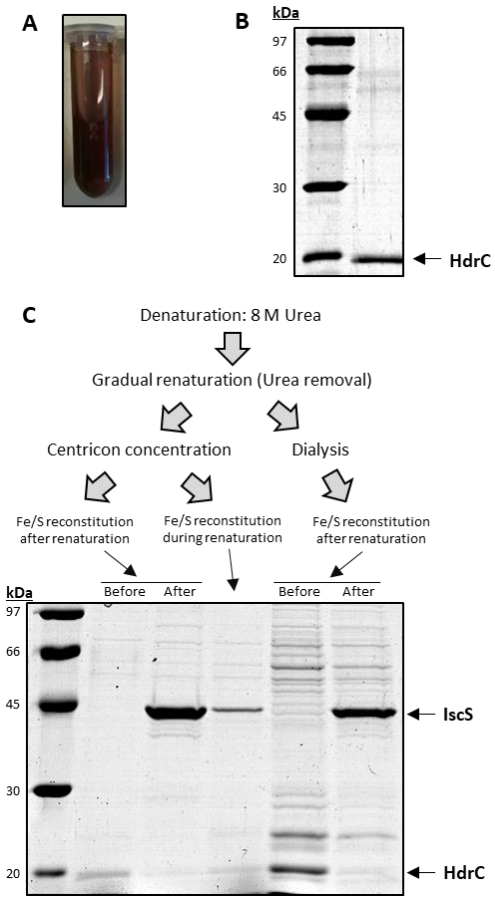

Figure 4.15 – Purification from inclusion bodies and with Fe-S cluster reconstitution. Color aspect of the inclusion bodies after treatment with 8 M Urea (**A**); SDS-PAGE gel for the inclusion bodies after treatment with 8 M Urea, HdrC-Strep highlighted (**B**); Diagram for the several protocols of renaturation plus Fe-S reconstitutions, with SDS-PAGE analysis highlighting HdrC-Strep and IscS enzyme.

The incubation with IscS resulted in denaturation of the low amount of HdrC available in solution. We also found out that, overtime, HdrC precipitates. In sum, this protocol allowed us to purify and refold HdrC, but due to its instability it was not possible to have enough protein to proceed for purification and biochemical assays.

4.4.3.7 – Expression level of *A. fulgidus* MvhAGD-HdrABC

Archaeoglobus is an archaeal genus of hyperthermophilic sulfate-reducers, such as *Archaeoglobus fulgidus* [67] and *Archaeoglobus profundus* [68]. These organisms encode the HdrABC protein complex together with the MvhAGD hydrogenase, putatively linking hydrogen oxidation with the reduction of ferredoxin and the DsrC trisulfide. Moreover, these organisms also encode the transmembrane HdrDE complex, which is involved in a redox loop mechanism where the oxidation of quinone-like cofactor methanophenazine by HdrE is coupled with the heterodisulfide reduction from the HdrD cytoplasmic subunit, which shares homology with HdrB regarding the CCG domain [69]–[71].

The HdrDE complex was already purified from *A. fulgidus* grown on lactate/sulfate media [44] and both the HdrDE and MvhAGD-HdrABC were purified from *A. profundus* grown on H_2/sulfate [18].

The *A. fulgidus* MvhAGD-HdrABC complex is likely more expressed under H_2-oxidizing conditions. In fact, *A. fulgidus* grows with H_2 as sole electron donor [18], but the growth under these conditions is very deficient. Furthermore, *A. fulgidus* grown in lactate/sulfate conditions does not exhibit hydrogenase activity: < 0.005 U/mg protein compared with 24 U/mg protein from *A. profundus* grown in H_2/sulfate [72].

To grow *A. fulgidus* and *A. profundus* on hydrogen-oxidizing conditions at a large-scale, the authors required the use of a 300 L fermenter working at the temperature of 85 °C and coupled with a supply system to continuously provide H_2/CO_2 (80/20 (v/v)) at rate of 50 $mL.L^{-1}.min^{-1}$ and a pressure of 3 bar [18], [44], [68], [72]. The high pressure and continuous gas supply is essential for growth, since H_2 in the culture media is even less soluble at higher temperatures [73]. The advanced technical challenges to create such a fermentation system for cell production, made it hard for us to mimic the described successful conditions, even at a lower scale. Despite not being the ideal conditions for cell growth for protein purification, *A. fulgidus* was grown in several 100 mL anaerobic flasks at 80 °C. For that, H_2/CO_2 (80/20 (v/v)) was pressurized in anaerobic flasks containing 50 mL of culture media with inoculum, and these flasks were displayed on horizontal position for a higher surface contact between the liquid media and the gas phase. *A. fulgidus* slightly grew under these conditions, and the H_2/CO_2 pressure of 3 atm diminished overtime,

requiring frequent over pressurization of the bottles. As previously referred, *A*. *fulgidus* has a deficient growth under hydrogen-oxidizing conditions which, together with the low H_2 diffusion/solubilization in the liquid culture media at high temperatures, reveals the reason for the modest growth observed.

Despite the challenges in growing *A*. *fulgidus*, the work proceeded to analyze the hydrogenase activity of this organism grown under two conditions (Lactate/Thiosulfate as a standard condition and H_2/CO_2/Thiosulfate), to assess its use for later Hdr purification. For this purpose, samples already available at the laboratory from previous experiments were used, namely several fractions from ionic exchange chromatography of the soluble fraction of *A*. *fulgidus* cells grown under Lactate/Thiosulfate conditions, and both soluble and membrane fractions from *A*. *fulgidus* grown in H_2/CO_2/Thiosulfate. **Figure 4.16** presents the hydrogenase activity of each of these conditions and fractions.

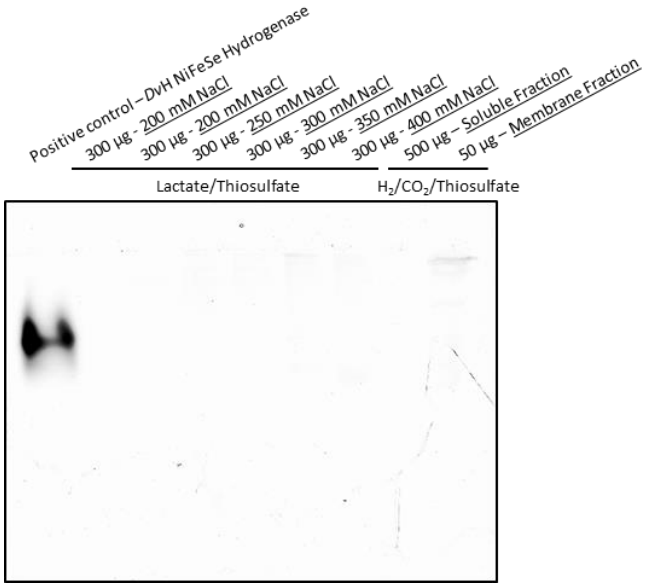

Figure 4.16 – Hydrogenase activity of samples deriving from *A*. *fulgidus* grown in Lactate/Thiosulfate and in H_2/CO_2/Thiosulfate. For the first several fractions from ionic exchange chromatography of the soluble fraction were used, and for the second growth condition only soluble and membrane fractions. 2 µg of *Dv*H NiFeSe Hydrogenase was used as a positive control.

The **Figure 4.16** shows that no hydrogenase activity was observed in the several fractions obtained from lactate/thiosulfate grown *A. fulgidus* cells, as well as not observed in the soluble fraction of *A. fulgidus* grown under H_2/CO_2/Thiosulfate conditions. A faint band was observed in the membrane fraction, which likely corresponds to the periplasmic membrane-anchored HynABC [NiFe] hydrogenase [20].

The MvhAGD-HdrABC is a soluble hydrogenase complex, and so a hydrogenase activity in the soluble fractions would be indicative of its presence. However, this was not observed, even considering the high amount of 500 µg of total protein loaded in the native gel.

4.4.3.8 – Homologous expression of *D. vulgaris* HdrABC-FlxABCD

Since *D. vulgaris* is a genetically manipulable organism, it was also tried to take advantage of that to homologously express HdrC. There were already previous attempts from our laboratory to grow *Dv*H WT in Ethanol-Sulfate, a condition in which the *hdr-flx* genes are more abundant [21], but it was not possible to obtain the Hdr-Flx complex in a sufficient amount that would discern from contaminant proteins. One alternative was to use *Dv*H IPFG04, a strain already available in the laboratory, which encodes for the *hdr-flx* (locus tag DVU2404-DVU2399) with a strep-tag coding sequence in the *flxA* gene (DVU2399), as depicted in **Figure 4.17A**. Therefore, *Dv*H IPFG04 was grown in MOY media supplemented with 40 mM ethanol and 20 mM sulfate. After reaching the stationary phase, the cells were anaerobically harvested, and the soluble fraction was separated by affinity chromatography. **Figure 4.17B** shows the SDS-PAGE analysis for each of the purification fractions, and **Figure 4.17C** shows the respective Western blot using an anti-FlxA antibody.

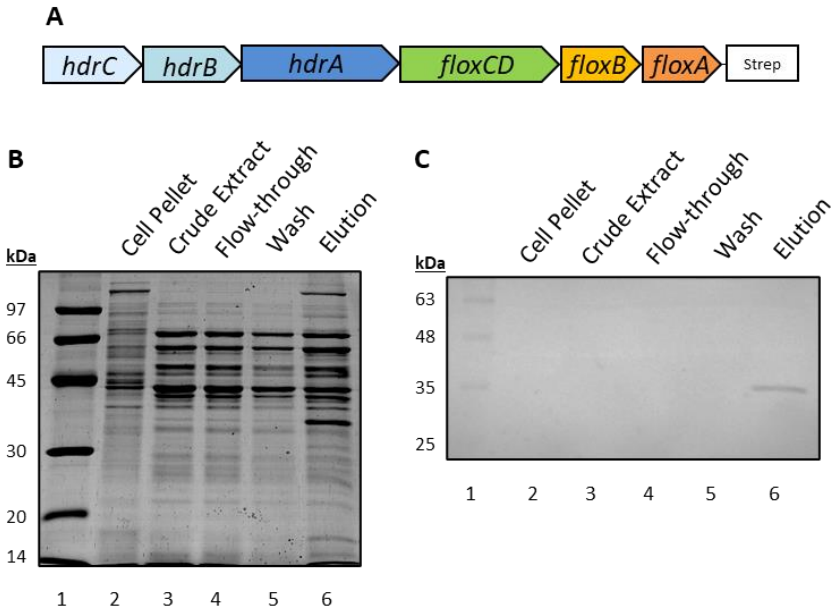

Figure 4.17 – Arrangement of the *hdr-flx* operon in *D*. *vulgaris* IPFG04, with the *flxA* gene encoding a strep-tag sequence at its C-terminus **(A)**; SDS-PAGE **(B)** and Western-blot **(C)** analysis of the cell pellet and crude extract after cell lysis (lanes 2 and 3), and flow-through, wash and elution fractions from affinity purification (lanes 4, 5 and 6).

Despite cell growth in ethanol-sulfate conditions, and the anaerobic environment along the cell growth and protein purification, FlxA expressed in very low amounts (see amount of FlxA band in Western blot versus total protein bands in SDS-PAGE). FlxA-Strep has a molecular mass of 33 kDa, and there is no band with this size that is clearly distinct from the contaminant protein bands.

On the other side, the Western blot analysis using the Anti-FlxA antibody detected FlxA in the elution fraction, but not in all the other fractions, as expected. This shows that FlxA is present in considerably low cellular amounts, even when *D*. *vulgaris* grows in conditions where *flxA* is more expressed, as suggested previously [21].

Overall, this system was also not effective in producing enough protein for characterization studies.

4.4.3.9 – Expression of *A. fulgidus* HdrC in *Desulfovibrio vulgaris*

Another approach was to use *D. vulgaris* Hildenborough to heterologously express the *A. fulgidus* HdrC. Despite not having bibliographic evidence for the use of *D. vulgaris* as heterologous expression host, there are several examples of its use for homologous recombinant protein expression in this strain, through the use of vectors such as pMO719 [21], [26], [28], [74], [75]. Moreover, the metabolic similarities between *A. fulgidus* and *D. vulgaris*, when comparing with *E. coli*, make *D. vulgaris* an hypothetical good bacterial host to try to overcome the issues in HdrC soluble expression.

For this purpose, the strain *D. vulgaris* IPDF01 was created, which is the *D. vulgaris* wild-type strain encoding a plasmid expressing HdrC and HdrB, both with a separate promoter and strep-tag. The decision to add HdrB was based on the literature showing an effective expression of soluble HdrC when coexpressed and copurified with HdrB [19], and to use HdrB as a control for the success in the protein purification. *D. vulgaris* cell growth was performed in MO medium supplemented with 0.5 g/L yeast extract, 30 mM lactate and 30 mM sulfate, a condition in which *D. vulgaris* growth is robust. Protein purification was performed anaerobically through affinity chromatography, by taking advantage on the strep-tag tail. **Figure 4.18** shows an SDS-PAGE with the eluted fraction stained with silver nitrate.

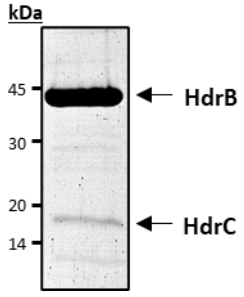

Figure 4.18 – SDS-PAGE gel stained with silver nitrate from the eluted fraction of *Dv*H IPDF01. HdrB (35 kDa) and HdrC (19 kDa) were identified by Mass Spectrometry.

The SDS-PAGE from the elution fraction showed a clear band corresponding to HdrB and a faint band with a size close to 20 kDa, likely corresponding to HdrC. The gel was subsequently treated with silver nitrate, a highly sensitive staining system, to increase the contrast of the latter band. Both bands were identified by mass spectrometry as HdrB and HdrC, respectively.

Using this methodology, it was possible to purify *A*. *fulgidus* HdrBC, but with HdrC in considerably low amounts and not in a 1:1 ratio. The low protein yield of 20 µg HdrBC per liter of *Dv*H cells would not be feasible to have HdrC in a sufficient amount for enzymatic assays and so, this led us to abandon this approach.

4.4.4 – Enzymatic assays: Is HdrB able to reduce DsrC trisulfide?

Despite the previously reported challenges around HdrC purification, an attempt was tried to observe electron transfer between HdrB and DsrC-trisulfide, to strengthen the hypothesis of the Hdr complex from sulfate-reducers being able to perform FBEB and participate in sulfate respiratory metabolism by reducing this species. For this, the reaction was performed in 50 mM K_2HPO_4/KH_2PO_4 buffer, by adding reduced methyl viologen as electron donor, then 500 nM HdrB and then 30 µM DsrC trisulfide as electron acceptor. The rationale is to observe the oxidation of methyl viologen by absorbance at 732 nm, upon reduction of DsrC trisulfide. No distinguishable differences were observed between the reaction with DsrC trisulfide and the negative control reaction, without HdrB enzyme. Additionally, another technique was used, which consisted in looking into the DsrC cysteines redox state. This technique consists in treating the samples with MalPEG after the enzymatic reaction. MalPEG is a high molecular reagent that binds to free thiol groups, such as cysteine reduced residues. When bound to the cysteine residue, the molecular weight of the protein will increase in ≈ 10 kDa per each cysteine residue, which can be observed by protein gel electrophoresis. Therefore, incubating samples with MalPEG after the reaction with HdrB and DsrC-trisulfide, can be used as a way to observe the alteration of the DsrC cysteines redox state from a trisulfide to the reduced state. An illustration of the expected reaction is presented in **Figure 4.19A**.

The wild-type DsrC from *A. fulgidus* contains 4 cysteine residues (C77, C85, C103 and C114), of which the two closer to the C-terminal are involved in the trisulfide formation. The plasmid used for DsrC expression (pET28b(+)-DsrC-Af) contains a mutant version of DsrC, in which the C77 and C85 residues were substituted to alanines, in order to simplify the results from the MalPEG gel-shift assay [28]. Therefore, only two cysteine residues present in DsrC, C103 and C114, can react with MalPEG. If the DsrC is in the oxidized form, forming a trisulfide, no MalPEG can bind to it, and so DsrC keeps its original molecular weight. On the other hand, if DsrC is fully reduced, both cysteine residues will be in thiol state and two MalPEG molecules will bind to DsrC, one in each cysteine, increasing the DsrC molecular weight by 2 x 10 kDa ≈ 20 kDa. However, if only one cysteine residue is reduced, but the sulfur atom from SO_3^{2-} is still bound to the other cysteine residue, only one cysteine binds to the MalPEG. The several possible results are represented in **Figure 4.19B**.

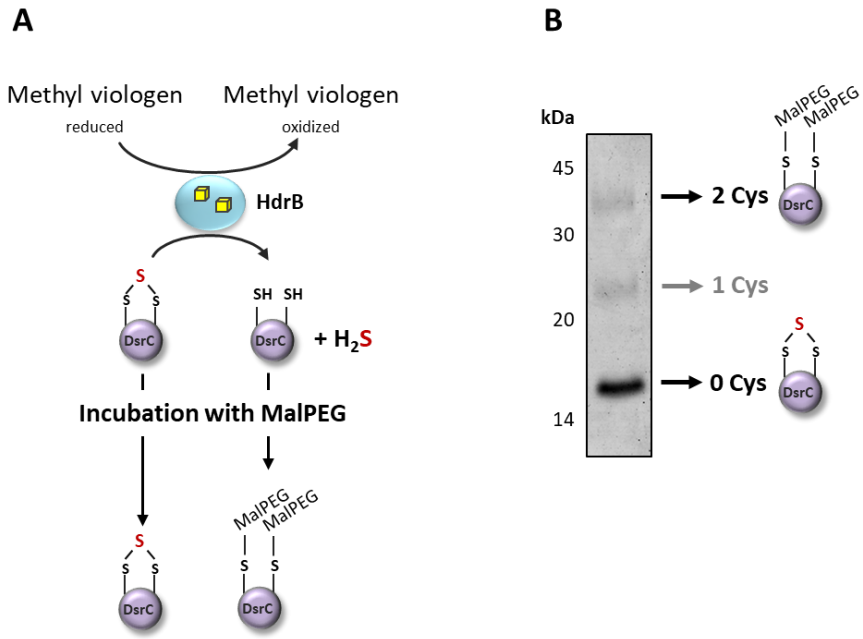

Figure 4.19 – Outcome from DsrC incubation with MalPEG. MalPEG gel-shift assay as methodology to evaluate electron transfer from HdrB to DsrC **(A)**. Possible scenarios for DsrC incubation with MalPEG, and respective illustration of DsrC-MalPEG oxidation status **(B)**.

The enzymatic reaction was performed in 50 mM K_2HPO_4/KH_2PO_4 buffer, by adding reduced methyl viologen, followed by 500 nM HdrB and then 30 µM DsrC trisulfide.

Figure 4.20 shows the reaction results looking into DsrC cysteines state after several time-points. Although it is not possible to observe the decrease in protein band intensity of DsrC trisulfide (lower molecular weight), it is possible to see that the band intensity corresponding to reduced DsrC is increasing over time. However, this increase in DsrC reduction is also observed to the same degree in HdrB as purified and in the negative control (without HdrB). This means that DsrC is likely being nonspecifically reduced by methyl viologen to a small degree.

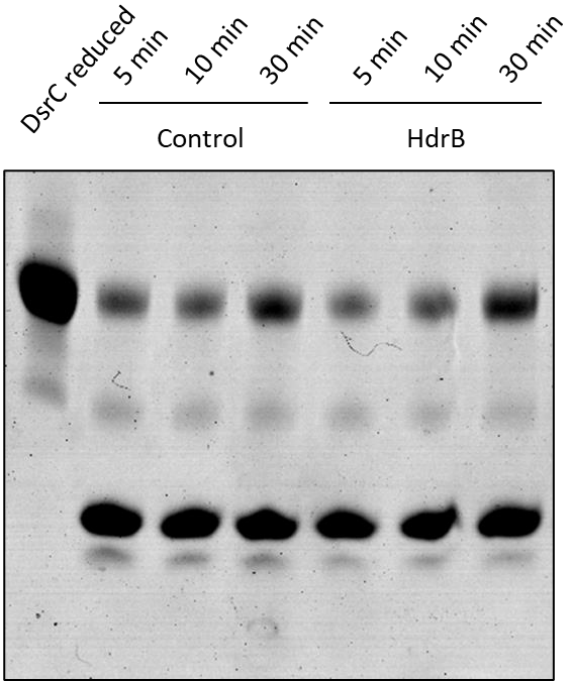

Figure 4.20 – MalPEG gel shift assay to evaluate the role of HdrB in the reduction of DsrC trisulfide. Assay samples were incubated after 5, 10 and 30 min of reaction with DsrC alone (control), with *A. fulgidus* HdrB. DsrC fully reduced with DTT was used as a control.

It is not possible to observe by SDS-PAGE the decrease of DsrC trisulfide over time, possibly due to the relatively high DsrC concentration (30 µM): this assay is not sensitive enough to detect a small reduction in the amount of DsrC trisulfide. One alternative would be to decrease the amount of DsrC.

Yan *et al*. [19] performed biochemical experiments with the HdrAB2C2 complex from *Methanosarcina acetivorans*, using CO and a CO dehydrogenase/acetyl-CoA synthase to donate electrons through HdrAB2C2 to CoM-S-S-CoB and ferredoxin. During the assay, a very low production of free thiol was observed when incubating only HdrB with CoM-S-S-CoB, but this was increased in the presence of HdrC. The failure of the experiment described above with *A*. *fulgidus* HdrB led us to perform a similar experiment, in the presence of HdrB and HdrC. Although HdrC could not be purified, cell extracts from *Dv*H IPDF01 express HdrCB, where HdrC is present in small amounts (**Figure 4.18**). As control, the same experiments were performed with *Dv*H WT cell extracts, to subtract any activity that could be caused by the cell background.

Two variables were tested, namely assay temperature and cell extract amount. The temperature tested was 70 °C and 80 °C, which is the ideal temperature for *A*. *fulgidus* growth. Prior to the enzymatic experiment, the cell extracts were incubated at these temperatures, in order to denaturate several proteins from the *D*. *vulgaris* host that is a mesophile. This approach could help reducing the background noise when performing the activity assays with *A*. *fulgidus* DsrC trisulfide.

The amount of cell extract was also tested, using the concentrations of 0.05 µg/µL and 0.01 µg/µL of cell extract. Although higher concentrations would be theoretically ideal, as more cell extract means more HdrCB, higher concentrations of cell extract would also increase the amount of background proteins that compete with DsrC for the MalPEG binding, making the SDS-PAGE results hard to read and interpret. The results of incubation of DsrC trisulfide with *Dv*H cell extracts containing *A*. *fulgidus* HdrCB can be seen in **Figure 4.21**.

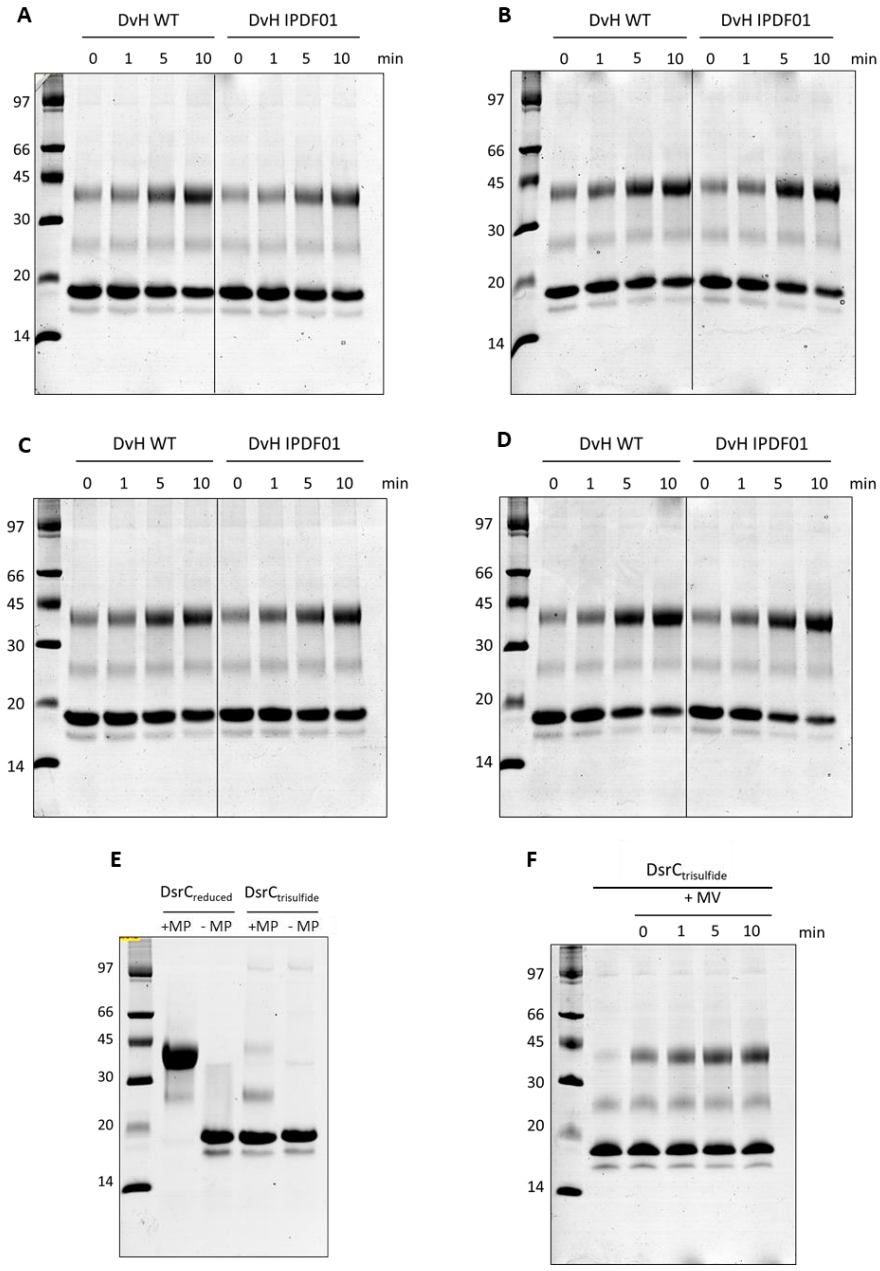

Figure 4.21 – MalPEG gel shift assays after 0, 1, 5, 10 minutes of incubation with 0.01 µg/µL cell extract at 70 °C **(A)**, 0.05 µg/µL cell extract at 70 °C **(B)**, 0.01 µg/µL cell extract at 80 °C **(C)**, 0.05 µg/µL cell extract at 80 °C **(D)**. Controls for DsrC were performed at 80 ºC, in the absence of cell extract **(E** and **F)**. MP: MalPEG; MV: Methyl viologen.

A similar result to what was seen in assays depicted in **Figure 4.20** was observed, with the extracts being able to reduce DsrC trisulfide over time, but this not being different from what was observed in the control experiments. Here the same happened, as assays and control experiments look the same, independent of the temperature and concentration of cell extract used.

The extracts seem to have an intrinsic ability to reduce the DsrC trisulfide, and the small amount of HdrCB in the extract from *Dv*H IPDF01 was not enough to make a difference in the efficiency to reduce DsrC trisulfide, when compared with the *Dv*H WT extract (control experiment). A somewhat similar issue was observed by Kaster [15] when using cell extracts to prove that MvhAGD-HdrABC is be able to oxidize H_2 and reduce CoM-S-S-CoB and ferredoxin, by observing that low amounts (≈ 25 μM) of benzyl viologen could reduce ferredoxin. The extract was catalyzing the reduction of ferredoxin with the oxidation of H_2, even in the absence of CoM-S-S-CoB. This was likely due to the electron transfer from H_2 through MvhAGD-HdrABC to the reduced viologen dye, which transferred electrons directly to ferredoxin, without the need to involve CoM-S-S-CoB in bifurcation.

4.5 – Discussion

The rising discovery of protein complexes able to perform FBEB, as well as their significance in prokaryotic metabolism, is very striking. Despite FBEB having been already described in methanogenesis, acetogenesis and several fermentation metabolisms, this mechanism is still poorly studied and not biochemically confirmed in dissimilatory sulfate reduction. Several hints indicate that heterodisulfide reductase HdrABC will interact with DsrC, coupling sulfate reduction with ethanol oxidation through the flavin oxidoreductase Flx in *D*. *vulgaris*, and with hydrogen oxidation through the [NiFe]-hydrogenase MvhAGD in *A*. *fulgidus*. Some of these hints include interactions deduced from coelution in pull-down assays and proteomic results in DsrC-affected strains, which were described previously in Chapter III.

One issue delaying the confirmation of FBEB by HdrABC in sulfate-reducers is the difficulty in purifying this protein complex. In this chapter, several strategies to express and purify Hdr proteins from *A*. *fulgidus* were discussed. The HdrA and HdrB subunits were successfully purified, and their spectroscopic properties were assessed. HdrA includes six [4Fe-4S] clusters and one FAD cofactor, and HdrB includes two non-cubane [4Fe-4S] clusters. The main issue around Hdr purification concerned the difficulty to purify the HdrC subunit in a soluble form. The best result was obtained from copurification with HdrB using *D*. *vulgaris* as expression host, but this still yielded low amounts of HdrC that were disproportional to HdrB. This chapter described a plethora of different approaches that were carried out to try to purify HdrC from the soluble fraction, as well as from inclusion bodies, and using different hosts for expression. The limiting time made us stop pursuing this topic, however, countless strategies could still be tried to eventually succeed in HdrC purification, namely:

In theory, the best approach could be to express the three HdrABC subunits together in the same strain, whether it is homologously in *Desulfovibrio* or *Archaeoglobus* species, or heterologously in *E*. *coli*. The challenges observed here with *D*. *vulgaris* and *A*. *fulgidus* were mainly regarding the lower expression, having this also been described in the literature, and the need to overcome by using large-scale fermenters with challenging settings. As for a heterologous expression in *E*. *coli*, cloning the whole *hdr* operon into a plasmid

would not be enough. This was tried, but there was a great expression disparity between genes: the first gene would be expressed together with the plasmid's enhanced ribosome-binding site, while the other two would still have the original rbs from the parent strain. To the best of my knowledge, there is no vector with three MCS, therefore three distinct rbs, to separately clone *hdrA*, *hdrB* and *hdrC*. One potential solution could be to use pDuet expressing *hdrB*/*C* together with a pET vector expressing *hdrA*, but this would require some both host and vector changes regarding antibiotic resistance.

Other suggestions could be: 1) from the solubility standpoint: testing other solubility tags besides GST, namely Trx or MBP [76]; 2) from the expression host standpoint: purify Hdr from a sulfate-reducing organism other than *A*. *fulgidus* or *D*. *vulgaris*. This study was focused on *A*. *fulgidus* because this strain is ideal for biochemical assays involving the DsrC trisulfide, which is important to prove the Hdr function. Nonetheless, biochemical activities could be performed using Hdr and DsrC from other organisms, or even a hybrid system with proteins from several organisms, for instance, the HdrABC from another sulfate-reducer and *A*. *fulgidus* DsrC. Despite this suggestion may be fallible and prone to challenges in interpreting the results, the interchangeability of proteins from organisms able to dissimilate sulfur was already shown to be possible: DsrJ from the sulfate-reducer *D*. *vulgaris* could functionally substitute *in vivo* the function of DsrJ from the sulfur-oxidizer *A*. *vinosum* [77]. This interchangeability has been also shown for organisms with an even more distant phylogenetic relationship, namely the ability of ferredoxin from *Clostridium tetanomorphum* to transfer electrons through *A*. *vinosum* DsrABL to NAD^+ [78].

Despite the failure in purifying HdrC from *A*. *fulgidus*, several new methods for protein expression and purification were learned through this process, for instance how to decrease the protein expression rate without decreasing the temperature or the inducer concentration, by inducing the cells at a higher bacterial density, near the stationary phase, in which the cells are metabolically less active.

Using the methodology described in the previous sections, it was not possible to prove the evidence of electron transfer between HdrCB and DsrC. The main issue lies around obtaining HdrCB with enough

quantity and quality, and future research on this topic should address this to show the Hdr capability to perform FBEB and contribute to dissimilatory sulfate reduction.

4.6 – Acknowledgements

I would like to thank Raquel Bernardino, which contributed to this work during her bachelor's. A special acknowledgment to Christiane Dahl and her group in the University of Bonn, particularly Maria Löffler, for an internship where I got training in expressing Fe-S proteins in *E*. *coli*. This work was funded by the Fundação para a Ciência e Tecnologia (Portugal) through fellowship PD/BD/128204/2016 (DF), grants PTDC/BIA-MIC/6512/2014 e PTDC/BIA-BQM/29118/2017, R&D unit MOSTMICRO-ITQB (UIDB/04612/2020 and UIDP/04612/2020) and LS4FUTURE Associated Laboratory (LA/P/0087/2020).

4.7 – Bibliography

[1] R. Thauer, K. Jungermann, and K. Decker, “Energy Conservation in Chemotrophic Anaerobic Bacteria”, *Bacteriol. Rev.*, vol. 41, no. 1, pp. 100–180, 1977.

[2] W. Buckel and R. K. Thauer, “Flavin-Based Electron Bifurcation, A New Mechanism of Biological Energy Coupling”, *Chem. Rev.*, vol. 118, no. 7, pp. 3862–3886, 2018.

[3] P. Mitchell, “The protonmotive Q cycle: A general formulation”, *FEBS Lett.*, vol. 59, no. 2, pp. 137–139, 1975.

[4] F. Baymann *et al.*, “On the natural history of flavin-based electron bifurcation”, *Front. Microbiol.*, vol. 9, no. JUL, 2018.

[5] L. Appel, M. Willistein, C. Dahl, U. Ermler, and M. Boll, “Functional diversity of prokaryotic HdrA(BC) modules: Role in flavin-based electron bifurcation processes and beyond”, *Biochim. Biophys. Acta - Bioenerg.*, vol. 1862, no. 4, p. 148379, 2021.

[6] W. Thamer *et al.*, “A two [4Fe-4S]-cluster-containing ferredoxin as an alternative electron donor for 2-hydroxyglutaryl-CoA dehydratase from Acidaminococcus fermentans”, *Arch. Microbiol.*, vol. 179, no. 3, pp. 197–204, 2003.

[7] W. Buckel and R. K. Thauer, “Energy conservation via electron bifurcating ferredoxin reduction and proton/Na+ translocating ferredoxin oxidation”, *Biochim. Biophys. Acta - Bioenerg.*, vol. 1827, no. 2, pp. 94–113, 2013.

[8] G. Herrmann, E. Jayamani, G. Mai, and W. Buckel, “Energy conservation via electron-transferring flavoprotein in anaerobic bacteria”, *J. Bacteriol.*, vol. 190, no. 3, pp. 784–791, 2008.

[9] F. Li, J. Hinderberger, H. Seedorf, J. Zhang, W. Buckel, and R. K. Thauer, “Coupled ferredoxin and crotonyl coenzyme A (CoA) reduction with NADH catalyzed by the butyryl-CoA dehydrogenase/Etf complex from *Clostridium kluyveri*”, *J. Bacteriol.*, vol. 190, no. 3, pp. 843–850, 2008.

[10] G. J. Schut and M. W. W. Adams, “The iron-hydrogenase of Thermotoga maritima utilizes ferredoxin and NADH synergistically: A new perspective on anaerobic hydrogen production”, *J. Bacteriol.*, vol. 191, no. 13, pp. 4451–4457,

2009.

[11] J. R. Sieber *et al.*, “The genome of *Syntrophomonas wolfei*: New insights into syntrophic metabolism and biohydrogen production”, *Environ. Microbiol.*, vol. 12, no. 8, pp. 2289–2301, 2010.

[12] M. C. Weghoff, J. Bertsch, and V. Müller, “A novel mode of lactate metabolism in strictly anaerobic bacteria”, *Environ. Microbiol.*, vol. 17, no. 3, pp. 670–677, 2015.

[13] A. R. Ramos, K. L. Keller, J. D. Wall, and I. A. Cardoso Pereira, “The membrane *qmoABC* complex interacts directly with the dissimilatory adenosine 5'-phosphosulfate reductase in sulfate reducing bacteria”, *Front. Microbiol.*, vol. 3, pp. 1–10, 2012.

[14] S. S. Venceslau, Y. Stockdreher, C. Dahl, and I. A. C. Pereira, “The ‘bacterial heterodisulfide’ DsrC is a key protein in dissimilatory sulfur metabolism”, *Biochim. Biophys. Acta - Bioenerg.*, vol. 1837, no. 7, pp. 1148–1164, 2014.

[15] A.-K. Kaster, J. Moll, K. Parey, and R. K. Thauer, “Coupling of ferredoxin and heterodisulfide reduction via electron bifurcation in hydrogenotrophic methanogenic archaea”, *Proc Natl Acad Sci U S A*, vol. 108, no. 7, pp. 2981–2986, 2011.

[16] T. Wagner, J. Koch, U. Ermler, and S. Shima, “Methanogenic heterodisulfide reductase (HdrABC-MvhAGD) uses two noncubane [4Fe-4S] clusters for reduction”, *Science.*, vol. 357, no. 6352, pp. 699–703, 2017.

[17] S. Madadi-Kahkesh, E. C. Duin, S. Heim, S. P. J. Albracht, M. K. Johnson, and R. Hedderich, “A paramagnetic species with unique EPR characteristics in the active site of heterodisulfide reductase from methanogenic archaea”, *Eur. J. Biochem.*, vol. 268, no. 9, pp. 2566–2577, 2001.

[18] G. J. Mander, A. J. Pierik, H. Huber, and R. Hedderich, “Two distinct heterodisulfide reductase-like enzymes in the sulfate-reducing archaeon *Archaeoglobus profundus*”, *Eur. J. Biochem.*, vol. 271, no. 6, pp. 1106–1116, 2004.

[19] Z. Yan, M. Wang, and J. G. Ferry, “A ferredoxin- and $F_{420}H_2$-dependent, electron- bifurcating, heterodisulfide reductase with homologs in the domains Bacteria and Archaea”, *mBio*, vol. 8, no. 1. pp. 1–15, 2017.

[20] I. A. C. Pereira, A. R. Ramos, F. Grein, M. C. Marques, S. M. da Silva, and S. S. Venceslau, “A comparative genomic analysis of energy metabolism in sulfate reducing bacteria and archaea”, *Front. Microbiol.*, vol. 2, no. 69, pp. 1–22, 2011.

[21] A. R. Ramos *et al.*, “The FlxABCD-HdrABC proteins correspond to a novel NADH dehydrogenase/heterodisulfide reductase widespread in anaerobic bacteria and involved in ethanol metabolism in *Desulfovibrio vulgaris* Hildenborough”, *Environ. Microbiol.*, vol. 17, no. 7, pp. 2288–2305, 2015.

[22] Y. Liu, S. Guo, R. Yu, J. Ji, and G. Qiu, “HdrC2 from *Acidithiobacillus ferrooxidans* owns two iron-sulfur binding motifs but binds only one variable cluster between [4Fe-4S] and [3Fe-4S]”, *Curr. Microbiol.*, vol. 66, no. 1, pp. 88–95, 2013.

[23] Y. Liu, J. Ji, R. Yu, and G. Qiu, “Expression, purification and molecular modeling of another HdrC from *Acidithiobacillus ferrooxidans* which binds only one [4Fe-4S] cluster”, *Curr. Microbiol.*, vol. 65, no. 4, pp. 416–423, 2012.

[24] C. T. Chung, S. L. Niemela, and R. H. Miller, “One-step preparation of competent *Escherichia coli*: transformation and storage of bacterial cells in the same solution”, *Proc Natl Acad Sci U S A*, vol. 86, pp. 2172–2175, 1989.

[25] K. L. Keller, J. D. Wall, and S. Chhabra, *Methods for engineering sulfate reducing bacteria of the genus Desulfovibrio*, 1st ed., vol. 497. Elsevier Inc., 2011.

[26] K. L. Keller, K. S. Bender, and J. D. Wall, “Development of a markerless genetic exchange system for *Desulfovibrio vulgaris* Hildenborough and its use in generating a strain with increased transformation efficiency”, *Appl. Environ. Microbiol.*, vol. 75, no. 24, pp. 7682–7691, 2009.

[27] M. Z. Li and S. J. Elledge, “Harnessing homologous recombination in vitro to generate recombinant DNA via SLIC”, vol. 4, no. 3, pp. 251–256, 2007.

[28] A. A. Santos *et al.*, “A protein trisulfide couples dissimilatory sulfate reduction to energy conservation”, *Science.*, vol. 350, no. 6267, pp. 1541–1545, 2015.

[29] M. K. Akhtar and P. R. Jones, “Deletion of *iscR* stimulates recombinant clostridial Fe-Fe hydrogenase activity and H2-accumulation in *Escherichia coli* BL21(DE3)”, *Appl. Microbiol.*

Biotechnol., vol. 78, no. 5, pp. 853–862, 2008.

[30] Y. Takahashi and M. Nakamura, “Functional assignment of the ORF2-*iscS-iscU-iscA-hscB-hscA-fdx*-ORF3 gene cluster involved in the assembly of Fe-S clusters in Escherichia coli”, *J. Biochem.*, vol. 126, no. 5, pp. 917–926, 1999.

[31] J. M. Kuchenreuther, C. S. Grady-Smith, A. S. Bingham, S. J. George, S. P. Cramer, and J. R. Swartz, “High-yield expression of heterologous [FeFe] hydrogenases in *Escherichia coli*”, *PLoS One*, vol. 5, no. 11, pp. 4–10, 2010.

[32] L. Kröninger, S. Berger, C. Welte, and U. Deppenmeier, “Evidence for the involvement of two heterodisulfide reductases in the energy-conserving system of *Methanomassiliicoccus luminyensis*”, *FEBS J.*, vol. 283, no. 3, pp. 472–483, 2016.

[33] G. M. Zane, H. C. Bill Yen, and J. D. Wall, “Effect of the deletion of *qmoABC* and the promoter-distal gene encoding a hypothetical protein on sulfate reduction in *Desulfovibrio vulgaris* Hildenborough”, *Appl. Environ. Microbiol.*, vol. 76, no. 16, pp. 5500–5509, 2010.

[34] A. Brandis and R. K. Thauer, “Growth of *Desulfovibrio* species on hydrogen and sulphate as sole energy source”, *J. Gen. Microbiol.*, vol. 126, no. 1, pp. 249–252, 1981.

[35] R. Rudolph and H. Lilie, “*In vitro* folding of inclusion body proteins”, *FASEB J.*, vol. 10, no. 1, pp. 49–56, 1996.

[36] K. Tsumoto, M. Umetsu, I. Kumagai, D. Ejima, J. S. Philo, and T. Arakawa, “Role of arginine in protein refolding, solubilization, and purification”, *Biotechnol. Prog.*, vol. 20, no. 5, pp. 1301–1308, 2004.

[37] S.-H. Lee, “Effects of solutes on solubilization and refolding of proteins from inclusion bodies with high hydrostatic pressure”, *Protein Sci.*, vol. 15, no. 2, pp. 304–313, 2006.

[38] A. Singh, V. Upadhyay, A. K. Upadhyay, S. M. Singh, and A. K. Panda, “Protein recovery from inclusion bodies of *Escherichia coli* using mild solubilization process”, *Microb. Cell Fact.*, vol. 14, no. 1, pp. 1–10, 2015.

[39] A. Singh *et al.*, “*Mycobacterium tuberculosis* WhiB3 responds to O_2 and nitric oxide via its [4Fe-4S] cluster and is essential for nutrient starvation survival”, *Proc. Natl. Acad. Sci. U. S. A.*,

vol. 104, no. 28, pp. 11562–11567, 2007.

[40] D. S. Fischer and D. C. Price, “A Simple Serum Iron Method Using the New Sensitive Chromogen Tripyridyl-s-triazine”, *Clin. Chem.*, vol. 10, pp. 21–31, 1964.

[41] S. S. Venceslau *et al.*, “Redox states of *Desulfovibrio vulgaris* DsrC, a key protein in dissimilatory sulfite reduction”, *Biochem. Biophys. Res. Commun.*, vol. 441, no. 4, pp. 732–736, 2013.

[42] L. Kröninger, S. Berger, C. Welte, and U. Deppenmeier, “Evidence for the involvement of two different heterodisulfide reductases in the energy conserving system of *Methanomassiliicoccus luminyensis*”, *FEBS J.*, vol. 283, pp. 472–483, 2016.

[43] H. Tegel, S. Tourle, J. Ottosson, and A. Persson, “Increased levels of recombinant human proteins with the *Escherichia coli* strain Rosetta(DE3)”, *Protein Expr. Purif.*, vol. 69, no. 2, pp. 159–167, 2010.

[44] G. J. Mander, E. C. Duin, D. Linder, K. O. Stetter, and R. Hedderich, “Purification and characterization of a membrane-bound enzyme complex from the sulfate-reducing archaeon *Archaeoglobus fulgidus* related to heterodisulfide reductase from methanogenic archaea”, *Eur. J. Biochem.*, vol. 269, no. 7, pp. 1895–1904, 2002.

[45] R. H. Pires, S. S. Venceslau, F. Morais, M. Teixeira, A. V. Xavier, and I. A. C. Pereira, “Characterization of the *Desulfovibrio desulfuricans* ATCC 27774 DsrMKJOP complex - A membrane-bound redox complex involved in the sulfate respiratory pathway”, *Biochemistry*, vol. 45, no. 1, pp. 249–262, 2006.

[46] C. H. Schein, “Production of soluble recombinant proteins in bacteria”, *Nat. Biotechnol.*, vol. 7, no. 11, pp. 1141–1149, 1989.

[47] K. Terpe, “Overview of bacterial expression systems for heterologous protein production: From molecular and biochemical fundamentals to commercial systems”, *Appl. Microbiol. Biotechnol.*, vol. 72, no. 2, pp. 211–222, 2006.

[48] J. G. Marblestone, S. C. Edavettal, Y. Lim, P. Lim, X. Zuo, and T. R. Butt, “Comparison of SUMO fusion technology with traditional gene fusion systems: Enhanced expression and

solubility with SUMO", *Protein Sci.*, vol. 15, pp. 182–189, 2006.

[49] M. T. Nguyen *et al.*, "Prokaryotic soluble overexpression and purification of oncostatin M using a fusion approach and genetically engineered *E. coli* strains", *Sci. Rep.*, vol. 9, no. 1, pp. 1–13, 2019.

[50] D. B. Smith and K. S. Johnson, "Single-step purification of polypeptides expressed in *Escherichia coli* as fusions with glutathione S-transferase", *Gene*, vol. 67, no. 1, pp. 31–40, 1988.

[51] R. J. Jenny, K. G. Mann, and R. L. Lundblad, "A critical review of the methods for cleavage of fusion proteins with thrombin and factor Xa", *Protein Expr. Purif.*, vol. 31, no. 1, pp. 1–11, 2003.

[52] E. Boisselier, M. Lou Audet, L. Cantin, and C. Salesse, "A strategy for purifying glutathio S-transferase in the presence of sodium dodecyl sulfate", *Biotechniques*, vol. 51, no. 3, pp. 193–194, 2011.

[53] J. F. Kane, "Effects of rare codon clusters on high-level expression of heterologous proteins in *Escherichia coli*", *Curr. Opin. Biotechnol.*, vol. 6, no. 5, pp. 494–500, 1995.

[54] T. L. Calderone, R. D. Stevens, and T. G. Oas, "High-level misincorporation of lysine for arginine at AGA codons in a fusion protein expressed in *Escherichia coli*", *J. Mol. Biol.*, vol. 262, no. 4, pp. 407–412, 1996.

[55] Z. Lipinszki *et al.*, "Enhancing the Translational Capacity of *E. coli* by Resolving the Codon Bias", *ACS Synth. Biol.*, vol. 7, no. 11, pp. 2656–2664, 2018.

[56] A. Krogh, B. Larsson, G. Von Heijne, and E. L. L. Sonnhammer, "Predicting transmembrane protein topology with a hidden Markov model: Application to complete genomes", *J. Mol. Biol.*, vol. 305, no. 3, pp. 567–580, 2001.

[57] J. Yang, R. Jang, Y. Zhang, and H. Bin Shen, "High-accuracy prediction of transmembrane inter-helix contacts and application to GPCR 3D structure modeling", *Bioinformatics*, vol. 29, no. 20, pp. 2579–2587, 2013.

[58] N. Sapay, Y. Guermeur, and G. Deléage, "Prediction of amphipathic in-plane membrane anchors in monotopic

proteins using a SVM classifier", *BMC Bioinformatics*, vol. 7, pp. 1–11, 2006.

[59] M. M. Carrió and A. Villaverde, "Localization of chaperones DnaK and GroEL in bacterial inclusion bodies", *J. Bacteriol.*, vol. 187, no. 10, pp. 3599–3601, 2005.

[60] A. Mitraki, B. Fane, C. Haase-petjingell, J. Sturtevant, and J. King, "Global Suppression of Protein Folding Defects and Inclusion Body Formation", *Science.*, vol. 253, pp. 54–58, 1991.

[61] I. Palmer and P. T. Wingfield, "Preparation and extraction of insoluble (Inclusion-body) proteins from *Escherichia coli*", *Curr. Protoc. Protein Sci.*, vol. 1, no. 70, pp. 1–25, 2012.

[62] L. F. Vallejo and U. Rinas, "Strategies for the recovery of active proteins through refolding of bacterial inclusion body proteins", *Microb. Cell Fact.*, vol. 3, pp. 1–12, 2004.

[63] H. Beinert, "Iron-sulfur proteins: Ancient structures, still full of surprises", *J. Biol. Inorg. Chem.*, vol. 5, no. 1, pp. 2–15, 2000.

[64] D. C. Johnson, D. R. Dean, A. D. Smith, and M. K. Johnson, "Structure, function, and formation of biological iron-sulfur clusters", *Annu. Rev. Biochem.*, vol. 74, pp. 247–281, 2005.

[65] M. R. Reyda, R. Dippold, M. E. Dotson, and J. T. Jarrett, "Loss of iron-sulfur clusters from biotin synthase as a result of catalysis promotes unfolding and degradation", *Arch. Biochem. Biophys.*, vol. 471, no. 1, pp. 32–41, 2008.

[66] E. M. Shepard and J. B. Broderick, "S-adenosylmethionine and iron-sulfur clusters in biological radical reactions: The radical SAM superfamily", *Compr. Nat. Prod. II Chem. Biol.*, vol. 8, pp. 625–661, 2010.

[67] K. O. Stetter, G. Lauerer, M. Thomm, and A. Neuner, "Isolation of extremely thermophilic sulfate reducers: Evidence for a novel branch of archaebacteria", *Science.*, vol. 236, no. 4803, pp. 822–824, 1987.

[68] S. Burggraf, H. W. Jannasch, B. Nicolaus, and K. O. Stetter, "*Archaeoglobus profundus* sp. nov., Represents a New Species within the Sulfate-reducing Archaebacteria", *Syst. Appl. Microbiol.*, vol. 13, no. 1, pp. 24–28, 1990.

[69] T. Ide, S. Báumer, and U. Deppenmeier, "Energy

conservation by the H_2:heterodisulfide oxidoreductase from *Methanosarcina mazei* Go1: Identification of two proton-translocating segments", *J. Bacteriol.*, vol. 181, no. 13, pp. 4076–4080, 1999.

[70] U. Deppenmeier, "The Membrane-Bound Electron Transport System of Methanosarcina Species", *J. Bioenerg. Biomembr.*, vol. 36, no. 1, pp. 55–64, 2004.

[71] F. Grein, A. R. Ramos, S. S. Venceslau, and I. A. C. Pereira, "Unifying concepts in anaerobic respiration: Insights from dissimilatory sulfur metabolism", *Biochim. Biophys. Acta*, vol. 1827, no. 2, pp. 145–160, 2013.

[72] J. Vornolt, J. Kunow, K. O. Stetter, and R. K. Thauer, "Enzymes and coenzymes of the carbon monoxide dehydrogenase pathway for autotrophic CO_2 fixation in *Archaeoglobus lithotrophicus* and the lack of carbon monoxide dehydrogenase in the heterotrophic *A. profundus*", *Arch. Microbiol.*, vol. 163, no. 2, pp. 112–118, 1995.

[73] C. Ziparo, A. Giannasi, L. Ulivi, and M. Zoppi, "Raman spectroscopy study of molecular hydrogen solubility in water at high pressure", *Int. J. Hydrogen Energy*, vol. 36, no. 13, pp. 7951–7955, 2011.

[74] M. C. Marques *et al.*, "The direct role of selenocysteine in [NiFeSe] hydrogenase maturation and catalysis", *Nat. Chem. Biol.*, vol. 13, no. 5, pp. 544–550, 2017.

[75] S. Zacarias, M. Vélez, M. Pita, A. L. De Lacey, P. M. Matias, and I. A. C. Pereira, "Characterization of the [NiFeSe] hydrogenase from *Desulfovibrio vulgaris* Hildenborough", *Methods Enzymol.*, vol. 613, pp. 169–201, 2018.

[76] D. Esposito and D. K. Chatterjee, "Enhancement of soluble protein expression through the use of fusion tags", *Curr. Opin. Biotechnol.*, vol. 17, no. 4, pp. 353–358, 2006.

[77] F. Grein *et al.*, "DsrJ, an essential part of the DsrMKJOP transmembrane complex in the purple sulfur bacterium *Allochromatium vinosum*, is an unusual triheme cytochrome c", *Biochemistry*, vol. 49, no. 38, pp. 8290–8299, 2010.

[78] J. Lofi, "Characterization of the Sulfite-Generating rDsrABL Complex of *Allochromatium vinosum*", 2020.

Chapter 5

Concluding Remarks

Sulfate-reducing microorganisms are essential to guarantee the balance of Earth ecosystems. Their metabolic process to obtain energy, dissimilatory sulfate reduction, drives the biogeochemical sulfur cycle and has a strong influence on other element cycles and on the redox balance of the oceans and atmosphere. It has a particular impact on marine sediments, where it accounts for up to 50% of carbon mineralization and prevents methane emissions through its involvement in anaerobic methane oxidation.

Besides maintaining a sulfur balance in the biosphere, dissimilatory sulfate reduction can be used for several biotechnological applications, such as bioremediation of contaminated environments. These applications are only possible due to the versatility of sulfate-reducing bacteria to use a wide range of organic compounds as electron donors for sulfate reduction.

One step of this metabolic process is the reduction of sulfite to hydrogen sulfide: the protein DsrAB, together with DsrC, catalyses a four-electron reduction of sulfite to S^0 in the form of a trisulfide bound to DsrC. This trisulfide is believed to be later reduced to sulfide by the DsrMKJOP transmembrane complex, and the DsrC recycled.

Despite the constant advances of science, there are still (and there will always be) a lot of mysteries to solve in this respiratory metabolism, and I could address some of them during my PhD journey:

1 - <u>Role of DsrD in the sulfate respiration metabolism.</u>

This has been a riddle over decades, as this protein is absent from sulfur-oxidizing organisms and present in most organisms able to perform the dissimilatory reduction of sulfite, and its respective gene *dsrD* is typically in the same operon as *dsrAB*. This characteristic has made *dsrD* a pivotal genetic marker to distinguish dissimilatory sulfur metabolisms.

We could assign the function of DsrD as an allosteric activator of DsrAB catalysis in sulfite reduction. We show here that DsrD is highly abundant in respiratory conditions but practically absent during fermentative growth, which is aligned with the observation that the absence of DsrD affects growth under sulfite respiration, but not fermentation. Despite its importance, this protein is not strictly essential as we could obtain a Δ*dsrD* deletion strain in *D. vulgaris* H,

in contrast to DsrC. The absence of DsrD in organisms encoding the putative earliest forms of DsrAB indicates that DsrD appeared later in the evolutionary history of the *dsr* genes. This is in line with its non-essential function, as observed in our studies.

2 - The role of DsrC goes beyond its function as a co-substrate of DsrAB in sulfite reduction.

The widespread presence of DsrC in sulfate, sulfite, thiosulfate and sulfur reducers, sulfur-disproportionators, organosulphonate degraders and in many photo- and chemotrophic sulfur-oxidizing prokaryotes, as well as the essentiality of this protein, suggests the ability of DsrC to be involved in something else than sulfite reduction.

We could show that DsrC is important for cellular functions other than sulfite reduction and suggest that it may also be involved in redox regulation, since its redox status is linked to the expression of several proteins, most notably Adh and the FlxABCD-HdrABC complex, for which direct interaction with DsrC was confirmed.

A defective DsrC causes the strain to growth in lactate/sulfate with fermentation and hydrogen consumption via hydrogen cycling model, with this being shown by proteomics and the products released, as well the slower growth and lower cell density in comparison with the wild-type strain. The defective DsrC also causes *D*. *vulgaris* to produce more ethanol, and the Adh alcohol dehydrogenase was also more abundant, in comparison with the WT in the same situation. This Adh is believed to be linked to the reduction of the DsrC trisulfide via FlxABCD-HdrABC, a protein complex likely able to perform FBEB. Despite this interaction between DsrC and FlxABCD-HdrABC having been proven by pull-down experiments, electron transfer between these two could not be shown *in vitro*, because of challenges in HdrC purification.

The rising discoveries of protein complexes able to perform FBEB, as well as their significance in prokaryotic metabolisms, have been striking. Despite FBEB being already described in methanogenesis, acetogenesis and several fermentation metabolisms, this mechanism is still poorly studied and not biochemically confirmed in dissimilatory sulfate reduction. This thesis presents several hints indicating that heterodisulfide reductase HdrABC interacts with

DsrC, this way coupling sulfate reduction with ethanol oxidation through the flavin oxidoreductase Flx in *D*. *vulgaris*, and with hydrogen oxidation through the [NiFe]-hydrogenase MvhAGD in *A*. *fulgidus*. The next step should be to confirm in vitro the ability of HdrABC to perform FBEB with DsrC.

To close, I want to emphasize the importance of perseverance and tenacity in scientific research. The road to discovery is rarely a smooth one, and setbacks are inevitable. But it's the small breakthroughs along the way that keep us going. Every experiment that yields a new insight, every data point that challenges our assumptions, every incremental improvement in our methods - these are the building blocks of scientific progress. I am joyful to have left my fingerprint in unveiling some of mysteries of life on Earth and I hope that my work inspires others to keep pushing the boundaries of knowledge.

ITQB NOVA, Avenida da República, 2780-157 Oeiras, Portugal | Tel +351 214 469 100 | itqb.unl.pt